



A2IM: Cookbook

An introduction to additive manufacture for astronomy

Carolyn Atkins and Bart van de Vorst – on behalf of the OPTICON A2IM team

29 June 2021



This research is part of the OPTICON project and is supported by the European Commission's H2020 programme grant number 730890).





Table of Contents

Table of Acronyms	11
1 Introduction	13
1.1 Purpose of Document	13
1.1.1 Scope of Document.....	13
1.1.2 Intended Audience.....	13
2 Applicable and Reference documents	14
2.1 Applicable Documents	14
2.2 Reference Documents.....	14
3 reference material	15
3.1 Manufacture methodology	16
3.1.1 Which manufacturing process to use?.....	17
3.2 Lightweight mirror manufacture.....	18
3.2.1 Lightweight mirror manufacture: casting	19
3.2.2 Lightweight mirror manufacture: subtractive	19
3.2.3 Lightweight mirror manufacture: fabricative	20
3.2.4 Lightweight mirror manufacture: additive.....	20
3.3 Additive Manufacturing process and material barriers.....	21
3.3.1 Processes.....	22
3.3.2 Polymers.....	23
3.3.3 Powder bed fusion - Polymers	24
3.3.4 Material Extrusion.....	25
3.3.5 Vat Photo Polymerisation	26
3.3.6 Metals	27
3.3.7 Powder Bed Fusion - Metals	29
3.3.8 Indirect metal processes	36
3.3.9 Binder Jetting	37
3.3.10 Advanced Ceramics	38
3.4 AM Material properties	40
3.4.1 General overview	40
3.4.2 Metals	41
3.4.3 Polymers.....	42



3.4.4	Ceramics.....	43
3.5	Software.....	44
3.5.1	Internal and external lattice structures	45
3.5.2	2D Grid structure.....	46
3.5.3	Periodic Lattices	46
3.5.4	Formula driven lattices	51
3.5.5	Stochastic lattice structures.....	52
3.5.6	Topology optimization & Generative Design	54
3.5.7	Biomimicry - Design with nature as example.....	58
3.6	AM design guidelines.....	62
3.6.1	Reference material.....	62
3.6.2	Key design guidelines for AM mirror development.....	63
3.6.3	Example: application of design guidelines for AM mirror fabrication.....	64
3.7	AM Defects.....	70
3.7.1	Porosity	73
3.7.2	Hidden material structure.....	74
3.7.3	Metallographic examination.....	74
3.7.4	Micro Porosity – Powder Bed Fusion	75
3.7.5	Micro-porosity – binder jetting.....	76
3.7.6	Reduction of porosity by hot isostatic pressing.....	77
3.8	Support structures	78
3.8.1	The role of support structures	78
3.8.2	Polymer support material	79
3.8.3	Metallic support material	82
3.9	Post-processing.....	85
3.9.1	The importance of post-processing	85
3.9.2	Post-processing techniques	86
3.9.3	Post processing considerations.....	91
3.9.4	Fixtures and clamping.....	92
3.9.5	Current development - Flexible post processing	93
3.9.6	Flexible Post Processing User case - Freeform mirror	94
3.9.7	Subtractive Machining Guidelines – Design for Manufacturing (DfM).....	95
3.9.8	Future developments – Hybrid Machining	96
3.9.9	Example 1: a lightweight Ti64 mirror.....	97
3.9.10	Example 2: a metallised polymer mirror.....	98



- 3.9.11 Example 3: metallisation of polymer components 99
- 3.9.12 Plating of AM substrates 100
- 3.9.13 Plating of Additive Manufacturing parts 102
- 3.9.14 Mechanical properties 103
- 3.9.15 Metal coating for optical post-processing: nickel phosphor (NiP)..... 104
- 3.9.16 Companies involved 104
- 3.10 Evaluation via dimensional metrology 105
 - 3.10.1 Overview 105
 - 3.10.2 Tools and examples 105
- References 113
- 4 Paradigm shift: Metal AM mirror development 119
 - 4.1 Fabrication chain 119
 - 4.2 Optical and manufacture requirements 120
 - 4.3 Design for additive manufacture 121
 - 4.4 Critical surfaces and drawing generation 122
 - 4.5 Preparation for build 123
 - 4.6 Build 124
 - 4.7 Post build 125
 - 4.8 Inspection and metrology 126
 - 4.9 Post-processing – subtractive machining 127
 - 4.10 Optical fabrication: polishing and SPDT 128
 - 4.11 Applications 129
- References 130
- 5 Case studies 135
- 6 Appendix: AM material properties references 149
 - 6.1 Metals 149
 - 6.2 Polymers 151
 - 6.3 Ceramics 153



List of Figures

Figure 1: manufacturing methodology – subtractive, formative, fabricative and additive, image credit: STFC..... 16

Figure 2: the benefits of metal manufacturing processes highlighted in terms of quantity required and geometric complexity. Image credit: G. N. Levy 2003 [2]. 17

Figure 3: sketches of different lightweight mirror styles - contoured back (a), open back (b), and sandwich (c). Image credit: STFC. 18

Figure 4: manufacturing processes used in lightweight mirror production – cross sections shown. Image credit: STFC. 18

Figure 5: casting of lightweight mirrors. *Left* - sketch of the casting process, *right* - example of the casting of the GMT 8.4 m mirrors, image credit: H. M. Martin 2019 [5]. 19

Figure 6: subtractive machining for lightweight mirrors. *Left* - a sketch of the subtractive (milling) process and *right* - an example of subtractive machining of a Zerodur mirror, image credit: SCHOTT AG [6]. 19

Figure 7: fabricative mirror manufacture; *left* - a sketch of a deconstruction of the manufacture process, *right* - an example of a fabricative primary mirror created for the NASA Kepler space telescope, image credit: D. Ebbets et al 2013 [7]. 20

Figure 8: additive mirror manufacture; *left* - a sketch of the manufacture process, *right* - an example of a prototype metallic mirror with a Voronoi lightweighting structure, image credit: E. Hilpert et al. 2019 [10]. 20

Figure 9: the interplay between different engineering material groups, image credit: TNO..... 21

Figure 10: the AM methodologies divided by engineering material group, image credit: TNO..... 22

Figure 11: thermoplastic performance pyramid (image credit: SABIC). 23

Figure 12: Polymer Powder Bed Fusion process, image credit: 3DHubs. 24

Figure 13: material extrusion process, image credit: 3DHubs. 25

Figure 14: VPP/SLA processing, image credit: 3DHubs. 26

Figure 15: additive manufacturing processes for engineering metals. Classification by direct and indirect processes, image credits: TNO..... 27

Figure 16: NNS part made with laser cladding technology. Secondary process steps such as CNC milling are used to realize the final shape. 28

Figure 17: different metallic groups that are suitable for metal PBF, image credits: TNO..... 28

Figure 18: metal PBF process, image credit: 3DHubs. 29

Figure 19: Current state-of-art PBF processes are equipped with multiple sensors to capture the melt-pool and build process for real time *in-situ* monitoring [11]. The complete build process is traceable and can be used for defect detection, qualification and certification [12]. 30

Figure 20: the Ishikawa diagram for the PBF process, image credit: Olaf Rehme, ILaS. 31

Figure 21: Laser beam distributions for a small laser spot and large multimode laser spot [14]. 34

Figure 22: Metal binder jetting parts from various companies 36

Figure 23: Material extrusion samples of highly filled metal filament. 36

Figure 24: Binder jetting process, image credit: 3DHubs. 37

Figure 25: Custom made ceramic optical substrate, image credit: 3D Ceram. 38

Figure 26: Solid state sintering of ceramics, image credits: TNO. 38

Figure 27: examples of 3D printed advanced ceramic parts. 39

Figure 28: Young's modulus as a function of density for AM metals, ceramics and polymers, image credit: STFC..... 40

Figure 29: Young's modulus as a function of density for AM metals – note the linear axes. Image credit: STFC..... 41

Figure 30: three examples demonstrating the use of metal AM in the creation of metal mirrors. Image credits: [17] [8] [18] respectively..... 41

Figure 31: Young's modulus as a function of density for AM polymers – note the linear axes. Image credit: STFC..... 42



Figure 32: two examples of printed plastic astronomical components. *a*) An ABS mirror (*left*) and actuator grid (*right*), image credit: Miller, C., et al. (2016) [19]; and *b*) a prototype housing to mimic a reflecting grating astronomical spectrograph, image credit: Steele, I., et al. (2018) [20]. 42

Figure 33: Young's modulus as a function of density for AM ceramics – note the linear axes. Image credit: STFC. 43

Figure 34: *left* - an AM alumina substrate for an active mirror prototype created as part of OPTICON A2IM, image credit Roulet, M. (2020) [21]; and *right* – AM RoboSic polished prototype mirrors, image credit Goodman, W., et al (2019) [22]. 43

Figure 35: Typical additive manufactured parts with complex structures that are difficult to design in traditional engineering software. 44

Figure 36: Some Additive manufactured parts with integrated functional lattice structures, which cannot be produced with other production technologies. 45

Figure 37: The four groups of lattices for implementation within product design (image credits: TNO). 45

Figure 38: Examples of the honeycomb 2D grid structure. 46

Figure 39: The seven primitive crystal systems, image credit: Encyclopaedia Britannica. 46

Figure 40: Periodic lattice structure nomenclature and applications..... 47

Figure 41: Selection of common lattice types available within the NetFabb structure library (image credit: NetFabb Autodesk). 47

Figure 42: Conformal lattice structures are preferred mechanically and production wise, image credits: J. Nguyen. . 48

Figure 43: The application of a graded lattice structure using Autodesk NetFabb, image credits: TNO. 48

Figure 44: NTopology Element Software used to generate a gradient lattice structure, image credits: TNO. 48

Figure 45: The influence of resolution on file size. Difference round and square beams, image credits: TNO. 49

Figure 46: Research study to the compressive properties of Al alloy lattice structures with three different unit cells fabricated by L-PBF, image credits: Lui, X., et al. [23]..... 50

Figure 47: Modulus and peak stress versus volumetric energy for different lattice structures and orientations, image credits: Muller, J. [24]. 50

Figure 48: Different type of triply periodic minimal surface structures, image credit: [25]..... 51

Figure 49: Sample of a TPMS structure made GEN3D software package, image credit: TNO..... 51

Figure 50: Stochastic and Voronoi lattice structures can be applied to 3D designs..... 52

Figure 51: Cellular solids in nature..... 52

Figure 52: Design study of optical mirror with an internal structure inspired by cellular solids, image credit: Hilpert, E. [26] 53

Figure 53: Grasshopper is a visual programming language and environment that runs within the Rhino 3D CAD application. A program is created by dragging components and functions onto a canvas; the outputs to these components are then connected to the inputs of subsequent components; and resulting in a 3D part. Image credit: Grasshopper3d.com..... 53

Figure 54: Trees influenced by their surroundings, image credit: Mattheck, C [27]. 54

Figure 55: Applying nature’s rules on conventional load conditions, image credit: Mattheck, C [27]..... 54

Figure 56: Finite Element Method used to optimise a structure, image credits: TNO. 55

Figure 57: Topology optimization of an actuator geometry, image credits: STFC & TNO. 55

Figure 58: Comparison between the tradition and generative design process, image credits: Autodesk..... 56

Figure 59: Generative design of a bracket where the target mass is varied and all other constraints are fixed, image credit: Ansys Workbench. 56

Figure 60: Screen capture of Autodesk Fusion 360 Generative design software with the comparison between multiple design studies, image credit: Autodesk. 57

Figure 61: Biomimicry - products inspired by structures found in nature..... 58

Figure 62: The workflow of the ELISE Algorithmic modelling software, image credit: ELISE GmbH. 59



Figure 63: Bionic Algorithms – By using a parameter slider the input values are altered. The design is re-calculated and automatic redrawn. Image credits: ELISE GmbH. 59

Figure 64: Generative engineering of highly stress B-Pillar poste with nature inspired bionic design features. Image credits: Hyundai and ELISE GmbH..... 60

Figure 65: A selection of additive manufactured parts - PBF aluminium (AlSi10Mg), image credits: Rolls Royce & BMW Group. 61

Figure 66: a poster, created by 3D Hubs, highlighting the design rules across the full spectrum of AM methodologies [32]. 62

Figure 67: AM design guidelines for metal PBF towards lightweight mirror fabrication, image credit: STFC..... 63

Figure 68: Common defects types encountered using AM, image credits: TNO & UoS..... 70

Figure 69: AM defects resulting from non-adoption of AM design rules, image credits: STFC & TNO. 71

Figure 70: AM defects caused by poor understanding of the AM build process - geometric and thermal. Image credits: STFC, NPL & UoS..... 72

Figure 71: The effect of types and locations of pores on the mechanical properties of AM processed material, image credit: Al-Maharma, A., et al. [35]. 73

Figure 72: Multiple types of porosity in AM parts..... 73

Figure 73: 3D printing of metal. Similar processes, different materials, different results. Image credits: TNO. 74

Figure 74: Preparation of Metallographic examination samples, (image credits: TNO) 74

Figure 75: Different types of porosity in PDF parts. Contour porosity in a result of dissimilar scan strategies, (image credit: GE Additive) [36]..... 75

Figure 76: Influence of process parameters and laser beam diameter on gas pore density. 75

Figure 77: By altering process settings, such as scan strategy and laser power, the porosity of a PBF part can be altered, image credits: SLM Solutions, KU Leuven 76

Figure 78: Optimised density obtained with Binder jetting printed after debinding and sintering, (image credit: TNO) 76

Figure 79: Schematic representation of the microstructure of Ti6Al4V in different heat-treated conditions, image credit: NLR..... 77

Figure 80: Microstructure of PBF Ti6Al4V without and after HIP, image credit: NLR. 77

Figure 81: the key roles undertaken by support material for AM components..... 78

Figure 82: an example of an SLA print and required support material (highlighted in red); the arrow demonstrates the build orientation (image credit: TNO & STFC). 79

Figure 83: SLA support material added to the part within the software (*left*); the connection points of the support material on the part (*middle-left*) and the non-connected top section (*middle-right*) prior to cleaning; and the part after cleaning. Image credits: CA Models & NSTP3-PF-007 team..... 79

Figure 84: soluble support structure used to build the OPTICON test geometry mark in VeroClear (acrylic-like), image credit: STFC. 80

Figure 85: the OPTICON test geometry with the majority of the support structure removed, image credit: STFC..... 80

Figure 86: selected laser sintering of the OPTICON benchmark; no supports are necessary as the powder bed acts as its own support, image credit: TNO. 81

Figure 87: heat transfer from the melt pool to the local environment. *Left* – poor conduction of the heat source within the surrounding metal powder; *middle* – improved conduction via the inclusion of the support structure (blue lattice); and *right* - an example of a metal support structure. Image credits: STFC. 82

Figure 88: removal of metal supports using cutting pliers (image credit: TNO)..... 82

Figure 89: *left & middle* - support material generated for an aluminium L-PBF circular mirror substrate and *right* – printed example (image credit: CA Models & NSTP3-PF2-008 team). 83



Figure 90: *left & middle* - support material generated for an aluminium L-PBF circular mirror substrate; *right* – roughness observed at the support – substrate interface (image credit CA Models & NSTP3-PF-007). 83

Figure 91: examples of three different types of support structure geometry used within EB-PBF (image credit: NSTP3-PF2-008 team). 84

Figure 92: support removal problems; the example highlights the support material used to support the vertical circular holes and the failure at the support removal. 84

Figure 93: profilometry data for different AM materials and methods prior to post-processing. Image credit: NSTP3-PF-007 team [42]. 85

Figure 94: Post-processing is an essential part of the AM workflow (image credits: Wohlers Report [43] & Gen3D) .. 91

Figure 95: Conventional workflow of post processing (image credits: 3D&FPP Project - Integrating Metal 3D Printing & Flexible Post Processing) 91

Figure 96: Multiple type of machine clamping solutions (image credits: BMW group - Rolls Royce, Blue Photon Grip, Matrix innovation) 92

Figure 97: Bespoke 3D printed jigs and fixtures (image credits: Renishaw, 3DSystems) 92

Figure 98: FAME mirror concept with bespoke 3D printed polishing jig (image credits: Konkoly Observatory) 92

Figure 99: The four generations of Industrial Revolution (image credit: www.behance.net). 93

Figure 100: Integrated CAD/CAM solution for 3D&FPP (image credit: 3D&FPP Project - Integrating Metal 3D Printing & Flexible Post Processing) 93

Figure 101: Integrated workflow of post-machining of 3D metal printed parts (image credit: 3D&FPP Project - Integrating Metal 3D Printing & Flexible Post Processing) 94

Figure 102: A fixed reference point during process steps can be implemented adding and additional handle or fixation point onto a 3D printed part (image credit: 3D&FPP Project) 94

Figure 103: Drilling of holes - guidelines for drilled part design (image credit: DFMPPro). 95

Figure 104: Milling - recommended design practices for milled parts (image credit: DFMPPro). 95

Figure 105: Turning - general guidelines for design of turned parts (image credit: DFMPPro). 95

Figure 106: Hybrid machining combines additive and subtractive processes in a single production machine (image credits: DMG Mori, Matsuura and Romi). 96

Figure 107: post-processing steps to create a Ti64 lightweight mirror. Image credit: NSTP3-PF2-008 team [45]. 97

Figure 108: the post-processing steps to create a reflective surface on a polymer mirror. Image credit: NSTP3-PF-007 team & CA Models [42]. 98

Figure 109: the post-processing steps in the metallisation of polymer components. Image credits STFC, CA Models & 3DDC Ltd. 99

Figure 110: Schematic representation of the electroless plating process. A conformal and uniform layer is applied regardless the geometry, image credits: Interplex. 100

Figure 111: Schematic representation of the electro plating process; a thickness variation will occur resulting from a non-uniform current distribution (image credits: Interplex) 101

Figure 112: Process flow of plating a polymer 3D printed structure. After a palladium seed layer, an electroless nickel plating process takes place, which is then followed by an electro plating step to thicken the nickel layer (image credits: TNO). 101

Figure 113: Cross-sectional view of the multiple metal coating layers on a stereo lithography polymer part (image credits: TNO). 102

Figure 114: A cross-section view of a Ni layer on a nylon PBF printed part (image credits: TNO). 102

Figure 115: Additive manufactured parts with an additional functional plating to improve mechanical strength (image credits: TNO) 103

Figure 116: a nickel phosphor coating allows AM substrates to be coated in a suitable material for precision optical processing via diamond turning or polishing (image credits: TNO. 104



Figure 117: contact evaluation methods. Image credits - STFC, TNO, Renishaw [49] & Kacmarcik et al. [50] 106

Figure 118: external non-contact evaluation methods. Image credits - STFC & TNO 108

Figure 119: internal non-contact evaluation methods. Image credits – NPL, Cooper et al. [51] & TNO..... 111

Figure 120: generic AM mirror fabrication chain, image credit: STFC..... 119

Figure 121: generic considerations from mirror requirements, to manufacture selection and optimal AM design, image credit: STFC. 120

Figure 122: a demonstration of design for additive manufacture, image credit: STFC..... 121

Figure 123: examples of DfAM in lightweight mirror development. Image credits: H. Herzog et al (2015) [9], M. Sweeney et al. (2015) [8], E. Hilpert et al. (2019) [10] and S. Tan et al. (2020) [18]..... 121

Figure 124: Identify critical surface and produce two drawings for manufacture (additive and subtractive), image credit: STFC..... 122

Figure 125: an example highlighting two drawings generated for AM mirror fabrication – source material C. Atkins et al. (2019) [45]..... 122

Figure 126: Europe represented in three STL files of different mesh sizes - a loss of detail is demonstrated in the coarse mesh in comparison to the fine mesh, image credit: STFC..... 123

Figure 127: a CAD file is first converted to an STL file and then edited in AM specific slicing software to add orientation, scaffold and AM build parameters (scaling), image credit: STFC. 123

Figure 128: four examples of AM mirrors highlighting build orientation and supports. Source material (left to right) Atkins et al. (2019) [45], N. Heidler et al. (2018) [53], E. Hilpert et al. (2019) [10] and S. Tan et al. (2020) [18]..... 123

Figure 129: the generic case for metal laser powder bed fusion (L-PBF) in mid build, image credit: STFC. 124

Figure 130: generic steps required in a metallic post build part. 125

Figure 131: powder removal process for electron beam - powder bed fusion (EB-PBF), image credit: C. Atkins et al. (2019)..... 125

Figure 132: examples of mirror substrates after build with supports attached (left) and with supports removed (right). Image credits: M. Sweeney et al. (2015) [8], N. Heidler et al. (2018) [53], E. Hilpert et al. (2018) [17] and S. Tan et al. (2020) [18]..... 125

Figure 133: contact profilometry of a raw aluminium build substrate prior to post-processing..... 126

Figure 134: 3D scanning and comparison to the original CAD file of a Viscal base plate, image credits TNO. 126

Figure 135: a) & b) the use of XCT to assess the internal cavity of a lightweight mirror substrate (image credits: Fraunhofer IOF) and c) an example of how microCT has been utilised to assess the fidelity of a part relative to the CAD and to quantify porosity within the substrate. Image credits: TNO. 126

Figure 136: a contact profilometer measurement of a raw aluminium substrate, image credit: M. Roulet et al. (2018) [54]..... 127

Figure 137: sketches of typical subtractive machining methods. Left - mill/drill using a simple translation stage. Right - a rotating lathe platform with a cutting tool shown in blue. Image credits: STFC. 127

Figure 138: example of subtractive machining used in AM mirror fabrication. Image credits: H. Herzog et al. (2015) [9], N. Heidler et al. (2018) [53], S. Tan et al. (2020) [18] and C. Atkins et al. (2019) [45]. 127

Figure 139: optical polishing used on AM mirror substrates. Left – a simplified sketch of a CNC polishing head, part and slurry delivery (blue tubing), image credit: STFC; right – examples of hand and mechanical polishing of AM substrates. Image credits: C. Atkins et al. (2018) [55] and H. Herzog et al. (2015) [9]. 128

Figure 140: SPDT of AM mirror substrates. Left – a simplified sketch of an AM substrate attached to the SPDT spindle and the diamond cutting tool (orange), image credit: STFC; right – three examples of AM substrates attached to a spindle for SPDT. Image credits: E. Hilpert et al. (2018) [17], C. Atkins et al. (2018) [55] and N. Heidler et al. (2018) [53]. 128



List of Tables

Table 2-1 Applicable Documents	14
Table 2-2 Reference Documents.....	14
Table 3: definitions of commonly used acronyms in AM processes.....	22
Table 4: Overview of possible variations at different levels in metal PBF production	32
Table 5: Comparison between a high-performance industrial PBF system and a high-resolution machine.....	33
Table 6: the OPTICON Test Geometry printed with two different types of machines in the same material. Image credits: TNO.	33
Table 7: Scanning electron microscope images of printed features in the OPTICON test geometry; both examples are printed in aluminium (AlSi10Mg) via PBF.	34
Table 8: The visual differences between two materials and two PBF systems as demonstrated using the OPTICON test geometry.....	35
Table 9: AM service bureaux for advanced ceramic parts.....	39
Table 10: Software vendors to implement 3D lattice structures in CAD design files; classified in STL format and native CAD format.....	49
Table 11: a selection of resources available in design for additive manufacture.....	62
Table 12: subtractive post-processing methods	87
Table 13: formative post-processing methods	89
Table 14: fabricative post-processing methods.....	90
Table 15: Improvement of material properties by application of a plating layer (Table credits: 3DDC) [47].	103
Table 16: Material properties of electroless nickel depending on content phosphorus [48]	104
Table 17: different tools available to evaluate dimensionally a part or surface.	105
Table 18: reported AM mirror fabrication in published literature since 2015.	129
Table 19: case studies highlighting different aspects of AM design, manufacture and post-processing.....	135



TABLE OF ACRONYMS

Acronym	Definition
2D	2 Dimensions
3D	3 Dimensions
3MF	AM print file format
A²IM	Additive Astronomy Integrated-Component Manufacturing
ABS	Acrylonitrile butadiene styrene
AI	Artificial Intelligence
AM	Additive manufacture
AMF	AM print file format
BCC	Body Centred Cubic (lattice style)
CAD	Computer aided design
CAE	Computer Aided Engineering
CAM	Computer Aided Modelling
CAO	Computer Aided Optimisation
CEA	Cost Effectiveness Analysis
CMM	Coordinate measuring machine
CNC	Computer numerical control
DED	Direct Energy Deposition
DfAM	Design for Additive Manufacture
DfM	Design for Manufacture
DLP	Digital Light Processing
DMLS	Direct Metal Laser Sintering
DOD	Drop on Demand
EBM	Electron Beam Melting \equiv EB-PBF
EB-PBF	Electron beam powder bed fusion
EDM	Electric Discharge Machining
ESA	European Space Agency
FAME	Freeform Active Mirror Experiment – OPTICON WP4
FDM	Fused deposition modelling
FE	Finite Element
FEA	Finite Element Analysis
FEM	Finite Element Modelling
GMT	Giant Magellan Telescope
HIP	Hot Isostatic Pressing
IAC	Instituto de Astrofísica de Canarias
IBF	Ion Beam Figuring
IGES	Initial Graphics Exchange Specification – a common file extension for CAD files
IR	Infrared
Konkoly	Konkoly Observatory, Hungary
LAM	Laboratoire d'Astrophysique de Marseille
LBM	Laser Beam Melting \equiv L-PBF
LED	Light Emitting Diode
LED	Light Emitting Diode
L-PBF	Laser powder bed fusion
Micro-CT	X-ray microtomography \approx XCT
MRF	MagnetoRheological Finishing
NASA	National Aeronautics and Space Administration



NiP	Nickel phosphorous
OPTICON	Optical Infrared Coordination Network for Astronomy
PA	Polyamide / Nylon
PBF	Powder Bed Fusion
PC	Polycarbonate
PEEK	Polyether ether ketone
PEI	Polyethylenimine
PEKK	Polyether ketone ketone
PP	Polypropylene
PPSU	Polyphenylsulfone
PS	Polystyrene
PV	Peak to valley
RMS	Root mean square
SKO	Soft Kill Option
SLA	Stereolithography
SLS	Selected Laser Sintering
SPDT	Single Point Diamond Turning
STEP	A common file extension for 3D objects within CAD
STFC	Science and Technology Facilities Council
STL	Common AM print file format
TNO	Netherlands Organisation for Applied Scientific Research
TPMS	Triply Periodic Minimal Surface
TPV	Thermoplastic vulcanizates
UAV	Unmanned aerial vehicle
UKATC	United Kingdom Astronomy and Technology Centre
UKRI	United Kingdom Research and Innovation
ULE	Ultra low expansion glass
UoS	University of Sheffield, UK
UV	Ultra violet
VPP	Vat Photo Polymerisation
w.r.t.	with respect to
WP	Work package
XCT	X-ray computed tomography

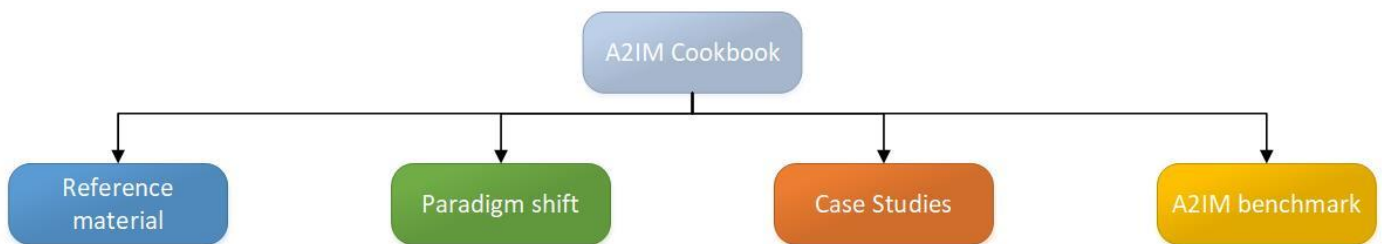


1 INTRODUCTION

1.1 Purpose of Document

The goal of the A2IM Cookbook is to provide scientists and engineers working within astronomical instrumentation with an overview of additive manufacture (AM) and how it can be leveraged to advance astronomical instrumentation in the future. The methodology of the Cookbook is to provide an overview of the fundamentals of additive manufacture, describing the processes, the benefits, the design rules etc., in addition to worked examples of how it has been applied to date.

1.1.1 Scope of Document



The Cookbook brings together reference material, case studies, a discussion of the paradigm shift and a benchmark study, which combined, highlights how AM has, and can be, implemented within astronomical instrumentation in the future. The document is not comprehensive in covering all operational environments and hardware required for astronomy, rather, the focus is broadly astronomical mirror development; the prime focus area of the OPTICON A2IM project.

The Reference Material introduces the implementation of AM, describing the different processes, design software, materials available, design rules, defects, post processing and metrology. For each topic, an overview is provided with reference links for further study. A series of Case Studies are provided to demonstrate the how AM has been implemented to date (including dimensions and cost) and importantly, to highlight how AM can provide benefits. The paradigm shift uses mirror fabrication as an example and explains the different steps in utilising AM. The Paradigm Shift connects the reference material and utilises it within a given research problem. The Benchmark, an open access model for download, utilises a number of specific geometric structures to highlight what can and cannot be achieved using AM. The role of the benchmark is as a ‘conversation starter’ for those that are interested in adopting AM, by highlighting the fidelity of the different structures relative to different printer capabilities.

1.1.2 Intended Audience

The intended audience of the Cookbook is scientists and engineers that are considering the adoption of AM within their discipline. Although the emphasis is orientated to the astronomical community, there will be cross over within other subject areas. The subject level is appropriate for physical scientists and mechanical engineers with undergraduate degree experience – i.e. with no pre-existing knowledge of AM.



2 APPLICABLE AND REFERENCE DOCUMENTS

2.1 Applicable Documents

The following documents are also deliverables of the OPTICON WP5, and combined, form the reference material (A1 & A2) and the prototype development (A3) undertaken within the project.

Table 2-1 Applicable Documents

Ref No	Document type	Document Title	Year
A1	A2IM report D5.1	Report on Additive Manufacturing Materials https://doi.org/10.5281/zenodo.3906026	2020
A2	A2IM report	A2IM Cookbook: test geometry	2021
A3	A2IM report D5.2 & D5.3	Report on Astronomical Components Prototypes and Prototype characterisation report.	2021

2.2 Reference Documents

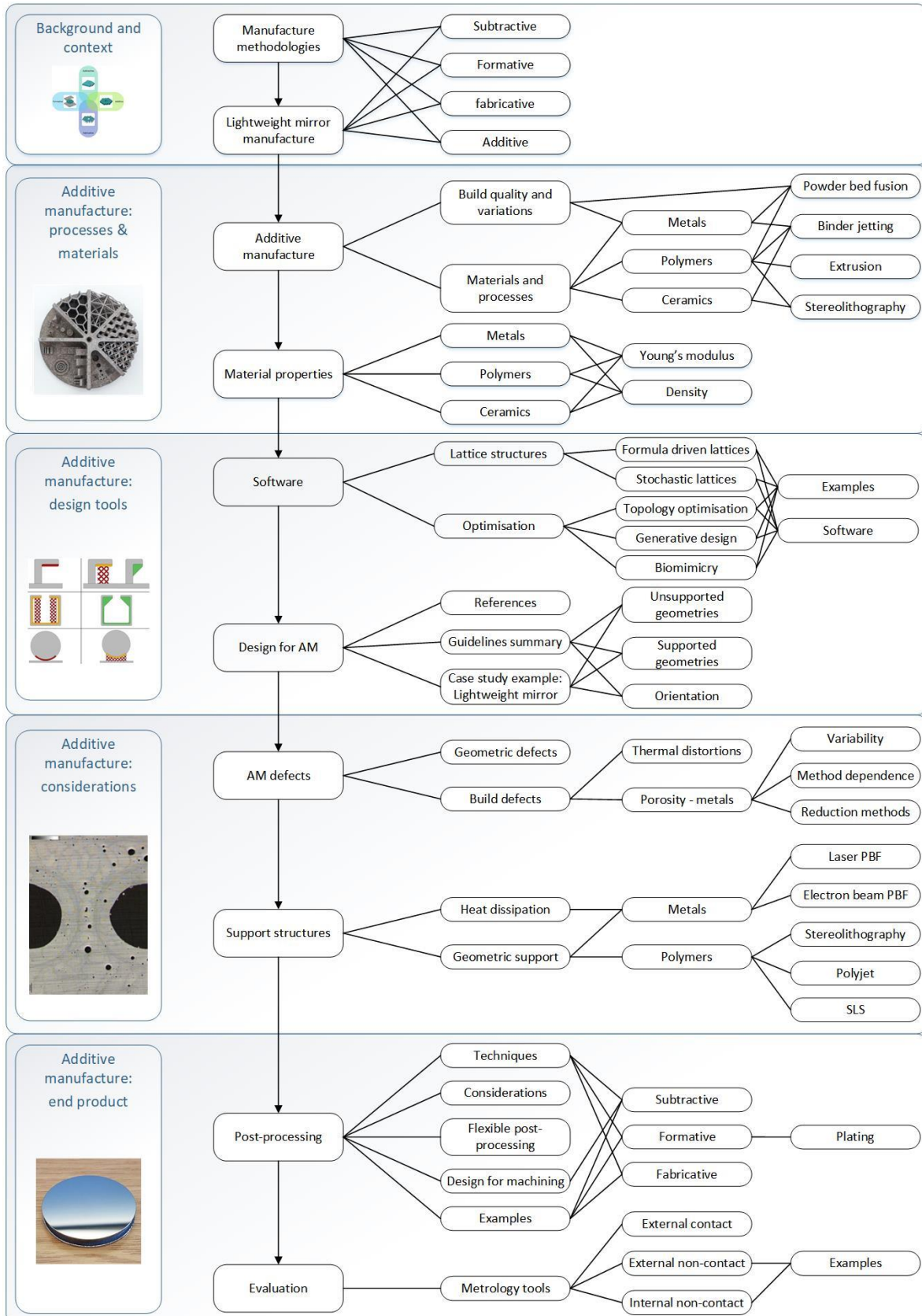
The following documents, published/submitted by members of the OPTICON WP5 project, detail individual prototyping projects (R1 → R4 & R6) and describe an overview of the project goals (R5).

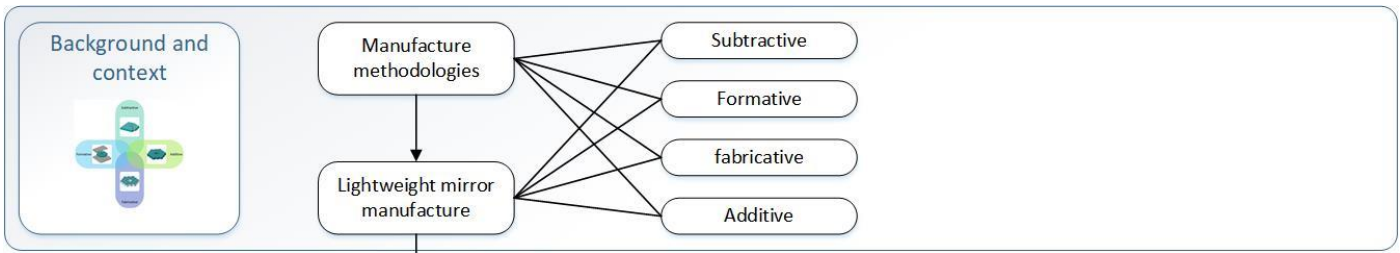
Table 2-2 Reference Documents

Ref No	Document type	Document citation	Year
R1	Conference proceedings	M. Roulet et al., 'Use of 3D printing in astronomical mirror fabrication', Proc. SPIE 11349	2020
R2	Conference proceedings	A. Vega et al., 'Design for additive manufacture (DfAM): the "equivalent continuum material" for cellular structures analysis', Proc. SPIE 11450	2020
R3	Conference proceedings	S. Farkas et al., 'Freeform active mirror designed for additive manufacturing', Proc. SPIE 11451	2020
R4	Conference proceedings	R. Snell et al., 'An additive manufactured CubeSat mirror incorporating a novel circular lattice', Proc. SPIE 11451	2020
R5	Conference proceedings	H. Schnetler et al., 'H2020 opticon WP5 overview: investigating the use of additive manufacturing AM for the design and build of multifunctional integrated astronomical components', Proc. SPIE 11451	2020
R6	PhD Thesis	M. Roulet, '3D printing for astronomical mirrors' / 'Impression 3D pour les miroirs spatiaux', Aix Marseille	2020

3 REFERENCE MATERIAL

The following figure outlines the scope and the interconnectivity within the provided reference material. The provided material is orientated towards astronomical hardware and, in particular, mirror fabrication. AM is a rapidly developing field and therefore the reference material should be considered a starting point for further investigation.





3.1 Manufacture methodology

Methods of manufacture can be divided into four processes: additive, formative, fabricative and subtractive [1], as demonstrated in Figure 1. Subtractive manufacture involves the removal of material from a bulk object to create the desired part (e.g. mill, drill and lathe). Formative manufacture uses a mould to create the desired shape from the raw material (e.g. forging and casting). Fabricative manufacture creates a component from bonding or fixing individual components together (e.g. bonding, welding and fixings). Additive manufacture (AM) uses a digital design file to build an object layer-by-layer to create the desired shape. However, to converge to the final object, more than one manufacturing method might be employed; e.g. a cast object (formative) might be sanded/smoothed (subtractive) to obtain the desired finish.

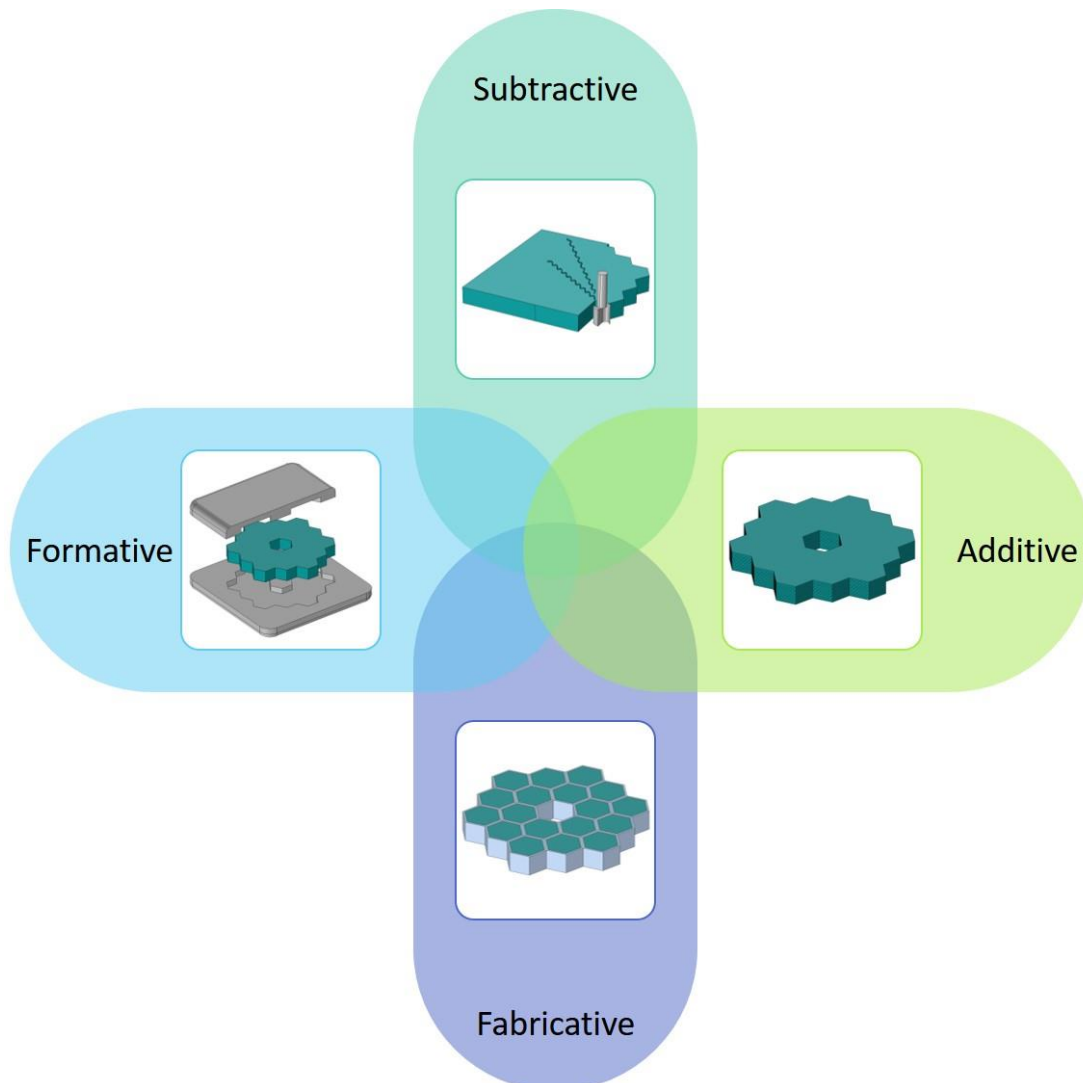


Figure 1: manufacturing methodology – subtractive, formative, fabricative and additive, image credit: STFC.

3.1.1 Which manufacturing process to use?

Selection of the optimum manufacturing process is dependent on a number of requirements, for example: cost, quantity, time and quality. Mass/continuous production involves the manufacture of thousands of identical parts at low cost and typically over a long duration, whereas one-off (unit) production requires a single count bespoke part, over a short duration, but the cost will be high. In the majority of cases, cost and time drives the selection of the optimum manufacture process.

Figure 2 highlights the metal specific case of manufacturing processes plotted against quantity required and geometric complexity (*G. N. Levy 2003 [2]*). In the figure, AM is termed *Layer manufacturing* and inhabits the region where low quantity and high geometric complexity is required and this is consistent with typical astronomical instrumentation which is often requires unit production with high precision.

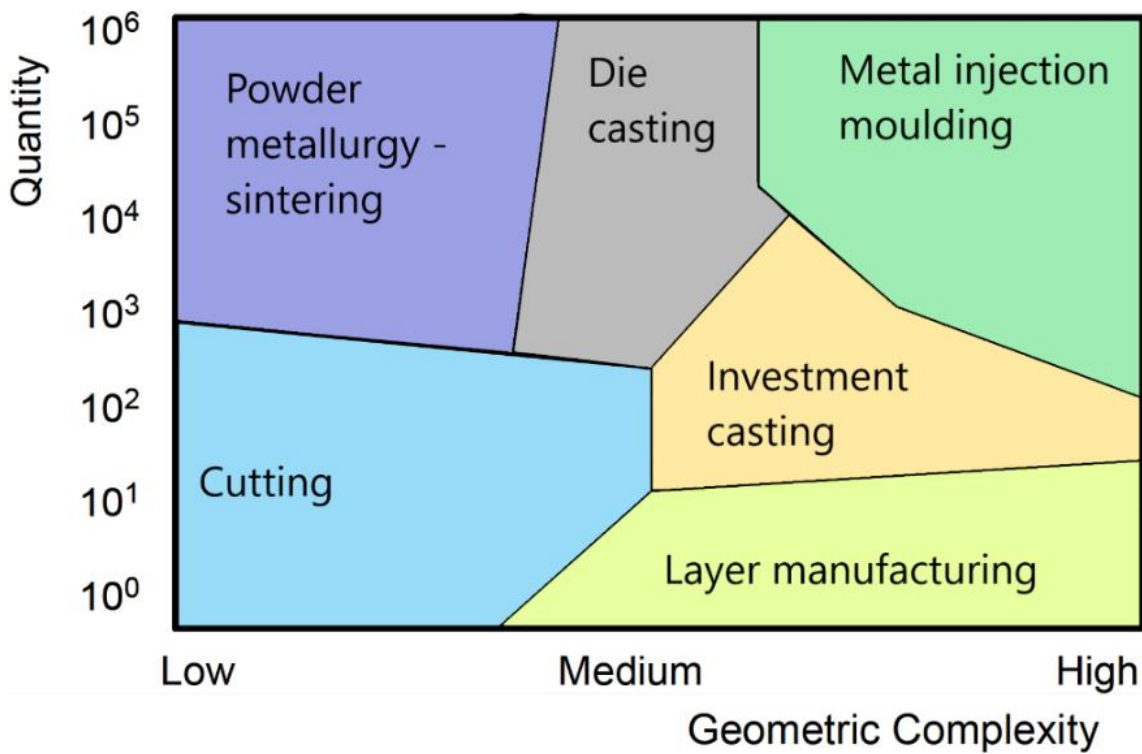


Figure 2: the benefits of metal manufacturing processes highlighted in terms of quantity required and geometric complexity. Image credit: G. N. Levy 2003 [2].

3.2 Lightweight mirror manufacture

Lightweight mirrors are defined as mirrors that have a percentage of mass removed from a given volume envelope. The advantage of lightweight mirrors is that the mass of the mirror can be reduced without adversely affecting the structural integrity. For example, one method to reduce the weight of the mirror would be to make the mirror very thin; however, mounting a thin mirror without distortion is challenging due to gravitational sag, therefore it is preferable to manufacture a thicker mirror for rigidity and then remove excess mass.

Conventional lightweight mirrors fall into three categories: contoured back, open back, and sandwich, as shown in Figure 3. Each variant has advantages and disadvantages in its manufacture and operation, and thorough descriptions can be found in *Vukobratovich, D. (1999) [3]* and *Schwartz, K. & Burge, J. H. (2012) [4]*. Contoured back mirrors are relatively easy to manufacture, but offer modest weight reduction; open back mirrors are more challenging to manufacture and are less rigid, but offer a greater weight reduction; whereas sandwich mirrors are more rigid, offer high levels of weight reduction, but are complex and expensive to manufacture.

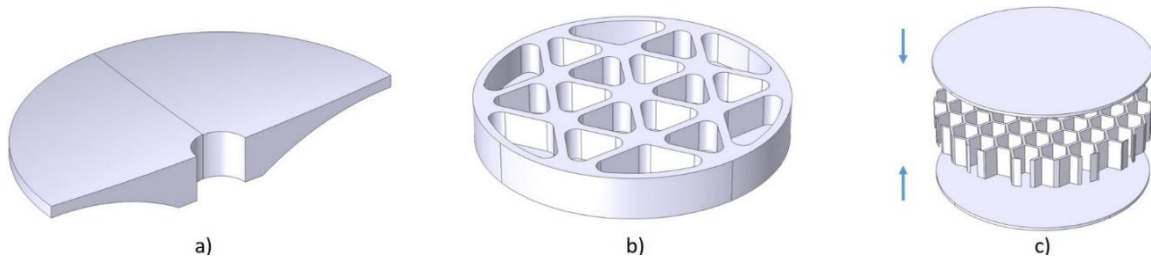


Figure 3: sketches of different lightweight mirror styles - contoured back (a), open back (b), and sandwich (c). Image credit: STFC.

To date, lightweight mirrors for astronomy have been created via the three conventional manufacturing methods – subtractive, formative and fabricative – and prototype mirrors have been trialled using AM. Figure 4 provides a graphical description of how each manufacturing methodology has been employed in lightweight mirror manufacture. The selection of methodology is dependent on the optical, physical and financial requirements of the mirror design.

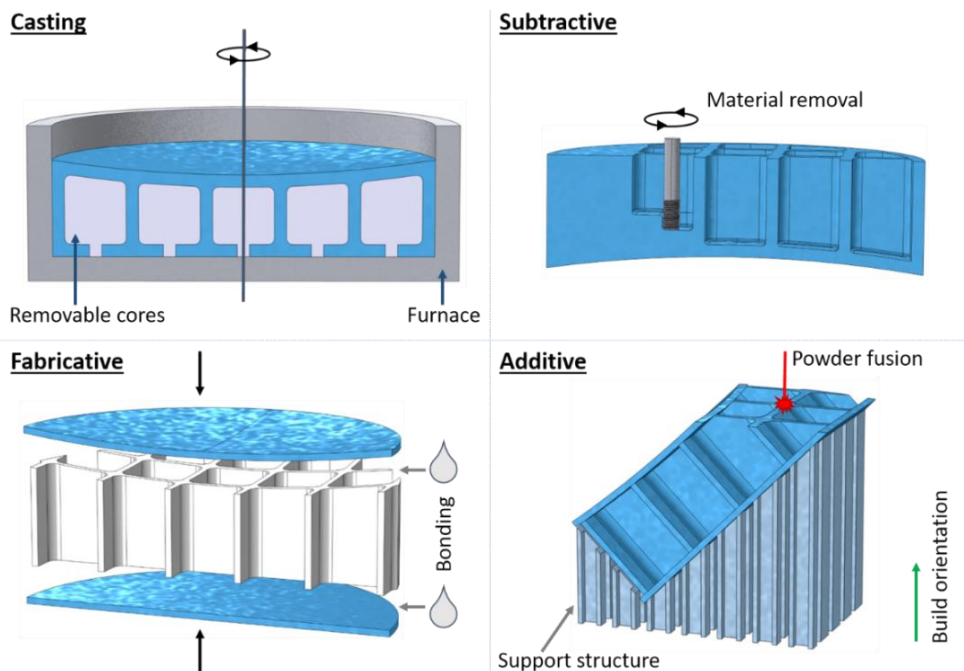


Figure 4: manufacturing processes used in lightweight mirror production – cross sections shown. Image credit: STFC.

In the following subsections, examples of lightweight mirror production are discussed in relation to the *primary* manufacturing methodology employed.

3.2.1 Lightweight mirror manufacture: casting

Casting is a replication process, where an inverse mould is used to generate the required shape of the part. This process is particularly beneficial if multiple parts with the same dimensions are required. Spin casting has been employed in the production of the Giant Magellan Telescope (GMT) telescope primary mirrors, which consist of seven individual mirrors of 8.4 m in diameter (Figure 5). As shown in the photo of Figure 5, solid glass is placed on top of a series of aligned and removable cores that create the hollow lightweight structure. When the furnace is closed, heated and spun, the molten glass seeps into the void between cores to create the lightweight structure. Once the mirror is cool and released from its housing, the cores can be removed resulting in an open-back/sandwich lightweight structure.

Casting

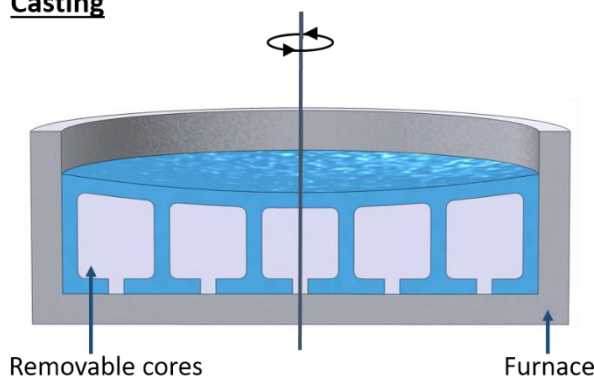


Figure 5: casting of lightweight mirrors. *Left* - sketch of the casting process, *right* - example of the casting of the GMT 8.4 m mirrors, image credit: H. M. Martin 2019 [5].

3.2.2 Lightweight mirror manufacture: subtractive

Subtractive manufacture of lightweight mirrors removes material from a solid block resulting in an open-back honeycomb structure. This process is performed frequently on ceramics and metals using computer numerical control (CNC) milling machines where one-off components are required. Figure 6 *right* highlights an example of a lightweight Zerodur mirror structure created via CNC machining; it has a diameter of 700 mm with 90% of its mass removed. In addition to creating the lightweight structure, subtractive manufacture is common in the generation of high performance optical surfaces, where material is removed via polishing (ceramics and metals) or single point diamond turning (SPDT; metals).

Subtractive

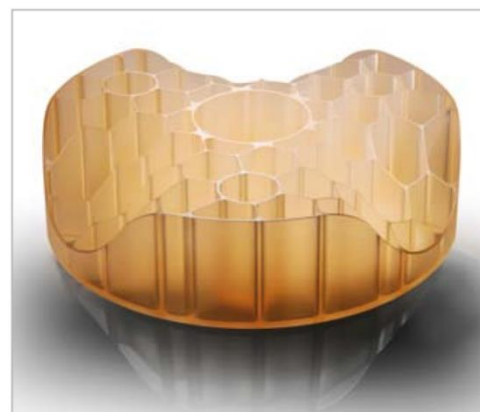
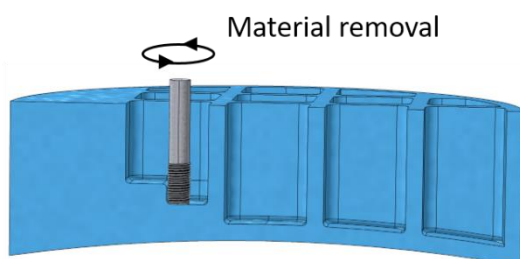


Figure 6: subtractive machining for lightweight mirrors. *Left* - a sketch of the subtractive (milling) process and *right* - an example of subtractive machining of a Zerodur mirror, image credit: SCHOTT AG [6].

3.2.3 Lightweight mirror manufacture: fabricative

Lightweight mirrors created via a fabricative method – i.e. the mirror structure created by more than one part – are termed sandwich, or closed-back, mirrors. These structures offer high levels of lightweighting capability and stiffness in comparison to subtractive mirrors, but they are more complex to manufacture. Figure 7 *right* presents the 1.4 m diameter primary mirror of the NASA Kepler space telescope, which is manufactured in ULE and is composed of a 9.75 mm thick faceplate (mirror surface), a 275 mm thick core and an 8 mm baseplate [7]. The fabricative method employed in the creation of the sandwich mirror resulted in 88% mass removal.

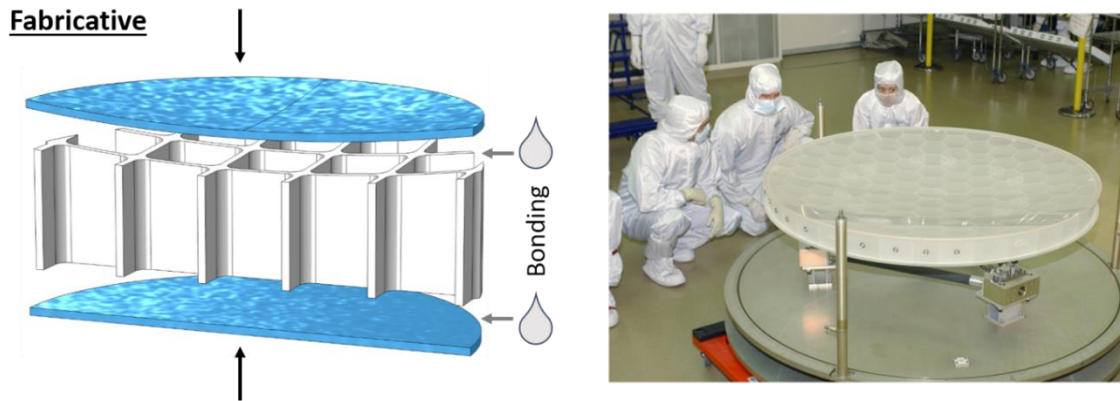


Figure 7: fabricative mirror manufacture; *left* - a sketch of a deconstruction of the manufacture process, *right* - an example of a fabricative primary mirror created for the NASA Kepler space telescope, image credit: D. Ebbets et al 2013 [7].

3.2.4 Lightweight mirror manufacture: additive

The production of lightweight mirrors via AM is a new and developing field with the first documented AM mirrors in 2015 [8] [9]. The advantage of AM over subtractive and fabricative approaches is that more intricate and optimised lightweight geometries can be produced as a single component. In addition, unlike casting where a precision mould needs to be created to replicate components, AM is suitable for batch production with no mould and with relatively easy design adjustments if required.

The majority of AM mirrors to date have been metallic, Figure 8 *right* highlights a prototype of an AM aluminium alloy mirror, which has been coated in nickel phosphorous and diamond turned. The lightweight structure is based upon Voronoi cells, where the density of the Voronoi cells is dependent upon the mirror mount locations [10].

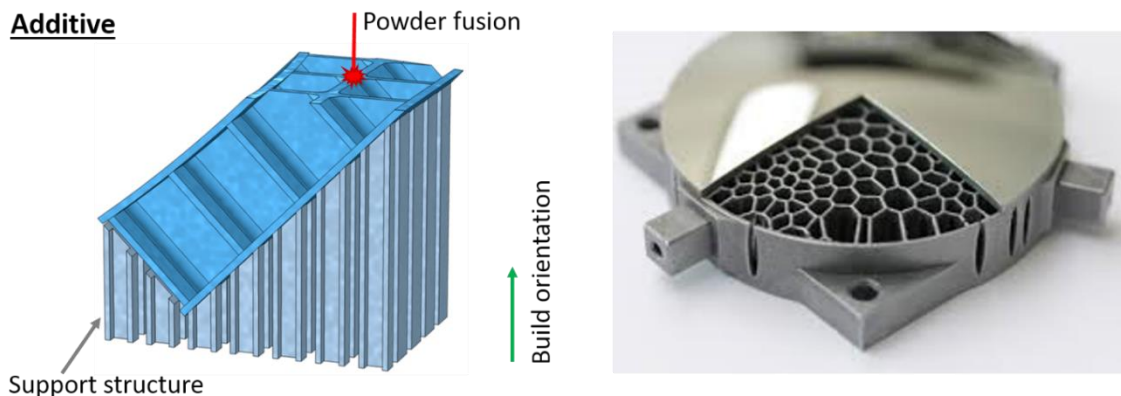
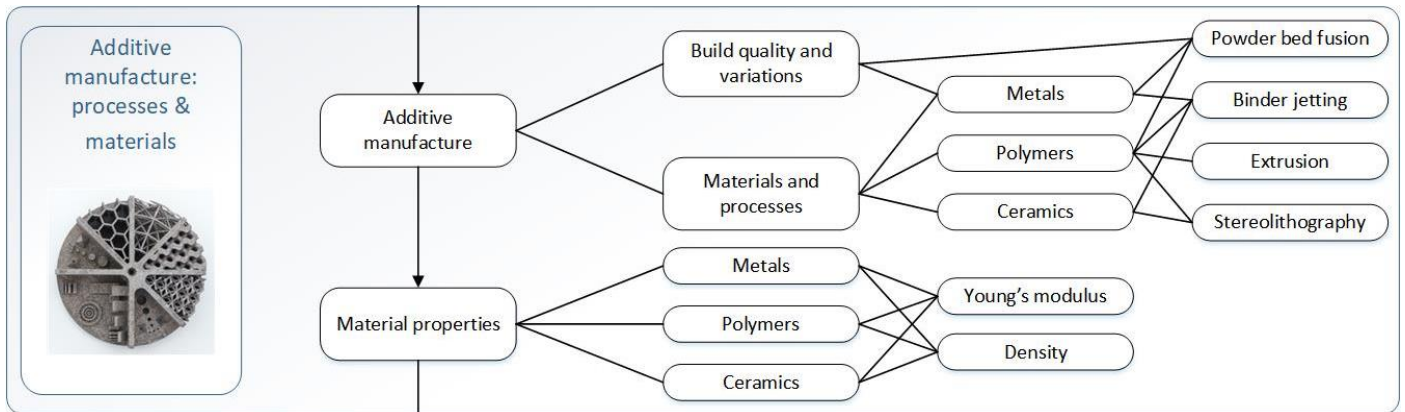


Figure 8: additive mirror manufacture; *left* - a sketch of the manufacture process, *right* - an example of a prototype metallic mirror with a Voronoi lightweighting structure, image credit: E. Hilpert et al. 2019 [10].



3.3 Additive Manufacturing process and material barriers

Virtually all types of materials can be used for AM. The materials that are used for any form of construction/manufacturing intended for an engineering application are known as *Engineering Materials*. These materials can be classified into the following broad groups - Figure 9.

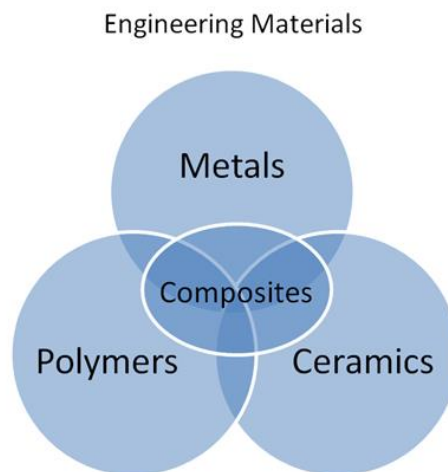


Figure 9: the interplay between different engineering material groups, image credit: TNO.

- Polymers** are usually long chain organic macro-molecules with covalent bonds. Each molecule is formed from a large number of unitary molecules known as *monomers*. For this reason, the polymers are deformable and stretched with ease. In certain polymers, some of the molecules cross-link with each other thereby increasing the strength across the molecules.
- Metals** are usually characterized by a well-defined crystal structure. They are bonded together by means of metallic bonds that maintain an electron cloud. This electron cloud is crucial for the high electrical and thermal conductivity characteristic of metals.
- Ceramics** are amorphous or complex crystalline structures with strong ionic bonds. Due to this amorphous nature, they do not have an electron community. This influences the electrical and thermal conductivity. Due to the strong ionic bonds, it takes a lot of energy to activate and displace the electrons. Therefore, ceramics are extremely heat resistant.
- Composites** are a macro-physical combination of different phases where the aim is to combine beneficial properties of the basic materials. Therefore, very clear and abstract knowledge of the properties of the basic materials are needed in order to select compatible materials for composite fabrication.

3.3.1 Processes

Figure 10 presents the different AM processes/methodologies divided into the different engineering material groups. AM processes/methodologies refer to the technology used to print the material and these are described further in Sections 3.3.3 to 3.3.7.

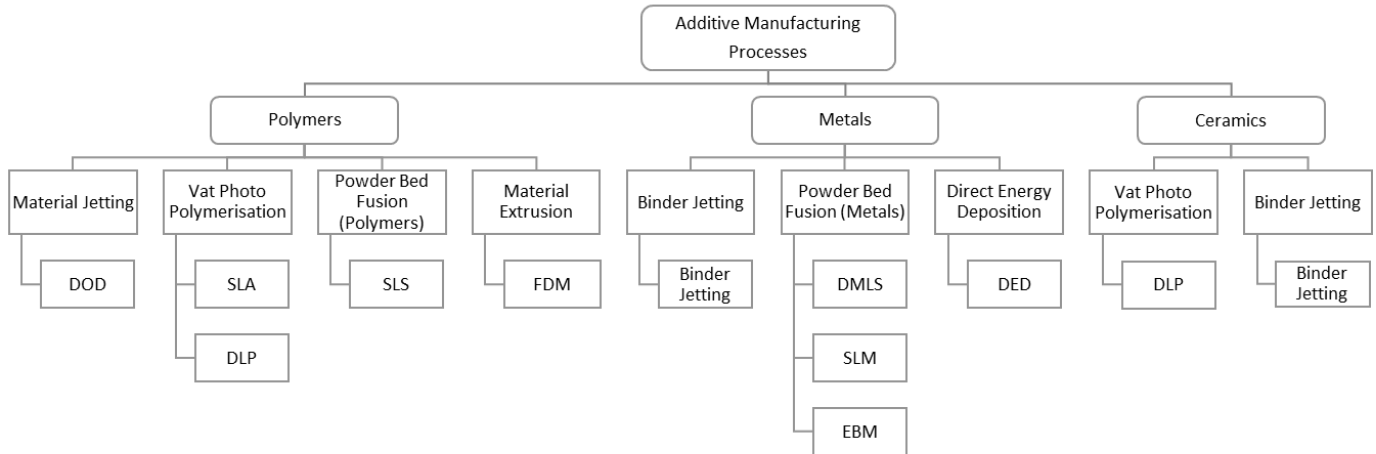


Figure 10: the AM methodologies divided by engineering material group, image credit: TNO.

Table 3 provides the definitions of the acronyms used within Figure 10.

Table 3: definitions of commonly used acronyms in AM processes.

Acronym	Definition	Acronym	Definition
DOD	Drop on Demand	DMLS	Direct Metal Laser Sintering
SLA	Stereolithography	SLM	Selected Laser Melting
DLP	Digital Light Processing	EBM	Electron-Beam Melting
SLS	Selected Laser Sintering	DED	Direct Energy Deposition
FDM	Fused Deposition Modelling		

3.3.2 Polymers

Polymers are the largest group of materials used in AM. Ranging from photo polymerization resin that mimics materials for plastic injection moulding, to high temperature resistant ultra-polymers such as Ultem® and PEEK® (Figure 11). Polymers used for AM differ significantly from those used for injection moulding. Even if the material is chemically identical, the material and mechanical properties differ significantly. Material that is completely molten and injected into a mould under high pressure, shows different properties compared to a material that is locally molten under atmospheric pressure. The addition of fillers, such as glass, aluminium, and ceramics, may improve mechanical properties to a certain extent.

Powder Bed Fusion (PBF) and Material Deposition (MP) are the two AM processes that use industrial grade thermoplastic polymers. Polymers can be divided into two main categories, semi-crystalline and amorphous, based on their difference in molecular structure. Semi-crystalline materials have a highly ordered molecular structure with sharp melt points. They do not gradually soften with a temperature increase. Semi-crystalline materials remain solid until a given quantity of heat is absorbed and then rapidly change into a low viscosity liquid.

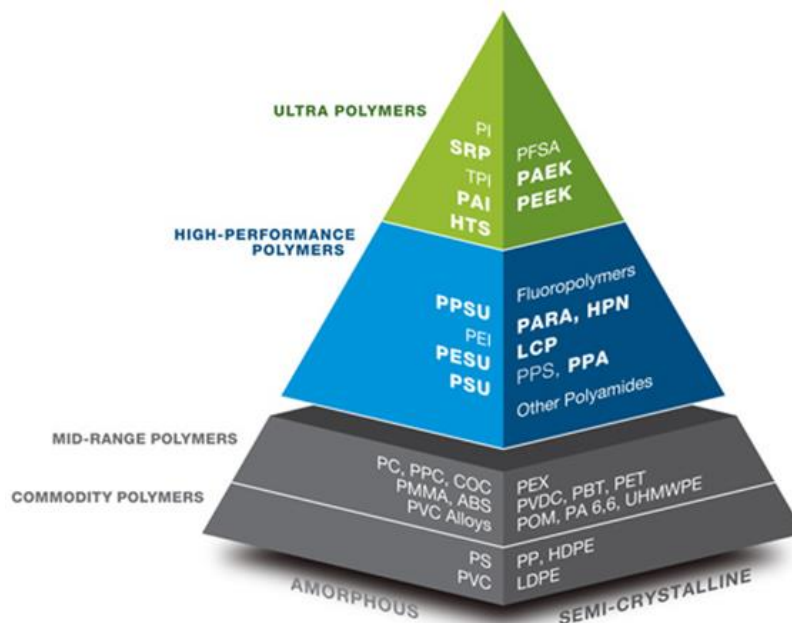


Figure 11: thermoplastic performance pyramid (image credit: SABIC).

3.3.3 Powder bed fusion - Polymers

Polymer PBF, or Selective Laser Sintering (SLS), is an AM technology where a thermal energy source is applied onto a powder layer for a short duration to selectively fuse regions (Figure 12). One advantage of polymer PBF is that it requires no support structures; the non-sintered powder supports the part. Polymer PBF can be used to create freeform geometries that are impossible to manufacture by other methods.

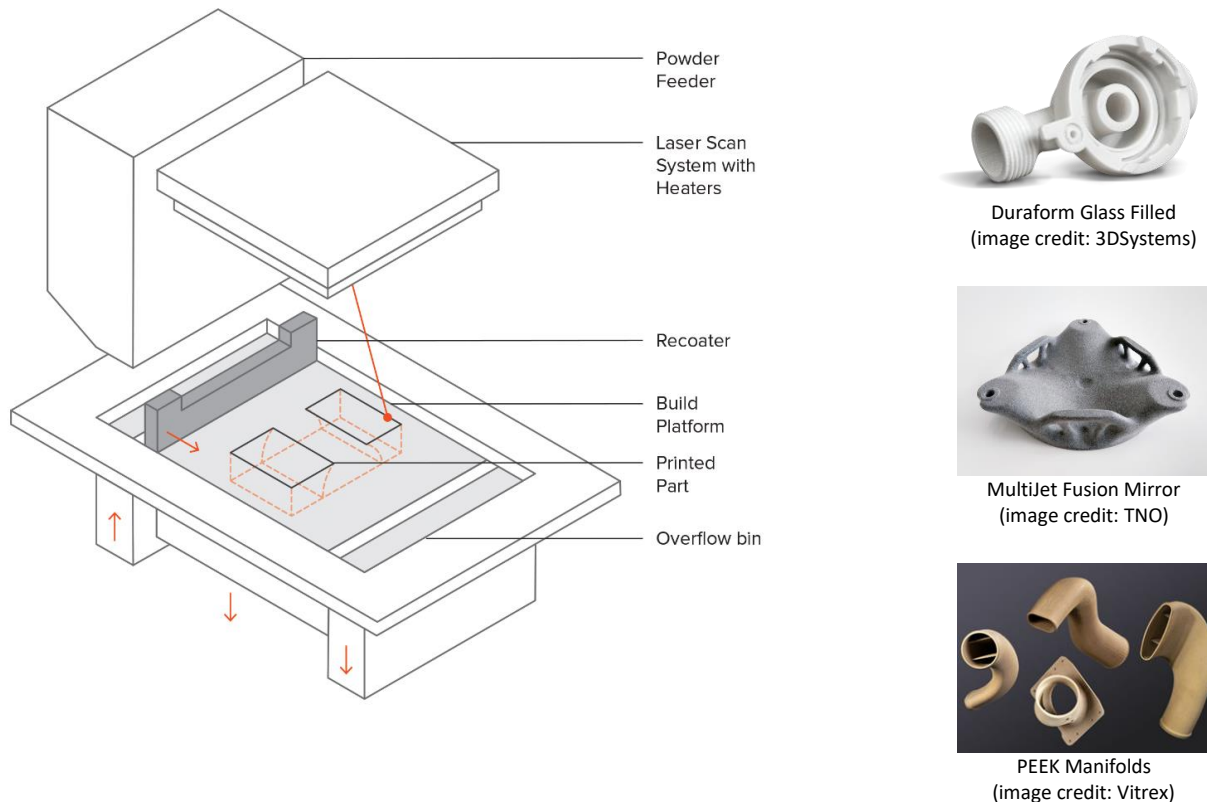


Figure 12: Polymer Powder Bed Fusion process, image credit: 3DHubs.

The polymer powder used for AM needs to melt, flow and solidify rapidly. Therefore, PBF is only applicable with certain semi-crystalline polymers that display a well-defined melting point. Widely used materials with such characteristics are Nylon, PA11 and PA12.

Other polymers that have successfully been used are PA6, PP, PS, TPU, PEEK and PEKK. To process ultra-polymers, such as PEEK and PEKK, specialized equipment is required. A process chamber with elevated temperatures up to 350°C is essential to obtain a robust and stable process. To enhance material properties fillers, such as carbon, glass and aluminium, are included.

3.3.3.1 Benefits and Limitations

- PBF parts have good, isotropic mechanical properties, making them ideal for functional parts and prototypes.
- Parts require no support material; designs with complex geometries are easily produced.
- The manufacturing capabilities of SLS are excellent for small to medium batch production.
- Parts have a grainy surface finish and an internal porosity that may require post processing.
- Large flat surfaces and small holes cannot be printed accurately with PBF, as they are susceptible to warping and over-sintering.

3.3.4 Material Extrusion

Material extrusion, or FDM, is an AM technology in which a material is selectively extruded through a nozzle. The extrusion head, or the building platform, moves in the X-Y plane. After a layer is completed, the build platform moves down or the head moves up. The following layer is then extruded and bonds to the previous layer (Figure 13).

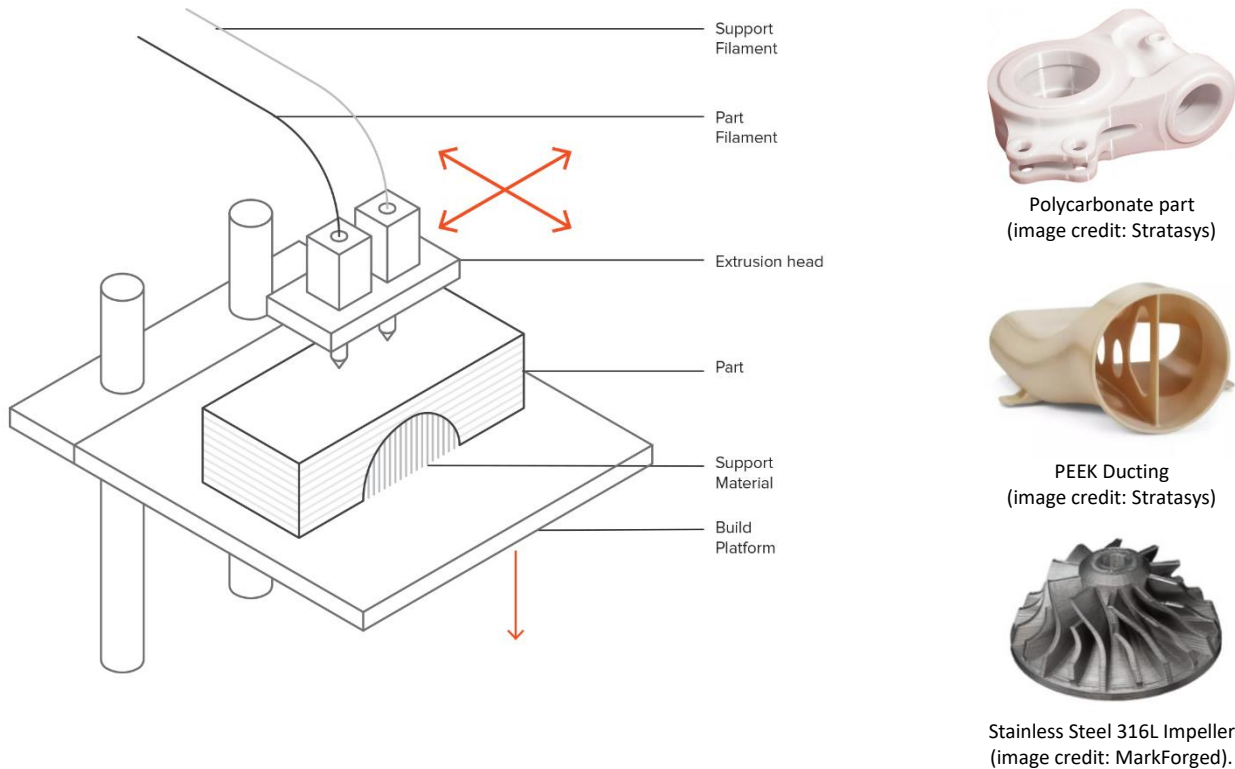


Figure 13: material extrusion process, image credit: 3DHubs.

Amorphous polymers with a wide melt trajectory are gradually heated within the extrusion head. The wide melt trajectory is essential to achieve sufficient bonding between the extruded material and previous layer. To process high performance materials, such as polycarbonate (PC), polysulfone (PPSU) and Ultem® (PEI), a heated build chamber up to 150 - 200°C is essential to obtain sufficient mechanical properties. The consumer “home printers” are usually not equipped with heated ovens and therefore not suitable for these engineering grade polymers.

Filaments with a high content of metal particles are available to print “green” parts. Afterwards debinding and sintering takes place to realise the functional metal component. The material is susceptible to porosity and therefore not suitable for AM mirrors.

3.3.4.1 Benefits and Limitations

- Material extrusion is the most cost-effective way of producing custom thermoplastic parts and prototypes.
- A wide range of thermoplastic materials is available, suitable for both prototyping and some non-commercial functional applications.
- Material extrusion has the lowest dimensional accuracy and resolution compared to other 3D printing technologies and therefore, is not suitable for high detailed parts.
- FDM parts are likely to have visible layer lines; therefore, post processing is required for a smooth finish.
- The layer adhesion mechanism makes FDM components inherently anisotropic in mechanical performance.

3.3.5 Vat Photo Polymerisation

Vat photo polymerisation (VPP), or SLA, uses an ultra violet (UV) laser and galvanometer scanning mirrors to scan the top surface of a liquid photopolymer that hardens once radiated (Figure 14). Alternative VPP systems use a lamp, or LED (light emitting diode), as a source of (near) UV energy in combination with Digital Light Processing (DLP) technology to cure the entire layer at once.

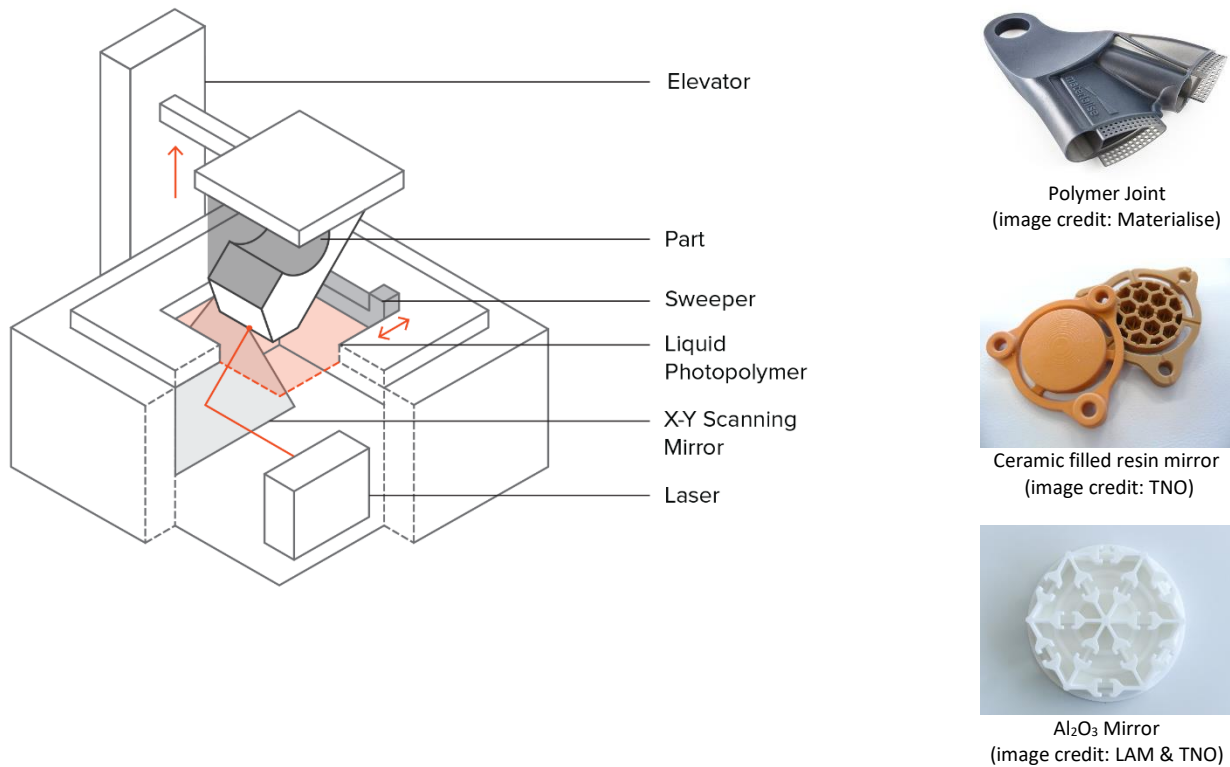


Figure 14: VPP/SLA processing, image credit: 3DHubs.

After completion, the parts are rinsed and cleaned to remove excess material. A post-curing step in an UV oven is required to obtain sufficient material properties. Since the process requires support structures, manual post-processing is essential and can be time/labour intensive. There are 100+ different photo-curable resins available simulating a variety of thermoplastic polymers. It is difficult to combine material properties in these resins and generally, there is a trade-off, such as impact strength versus heat deflection temperature. Stability over time and moisture absorption are also an issue. Using fillers, such as ceramic nanoparticles, allow some limitations to be partly overcome.

The process is also suitable to process high filled ceramic or metal resins. After printing, these parts are debinded and sintered to create a fully dense material.

3.3.5.1 Benefits and Limitations

- SLA can produce parts with very high dimensional accuracy and with intricate details.
- SLA parts have a very smooth surface finish, making them ideal for visual prototypes.
- Speciality SLA materials are available, such as clear, flexible and cast-able resins.
- SLA parts are generally brittle and not suitable for functional prototypes.
- The mechanical properties and visual appearance of SLA parts will degrade overtime when the parts are exposed to sunlight.
- Support structures are always required and post-processing is necessary to remove the visual marks left on the SLA part.

3.3.6 Metals

There are a number of different technologies used in the metal AM systems available today. Systems can be classified by the energy source or by the way the material is being joined, for example by using either a binder, laser, electron beam, heated nozzle etc. Classification is also possible by the direct or indirect method to realize the end product. With the indirect processes, a green part is realised by bonding metal powder with an organic binder. When the print is completed the part is debound and sintered to reach the final size and strength. A benefit of these systems is that the build is undertaken at room temperature and ambient atmosphere without the partial melting that occurs with a high power laser or electron beam. Debinding and sintering is a batch process and takes place at a later time in a controlled atmosphere.

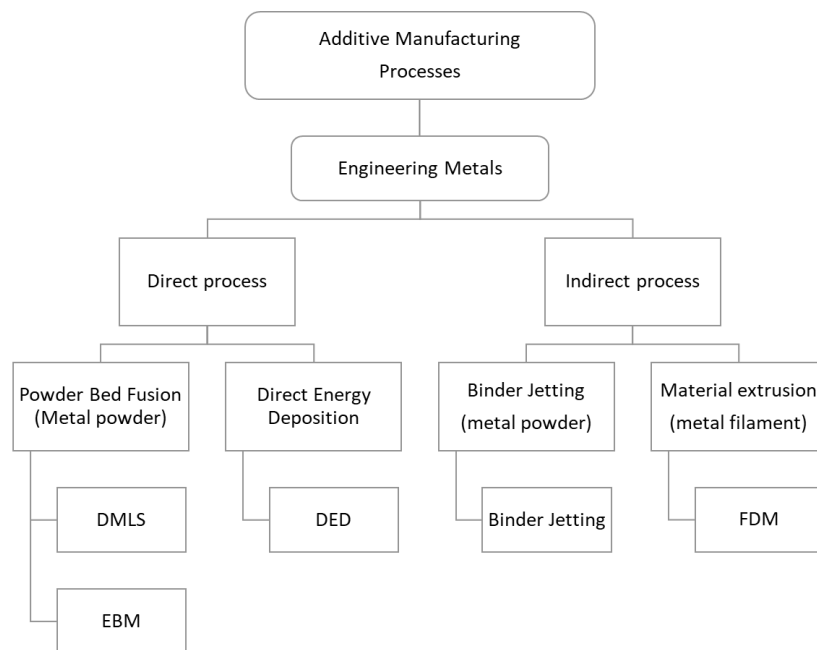


Figure 15: additive manufacturing processes for engineering metals. Classification by direct and indirect processes, image credits: TNO.

3.3.6.1 Direct process

In comparison to polymers, the high thermal conductivity, tendency to oxidize, high surface energy and low absorption, make metals significantly more difficult to process than polymers. With the availability of high power Yb fibre lasers PBF of metals became viable. Due to the shorter wavelength of 1032 nm and a small spot size (30 - 100µm) it was possible to apply the required energy to melt the metal powder. Higher absorption in metals results in higher effective power and higher possible build speeds. To prevent oxidation and contamination, direct processes take place in a protective and controlled nitrogen or argon atmosphere. For the electron beam process, a vacuum is essential.

Direct Energy Deposition (DED), or cladding, is a Near Net Shape (NNS) technology that has the capability to build up complex structures on a base plate or existing components. Cladding is a process wherein a laser source is used to melt metal powder or wire onto a substrate. The main application area in industry is the repair of high value components such as turbine blades. A wide range of metals can be used as feedstock material. Besides laser based systems, there are DED processes based upon plasma or an electron beam source.

3.3.6.2 Near Net Shape production

Laser cladding manufacturing processes are a fast and low cost method to produce metal parts. The resolution and accuracy are insufficient to meet the final specifications. Secondary high resolution process are used to refine the part to its final shape (Figure 16). The advantage of NNS manufacturing is that no tooling is required for casting or forging. Direct CNC milling or wire EDM from a billet would require more material to be removed, resulting in more waste material and machine time.



Laser cladding process
(image credits: Voest Alpine)



From Near Netshape Titanium part to the final shape
(image credits: Norsk Titanium)

Figure 16: NNS part made with laser cladding technology. Secondary process steps such as CNC milling are used to realize the final shape.

3.3.6.3 Metals for Additive Manufacturing

Numerous engineering metals are available for 3D printing (Figure 17). They range from ferrous metals such as stainless steel and tool steel, to non-ferrous metals such as super alloys, refractory metals and precious metals. Metal powders can be obtained from machine manufactures and various material suppliers. The number of process-able materials is continuously growing; however, a service provider usually offer a selective range of common materials. Therefore it can be difficult to find special and exotic materials.

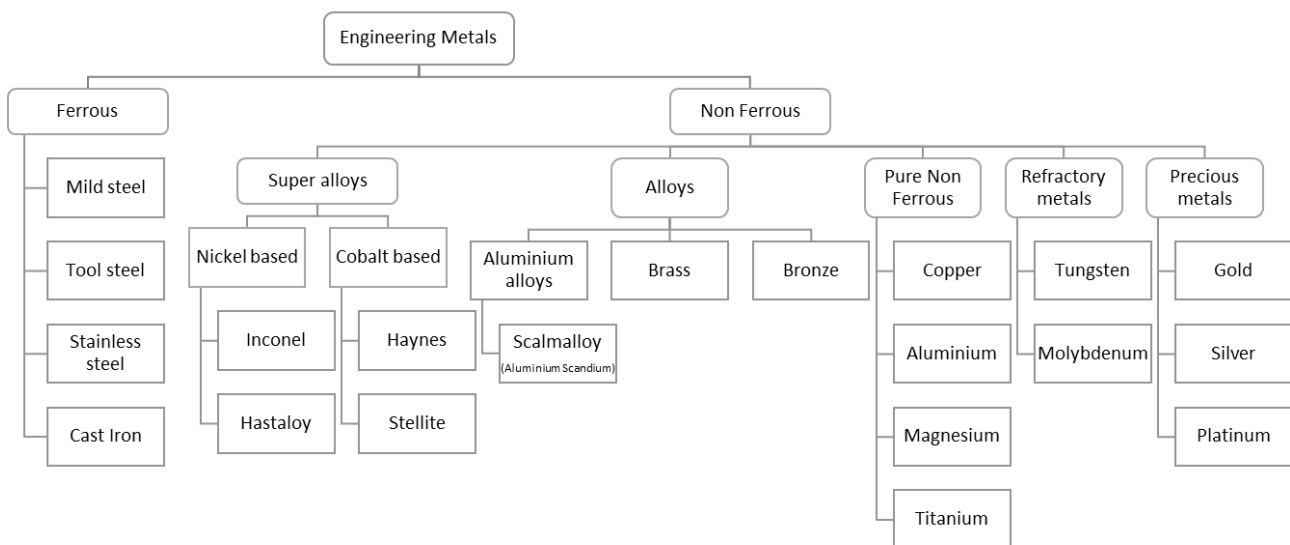
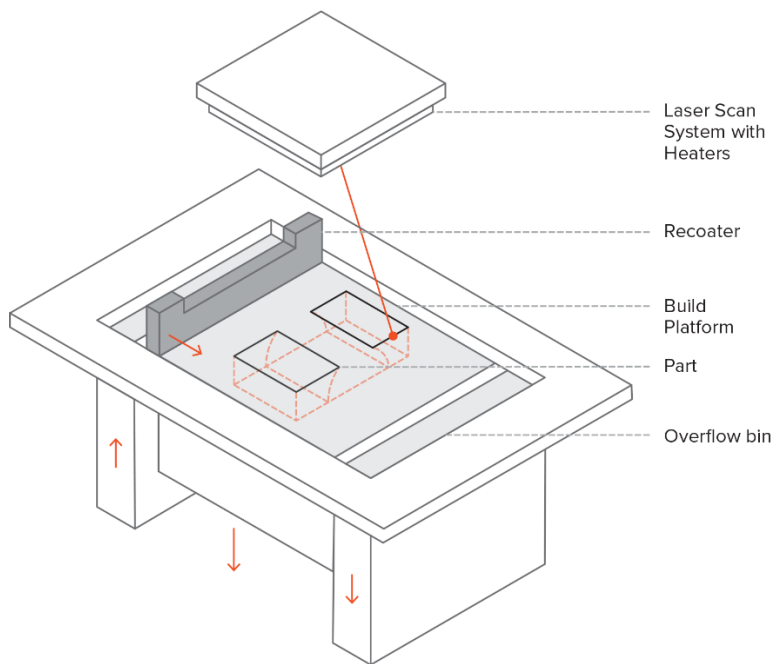


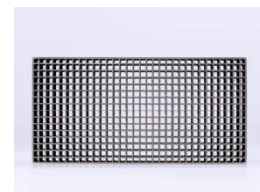
Figure 17: different metallic groups that are suitable for metal PBF, image credits: TNO.

3.3.7 Powder Bed Fusion - Metals

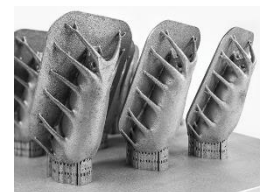
Powder bed fusion of metals is comparable with the polymer-based variant (Figure 18). The main difference is the necessity of support structures and these structures are required for most metals. The high residual stresses experienced when processing metals means that support structures are used to keep the part from deforming and to dissipate heat.



Ti6Al4V Titanium Actuator
(image credit: STFC & TNO)



Tungsten Anti-scatter grids
(image credit: Dunlee)



AlSi Aluminium Scanning Mirror
(image credit Fraunhofer IOF)

Figure 18: metal PBF process, image credit: 3DHubs.

For the AM of metals: stainless steel, tool steel, CoCr alloys, titanium and aluminium alloys, are all available, plus many more. Process parameters, such as applied energy power, scan strategy, process control and powder dispensing, have to match the material in use. Materials with a low thermal conductivity result in better accuracy as the melt pool and solidification area can be controlled more accurately. The process aims to produce fully dense functional parts. Metals with high reflectivity and thermal conductivity are difficult to process, such as aluminium and copper. In general, metallic materials that exhibit good weld-ability are easy to process by AM. Residual stresses are generated as a result of solidification. This may lead to cracking during, or after, part construction. Thermal post-processing steps, such as stress relief heat treatment and Hot Isostatic Pressing (HIP), are essential to realise stress free and fully dense parts.

3.3.7.1 Benefits and Limitations PBF

- Metal PBF can be used to manufacture complex, bespoke parts with geometries that traditional manufacturing methods are unable to produce.
- Metal PBF parts have excellent physical properties and the available material range includes difficult to process otherwise materials, such as metal super-alloys.
- The material and manufacturing costs connected with metal PBF are high, so these technologies are not suitable for parts that are easily manufactured by traditional methods.
- The build size of the metal PBF is limited, as precise manufacturing conditions and process control are required.
- Already existing designs may not be suitable for metal PBF and may require redesign for AM.

3.3.7.2 Powder Bed Fusion – Process developments

A high-power laser (in DMLS/SLM), or an electron beam (in EBM), is used to selectively bond metal powder particles together layer-by-layer forming the metal part (Figure 19). In SLM and DMLS, almost all process parameters are set by the machine manufacturer. The layer height used in metal PBF varies between 20 to 50 microns and depends on the properties of the metal powder (flow-ability, particle size distribution, shape etc.).

The typical build size of a metal PBF system is 250 x 150 x 150 mm, but larger machines are available (up to 500 x 280 x 360 mm). The dimensional accuracy that a metal PBF printer can achieve is approximately ± 0.1 mm. Current developments are mainly relating to inline process control and an increase in production speed. High power, multiple fibre lasers and advanced scanning systems are implemented to achieve higher build rates. Current machines are capable of building 25 cm³/hr material for high accurate machines and up to 175 cm³/hr for industrial production machines. At the end of 2021, SLM Solution introduced the NXG XII 600 serial production machine with 12x 1000Watt lasers. The system is capable to build over 1000 cm³/hr with a build volume of 600 x 600 x 600 mm.

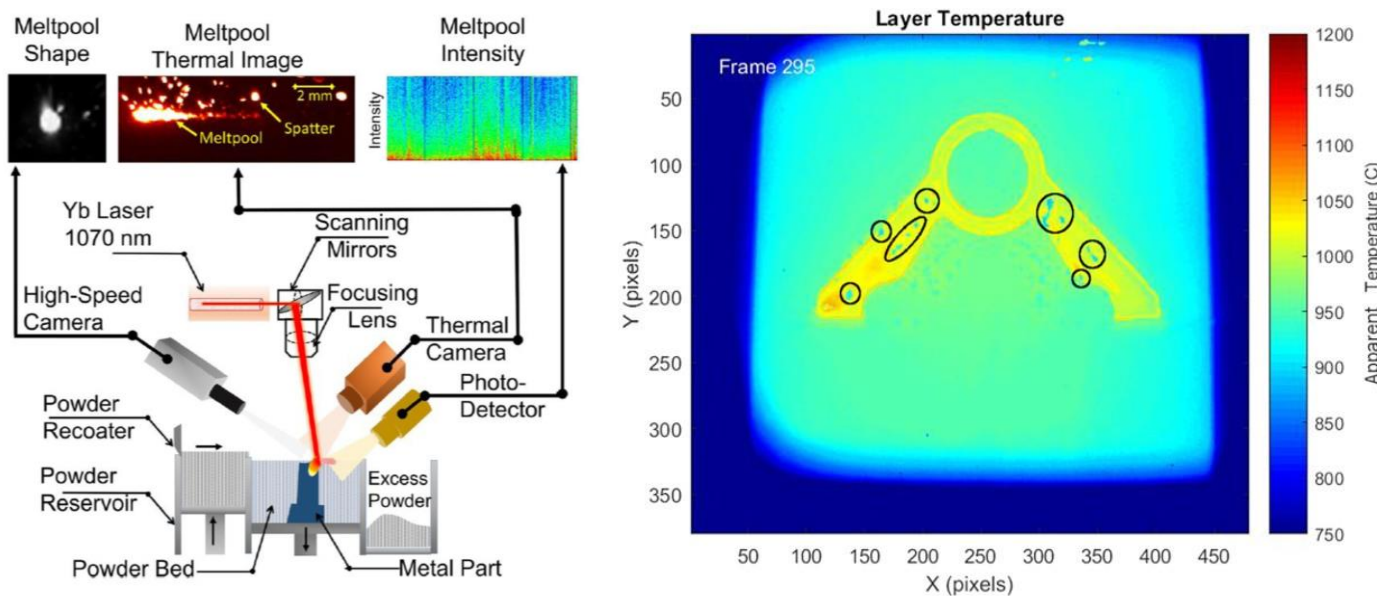


Figure 19: Current state-of-art PBF processes are equipped with multiple sensors to capture the melt-pool and build process for real time *in-situ* monitoring [11]. The complete build process is traceable and can be used for defect detection, qualification and certification [12].

The 3D printing step is only the beginning of the PBF manufacturing process. After the print is complete, several necessary/optional, post-processing steps are required before the parts are ready to use. Compulsory post-processing steps include:

- Stress relief: internal stresses develop due to the very high processing temperatures during printing. These need to be relieved through a thermal cycle before any other operation.
- Removal of the parts: in DMLS/SLM the parts are essentially welded onto the build platform. A band saw or EDM wire cutting is used to remove the parts.
- Removal of the support: supports in DMLS/SLM are always required to mitigate the thermal warping and distortion that occurs during printing. The support is removed manually or by CNC machining.

3.3.7.3 Part quality

Realising a qualitatively correct part with the PBF process is complex and depends on multiple factors. The influencing parameters are displayed in the Ishikawa/fishbone diagram that show the potential causes of a specific event [13] (Figure 20). A further application of a fishbone diagram is in the identification of potential factors leading to AM defects.

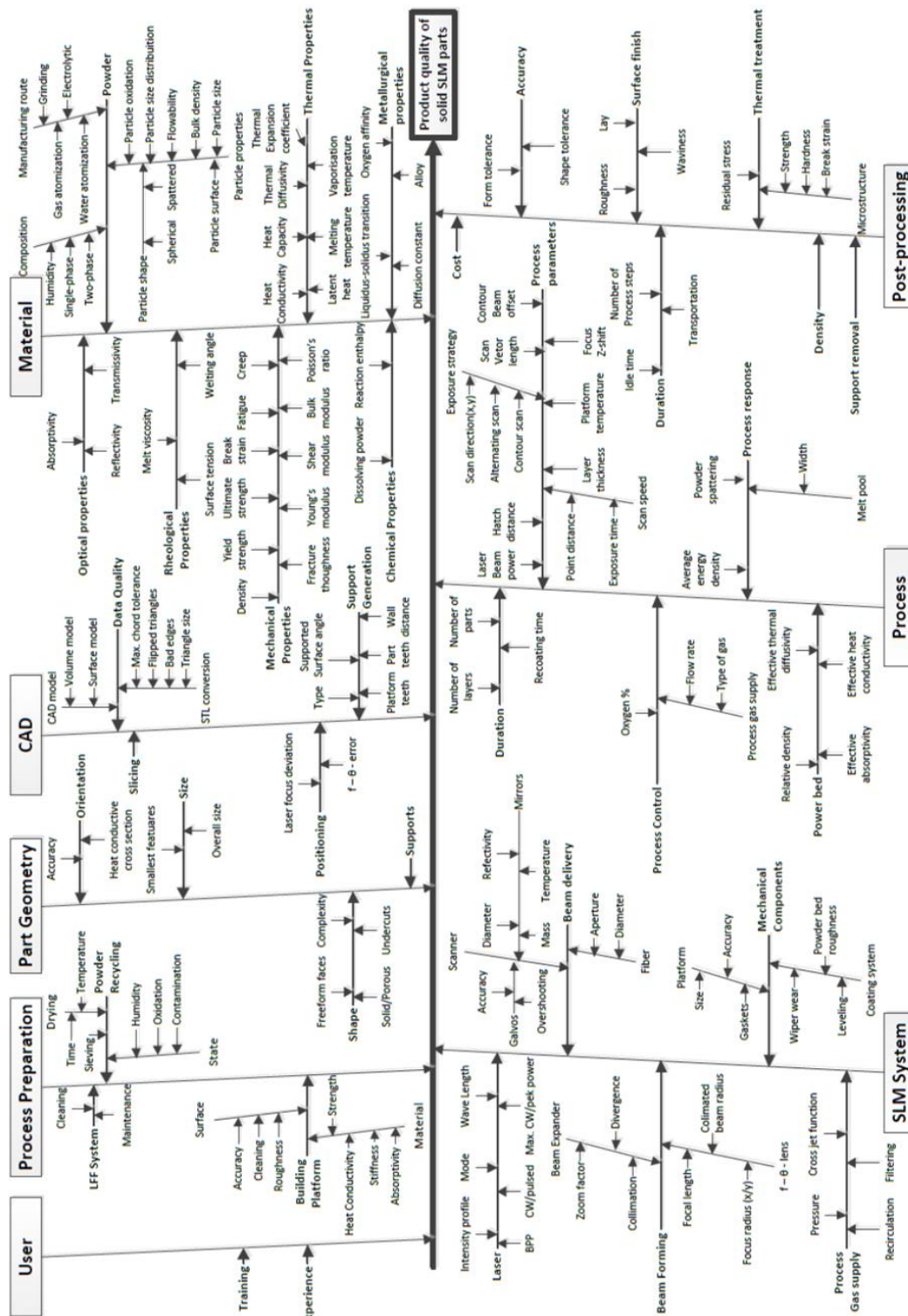


Figure 20: the Ishikawa diagram for the PBF process, image credit: Olaf Rehme, ILaS.

3.3.7.4 Influence of variations

There can be large differences between parts manufactured by PBF, as the initial build quality is determined by several factors. The main categories are part design, build orientation, material, process parameters and the machine architecture. The build parameters are dependent upon the powder material and the capabilities of the equipment; the equipment owner, or service bureau, usually controls these parameters. An overview of possible variations that may occur in a given build is provided in Table 4.

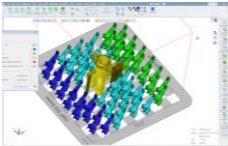
Process level at which variation can occur	Material Parameters	Process Parameters
 <p>Different metal AM processes</p>	Different material specifications	Different processes = different process parameters
 <p>One process, different machines</p>	Raw material properties such as particle size distribution. Difference in powder specifications. Chemical composition in range of standard specification	<ul style="list-style-type: none"> Selected parameters by process engineer Powder layer application systems Laser characteristics Different inert gas systems ...
 <p>Different machines of same brand & type</p>		<ul style="list-style-type: none"> Laser characteristics Environmental conditions Different machine settings ...
 <p>Different build jobs in one machine</p>	Virgin or recycled material. Change of particle size distribution, moisture, oxygen or nitrogen content	<ul style="list-style-type: none"> Powder layer thickness Irregularities Laser glass pollution Inert gas filter resistance
 <p>In one build job</p>		<ul style="list-style-type: none"> Location in build chamber Homogeneity of gas flow Temperature variations Variation in layer thickness Temperature variation optical system
 <p>In one part</p>		<ul style="list-style-type: none"> Variation in layer thickness Time between layers Height on platform Temperature variations

Table 4: Overview of possible variations at different levels in metal PBF production

3.3.7.5 One process, different machines

Currently there are multiple manufactures of PBF systems each with specific machines and processes. Machines are developed with different applications and requirements in mind. From small-scale machines for high-resolution parts, to large high-performance system for series production – this difference in performance is highlighted in Table 5.

Machine	MLab - R	SLM 500HL
		
Manufacturer	ConceptLaser by GE	SLM Solutions
Build volume (XYZ)	90 x 90 x 80 mm	500 x 280 x 365 mm
Layer Thickness	15 – 30 µm	20 – 200 µm
Laser system	100W	Twin 2x 400W Quad 4x 400W
Beam Focus Diameter	50 µm	80 – 120 µm
Maximum Scan Speed	7 m/s	10 m/s
Build rate	1 – 5 cm ³ /h	up to 175 cm ³ /h
Cost	>175 K Euro	>1M EURO

Table 5: Comparison between a high-performance industrial PBF system and a high-resolution machine.

Table 6 provides a visual comparison between PBF processes, in the example, the OPTICON test geometry was printed in aluminium (AlSi10Mg) by two service bureaux. One sample is produced on a high resolution system and the other on an industrial grade machine.

Print	High Resolution System	Industrial System
Test Geometry		
Material	CL31Al (AlSi10Mg)	AlSi10Mg
Process	Powder Bed Fusion	Powder Bed Fusion
Equipment	MLab – R	SLM 500HL
Manufacturer	ConceptLaser – GE	SLM Solutions
Post processing	Heat treatment	Heat treatment

Table 6: the OPTICON Test Geometry printed with two different types of machines in the same material. Image credits: TNO.

3.3.7.6 Difference in resolution

There is a clear difference in the resolution visible when comparing the two processes (Table 7): small features are absent or lack detail; sharp corners are rounded; and there is an excess of material. This is a result of the different laser beam distribution between the two systems and energy input. The beam focus diameter of the high resolution system is 50 μm , while the multimode laser of the industrial system may vary from 80 – 120 μm (Figure 21).

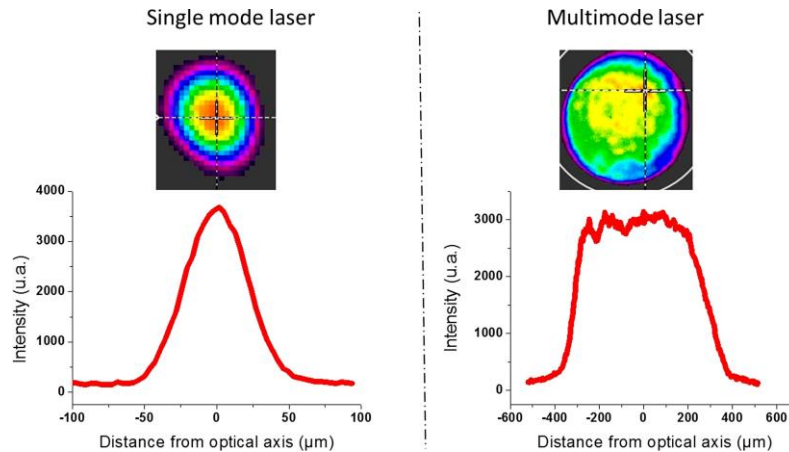


Figure 21: Laser beam distributions for a small laser spot and large multimode laser spot [14].

Feature	Vertical holes	Cube Pyramid	Debossing & Embossing
High Resolution system AlSi10Mg	<p>The \varnothing 0.25 mm hole is present and has a diameter of 0.218 mm. The diameter of the large hole is 0.49 mm.</p>	<p>The stacked cubes are well defined and hole in the middle is open</p>	<p>Features are present and well defined.</p>
Industrial System AlSi10Mg	<p>The \varnothing 0.25 mm holes are blocked with powder.</p>	<p>The corners of the stacked cubes are rounded and the middle hole is not present</p>	<p>Features are present. Corners are rounded.</p>

Table 7: Scanning electron microscope images of printed features in the OPTICON test geometry; both examples are printed in aluminium (AlSi10Mg) via PBF. Image credits: TNO.

3.3.7.7 Difference in materials

There is also a large difference in process-ability of materials. There are materials with low reflectivity and low thermal conductivity such as titanium, ferrous, and nickel alloys, and materials with high reflectivity and high thermal conductivity, such as aluminium and copper alloys. The later are more difficult to process due to the low absorptivity of laser energy and the high coefficient of thermal expansion. In addition, the latent heat of fusion for aluminium (the energy required for melting) is the highest for any metal. Therefore, applying sufficient energy in the laser-powder bed interaction zone and keeping that energy within the melting zone is challenging. Controlling the melt pool and to achieve thin wall thicknesses and small features is difficult. The reactivity and presence of oxides and hydrogen makes aluminium even more susceptible to porosity and micro crack formation.

Material & Systems	Titanium High Resolution TiAl6V4	Aluminium Industrial System AlSi10Mg	Aluminium High Resolution AlSi10Mg
Top view (XY plane)			
Quality of top surface (XY Plane)			
Quality of side walls (XZ Plane)			

Table 8: The visual differences between two materials and two PBF systems as demonstrated using the OPTICON test geometry. Image credits: TNO.

An extensive comparison between multiple AM process, systems and materials is collated within the OPTICON Test Geometry report [A2].

3.3.8 Indirect metal processes

Recently various indirect metal systems have introduced to the market and these are based upon the binder jetting and material extrusion processes (Figure 22). After debinding and sintering, a near fully dense part is realised with binder jetting systems; values up to 99.9% are achievable. Some processes use capillary infiltration with bronze to obtain fully dense material. One advantage of the binder jetting systems is the absence of support material or structure; however, part shrinkage of 17% to 20% needs to be considered. The printed layer thickness depends on material, system and manufacture, and typically ranges from 20 to 50 μm . The XY print resolution ranges from 600 to 1200 dpi.



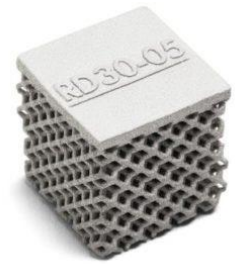
Light weight screws
(image credit: Digital Metal)



Venturi valves printed in 316L stainless steel
(image credit: ExOne)



Power steering unit
(image credit: Desktop Metal)



Metal Jet part
(image credit: HP)

Figure 22: Metal binder jetting parts from various companies

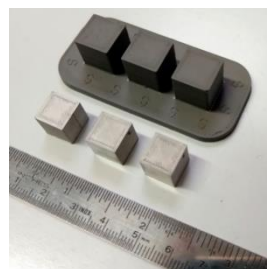
An alternative approach of indirect manufacturing of metal parts, is material extrusion (Figure 23). A high metal particle filled polymer filament is extruded through a nozzle and deposited. Support structures are essential during the build process. Porosity due to filament production is inherent to material extrusion and also present after debinding and sintering. Pores are dominantly found at the edges and corners. Typical density values range between 90% and 99%. Since parts are printed with a layer thickness of 0.15 to 0.25 mm and a nozzle diameter of 0.4 mm, high resolution features are not achievable.



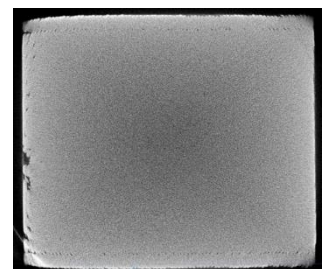
316L Piston
(Image credits: Desktop Metal)



Ultrafuse material from BasF
(image credits: Sculpteo)



Cubic sample before and after the sintering process. Shrinkage percentage of over 17% [15]

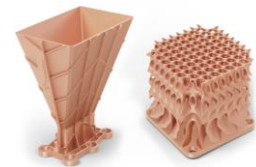
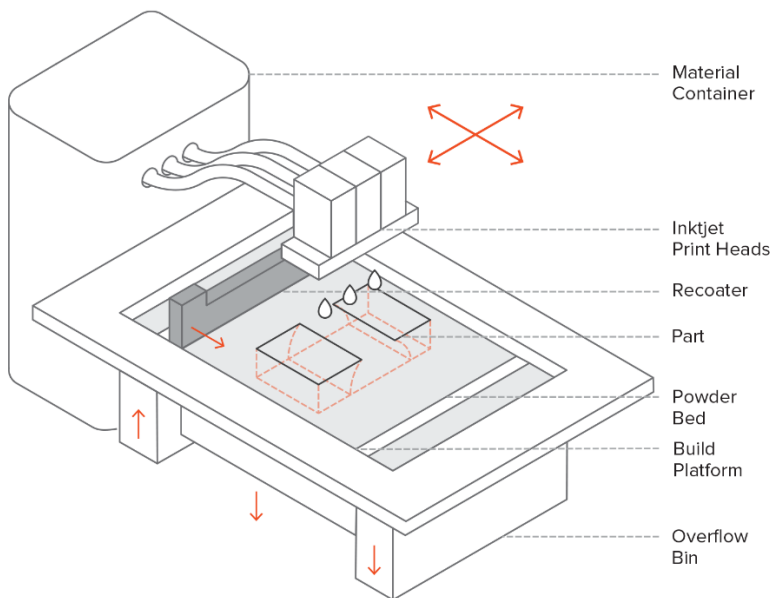


CT image displays a density of 98% in the centre of a build
(image credits: BasF)

Figure 23: Material extrusion samples of highly filled metal filament.

3.3.9 Binder Jetting

The binder jetting concept is suitable to process a wide range of materials: from gypsum and polymers, to ceramics and metals. In this process, a binding agent is selectively deposited upon a thin layer of the powdered material of interest to create the object of successive layers (Figure 24). Binder jetting is used in various applications, including large sand casting cores and the manufacturing of metal and ceramic parts.



Pure copper antenna and heatsink
(image credit: Digital Metal)



SiSiC Mirrors by SGL Ceramics
(image credit: IAC & TNO)



316L Actuator by Digital Metal
(image credit: STFC & TNO)

Figure 24: Binder jetting process, image credit: 3DHubs.

The process: first, a recoater blade spreads a thin layer of powder over the build platform; then an inkjet print-head deposits selectively droplets of a binder (glue) that bond the powder particles. When the layer is complete, the platform lowers and a new powder layer is applied. Similar to PBF of polymers, no support structure is needed. After printing, the parts are removed from the powder bed and depowdered. These “green” parts are brittle and highly porous. A post-processing step is required to achieve mechanical properties. The parts need to be sintered, or infiltrated with a low melting material. This is a batch process.

A wide range of metals and ceramics are available, such as stainless steel 316L, Inconel 718, copper, silicon infiltrated silicon carbide (SiSiC), zirconia.

3.3.9.1 Benefits and Limitations

- Binder jetting produces metal parts at a fraction of the cost compared to PBF.
- Binder jetting can manufacture complex metal geometries as it is not limited by thermal effects (e.g. warping) and batch wise thermal post processing steps.
- The manufacturing capabilities of binder jetting are excellent for low to medium batch production.
- Metal binder jetting parts have lower mechanical properties than PBF parts, due to their higher porosity.
- Only rough details can be printed with binder jetting, as the parts are very brittle in their green state and may fracture during post processing.

3.3.10 Advanced Ceramics

Recently, several indirect AM processes have become commercially available to print ceramic green components (Figure 25). Crack- and pore-free ceramics can be manufactured after performing additional densification steps after the AM process, such as debinding and sintering. With some AM ceramic processes, full density is not achievable and infiltration with silicon at elevated temperatures results in fully dense parts. The success depends on good AM design, 3D printing and the correct heat treatment. Crystal growth, residual stress and shrinkage are some of the important and influencing factors.

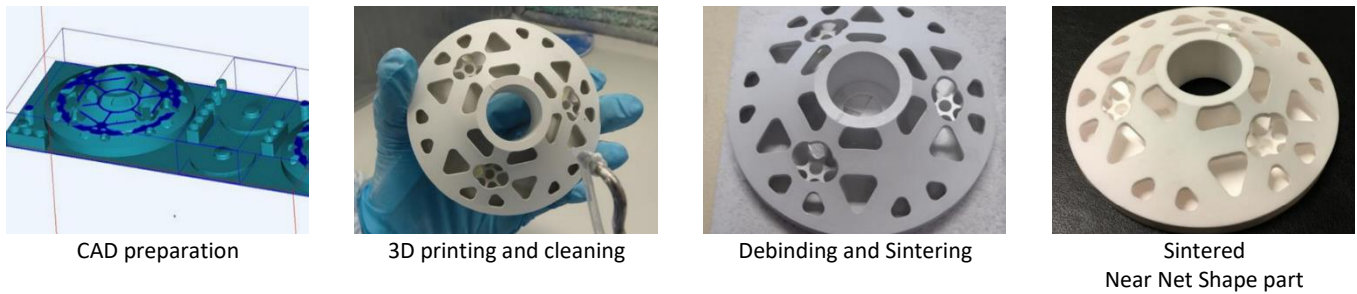
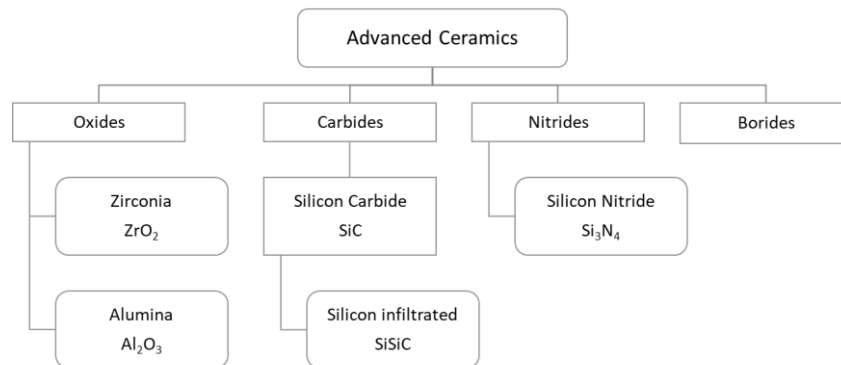


Figure 25: Custom made ceramic optical substrate, image credit: 3D Ceram.

There are multiple advanced ceramic materials, but only a small selection of materials is currently available for AM, as shown below.



The two most common processes to produce ceramic parts are VPP and binder jetting. The AM processes shape the part by binding ceramic particle together. In the ‘green state’, the strength is determined by the binding agent, which acts as a glue. The binder is removed by a chemical, or a thermal, debinding process that leaves the part in a ‘brown state’. The parts in the brown state are fragile and porous. A thermal sintering step is essential to bond the particles. The closely packed particles agglomerate at temperatures above a certain temperature as they seek to minimize free energy by decreasing the surface area - the processes is termed necking. As sintering progresses, neck size increases and the pore size decreases – as demonstrated in Figure 26.

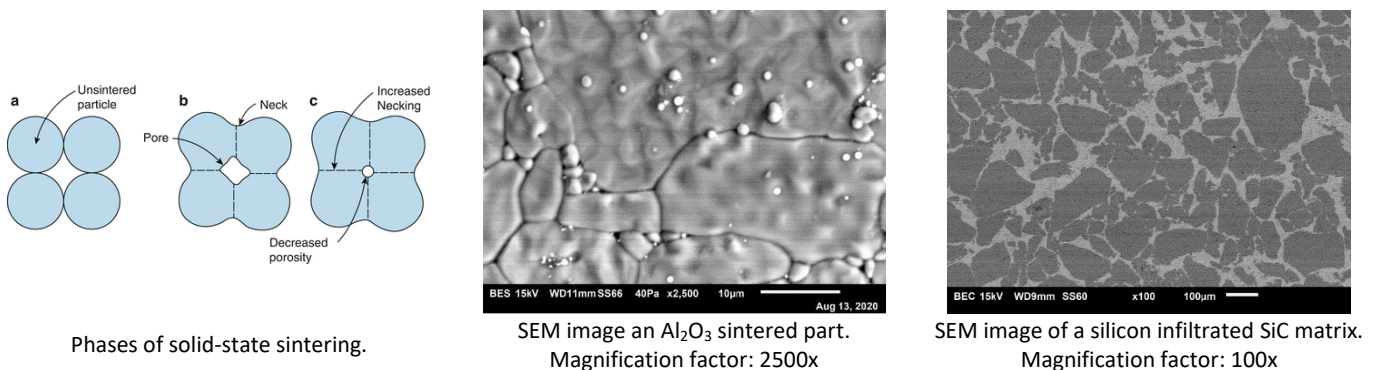


Figure 26: Solid state sintering of ceramics, image credits: TNO.

3.3.10.1 Service providers

Several European service providers are specialised in the design and production of advanced ceramic parts. Most companies are experienced in ceramic injection moulding or processing and are knowledgeable in sintering and post-processing of advanced ceramics. They are using similar VPP processes from Admatec, Lithoz, or 3D Ceram. The sintering and infiltration of silicon carbide requires specialised high temperature oven equipment. Companies such as SGL Carbon and Schunck are offering a 3D Printing and post-processing service (Table 9).

Advance Ceramics	Service Provider	Process
Alumina – Al ₂ O ₃ Zirconia – ZrO ₂	Formatec - Admatec Lithoz 3D Ceram - Sinto Cerix – Bosch Steinbach	DLP DLP SLA DLP DLP
Silicon Nitride - Si ₃ N ₄	International Syalons	SLA
Silicon Infiltrated Silicon Carbide – SiSiC	SGL Carbon Schunck GmbH	Binder Jetting Binder Jetting

Table 9: AM service bureaux for advanced ceramic parts

3.3.10.2 Considerations

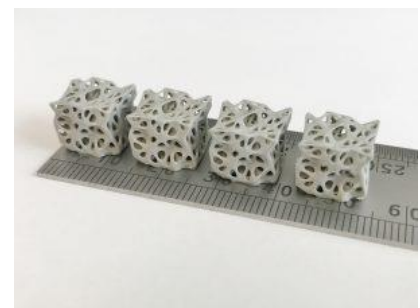
Successful ceramic 3D printed parts require several processes, dependent upon the design rules, to be followed. Build volume is restricted to certain dimensions and the use of support structures has to be limited with VPP. To prevent micro cracking, a result of stress concentration, sharp corners must be avoided. Tight tolerances are difficult to reach due to shrinkage factors of up to 20%. The cost and the lead times can be high. Examples of successful 3D printed ceramic parts are shown in Figure 27



Alumina Oxide mirrors printed by Vat Photo Polymerisation
(image credit – TNO & LAM)



Si-SiC Mirror blanks printed by Binder Jetting technology. Produced by SGL Carbon
(image credit – TNO & IAC)



Silicon Nitride 3D printed Lattice cubes
(image credit – International Syalons)

Figure 27: examples of 3D printed advanced ceramic parts.

3.4 AM Material properties

AM material properties are known to vary not only from their bulk counterparts, but also between different AM machines – i.e. the same powder sample printed on two different machines will behave differently. A thorough description of the AM material properties and the prioritisation of the different properties for astronomical applications has been discussed within the OPTICON A2IM Deliverable D5.1 [16].

In this section, the priority is to provide a visual description of the variability of two key material properties - Young's modulus and density - for AM polymers, ceramics and metals. The methodology employed to achieve this has been to collate material properties from either online databases, or from company published datasheets, for like-for-like materials (or as near as possible) and to represent the range of this data as an area - the objective was not to provide definitive values. It should be noted that in the case of an anisotropic Young's modulus, an average of the different axial values has been plotted. The data sheets used within this section are listed in the Appendix.

3.4.1 General overview

Figure 28 presents an overview of the three primary materials groups used in AM (polymers, ceramics and metals) and the range of material property values for a given material within that group.

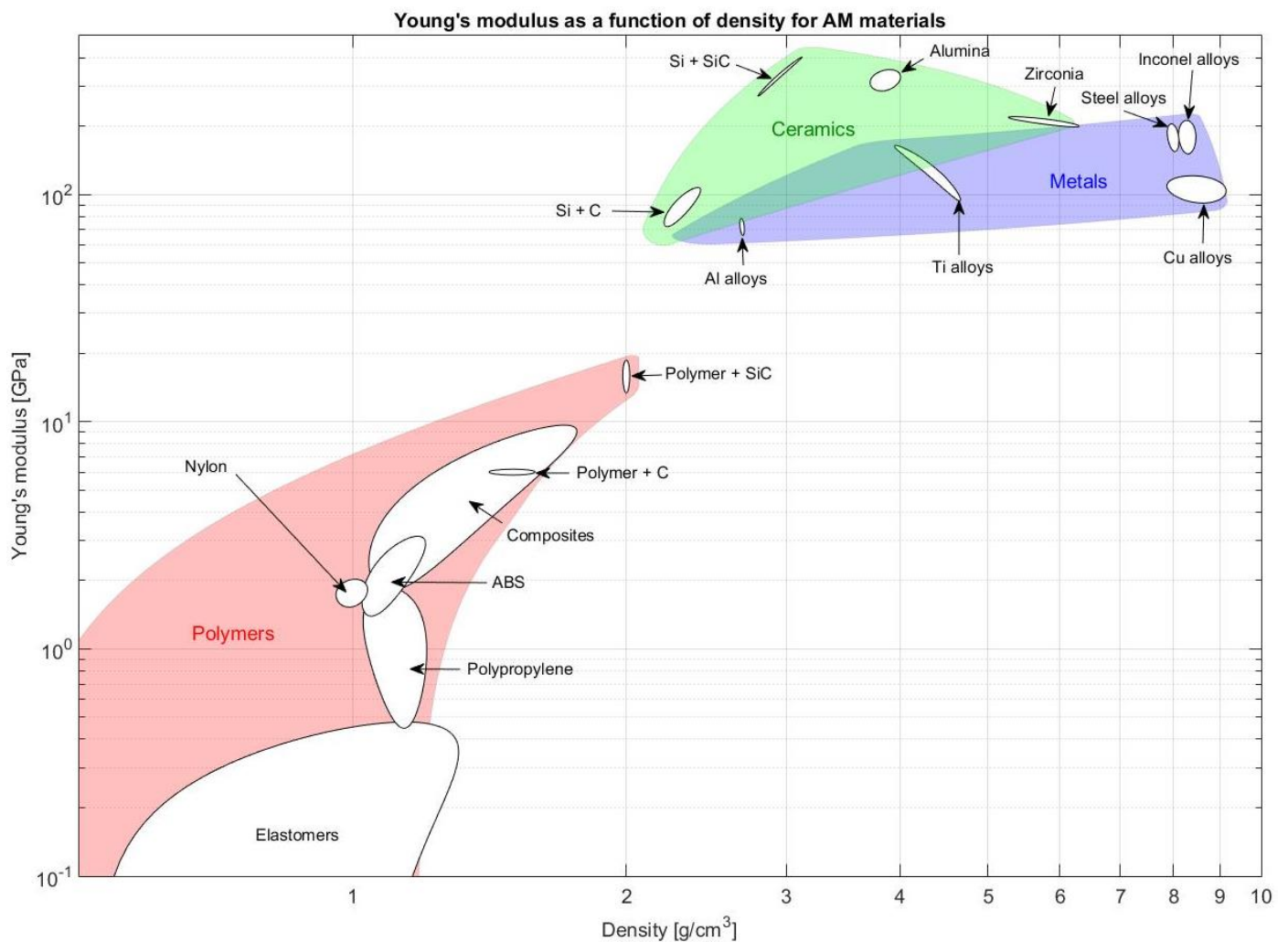


Figure 28: Young's modulus as a function of density for AM metals, ceramics and polymers, image credit: STFC.

3.4.2 Metals

Figure 29 highlights only the common metal alloys available via AM to date. The metal groupings include different alloys of the dominant metal. The values used within the graph include both raw and post-processed (heat treated or hot isostatic press (HIP)) material property data and therefore, demonstrate the range in potential material performance. Inconel is the tradename for a family of high performance nickel alloys – two Inconel alloys are presented within the graph. Figure 30 presents three examples of AM metals used in mirror fabrication.

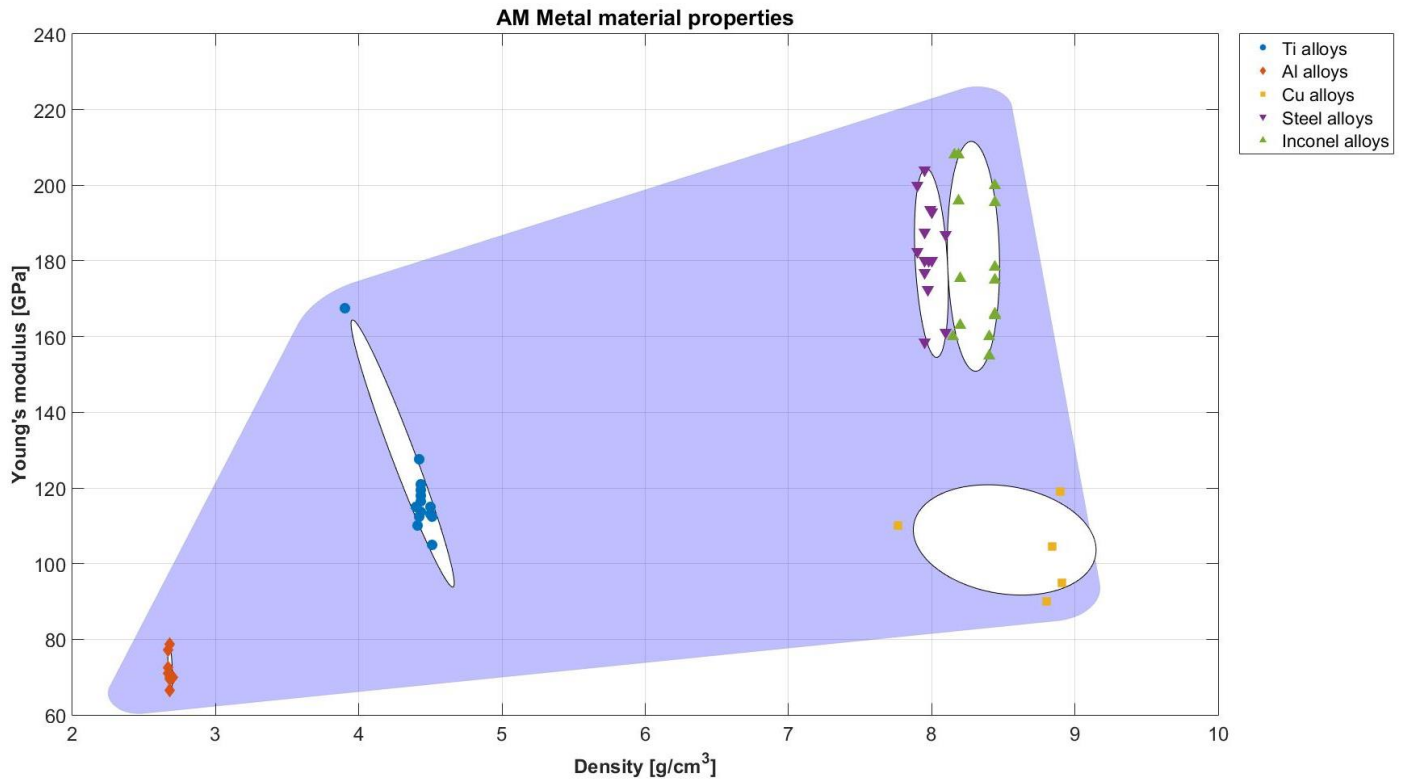
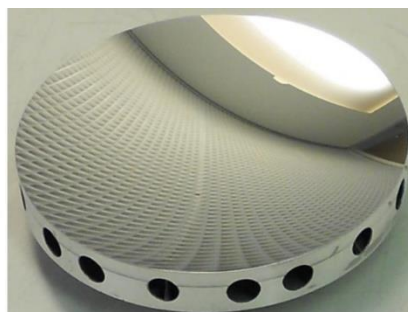


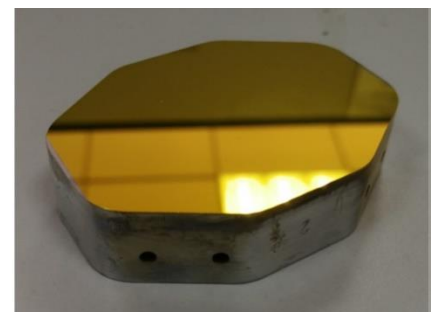
Figure 29: Young's modulus as a function of density for AM metals – note the linear axes. Image credit: STFC.



a) Hilpert, E., et al. (2018)



b) Sweeney, M., et al. (2015)



c) Tan, S., et al. (2020)

Figure 30: three examples demonstrating the use of metal AM in the creation of metal mirrors. Image credits: [17] [8] [18] respectively.

3.4.3 Polymers

Figure 31 plots the broad range of polymers that are possible via AM. Some of the polymers are considered ‘standard’ – i.e. commonly used in AM – whereas the other polymers are either high performance or composites. Due to the linear scale within the plot, the breadth of the Young’s modulus property for elastomers is not as clearly demonstrated as in Figure 28. When defining polypropylene (PP) and ABS (acrylonitrile butadiene styrene) within the plot, the data includes sources that are defined as PP-like or ABS-like. In the case of carbon + polymer and silicon carbide + polymer, these materials are composites where the polymer acts as the binding agent. Figure 32 provides two examples of AM polymer prototypes designed for astronomical applications.

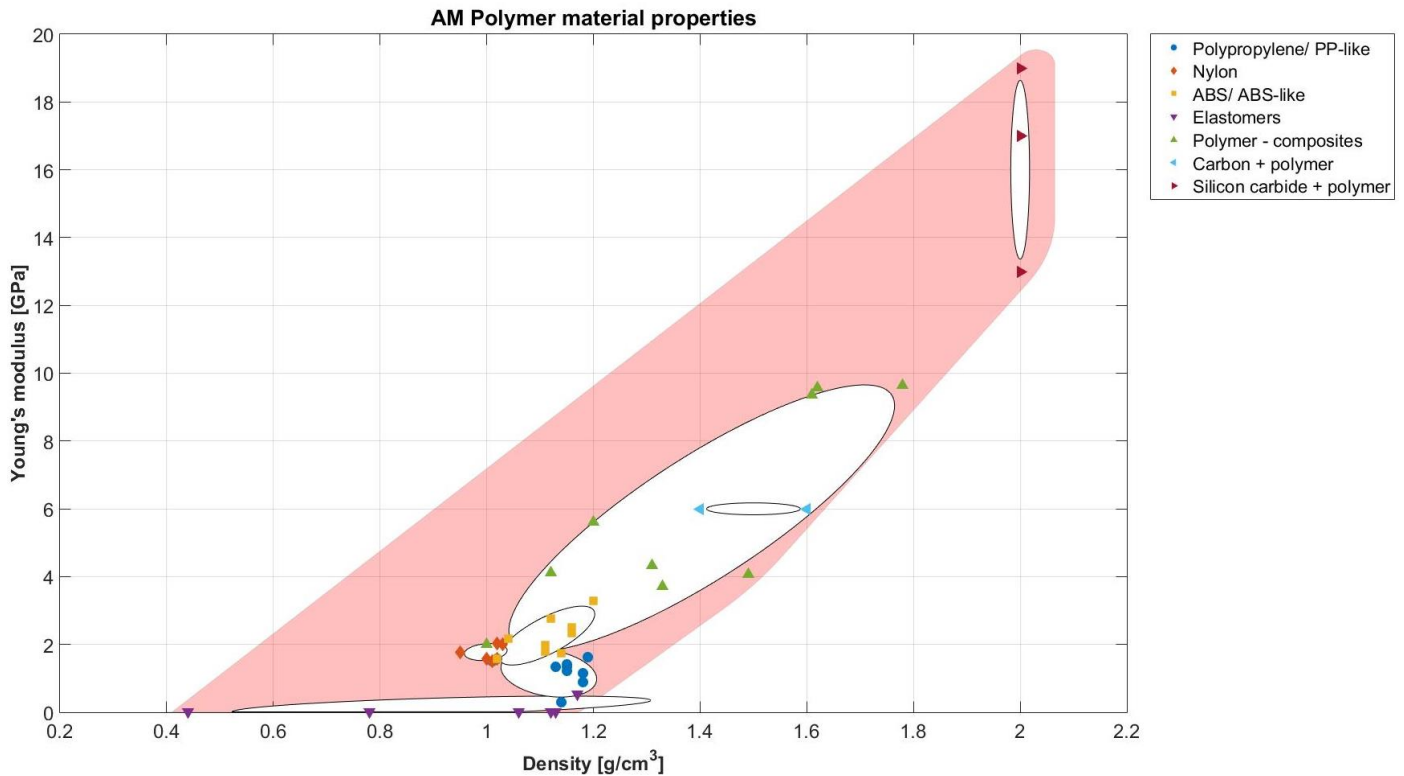


Figure 31: Young's modulus as a function of density for AM polymers – note the linear axes. Image credit: STFC.

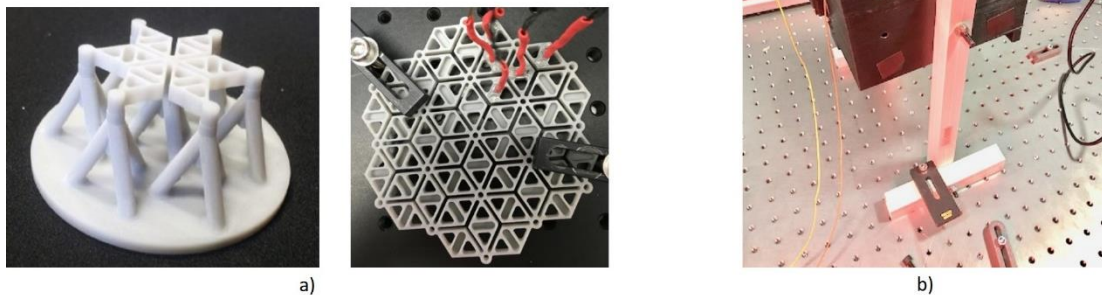


Figure 32: two examples of printed plastic astronomical components. a) An ABS mirror (*left*) and actuator grid (*right*), image credit: Miller, C., et al. (2016) [19]; and b) a prototype housing to mimic a reflecting grating astronomical spectrograph, image credit: Steele, I., et al. (2018) [20].

3.4.4 Ceramics

Figure 33 presents ceramic (or ceramic-like) materials available for AM. This is a developing area in terms of breadth of materials available, which means that in some cases there is only one supplier (and therefore datasheet). Alumina and zirconia are the most common AM ceramics available to date. In the cases of silicon + carbon and silicon + silicon carbide, silicon acts as the binding agent. Figure 34 provides two examples of AM ceramic mirrors: (*left*) an example of an alumina mirror prototype designed to incorporate mirror surface and actuator holders as a single object while minimising the print-through effect [21]; and (*right*) five AM RoboSiC prototype mirrors polished to a surface roughness of ~ 2 nm RMS [22].

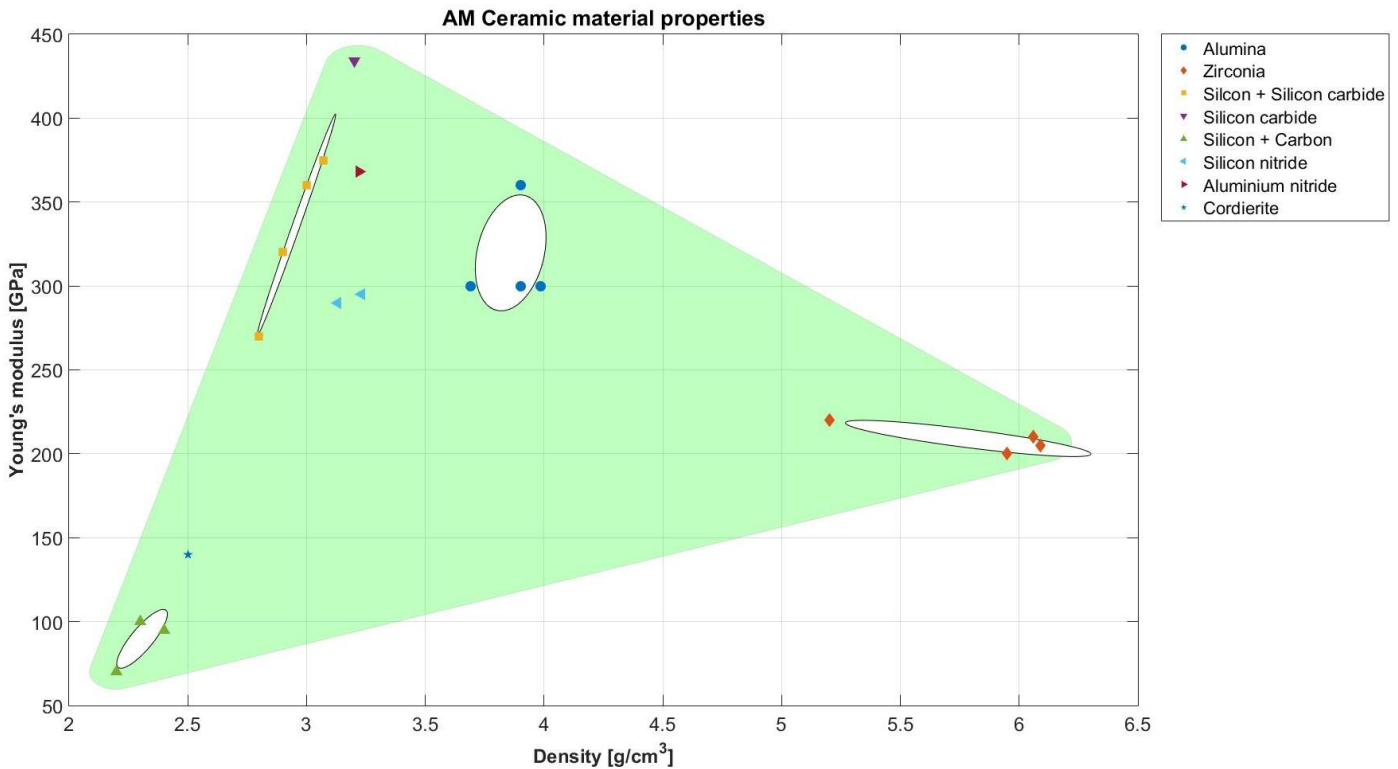
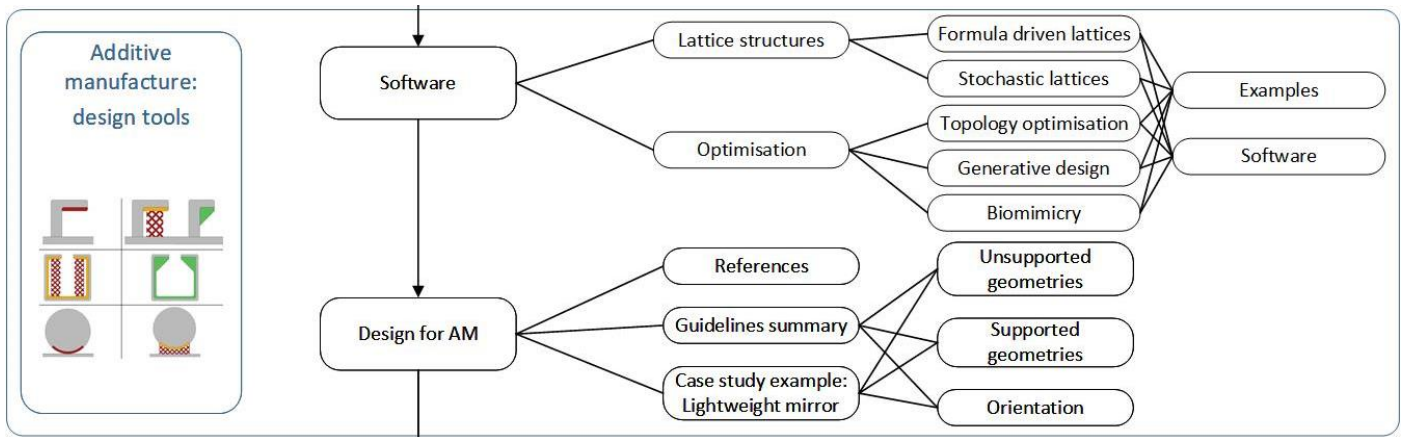


Figure 33: Young's modulus as a function of density for AM ceramics – note the linear axes. Image credit: STFC.



Figure 34: *left* - an AM alumina substrate for an active mirror prototype created as part of OPTICON A2IM, image credit Roulet, M. (2020) [21]; and *right* – AM RoboSiC polished prototype mirrors, image credit Goodman, W., et al (2019) [22].



3.5 Software

The layer-by-layer production method that is common for AM lends itself to generate freeform parts with complex internal and external structures (Figure 35). The design can become very complex and the engineering of these components is time consuming. Standard engineering software programs are usually not sufficient. Additional plug-ins and dedicated software suites are essential to design parts that take full advantage of the AM capabilities. Current trends in AM design are:

- Internal & external lattice structures
- Topology optimisation
- Generative design and Biomimicry
- Algorithmic modelling



AM part with a lattice structure; (image credit: EOS GmbH).



Freeform AM part optimised using topology software; (image credit: nTopology – ZenithTechnica).



Biomimicry inspired structural building element; (image credit: Arup).

Figure 35: Typical additive manufactured parts with complex structures that are difficult to design in traditional engineering software.

This section will explore the different geometries now possible with AM, examples in how they have been implemented within components and the software that is currently available to achieve this.

3.5.1 Internal and external lattice structures

Lattice structures are space-filling unit cells that tessellate along any axis with no gaps between cells (Figure 36). There are several reasons to implement internal or external lattice structures in a design:

- Structural optimisation,
- Weight reduction,
- Cost reduction,
 - Reduce material usage,
 - Reduce build time,
- Surface area increase,
- Promote bone ingrowth.



Copper heat exchange
(image credit: Hyperganic).



Nexxt Matrixx Spinal cages with tailored surface topology
(image credit: NexxtSpine).

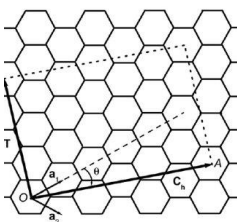


3D printed midsole
(image credit: Under Armour).

Figure 36: Some Additive manufactured parts with integrated functional lattice structures, which cannot be produced with other production technologies.

Numerous lattice variations are available for implementation within product designs. They can be categorised in four distinguished groups - Figure 37.

2D Grid structure



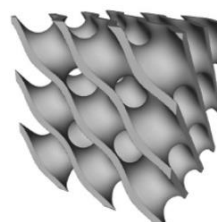
Honeycomb lattice

Periodic Lattice



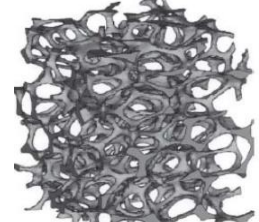
Face and Body Centred Cubic (BCC) with Z struts unit cell

Formula Driven lattice



Schwarz-D Triple periodic lattice

Stochastic lattice



Random lattice structure

Figure 37: The four groups of lattices for implementation within product design (image credits: TNO).

3.5.2 2D Grid structure

The hexagonal honeycomb sandwich is a well-known 2-dimensional (2D) grid structure designed to have a high stiffness-to-mass ratio (Figure 38). The stiff, strong face sheets carry the bending loads, while the core resists shear loads.

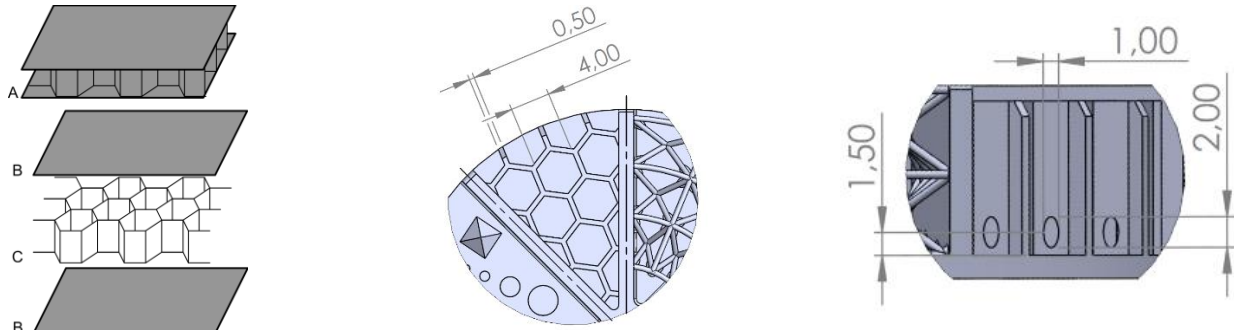


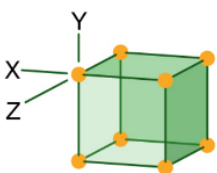
Diagram of an assembled composite sandwich (A), and its constituent face sheets or skins (B) and honeycomb core (C) (image credit: George William Herbert).

For easy residual material removal multiple oval holes are incorporated in the design at the bottom of the cavity (image credits TNO).

Figure 38: Examples of the honeycomb 2D grid structure.

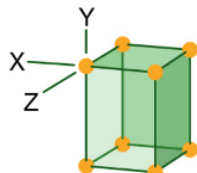
3.5.3 Periodic Lattices

Cellular solid lattice structures are space filling unit cells in an ordered arrangement. These ordered structures are usually symmetric patterns that repeat along the principal directions of the 3-dimensional (3D) space. There are many similarities with crystallography. There are seven primitive crystal systems and multiple derivatives of these concepts - Figure 39.



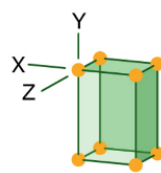
Simple Cubic

All three axes are equal in length and all are perpendicular to one another.



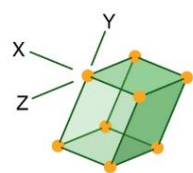
Tetragonal

Two of the three axes are equal in length and all three axes are perpendicular to one another.



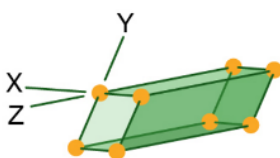
Orthorhombic

All three axes are unequal in length and all are perpendicular to one another.



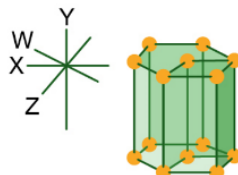
Monoclinic

All three axes are unequal in length, and two axes are perpendicular to each other.



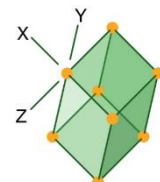
Triclinic

All three axes are unequal in length and are not perpendicular to another.



Hexagonal

Of four axes: three are of equal length, separated by equal angles and lie in the same plane. The fourth axis is perpendicular to the plane of the other three axes. Hexagonal cells have lattice points in each of the two six-sided faces.



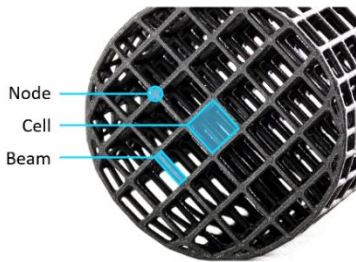
Rhombic

All three axes are of equal length and the axes are not perpendicular to another, but the crystal faces all have the same size and shape.

Figure 39: The seven primitive crystal systems, image credit: Encyclopaedia Britannica.

3.5.3.1 Patterns selection

There are numerous lattice structures, a designer can mix and match these shapes to create specific material characteristics (Figure 40). Since not all structures behave the same, it is important to choose suitably. Cell size, density, beam thickness and overhanging features are key factors. In general, larger cells are easily printable. Smaller cells allow for a more consistent system response, but are limited by feature dimensions. All are dependable on the AM process and material used. Cell orientation can alter the properties of a lattice structure and the necessity of support structures; self-supporting structures are preferable.



Nomenclature of lattices;
(image credit: Fast Radius)



Low-density 3D lattice structures printed for the LIGHT additive manufacturing project consortium; (image credit: Delcam).



Optical mirror concept with internal lattice structure
(image credit: TNO & IAC).

Figure 40: Periodic lattice structure nomenclature and applications.

In software, different lattice base structures are in-built and can be altered based upon unit size and beam diameter. Software packages, such as NetFabb and Magics, offer a library of standard and exotic structures. A sub-selection of these base lattices are shown below - Figure 41.

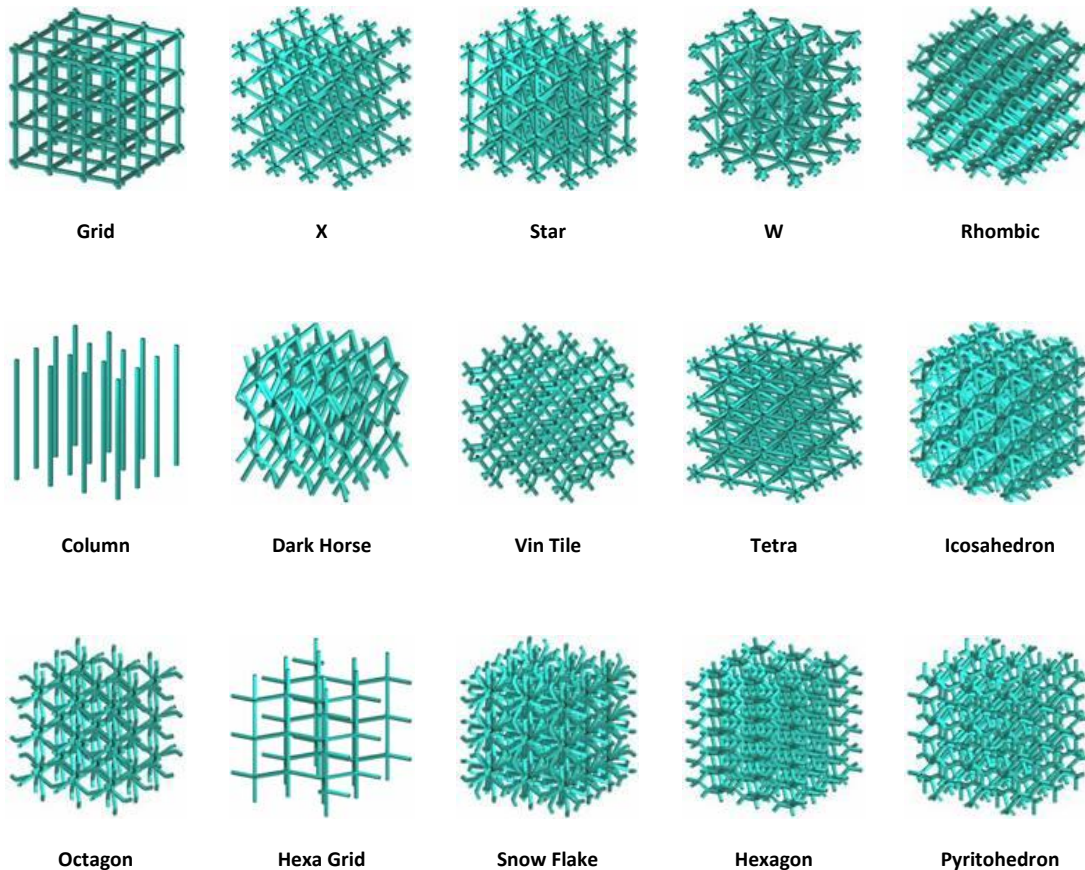
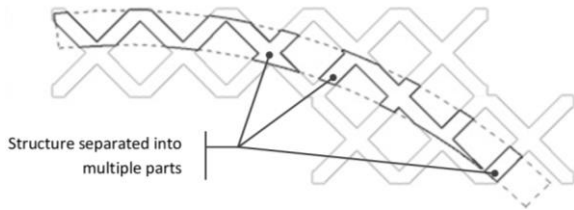


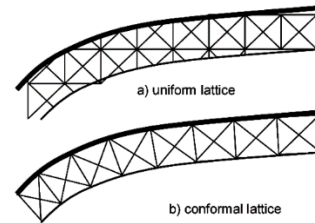
Figure 41: Selection of common lattice types available within the NetFabb structure library (image credit: NetFabb Autodesk).

3.5.3.2 Conformal and graded lattices

With several 3D software packages, it is possible to automatically generate and edit complex lattice structures. Conformal lattice structures that follow the outer hull prevent loose nodes and struts; when considering AM processing, this prevents misprints (Figure 42). Within the software, it is possible to perform Boolean operations to clean up the structure and to remove loose elements; re-shuffling and repositioning of nodes is possible.



When a lattice merges with a 3D shell, beams and nodes can become be unconnected, resulting in loose and incorrect structures.



The unit cells are conformal to the surface.

Figure 42: Conformal lattice structures are preferred mechanically and production wise, image credits: J. Nguyen.

The application of a gradient in beam thickness throughout a lattice structure is possible. In the example below, Figure 43, Autodesk Netfabb Premium has created a complex, graded volume lattice structure based upon a 3D STL file.

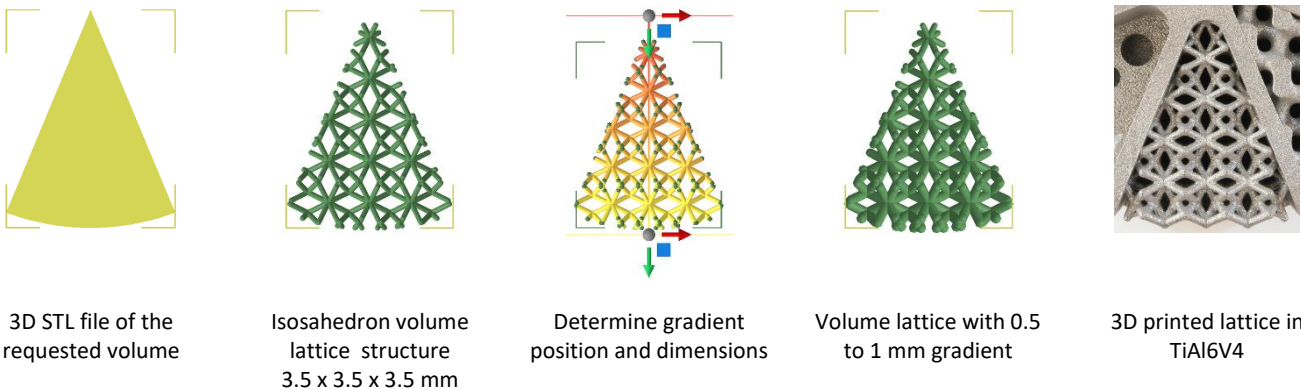


Figure 43: The application of a graded lattice structure using Autodesk NetFabb, image credits: TNO.

NTopology is powerful software solution that is capable of both applying complex predefined lattice structures and locally varying the beam thickness with custom modifiers. Furthermore, NTopology supports the combining of multiple lattice structures and lattice editing (Figure 44).

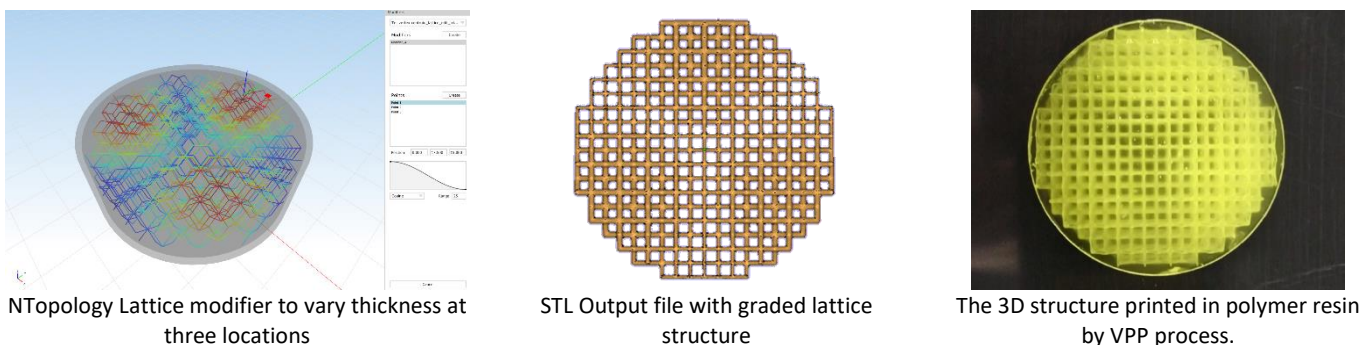


Figure 44: NTopology Element Software used to generate a gradient lattice structure, image credits: TNO.

3.5.3.3 Handling and file size reduction

The implementation of lattices has become popular due to the capabilities of AM. Within appropriate software, a lattice is selected from a library containing a catalogue of predefined unit cells and then the lattice is integrated into the required geometry; this design process is frequently not optimal as it is difficult to predict the mechanical properties of a part with internal lattice structures. However, Finite Element Analysis (FEA) methods can simulate and predict this behaviour, but this analysis is potentially difficult and time consuming. Predominately, this is caused by the volumetric expansion of data when applying lattices. Furthermore, the file size of 3D CAD and STL models can become extremely large and unmanageable (Figure 45). A selection of software programs solve this problem by working with virtual lattice structures and create the final 3D structure when exported to STL or slice format.

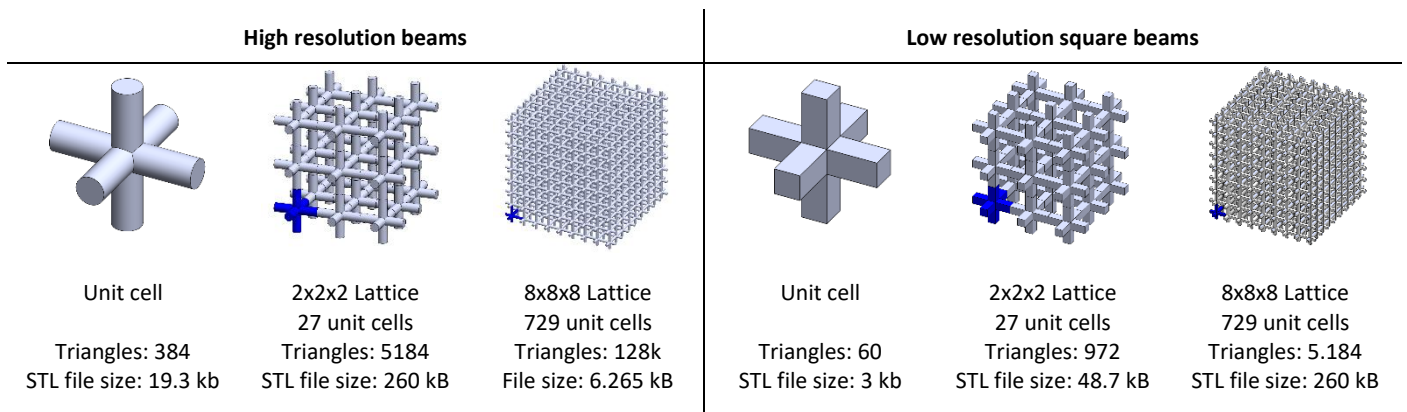


Figure 45: The influence of resolution on file size. Difference round and square beams, image credits: TNO.

The use of low-resolution unit cells will reduce the computational power needed. The data reduction is obtained by using larger unit cells and by using square beams in place of round and filleted beams. Usually the resolution of the printing system is not capable of printing the fine features in the 3D CAD file.

3.5.3.4 Periodic Lattice software

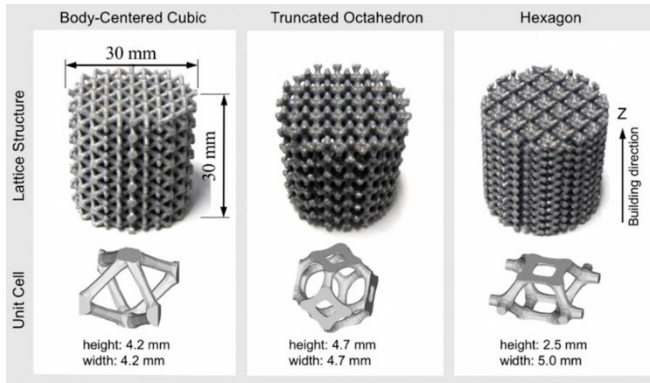
There are multiple options to generate lattice structures within 3D CAD. Constructing each lattice cell by hand is tedious and not practical, especially for complex structures. In recent years, 3D CAD and STL editing software now include lattice geometric modelling tools. In addition, more advanced AM software packages blend lattices with generative design and topology optimisation. Table 10 provides a summary of the different AM software currently available within the market.

STL editing software - Filling voids with unit cells	CAD and CAE software – Using native CAD format	
<ul style="list-style-type: none"> • 3-Matic – Materialise • NetFabb – Autodesk • 3DXpert – 3DSystems • Fabpilot – Sculpteo • NTopology 	<ul style="list-style-type: none"> • Hyperworks – Altair • NTopology • Within – Autodesk • Gen3D • Hyperganic • IntraLattice 	<ul style="list-style-type: none"> • Creo – PTC • Paramatters • Hexagon – MSC Apex • NX – Siemens • BetaType • Elise GmbH

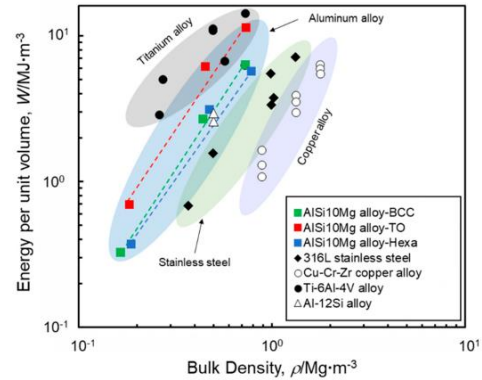
Table 10: Software vendors to implement 3D lattice structures in CAD design files; classified in STL format and native CAD format

3.5.3.5 Mechanical performance of Lattice structures

Multiple extensive research studies have been performed to determine the mechanical behaviour of lattices and to find the optimal structure (Figure 46). There is no simple solution when implementing lattices as each application, shape, material and AM process, may require a different type of internal lattice structure. However, when applied correctly, the use of lattices can result in strong, lightweight and cost efficient part production.



3D printed Lattice structures in AlSi10Mg and corresponding CAD models

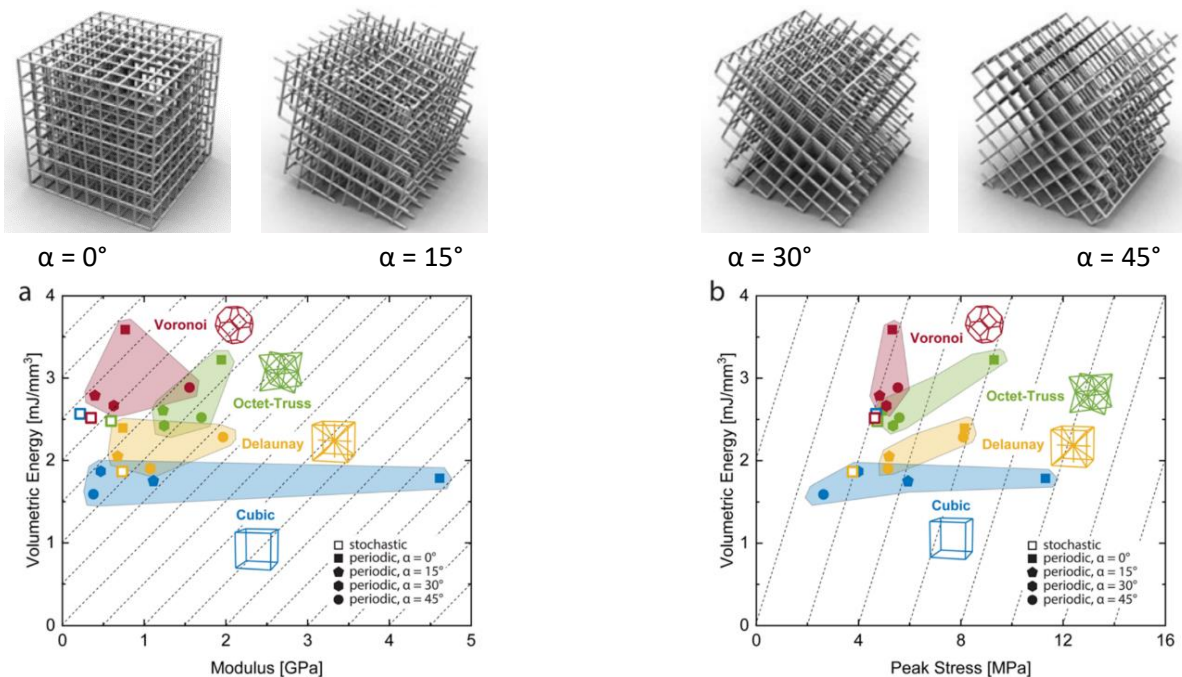


The relationship between energy per unit and bulk density of AlSi10Mg lattice structures compared with lattice structures in different materials [23].

Figure 46: Research study to the compressive properties of Al alloy lattice structures with three different unit cells fabricated by L-PBF, image credits: Lui, X., et al. [23].

3.5.3.6 Influence of unit cell orientation

The orientation of the unit cell determines the mechanical properties and compressive behaviour of the final geometry. Tensile and compressive strength may vary depending on load angle and requires consideration. Multiple studies are available where a comparison between rotation angle (α) and lattice type has been evaluated (Figure 47).



Voronoi and stochastic structures provide the lowest moduli to energy ratio. This is advantageous for crash absorption. Stiff structures exhibit less energy absorption capability

Voronoi structures are the first choice in energy absorption applications

Figure 47: Modulus and peak stress versus volumetric energy for different lattice structures and orientations, image credits: Muller, J. [24].

3.5.4 Formula driven lattices

There are multiple Triply Periodic Minimal Surface structures (TPMS) known. The most common surfaces are shown in Figure 48.

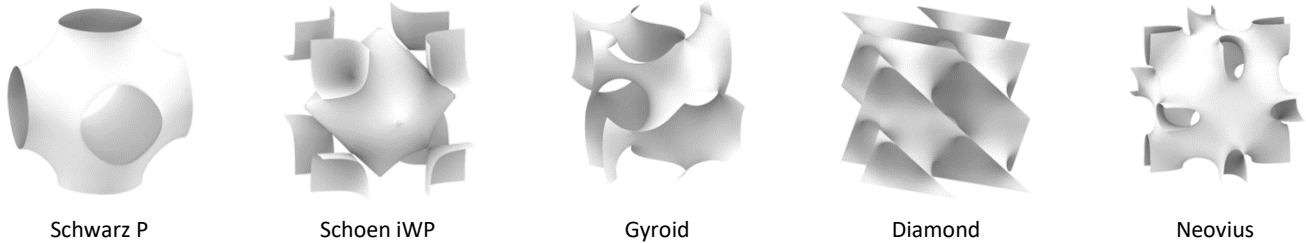


Figure 48: Different type of triply periodic minimal surface structures, image credit: [25].

The gyroid is the only known embedded TPMS that possesses triple junctions and no lines of reflectional symmetry. A gyroid surface is trigonometrically approximated by the following equation:

$$\sin x \cos y + \sin y \cos z + \sin z \cos x = 0$$

The TPMS structures are ideal for AM technologies since they are self-supporting; there are no large horizontal overhanging structures and therefore no requirement for support structures.

3.5.4.1 Software for formula driven lattices

There are several software packages available to implement 3D TPMS structures into a 3D CAD model. They are usually mesh-based programs. The gyroid structure presented in Figure 49 is designed with Gen3D software.

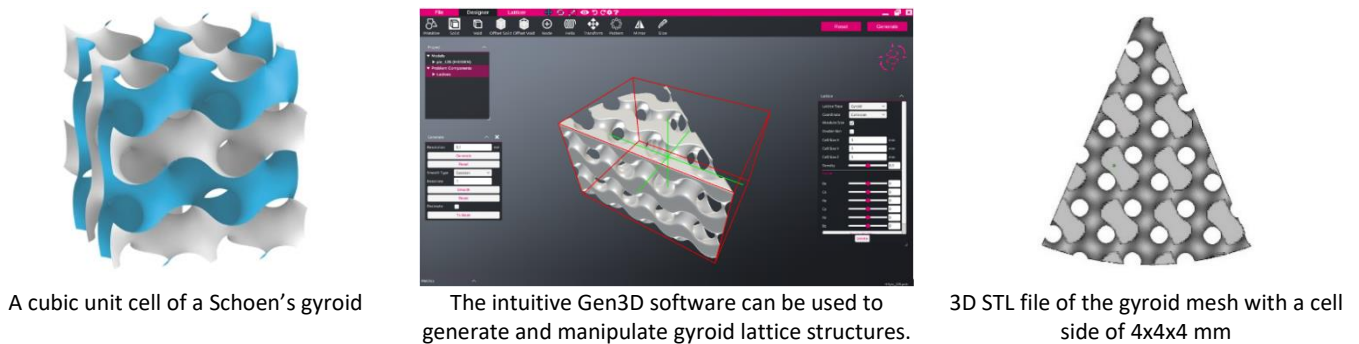
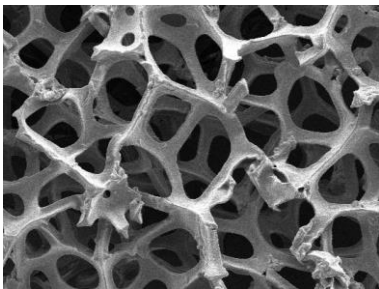


Figure 49: Sample of a TPMS structure made GEN3D software package, image credit: TNO.

In 2020, Siemens NX introduced the Implicit Modelling module for the creation of equation driven structures. Robust modelling operations on complex designs can be performed using “Implicits” that are not feasible using traditional CAD models. Features include implementing TPMS structures and Shell and Boolean operations.

3.5.5 Stochastic lattice structures

Stochastic lattices use randomised cells to create a foam-like structure that can conform to a bound surface (Figure 50). These structures can absorb shock and sound waves and are commonly used for filtration, or, to fill in sandwich structures. In medical applications stochastic lattices can be used to promote bone ingrowth. For AM, open-cell foam cellular solids are preferred to facilitate the removal of unused material. A mathematical representation of such structures are 3D Voronoi cells; a Voronoi diagram is a partition of a plane into regions equally close to each of a given set of objects. In the simplest case, these objects are just finitely many points on the plane (called seeds, sites, or generators). For each seed, there is a corresponding region called the Voronoi cell, consisting of all points of the plane closer to that seed than to any other.



Graphene open cell foam structure,
(image credit: MTI Corporation)



Silicon Carbide solar absorber based on
Voronoi cell structure,
(image credit: EnginCer)



Porous structure for bone ingrowth,
(image credit: EOS GmbH)

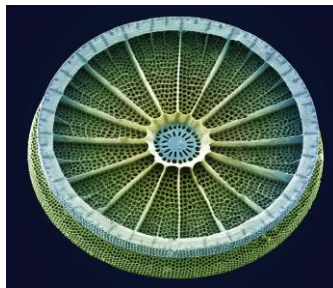
Figure 50: Stochastic and Voronoi lattice structures can be applied to 3D designs.

3.5.5.1 Cellular Solids

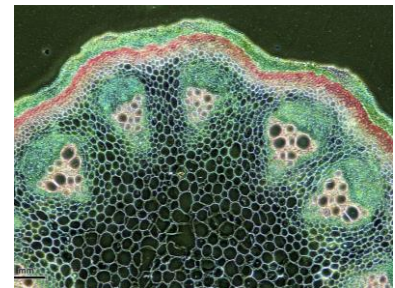
Cellular solids are an assembly of cells with solid edges or faces packed together so they fill a space. Such materials are common in nature and can be found, for example, in diatoms, corals, sponges and plant stems (Figure 51). Cellulose is from the Latin diminutive cellula: full of little cells.



Coral cell structure,
(Image credit: OnionLab)



Diatome via SEM,
(image credit: Steve Gschmeissner)

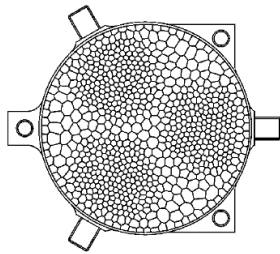


Cross-section of stem of Aristolochia,
(image credit: Josef Reischig)

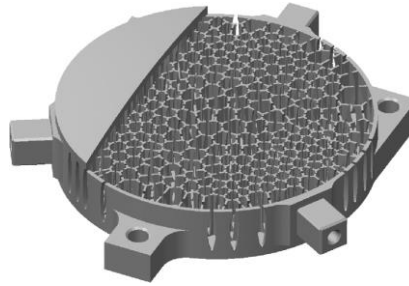
Figure 51: Cellular solids in nature.

3.5.5.2 Demonstrator

The lightweight optical mirror design concept by Fraunhofer IOF was inspired by nature (Figure 52). A stochastic interior was implemented using extruded 2D Voronoi cells.



2D Cellular solid structure



3D CAD model



Additive manufactured mirror with internal structure made visible.

Figure 52: Design study of optical mirror with an internal structure inspired by cellular solids, image credit: Hilpert, E. [26] .

3.5.5.3 Software for Stochastic Lattice Structures

Random structures are very complex and it is not possible to generate them by hand within a normal CAD environment. Mathematical programming software is used to generate Voronoi structures. Software, such as Rhino Grasshopper, Meshlab, Elisa and Siemens NX, have specialised scripts/plugins to automatically generate 3D Voronoi structures based upon mathematical formulae (Figure 53). *Algorithmic Modelling* is the latest development in CAD engineering.

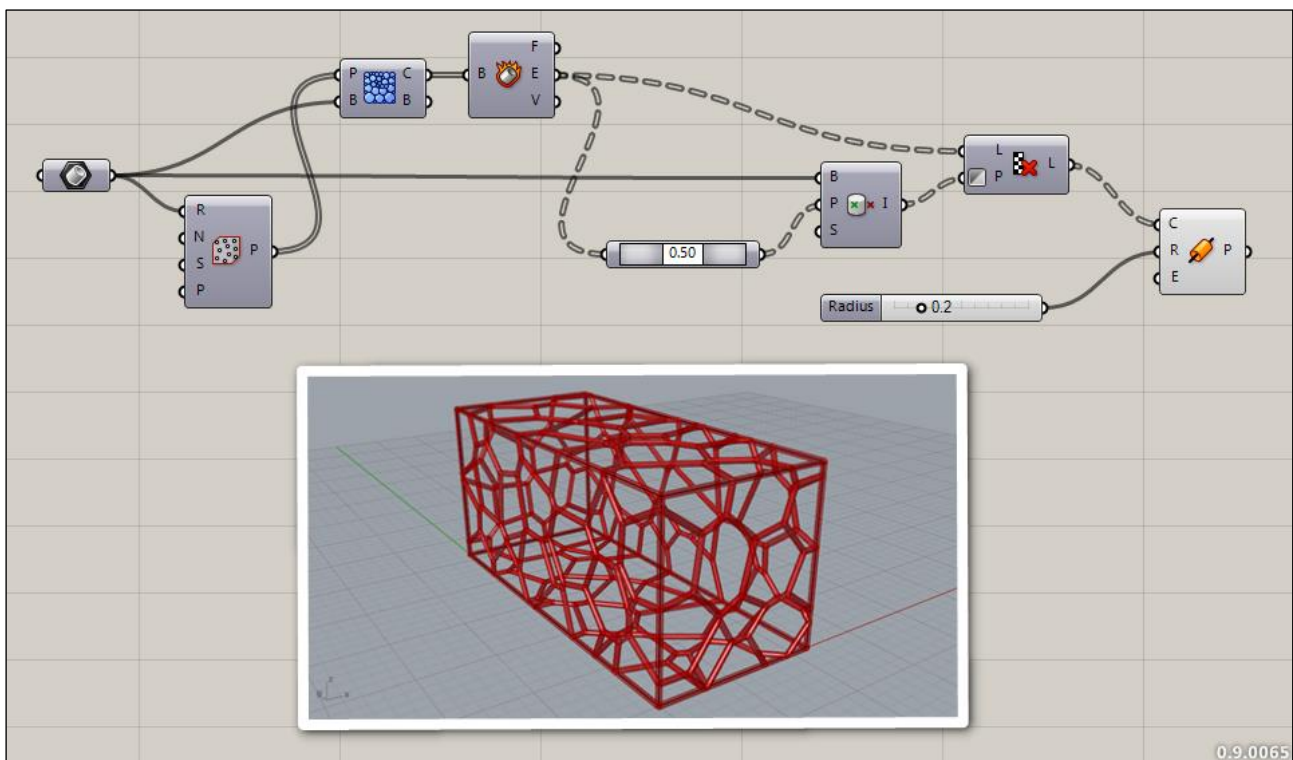


Figure 53: Grasshopper is a visual programming language and environment that runs within the Rhino 3D CAD application. A program is created by dragging components and functions onto a canvas; the outputs to these components are then connected to the inputs of subsequent components; and resulting in a 3D part. Image credit: Grasshopper3d.com.

3.5.6 Topology optimization & Generative Design

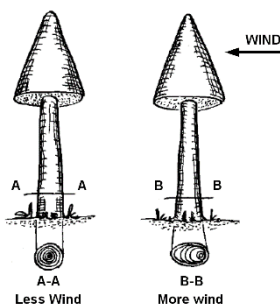
With topology optimisation, the software converges on a single solution, based upon functional objectives, constraints and loads. In generative design, multiple solutions are calculated simultaneously to create the most optimal solutions based upon functional and non-engineering requirements, such as manufacturability.

3.5.6.1 Topology optimisation

Topology optimisation is used to derive an optimal material distribution for a design under given functional use conditions. An algorithm reduces the mass of an existing object; the concept has been in use since 1990.

Claus Mattheck performed research on biomechanical engineering for parts using nature as example [27]. His work comprehends tree biomechanics, shape optimisation and failure analysis. Within his research, trees play an important role and many of his conclusions are based upon tree growth. Tree design is founded on the principle of constant surface tension. A tree attempts to keep its inner tension equal by adjusting its cross-section of the trunk so that it can achieve a balanced stress concentration. In nature, numerous of examples can be found; a comprehensive overview of cases is discussed within website of the non-profit Biomimicry institute - Asknature.org [28].

- The influence of the wind determines the shape of a tree as their cross-section will be altered. For example, trees in the mountains often grow with a spiral twist to make them stronger against the wind.
- As stated, nature is always trying to reach equilibrium with its surrounding. Trees are capable of growing around obstacles and assimilating unnatural objects during their growth process. Examples, such as encapsulated barbwire and fences in trees, are well known (Figure 54).



Trees will adjust their shape to resist wind



Spiral Twist of a mountain tree



Ancient fence assimilated by a tree

Figure 54: Trees influenced by their surroundings, image credit: Mattheck, C [27].

Applying the rules of nature to a product will mean that form follows function – i.e. to use material where required to achieve strong yet lightweight parts. This concept is commonly referred as *topology* and the method of ‘washing’ unnecessary material away *optimises* the structure. Based upon Mattheck’s research, optimised shapes can be derived from conventional design principles. When applied on conventional load conditions this results on the following optimized design (Figure 55).

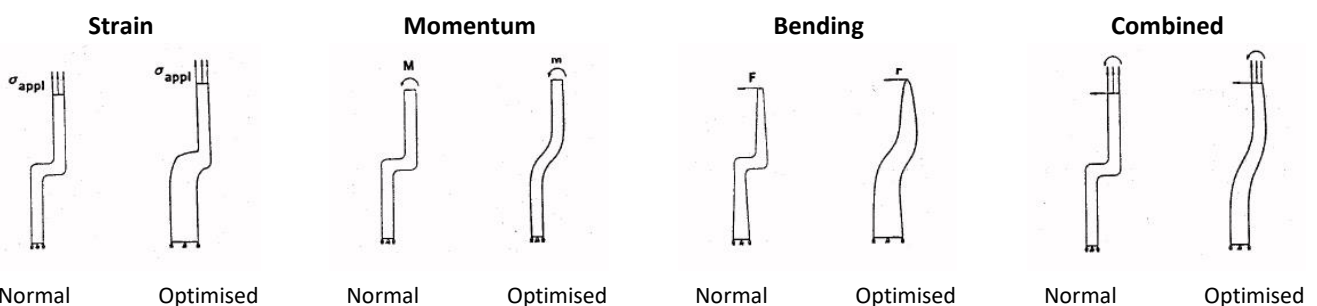


Figure 55: Applying nature’s rules on conventional load conditions, image credit: Mattheck, C [27].

3.5.6.2 Computer Aided Engineering & Topology

Using this knowledge of ‘natural construction’, software has been developed to achieve the optimised shape of a part. Existing Computer Aided Engineering (CAE) programs can be helpful tools when developing new products. Besides movement analysis and software to predict the flow of polymers for injection moulding, software packages to calculate strength by using Finite Element Method (FEM) or Analysis (FEA) are available (Figure 56).

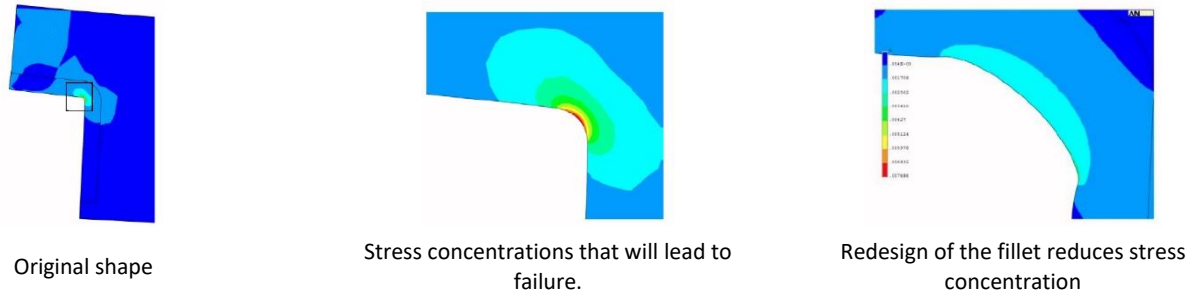


Figure 56: Finite Element Method used to optimise a structure, image credits: TNO.

Software driven design of optimized structures is commonly referred to as Computer Aided Optimization (CAO). Topology optimization will calculate an optimal design from a given design space by using the Soft Kill Option (SKO). This technology is commercially available and used widely in the automotive industry where lightweight is an important issue.

Within the design-space the loads and boundary conditions are specified. This will result in a design proposal that can be used for further development. Besides saving material and weight, the part will be optimized for its function. The end product will have optimal strength coupled with stress reduction (Figure 57).

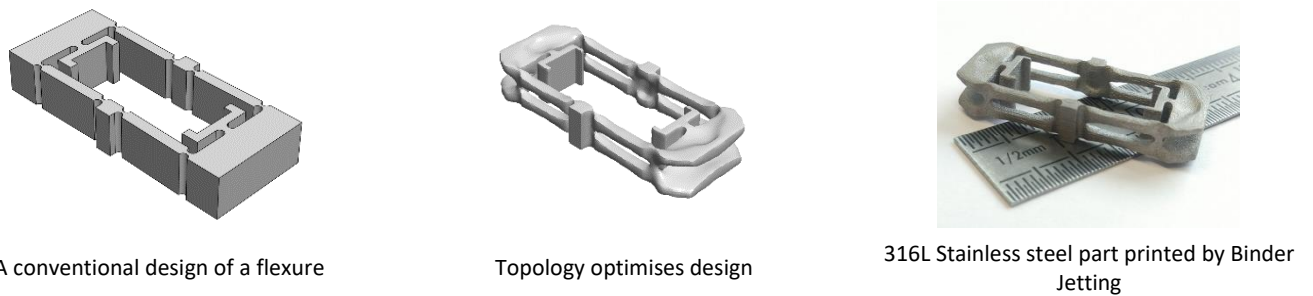


Figure 57: Topology optimization of an actuator geometry, image credits: STFC & TNO.

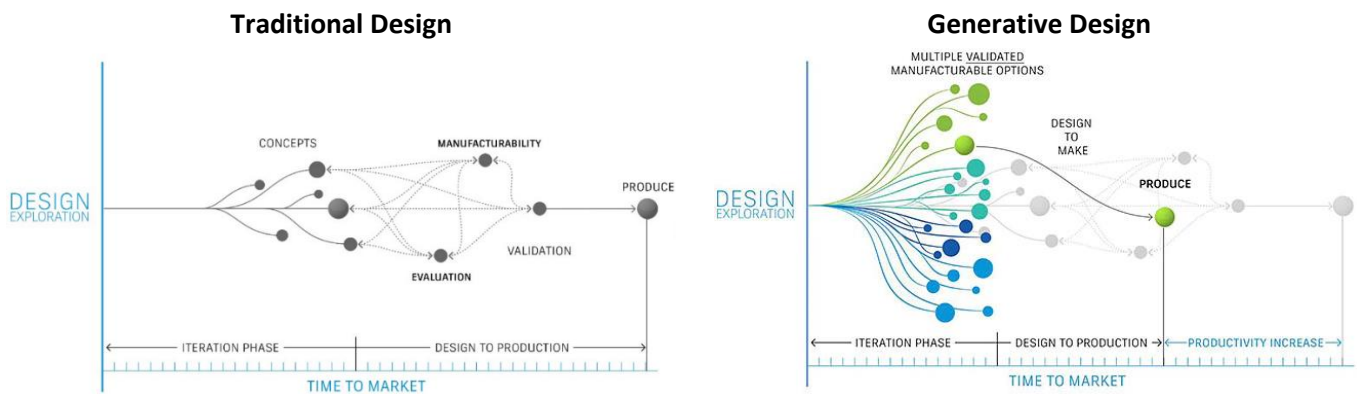
Topology optimization can be performed with several software systems. Ansys Mechanics and Altair Optistruct are examples of modular systems for structural optimization of mechanically stressed components. The program generates an optimal design proposal for a given design space, boundary and loads. With the software, STL or universal export files can be generated, such as STEP or IGES. Afterwards, optimization and redesign of parts need to take place. The proposed geometry generated by the FEA and optimization software can be used as a template by the engineer. Current CAD engineering software have powerful and user-friendly functionalities and add-ons available to fulfil this task.

3.5.6.3 Generative design

In recent years powerful new software, aided by cloud computing and artificial intelligence (AI), has been developed that will transform the design process. Instead of evaluating design concepts after they are developed, generative design lets engineers input design parameters, such as material properties, size, weight, strength, manufacturing methods and cost constraints. The software, using AI-based algorithms and cloud computing, generates an array of design options.

Generative design and topology optimisation are a paradigm shift from the traditional CAD approach to predictive and intelligent design. With the introduction of several programs such as CogniCAD by ParaMatters, NTopology, ELISA, Fusion 3D by AutoDesk and Hyperganic, the inclusion of generative design into the everyday design process takes place. Besides part cost and weight reduction, the development and engineering time will be reduced. Within the generative design engine, functional requirements such as material, strength, weight, heat transfer and other factors are implemented. The engine explores multiple combinations of a solution and automatically generates the optimal design options. Optimisation of 3D printing orientation, design of support (less) generation and design rules for manufacturing (DfM) are integrated.

The software applications use a form of machine learning and AI that leverage the power of cloud computing to create the multiple solutions in a short time (Figure 58). The engineer can explore these solutions and evaluate several manufacturing methodologies, such as additive, subtractive and formative.



Traditional Design process with several iteration steps.

Generative design process with multiple iterations steps.

Figure 58: Comparison between the tradition and generative design process, image credits: Autodesk.

Generative design software automatically analyses the design space and gives the engineer a spectrum of design solutions. The generation of options happens in parallel and no further user input is required. To avoid infinite variations, generative design uses AI algorithms and search engines to prevent unfeasible possibilities. Once a design has been chosen, the software can export the design as an editable CAD file that can be used within engineering software, such as FEA, CAM, or AM (Figure 59).

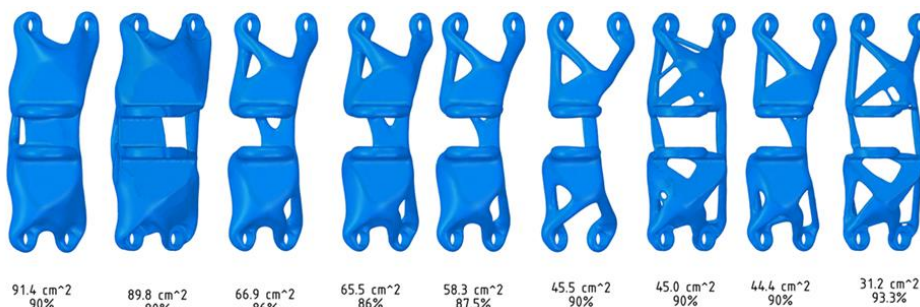


Figure 59: Generative design of a bracket where the target mass is varied and all other constraints are fixed, image credit: Ansys Workbench.



3.5.6.4 Concept evaluation

Using filters an engineer can make a selection from the outcome of multiple studies. Selection criteria could be mechanical performance, weight, safety factors, production cost, needed support structure, etc. - Figure 60.

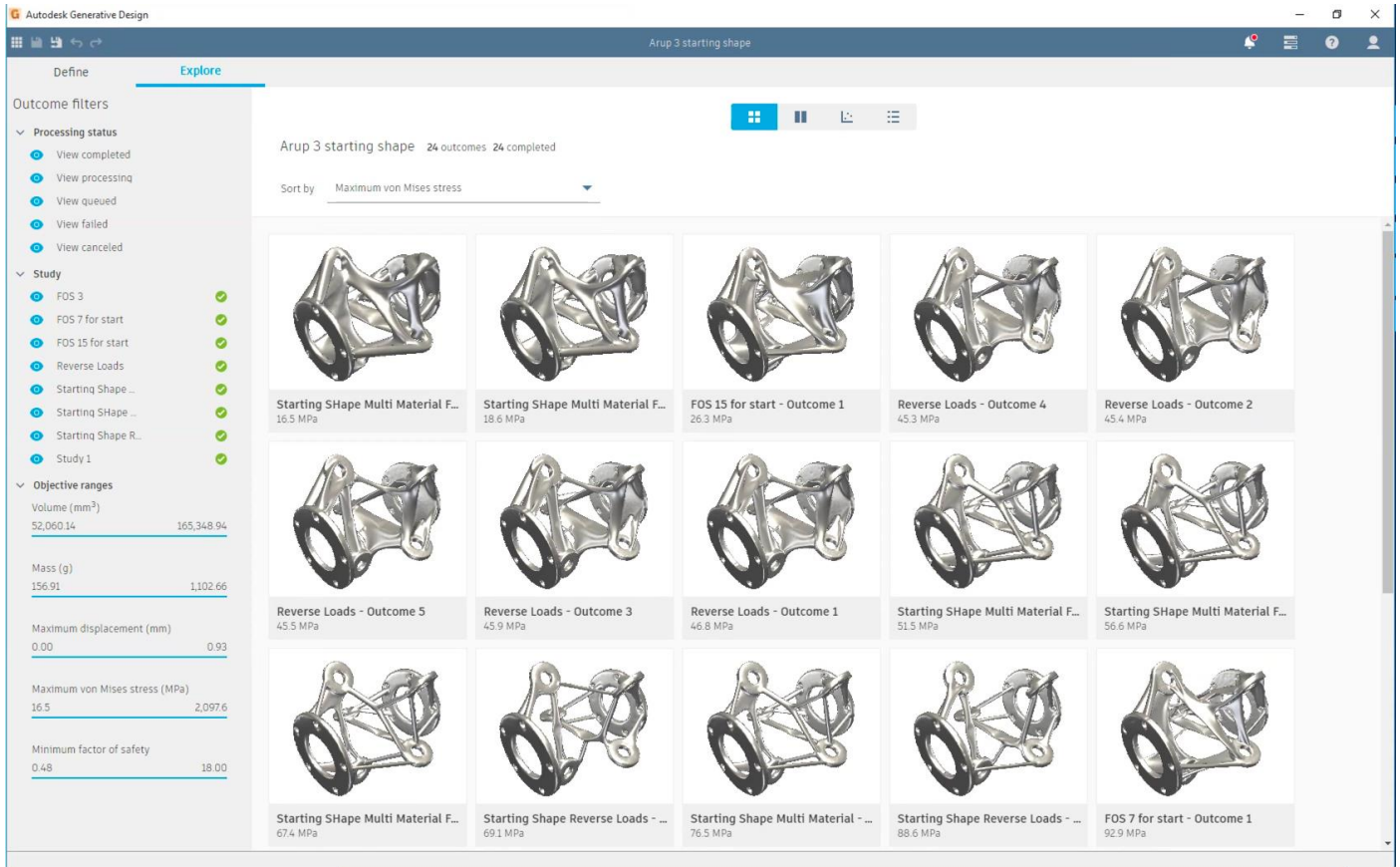


Figure 60: Screen capture of Autodesk Fusion 360 Generative design software with the comparison between multiple design studies, image credit: Autodesk.

3.5.6.5 Software providers

Established CAD and new software companies offer solutions for generative design and additive manufacturing

- Fusion 360 – Autodesk
- Paramaters – CogniCad
- Siemens NX
- Gen3D
- ToffeeAM
- NTopology
- Creo – PTC (Previously Fustrum Generate 2018)
- Apex – MSC Software
- Hyperganic
- Topos & Millipede Grasshopper Rhino

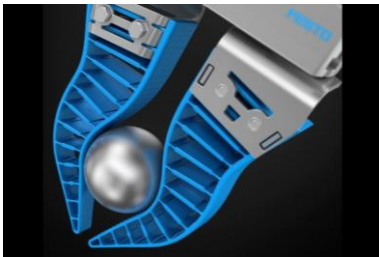
3.5.7 Biomimicry - Design with nature as example

Regarding lightweight structures, solutions provided by nature are often superior to man-made. The leaves of the giant lily, *Victoria regia amazónica*, can get up to 2 meters in diameter and carry a load of 50 kg. Yet the leaf has an overall wall thickness of approximately 2 mm. This act of strength is possible due to the inner structure of the leaf. Lightweight and strong constructions are universal in nature. Structures like honeycomb, tree stems, and soap bubbles, all have in common that they are made of a minimum of material to create a structure suitable for its function - *form follows function*. The structures in nature try to reach equilibrium with the material available. The approach of mimicking nature is termed *biomimetics* or *bionics* - Figure 61.

Product design inspired by nature



Silicon Carbide Laser scanning mirror.
Image credit: OptiSiC by Mersen



Adaptive Fin Ray gripper.
Image credit: Festo



Bespoke bike helmet
Image credit: Hexr in cooperation with EOS GmbH

Structures found in nature



Inner structures of the Giant Lily



Dorsal fins inspiration of the Fin-ray effect



Bee on a honey comb

Figure 61: Biomimicry - products inspired by structures found in nature.

Bionics deals with the transfer of phenomena from nature to technology. It is an interdisciplinary field research that attracts scientists, engineers, architects, philosophers and designers. Direct implementation of nature in functional designs is generally not possible. Natural structures are optimised and the load cases are usually different; however, nature can guide engineers to develop innovative ideas and concepts.

3.5.7.1 Algorithmic Modelling & Design

The design of products with current 3D CAD software packages can become very complex and time consuming, especially with the implementation of CEA (Cost Effectiveness Analysis) and topology optimisation software. Small modification in the technical specifications can result in time intensive and costly new multiphysics simulations (FE), extended redesign, manufacturing pre-processing, and cost evaluation processes.

The manual iteration via current 3D CAD may also cause multiple errors and therefore additional engineering time. The automated and simultaneous workflow of an *algorithmic modelling* tool combines many automated iterations and the integration of expert knowledge. For example, the bionic design rules developed by Fraunhofer IAPT are integrated as an app (application) in the ELISA software suite. The philosophy of the software, developed by the company ELISE, is to build the path and not the part (Figure 62).

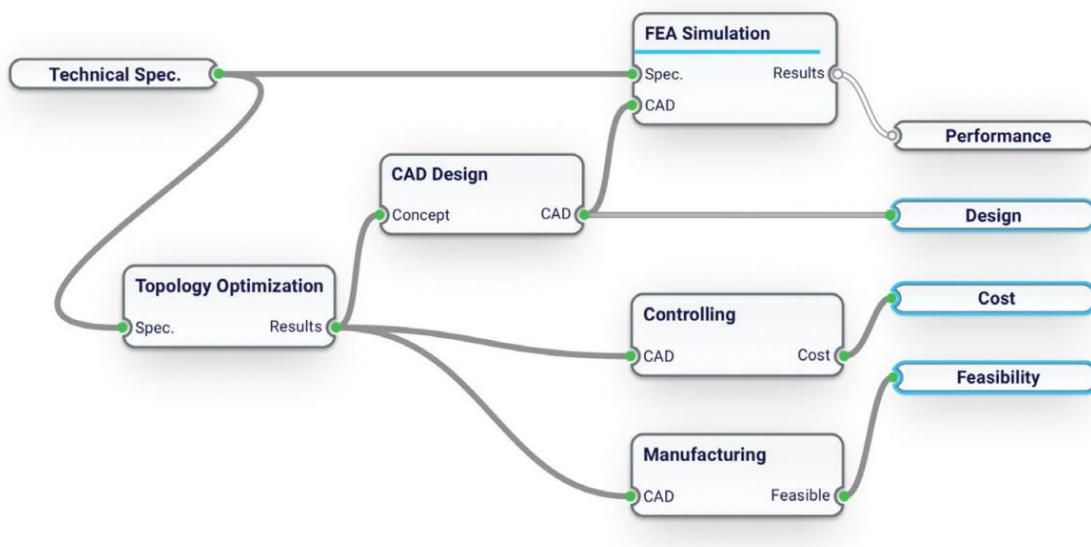


Figure 62: The workflow of the ELISE Algorithmic modelling software, image credit: ELISE GmbH.

By linking multiple building blocks with adjustable parameters together, the outcome is automatically generated. Changing a value in a building block, results in a new design. By using parameter sliders, the design is re-calculated and automatic redrawn by the software (Figure 63). No time consuming and manual engineering time is needed. Several analysis tools are implemented in the software and function as an open platform; new add-ons are being developed with partners such as Fraunhofer IAPT, HxGN Emendate and Amphyon.



Figure 63: Bionic Algorithms – By using a parameter slider the input values are altered. The design is re-calculated and automatic redrawn. Image credits: ELISE GmbH.

3.5.7.2 Automotive B-Pillar Demonstrator

In the automotive and aerospace industries, research is ongoing to implement generative designed AM parts in future models. For efficient design of highly stressed nodes, complex bionic structures are required. These structures can be created in conventional CAD programs only with great effort. Generative engineering will lead to better and more efficient products and may reduce development times [29] - Figure 64.

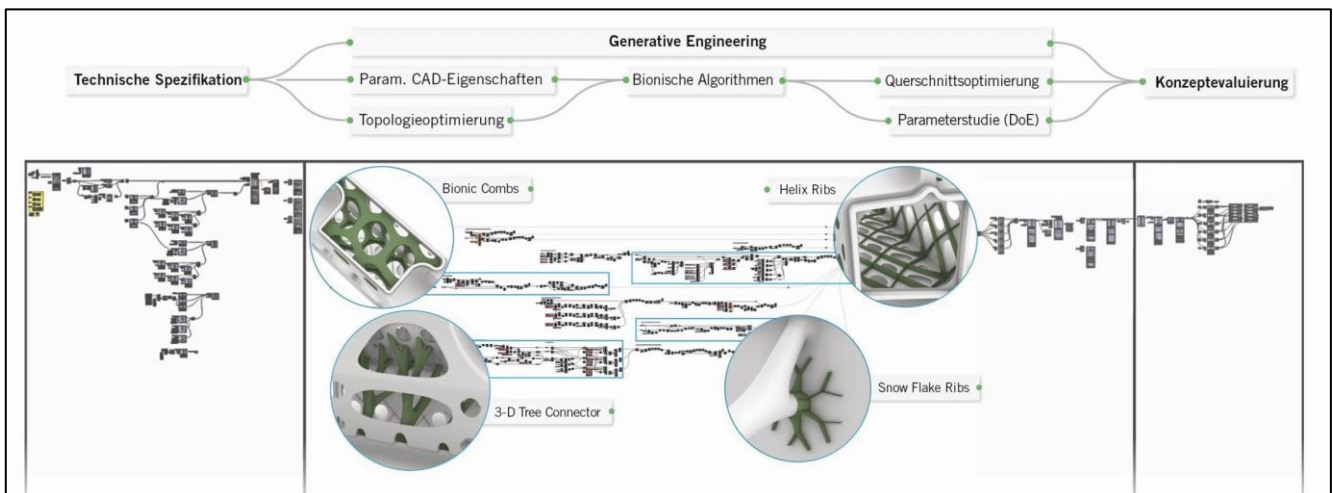
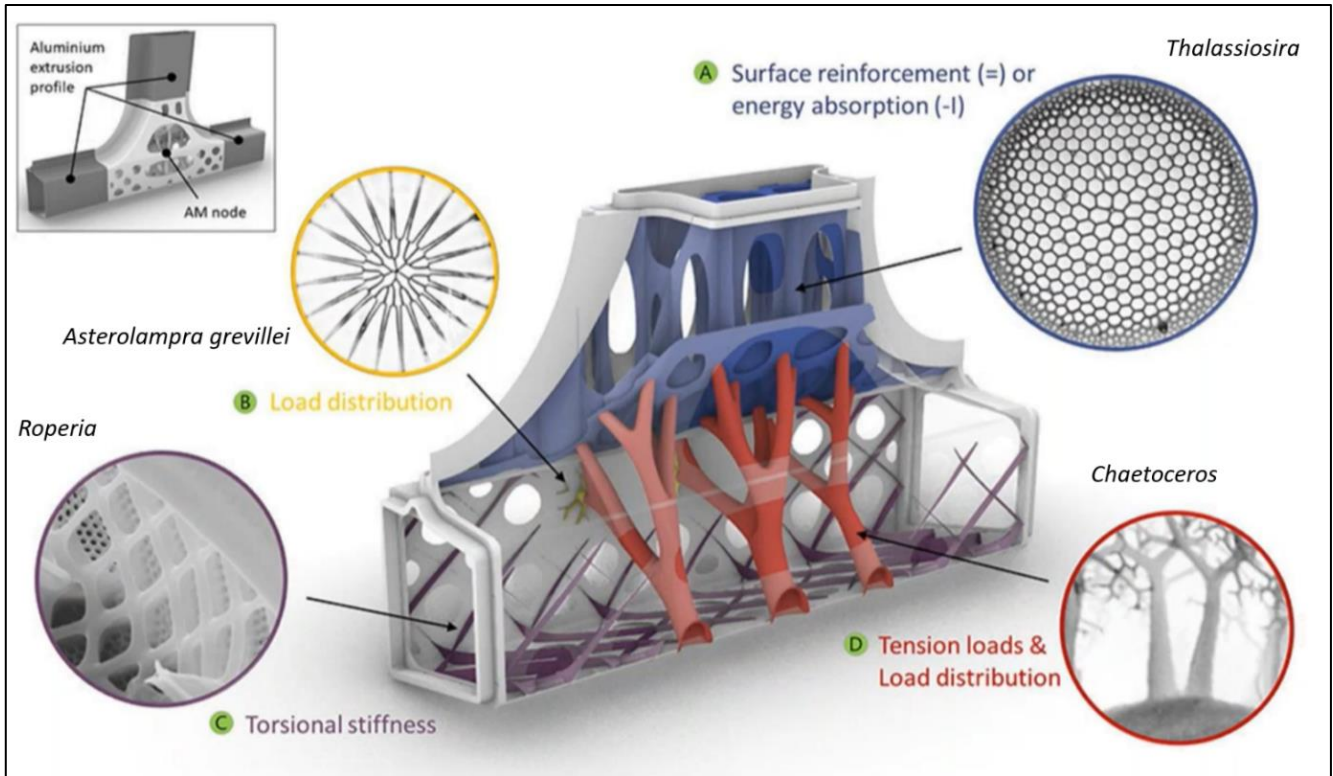


Figure 64: Generative engineering of highly stress B-Pillar poste with nature inspired bionic design features. Image credits: Hyundai and ELISE GmbH.

3.5.7.3 Automotive parts Brackets by BMW - Rolls Royce

Parts that had previously been virtually impossible to realise can be engineered by generative design, which uses computer algorithms for rapid component development. Together, experts and computers create parts that make the best possible use of materials in production. Many potential applications are only possible due to generative design and 3D printing technologies that create the optimised design, as these design could not have previously been made by conventional tools.



Metal components produced by metal PBF in AlSi10Mg4



Removal of part from build plate



Welding the aluminium parts to the chassis of a Roll-Royce Ghost car body

Figure 65: A selection of additive manufactured parts - PBF aluminium (AlSi10Mg), image credits: Rolls Royce & BMW Group.

For the BMW Group, generative design results in topology-optimised solutions, where form and function have been significantly enhanced. The components are around 50 percent lighter than comparable conventional components and make the best possible use of the space available [30] - Figure 65.

3.6 AM design guidelines

Each AM methodology (Section 3.3) has its own set of design guidelines and there are numerous resources available that describe the generic best practice design for an each methodology – a selection of resources are provided in Table 11. Therefore, the objective of this section is to outline the guidelines that are relevant to lightweight metal AM mirror fabrication for astronomy. Section 3.6.2 presents a one-page graphic illustrating the key design rules for metal PBF methodologies and Section 3.6.3 provides a multipage example of how to apply the AM design rules to a cylindrical lightweight metal mirror design.

3.6.1 Reference material

Table 11 lists a selection of generic AM design guidelines available. It is common for each printer type to have its own recommendations regarding design limitations.

Table 11: a selection of resources available in design for additive manufacture.

Reference source	Access information
3D Hubs / Book	'The 3D Printing Handbook: Technologies, Design and Applications', Ben Redwood, Brian Garret and Filemon Schöffner, 3D Hubs B.V. (2017) [31]
3D Hubs / poster (open access)	'Design rules for 3D printing', poster (shown in Figure 66: a poster, created by 3D Hubs, highlighting the design rules across the full spectrum of AM methodologies .) [32] https://www.3dhubs.com/get/3d-printing-design-rules/
Research paper (open access)	'Design guidelines for laser additive manufacturing of lightweight structures in TiAl6V4', J. Kranz, D. Herzog and C. Emmelmann, J. Laser Appl. 27, S14001 (2015) [33]
Book	'A Practical Guide to Design for Additive Manufacturing', Olaf Diegel, Axel Nordin and Damien Motte, Springer series in Advanced Manufacturing, Springer, (2020) [34]

DESIGN RULES FOR 3D PRINTING



	Supported walls	Unsupported walls	Support & overhangs	Embossed & engraved details	Horizontal bridges	Holes	Connecting /moving parts	Escape holes	Minimum features	Pin diameter	Tolerance
	Walls that are connected to the rest of the print on at least two sides.	Unsupported walls are connected to the rest of the print on less than two sides.	The maximum angle a wall can be printed at without requiring support.	Features on the model that are raised or recessed below the model surface.	The span a technology can print without the need for support.	The minimum diameter a technology can successfully print a hole.	The recommended clearance between two moving or connecting parts.	The minimum diameter of escape holes to allow for the removal of build material.	The recommended minimum size of a feature to ensure it will not fail to print.	The minimum diameter a pin can be printed at.	The expected tolerance (dimensional accuracy) of a specific technology.
Fused deposition modeling	0.8 mm	0.8 mm	45°	0.6 mm wide & 2 mm high	10 mm	Ø2 mm	0.5 mm		2 mm	3 mm	±0.5% (lower limit ±0.5 mm)
Stereolithography	0.5 mm	1 mm	support always required	0.4 mm wide & high		Ø0.5 mm	0.5 mm	4 mm	0.2 mm	0.5 mm	±0.5% (lower limit ±0.15 mm)
Selective laser sintering	0.7 mm			1 mm wide & high		Ø1.5 mm	0.3 mm for moving parts & 0.1 mm for connections	5 mm	0.8 mm	0.8 mm	±0.3% (lower limit ±0.3 mm)
Material jetting	1 mm	1 mm	support always required	0.5 mm wide & high		Ø0.5 mm	0.2 mm		0.5 mm	0.5 mm	±0.1 mm
Binder jetting	2 mm	3 mm		0.5 mm wide & high		Ø1.5 mm		5 mm	2 mm	2 mm	±0.2 mm for metal & ±0.5 mm for sand
Direct metal Laser sintering	0.4 mm	0.5 mm	support always required	0.1 mm wide & high	2 mm	Ø1.5 mm		5 mm	0.6 mm	1 mm	±0.1 mm

Figure 66: a poster, created by 3D Hubs, highlighting the design rules across the full spectrum of AM methodologies [32].

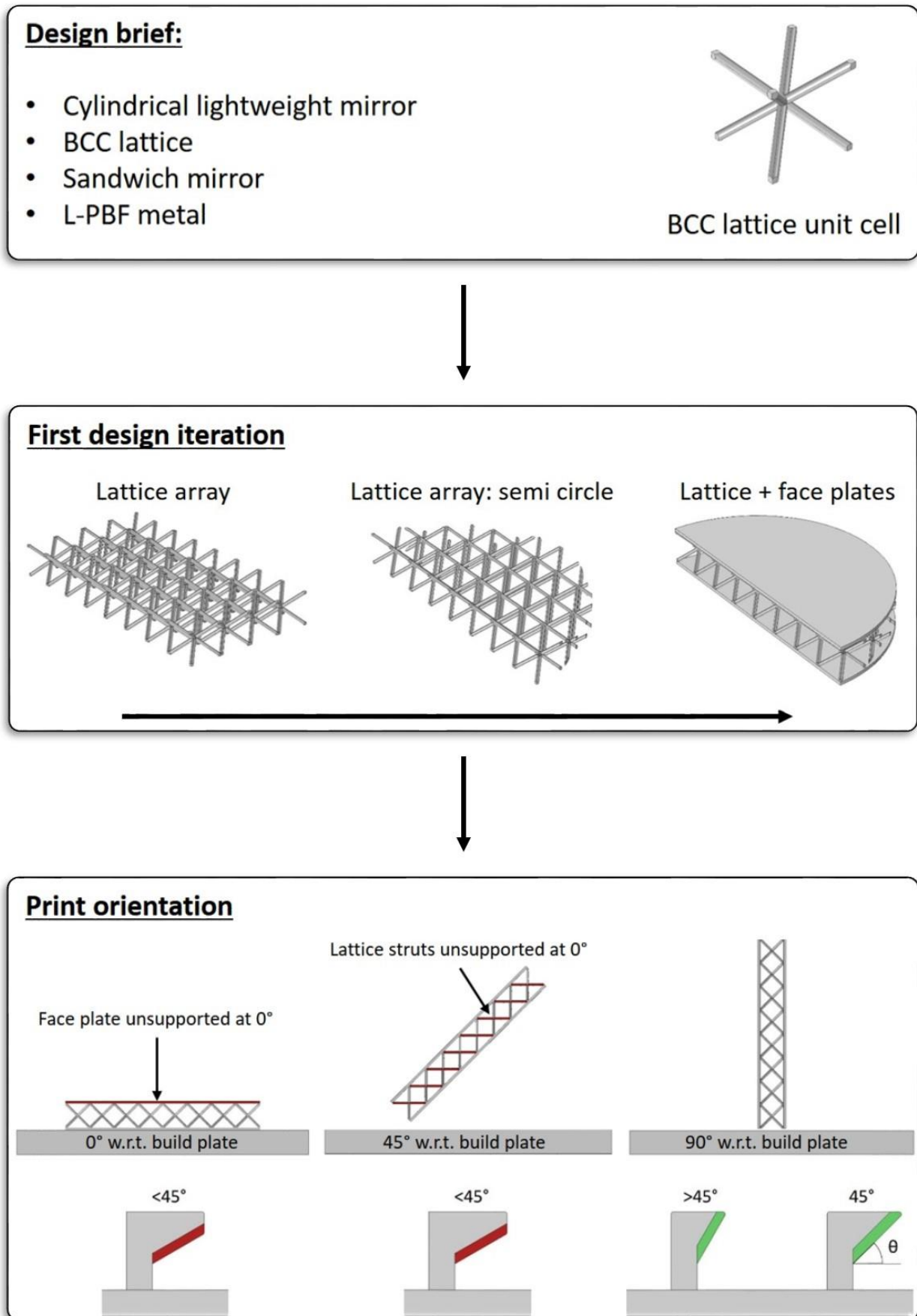
3.6.2 Key design guidelines for AM mirror development

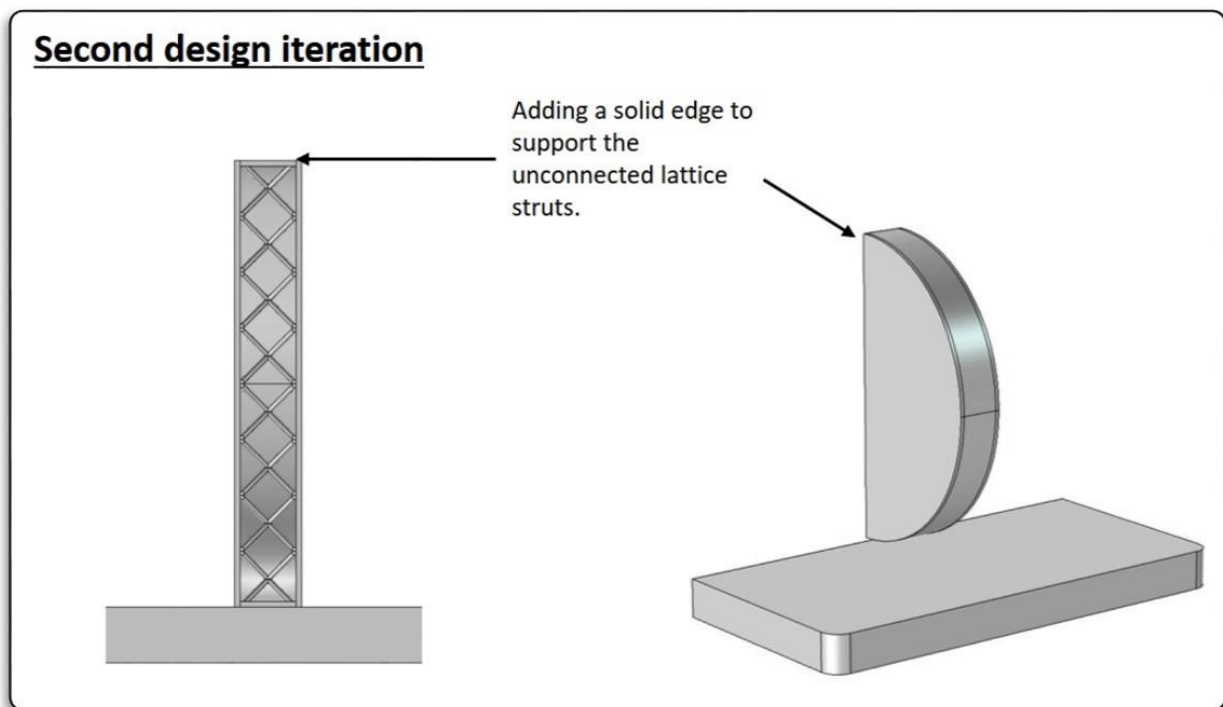
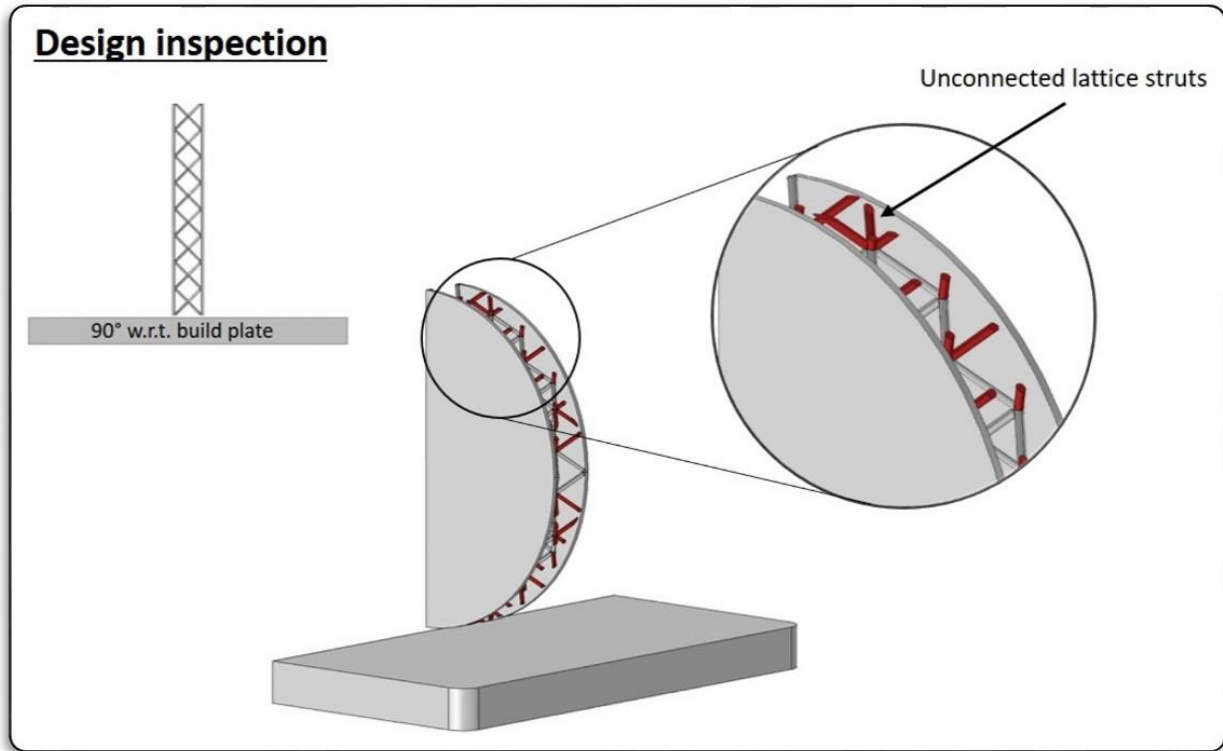
Powder bed fusion (PBF) Metals AM		
Unsupported geometries		
Overhangs at an angle $< 45^\circ$ lead to increased roughness and risk of failure.	Build direction ↑	
Unsupported circles/bores lead to increased roughness, deformed shape and risk of failure.	↑	
Supported geometries		
Overhangs at an angle $< 45^\circ$ require support material or a redesign.	↑	
Support material is temporary; adequate access should be ensured to remove supports, or redesign if necessary.	↑	
For metal PBF, supports are required to provide heat dissipation.	↑	
Orientation independent		
Enclosed volumes should be avoided as unsintered material cannot be removed.		
Sharp corners will not be accurately reproduced and lead to the potential for increased internal stress; fillets minimise these effects.		

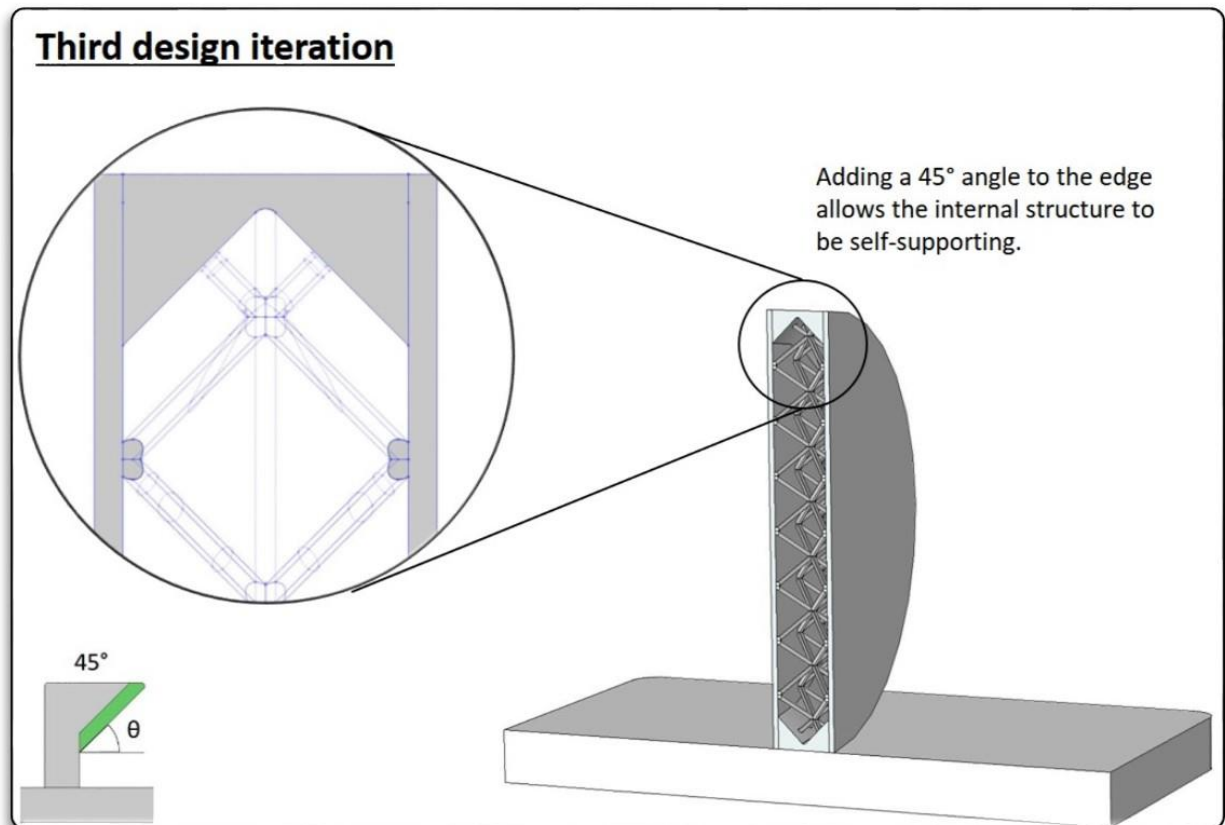
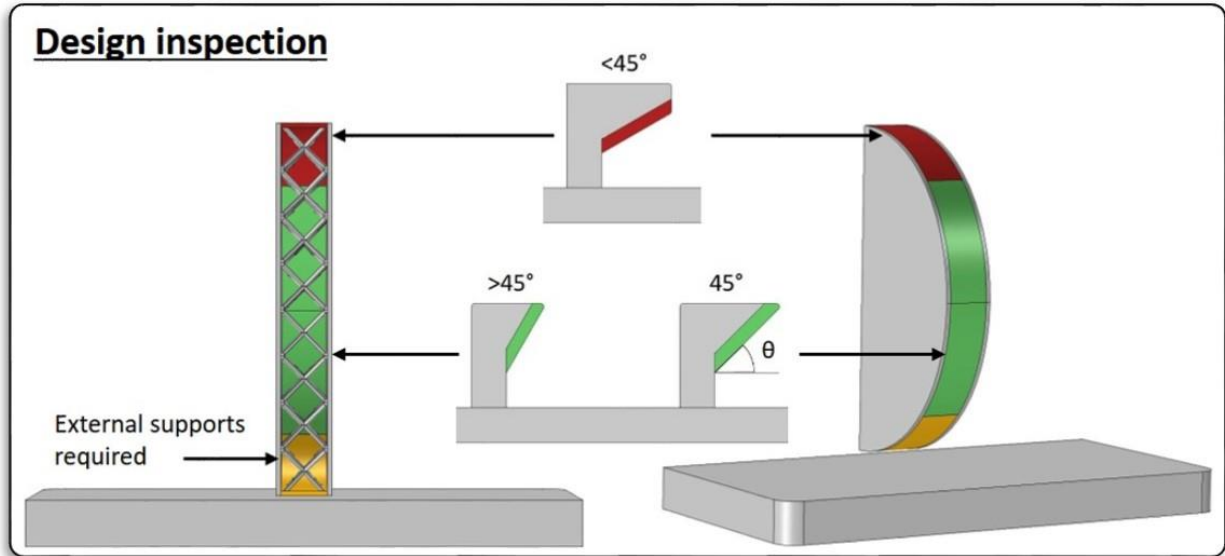
Figure 67: AM design guidelines for metal PBF towards lightweight mirror fabrication, image credit: STFC.

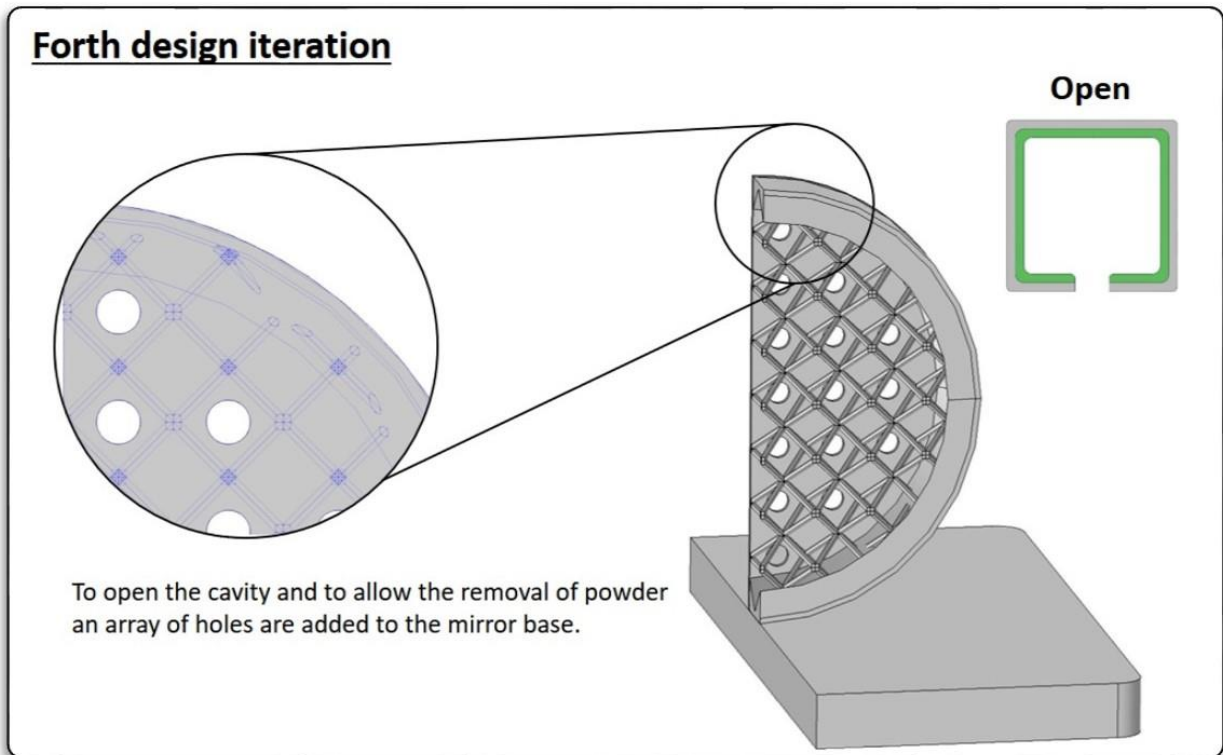
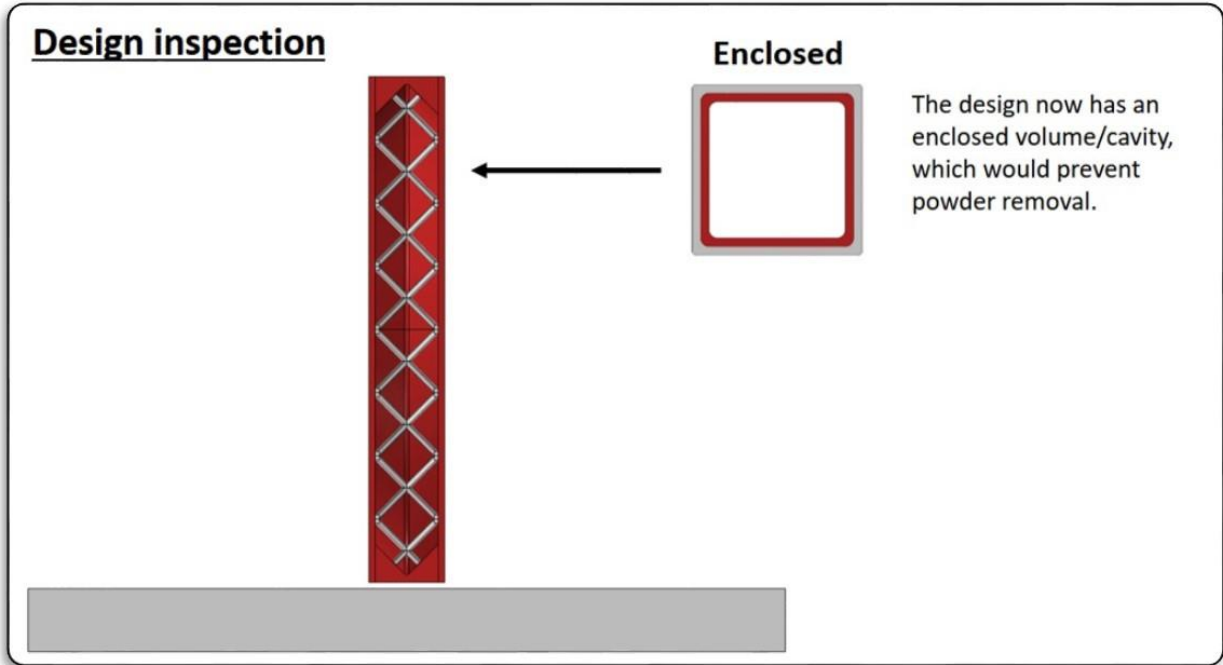
3.6.3 Example: application of design guidelines for AM mirror fabrication

Note – that the graphics highlight only half of the mirror design for clarity. Image credits: STFC & UoS.







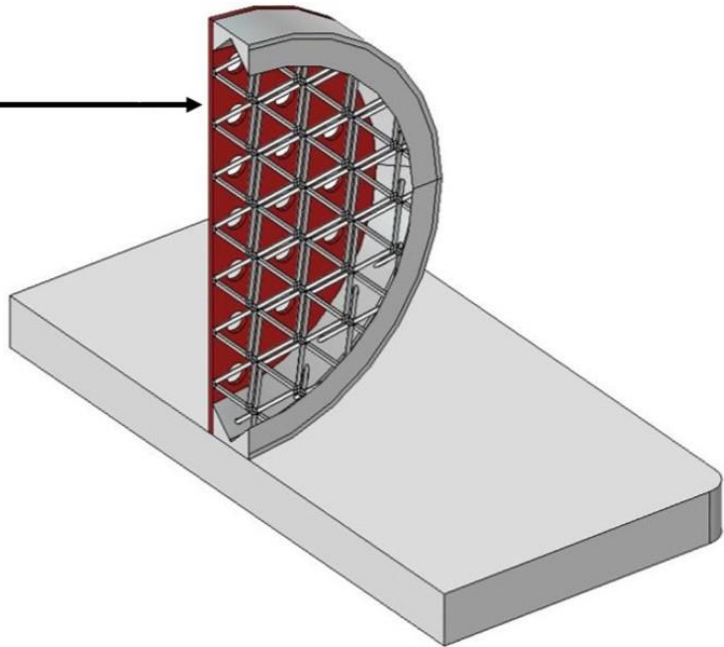




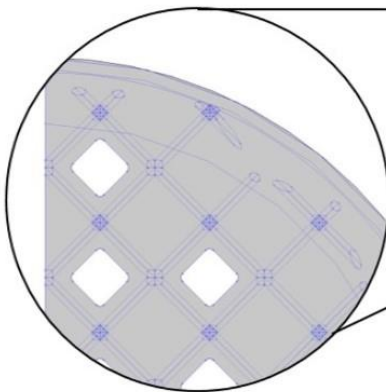
Design inspection



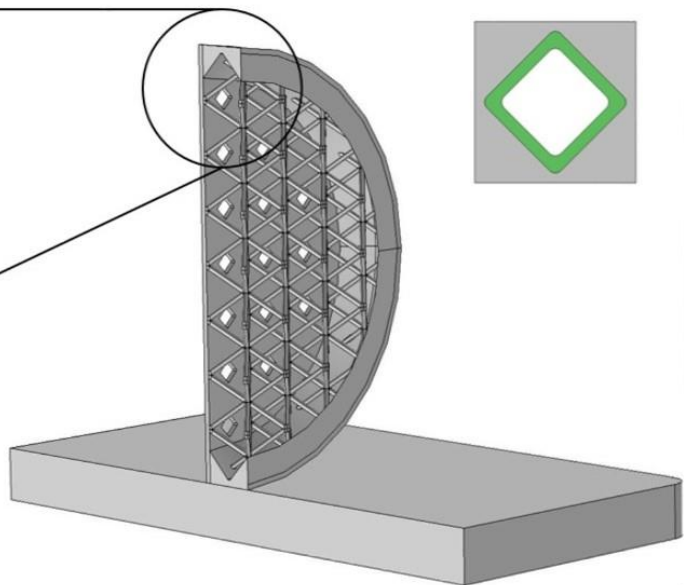
The holes to allow the removal of the powder are circles, which are not self supporting and would require support material.



Fifth design iteration

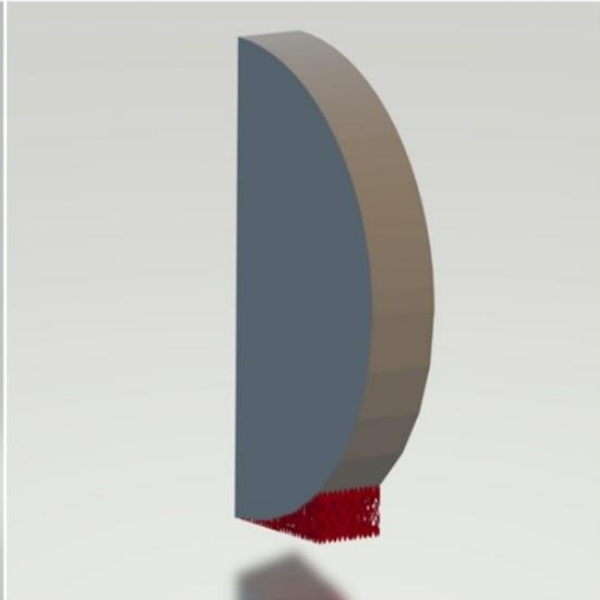
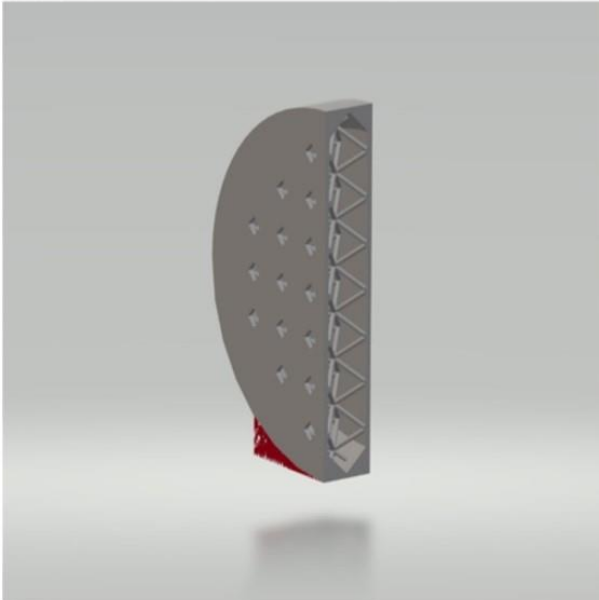


The circular holes have been converted into diamonds which are self supporting and do not require supports.



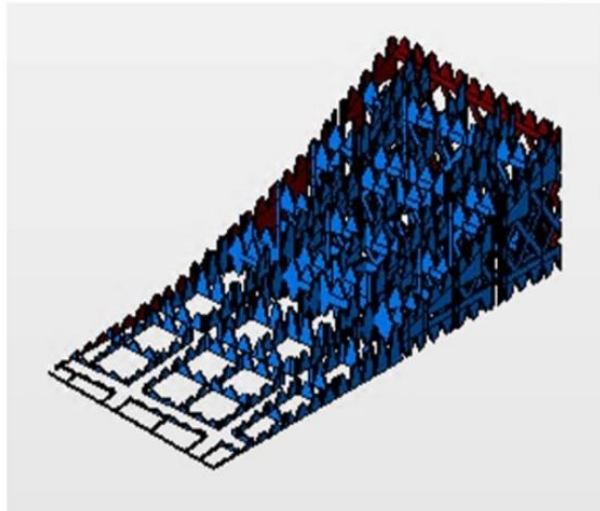


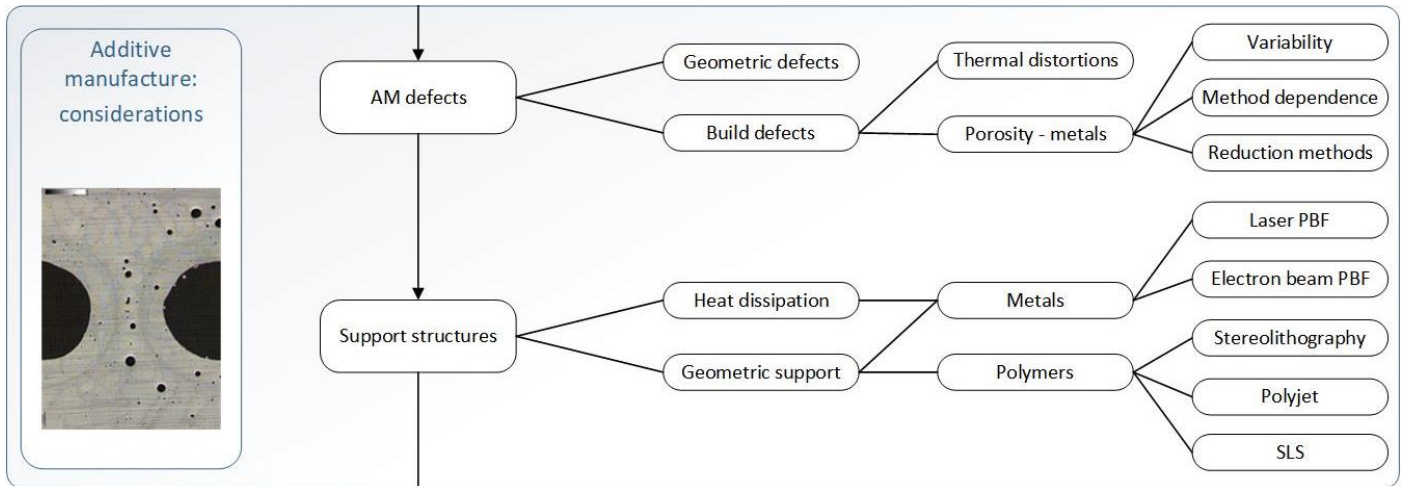
Support generation



The required supports to build the part are shown in red above – only external support is required due to following the design rules.

The geometry of the support structure is shown in blue on the right. In this example the default geometry was used, but other support geometry styles are available depending on software and printer.





3.7 AM Defects

Defects relating to AM builds are common and can be characterised by either: poor adherence to design rules, thermal distortions, or non-optimal build parameters (i.e. the parameters used by the AM machine) - Figure 68.

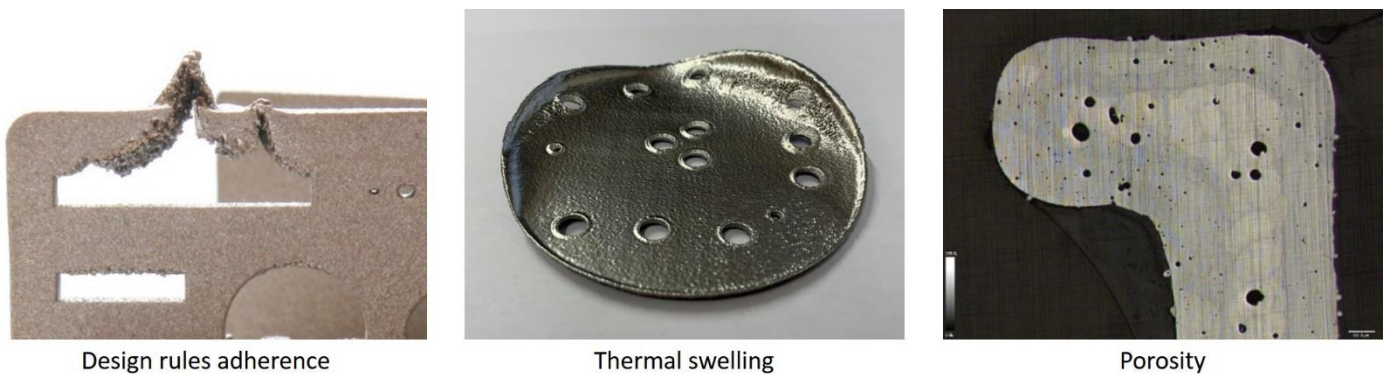


Figure 68: Common defects types encountered using AM, image credits: TNO & UoS.

Poor adherence to design rules typically leads to external defects such as increased roughness, poor fidelity with the original geometry and loss of structure – Figure 69 highlights common defects incurred due to design.

Thermal distortions primarily occur in metallic substrates created via PBF techniques, where a solid structure is created within volume of metallic powder. The volume of loose powder acts as an insulator, which inhibits the ability of the printed structure to dissipate heat – further discussed in Section 3.8.3. Without the implementation of suitable heat transfer conduits, the excess heat leads to swelling and deformation – highlighted in Figure 70.

Internal defects, such as porosity or poor layer adhesion, are effects created via non-optimum build parameters. Often, machines are provided with an optimum setting for a given material and with an operating assumption that the part will function in a non-specialised environment – i.e. room temperature and pressure. However, although these settings may work for the majority of applications, for specialised environments, often seen in astronomy and space science, the generic build parameters may not be optimal. A common defect is porosity within the internal structure, which is potentially problematic for parts intended for vacuum or cryogenic environments. The creation of pores within a substrate is linked to the machine/process parameters and a thorough description of this defect is provided in Section 3.7.1.

Geometric defects			
Unsupported geometries			
<p>Increasing roughness observed on the underside of the ledge for decreasing angle relative to the build plate.</p>			
<p>Roughness and distortion observed on unsupported horizontal bores.</p>			
<p>Increased roughness and distortion observed on an unsupported slot.</p>			
<p>Distortion and loss of structure for unsupported horizontal lattice struts.</p>			
<p>Loss of object definition due to AM machine resolution – layer thickness, laser spot size, etc..</p>			

Figure 69: AM defects resulting from non-adoption of AM design rules, image credits: STFC & TNO.

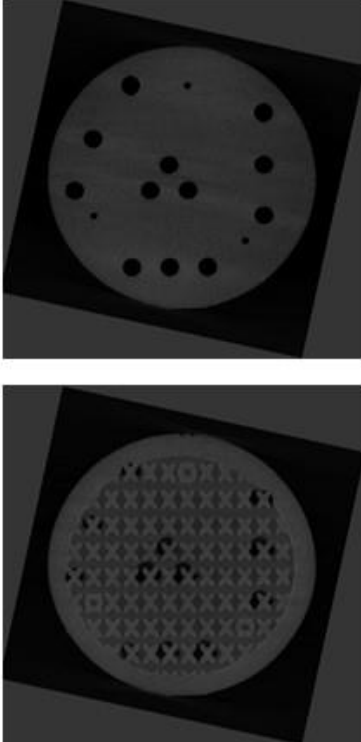
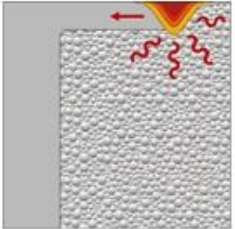
Geometric defects		
Unsupported geometries		
<p>Insufficient access to remove powder from an internal cavity when using EB-LPF.</p> <p>XCT cross sections highlight the insufficient access holes to remove the semi-sintered powder (top) and semi-sintered powder in between the internal lattice structure of the cavity (bottom).</p>		
Build defects: swelling and thermal distortion		
<p>Swelling and thermal distortion in metal AM is caused by an inability to adequately dissipate heat leading to excess powder being melted (swelling) and distortion.</p>		

Figure 70: AM defects caused by poor understanding of the AM build process - geometric and thermal. Image credits: STFC, NPL & UoS.

3.7.1 Porosity

Parts made with powder and filament based 3D printing technologies, i.e. PBF and material extrusion, are prone to display a significant amount of porosity. There are pores with irregular shapes (keyhole) and uniform shapes (spherical). Pores are present at different locations within a part and the position affects the mechanical and physical properties (Figure 71).

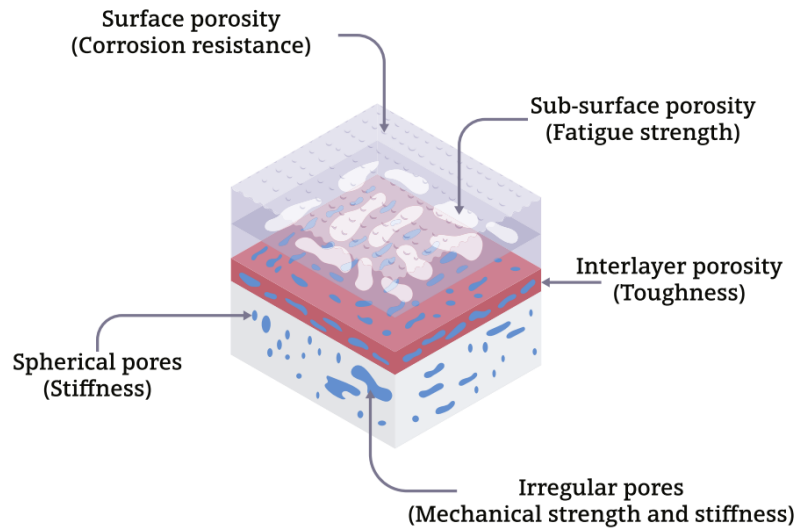
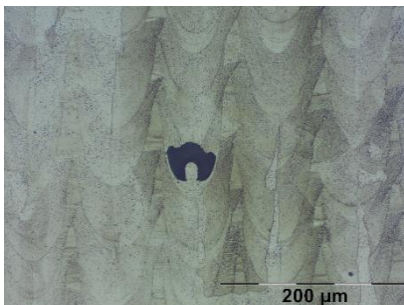


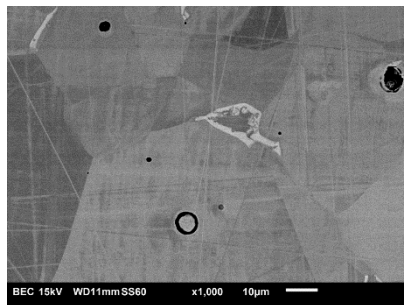
Figure 71: The effect of types and locations of pores on the mechanical properties of AM processed material, image credit: Al-Maharma, A., et al. [35].

Many AM parts are produced for critical applications in aerospace, industrial and medical sectors. Inter-layer pores are very critical to the toughness properties of the part when loads are applied transverse to the layer orientation as these defects induce delamination. Other locations critically affect the tensile and fatigue strength, since they act as initiation points under stress. Furthermore, a rough surface decreases corrosion resistance.

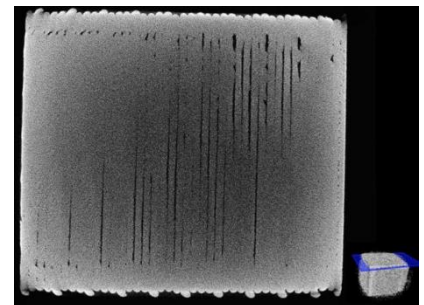
There are multiple types of microstructural pores in parts fabricated by AM processes (Figure 72). There are spherical pores (intra granular pores) resulting from a powder containing entrapped gas introduced by the gas atomization process of the powder particles. Whereas, keyhole porosity and micro-cracks usually form when processing parameters are incorrect. Parts fabricated by material extrusion display linear pattern pores between the deposited beads at the interfacial region. The inter- and intra-layer pores create anisotropy in the material properties.



Optical microscopy image of a 316L PBF part; keyhole porosity is located on the granular boundaries. Image credit: ECN



SEM image of intra-granular pores within a 316L Binder Jetting part. These pores are usually small and closed. Image credit: TNO



Micro CT scan of linear pattern pores in 316L UltraFuse part. Image credit: BASF.

Figure 72: Multiple types of porosity in AM parts.

3.7.2 Hidden material structure

The images in Figure 73 clearly display that there is a significant difference internally between metal AM processes and materials. The presence of porosity is not apparent from the outside of an AM part; however, metallographic examination is a common method to investigate the internal microstructure.

Powder Bed Fusion AlSi10Mg	Powder Bed Fusion TiAl6V4	Binder jetting steel
<p>Shot peened SEM image - 50x magnification</p>	<p>No cleaning SEM image - 50x magnification</p>	<p>Bead blasting SEM image - 50x magnification</p>
<p>50x magnification</p>	<p>50x magnification</p>	<p>50x magnification</p>
<p>Large pores are present throughout the cross section - keyhole porosity caused by incorrect process settings.</p>	<p>Larger pores located dominantly at the edge; known as sub-contour porosity.</p>	<p>Near optimum. Fine intra-granular porosity uniformly distributed throughout the cross section.</p>

Figure 73: 3D printing of metal. Similar processes, different materials, different results. Image credits: TNO.

3.7.3 Metallographic examination.

The microstructure and porosity of a sample can be observed via cross-sectional analysis. This examination requires a specimen to be embedded in a slow setting epoxy. Then, by using multiple grinding, polishing and etching steps, the micro and grain structure is exposed. Optical microscopy and Scanning Electron Microscopy (SEM) can be used to examine the structure (Figure 74).

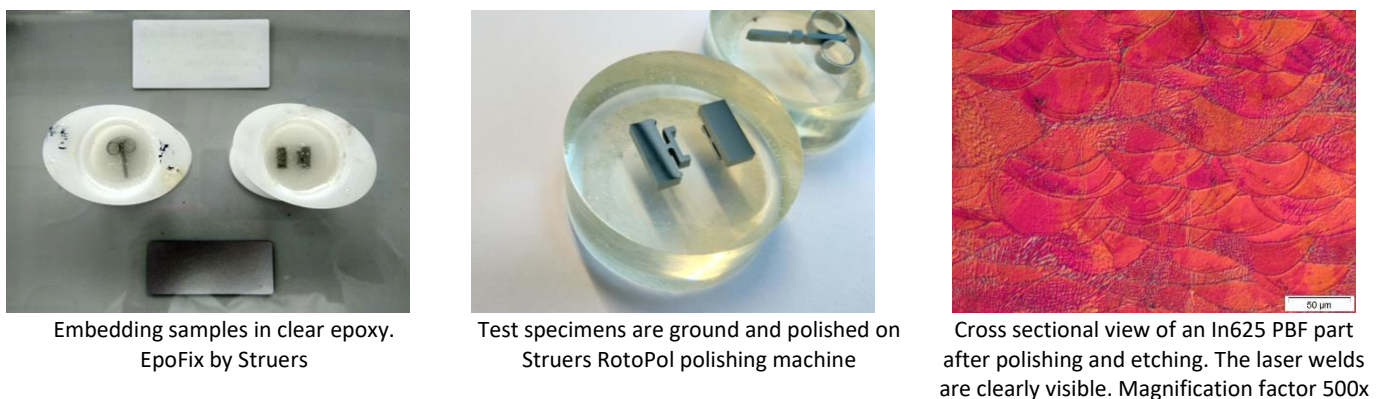


Figure 74: Preparation of Metallographic examination samples, image credits: TNO.

3.7.4 Micro Porosity – Powder Bed Fusion

Current levels of porosity have improved when compared against early AM processes. Typical PBF parts are approximately 99.5% dense and in many cases, 0.5% porosity does not have an influence on the mechanical properties of the part. This level of porosity is comparable with forged materials. Porosity types, such as keyholes, lack of fusion and gas porosity, are detected in PBF parts at preferential locations (Figure 75).

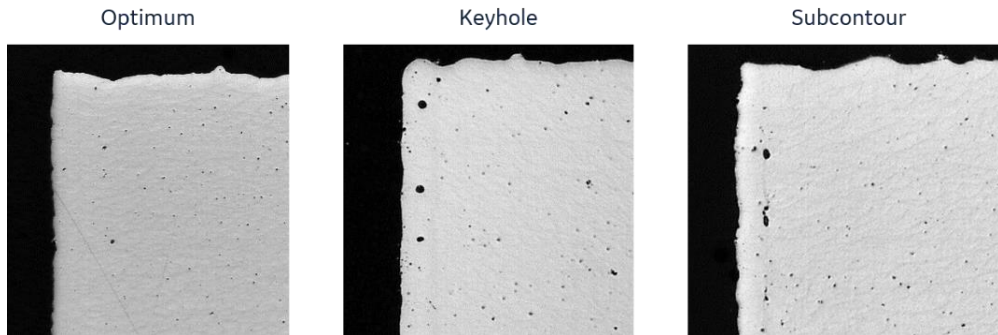
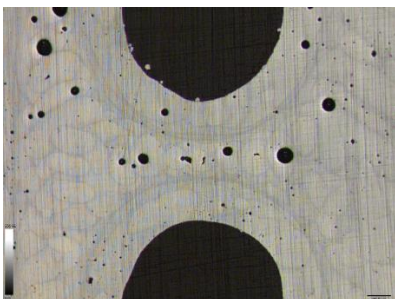


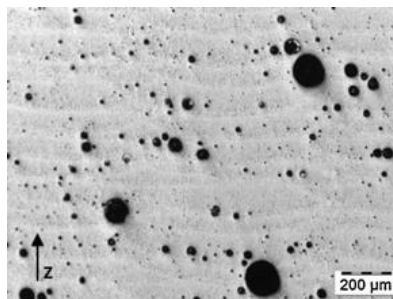
Figure 75: Different types of porosity in PDF parts. Contour porosity in a result of dissimilar scan strategies, image credit: GE Additive [36].

The presence of porosity is reflected in elongation and in reduced tensile strength. Fatigue life is negatively impacted by surface conditions and porosity. Pores can act as crack initiation sites and accelerate crack growth. The shape and location of the pores need to be considered. Randomly distributed gas pores are less impactful than patterned porosity. Where pores are located in a row, a crack will migrate and failure will occur more quickly. Thin walls require additional care due to heat dissipation as the thin walls are surrounded by loose powder. This will limit the ability to conduct the heat out of the part and leads to heat build-up - resulting in over melting and gas porosity. The risk on creating porosity is also present with overhanging surfaces – also termed *downskins*.

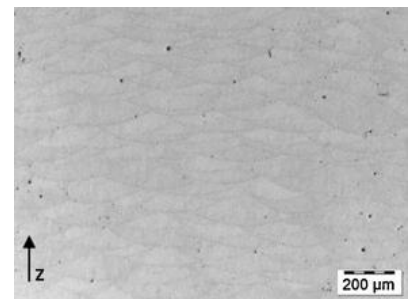
Process parameters related to the laser scan strategy, such as hatching distance and energy input, in addition to material quality and conditioning, all impact the generation of porosity (Figure 76). Aluminium, in particular, is susceptible for nucleation and growth of hydrogen pores in the melt pool. Moisture on the powder particle surface, as well as dissolved hydrogen in the powder material, leads to pore formation. Hydrogen pores can be reduced by external powder drying and optimised scan strategy [37].



PBF AlSi10Mg Flexible hinge with hydrogen Pores (image credit: TNO)



AlSi10Mg PBF sample with large laser beam diameter ($d_s = 1\text{mm}$) and low scan speed ($v_s = 2250\text{ mm/s}$). Image credit: Fraunhofer.



AlSi10Mg PBF sample with small laser beam diameter ($d_s = 0.3\text{mm}$) and high scan speed ($v_s = 2250\text{ mm/s}$). Image credit: Fraunhofer.

Figure 76: Influence of process parameters and laser beam diameter on gas pore density.

PBF processes allow the user to alter multiple process settings and this will influence the part quality and build-up speed. By changing process settings, such as scan strategy, layer thickness and (multi) laser power, the micro porosity, grain structure and internal properties can be altered. Recent methodologies, such as remelting and Hull – Core strategies, do not affect the outside of a 3D printed part, but may influence the mechanical properties to great extent (Figure 77).



Hull – Core scan strategy. The outer edge of the part is laser melted with optimised process settings for accuracy and density. The core is printed with settings optimised for speed and productivity [38].



SLM Only



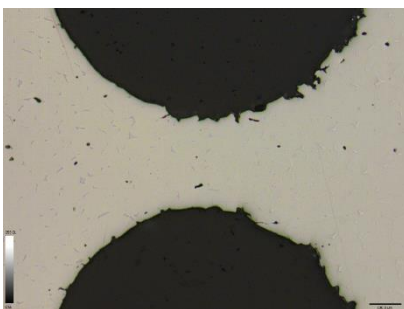
SLM and remelting

Remelting scan strategy to reduce porosity and improve surface quality [39]

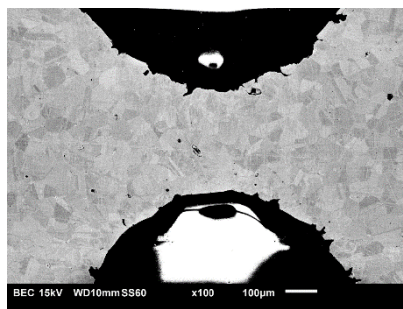
Figure 77: By altering process settings, such as scan strategy and laser power, the porosity of a PBF part can be altered, image credits: SLM Solutions, KU Leuven.

3.7.5 Micro-porosity – binder jetting

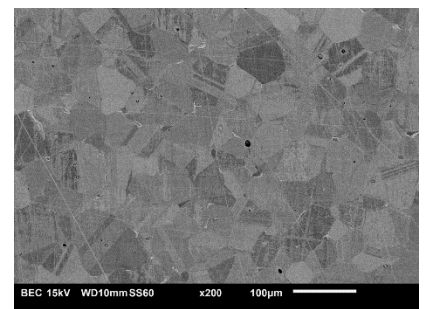
With binder jetting processes, the consolidation process takes place outside the machine in the form of a sinter step. Incomplete sintering causes inadequate sinter necking and diffusion, which results in residual porosity. Over sintering, or sintering at too high a temperature, causes pores to become exaggerated. Microscopic analysis of the 316L binder jetting sample (Figure 78), displays closed, intra-granular porosity, with pore size in the range of 5 – 75 μm. According literature, a density of approximately 96% of theoretical can be achieved for 316L [40]. Higher densities can be achieved by performing HIP (Hot Isostatic Pressing); with this technology almost 100% dense is possible.



Optical Microscopy of Flexible hinge.
100x magnification



Scanning Electron Microscope image in
Back-scatter mode.
Magnification factor 100x



Uniform micro-grain structure, which is
characteristic for binder jetting, is observed.
Magnification factor 200x

Figure 78: Optimised density obtained with Binder jetting printed after debinding and sintering, image credit: TNO.

3.7.6 Reduction of porosity by hot isostatic pressing

Powder Bed parts are prone to internal stresses and, occasionally, pores. HIP can be a part of the thermal post-processing steps and through this common practice a closure of internal gas pores in AM metal parts is possible (Figure 79). At an elevated temperature and pressure, a 50 μm gas pore will shrink to a diameter of $\sim 2\ \mu\text{m}$, using this process almost 100% density may be obtained.

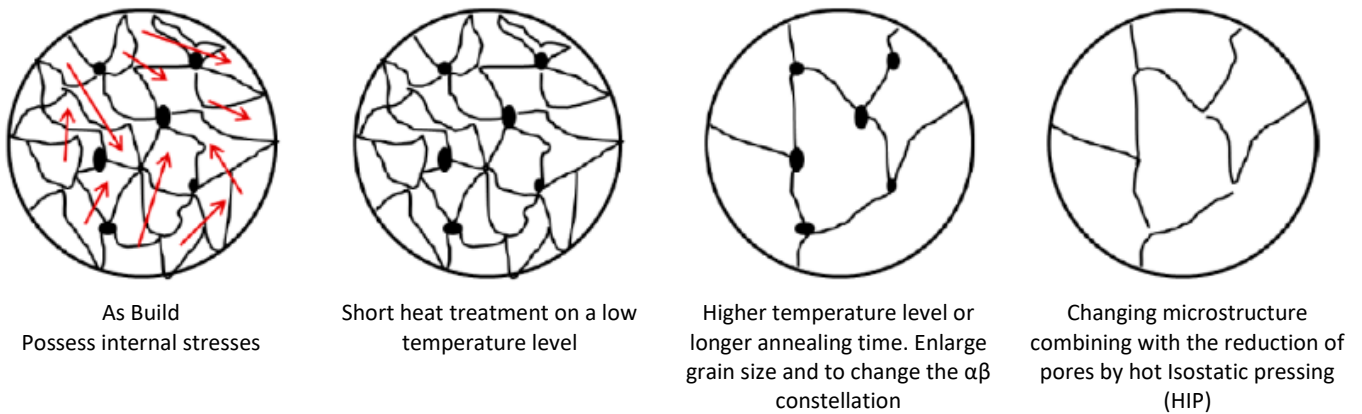


Figure 79: Schematic representation of the microstructure of Ti6Al4V in different heat-treated conditions, image credit: NLR.

Besides the decrease and closure of pores, HIP also has an effect on the microstructure of the contour lines and hatches, where the consistency of mechanical properties are improved - increased tensile strength, impact strength and ductility are detected (Figure 80). There is no need to HIP components if the existing mechanical properties are acceptable for the performance of the part, as the cost will increase with the additional post-processing step.

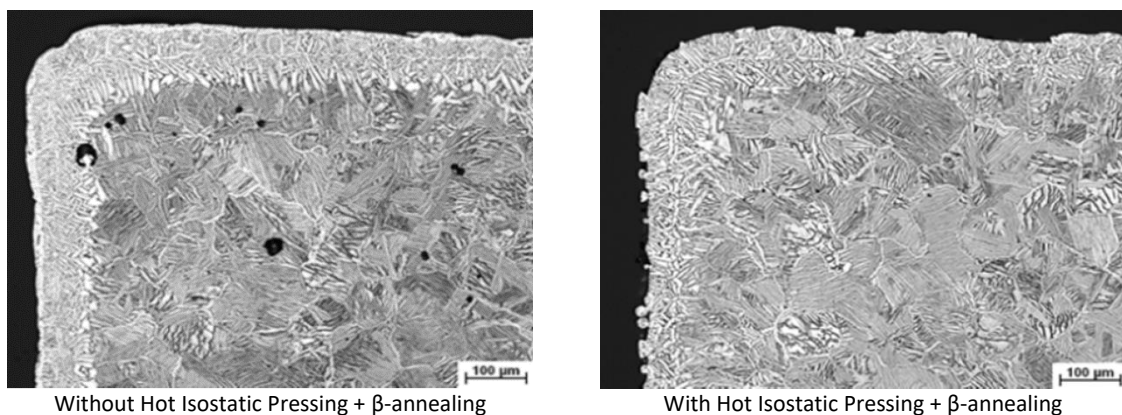


Figure 80: Microstructure of PBF Ti6Al4V without and after HIP, image credit: NLR.

HIP is a specialised process and requires dedicated equipment; several companies within Europe provide the process as a service, for example:

- Bodycote – Belgium
- Isostatic Toll Services – Spain
- Quintus - Sweden

3.8 Support structures

The support structure generation is dependent upon the AM method and material – for example, some polymers use a support structure made of a different soluble material, whereas metals use the same material for the supports and component. Due to the breadth of AM methods and materials and the unique construction, in terms of geometry and material, of the support structures for the different methods, this section will only provide a broad overview of the topic. The following key information is provided: the role of support structures, support structures for polymers and support structures for metals.

3.8.1 The role of support structures

Figure 81 highlights the two key roles that support structures and material play in AM. The first role, across all materials (Section 3.3.7.6) and methods (Section 3.3), is to support the geometry during build, by either providing support for overhanging regions, or by anchoring a part onto the build plate. The second key role is metal PBF specific and refers to the role that support structures play in dissipating heat from the *melt pool* to the build plate, which prevents swelling and thermal distortion (Figure 70).

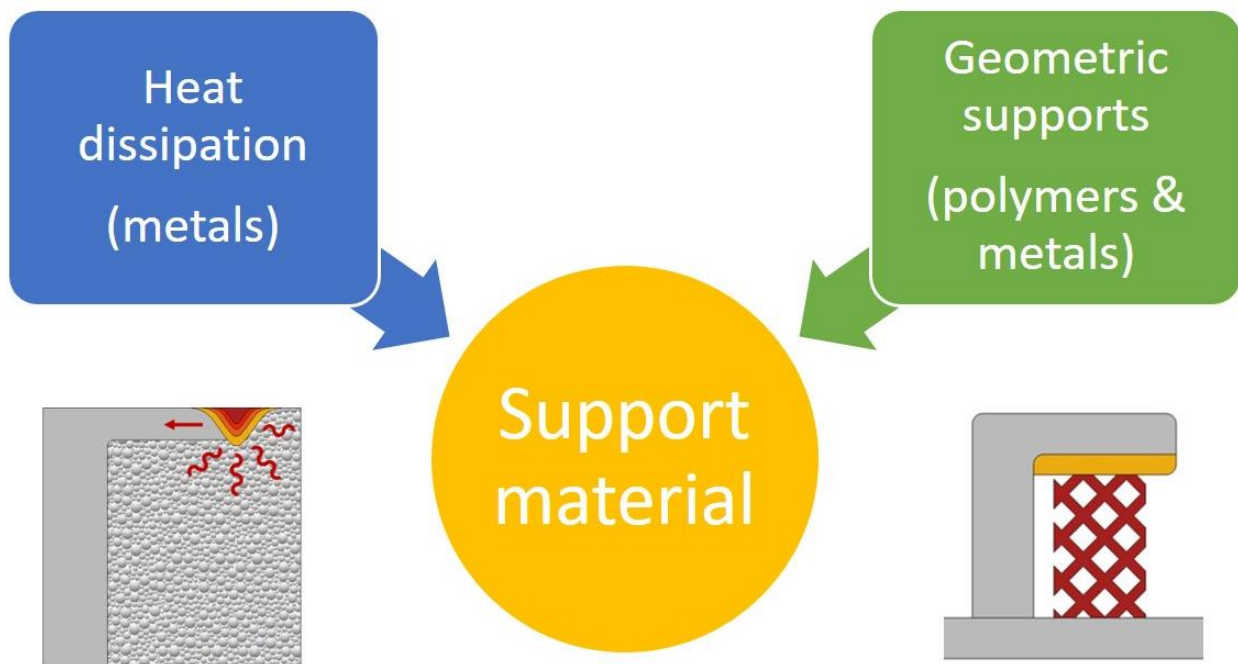


Figure 81: the key roles undertaken by support material for AM components, image credit: STFC.

3.8.2 Polymer support material

There are a number of polymer printing methods available: FDM, SLA, material jetting (polyjet) and SLS. Due to the prevalence of FDM within the 3D printing market, there is a broad range of support material information already available and therefore this section will focus on the less common polymer printing methods: SLA, polyjet and SLS.

3.8.2.1 Stereolithography

SLA uses photo-polymerisation to cure liquid resin into a solid part. Support material is required to support the part physically during the build process and to attach it to the build plate. Figure 82 highlights the OPTICON test geometry printed via SLA using VisiJet Flex and the required support material, emphasised in red, to support the geometry.

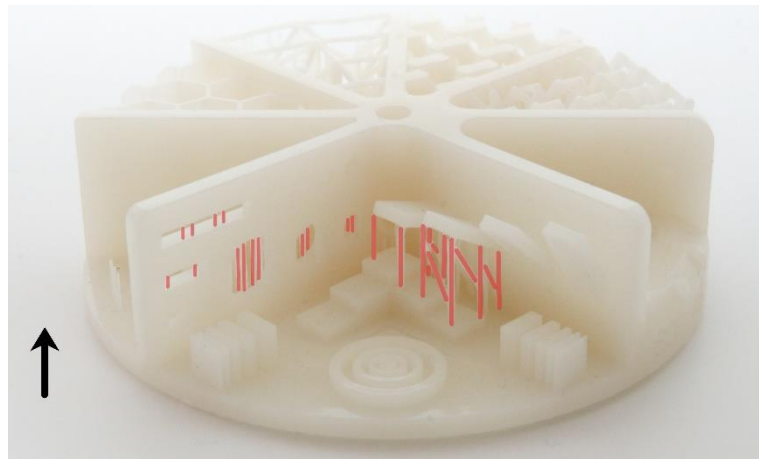
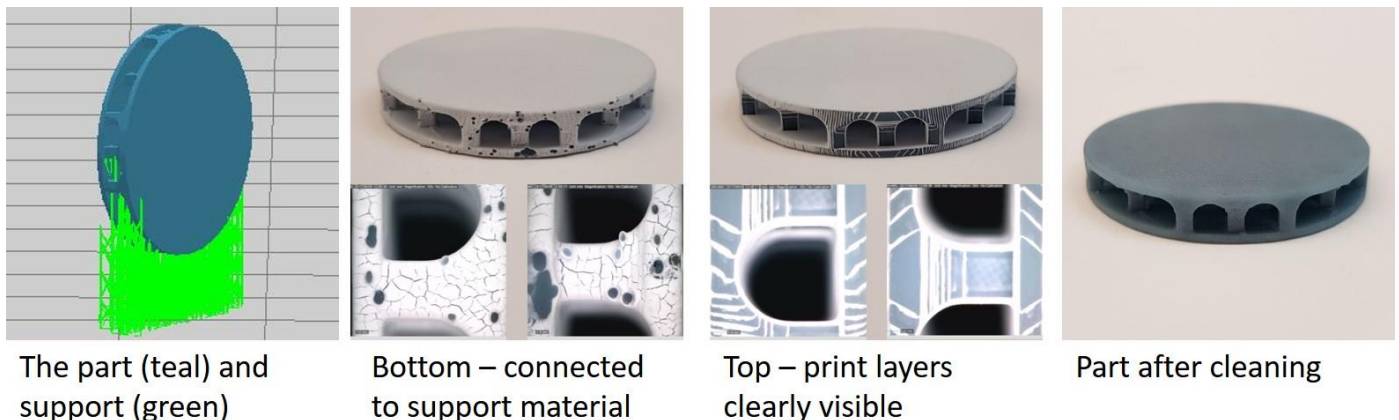


Figure 82: an example of an SLA print and required support material (highlighted in red); the arrow demonstrates the build orientation, image credit: TNO & STFC.

In SLA, the support structure and the part share the same material and there is a physical continuation between the part and the supports. Therefore, upon removal of the support material there is an area of increased roughness, as demonstrated in Figure 83. In the figure, the part was printed via SLA using the high performance polymer Bluestone and the two images in the middle of the figure highlight the part prior to cleaning to remove the excess SLA residue.



The part (teal) and support (green)

Bottom – connected to support material

Top – print layers clearly visible

Part after cleaning

Figure 83: SLA support material added to the part within the software (*left*); the connection points of the support material on the part (*middle-left*) and the non-connected top section (*middle-right*) prior to cleaning; and the part after cleaning. Image credits: CA Models & NSTP3-PF-007 team.

3.8.2.2 Polyjet

Figure 84 and Figure 85 highlight the role of support structure for polyjet printing. The support material is a requirement even on overhangs that are $> 45^\circ$ to the build plate. In the examples shown, the support material is soluble and removed via waterjet, but as demonstrated in Figure 85, access to remove all support material is required. An aesthetic result of the support material is a limitation on the gloss/matt finish of the part, if support material is required, a matt finish will result.

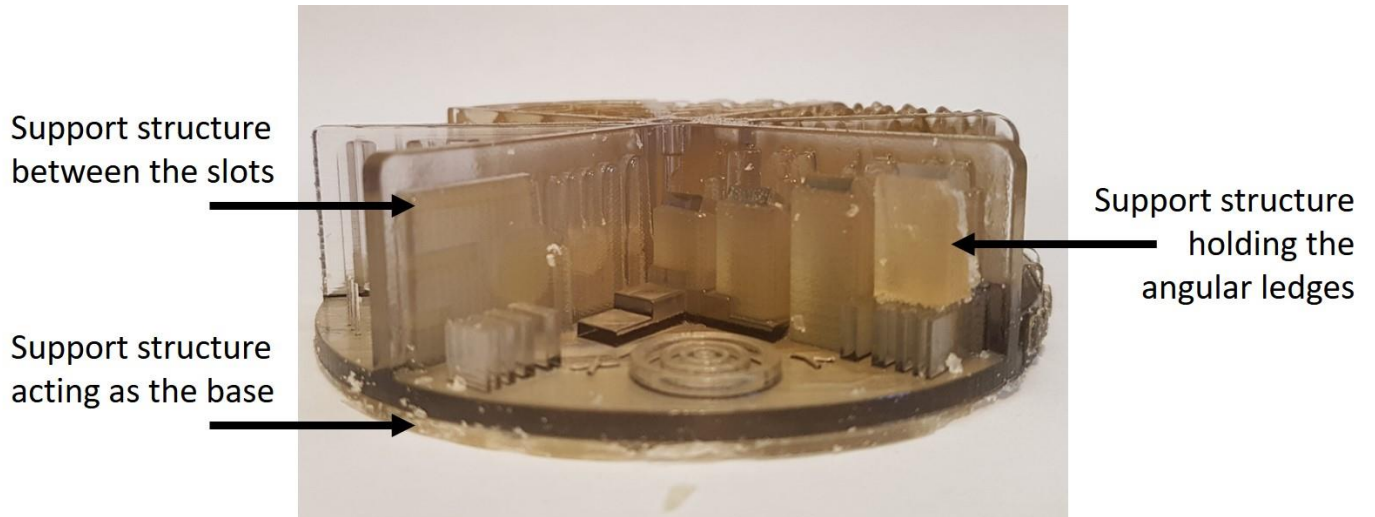


Figure 84: soluble support structure used to build the OPTICON test geometry mark in VeroClear (acrylic-like), image credit: STFC.

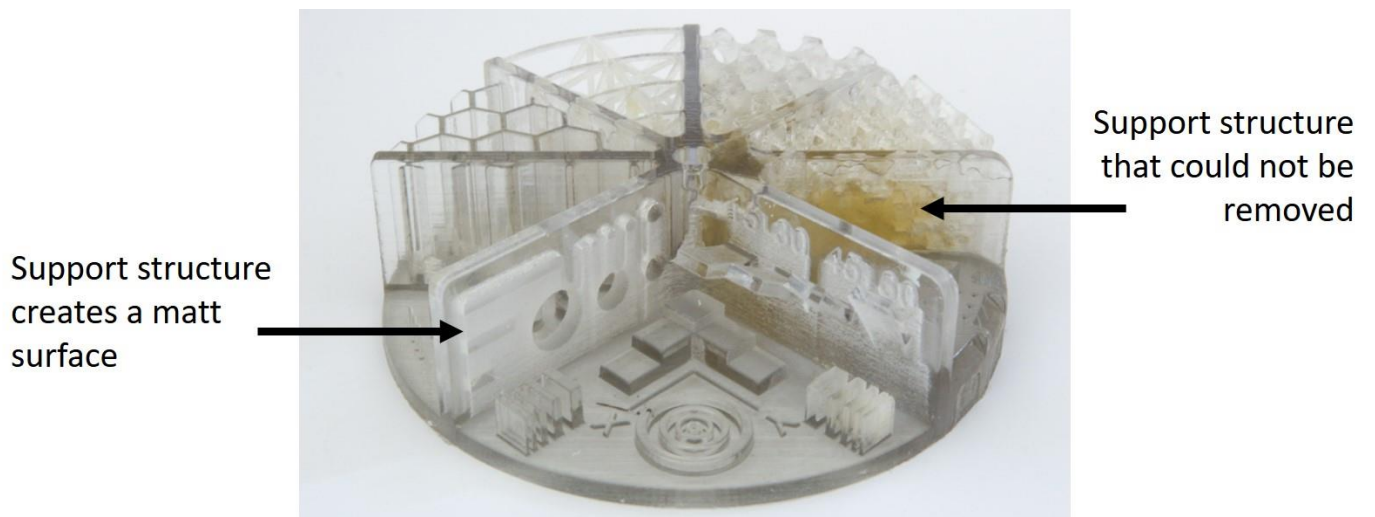


Figure 85: the OPTICON test geometry with the majority of the support structure removed, image credit: STFC.

3.8.2.3 Selected laser sintering

Figure 86 highlights a glass filled nylon benchmark created via SLS with no support material. SLS is a powder process where successive layers of powder are sintered together using a laser. Unlike the equivalent metallic PBF methods, SLS does not require support material for heat dissipation (discussed in Section 3.8.3) and, therefore, the sintered part is self-supported by the surrounding loose powder. To minimise heat related defects (warping, shrinking), the powder bed is heated to just below the sintering temperature [32].

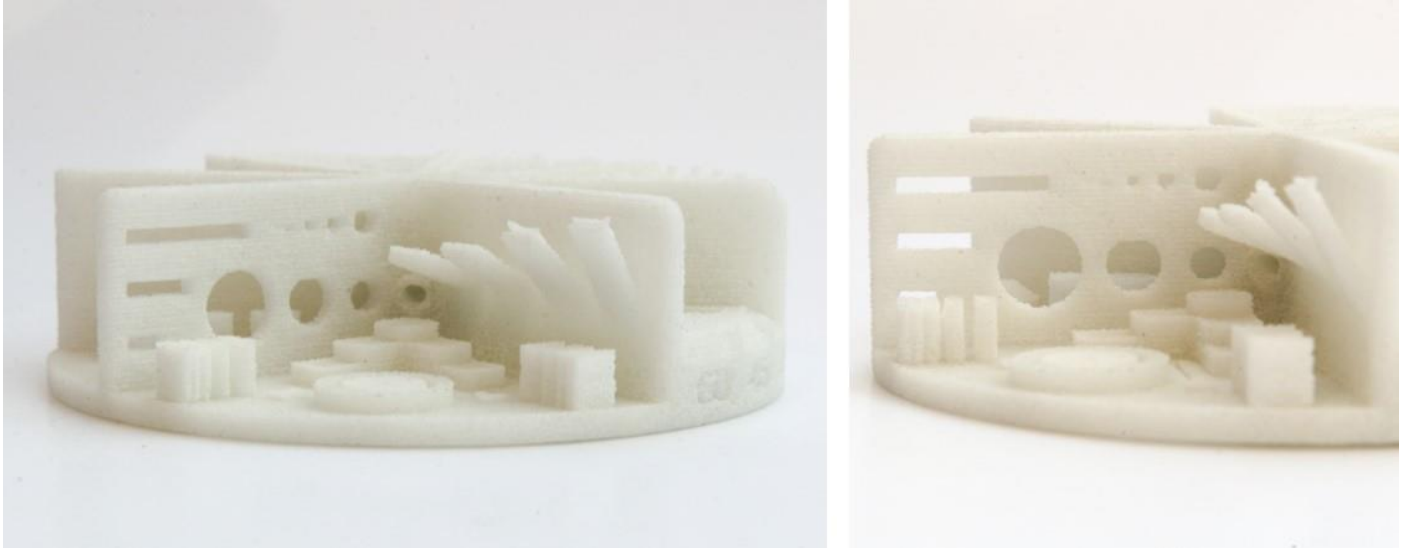


Figure 86: selected laser sintering of the OPTICON benchmark; no supports are necessary as the powder bed acts as its own support, image credit: TNO.

3.8.3 Metallic support material

In metallic PBF methodologies, support structures have the primary role of heat dissipation and a secondary role for geometric support. In theory, overhanging structures could be supported by the powder bed as demonstrated by SLS of polymers; however, the high temperature required to fuse the metallic powder needs to be dissipated to prevent thermal distortions and swelling (Section 3.7). The thermal conductivity of the metallic powder is generally ~ 100 times less than that of a fused solid [41], therefore, to ensure that the heat is dissipated and to prevent thermal defects, support structure is required to conduct the heat efficiently from the overhang to the base plate – as demonstrated Figure 87.

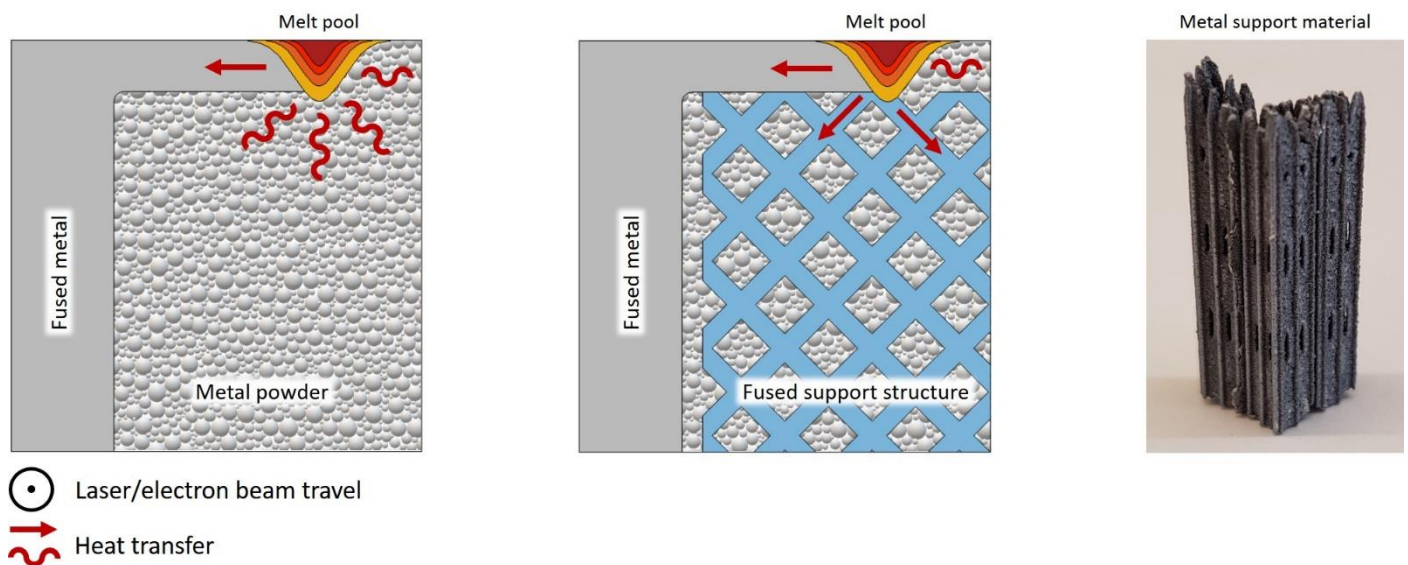


Figure 87: heat transfer from the melt pool to the local environment. *Left* – poor conduction of the heat source within the surrounding metal powder; *middle* – improved conduction via the inclusion of the support structure (blue lattice); and *right* - an example of a metal support structure. Image credits: STFC.

Removal of metallic support material is generally more challenging than for polymers. First, the part is removed from the build plate, in EB-PBF this can sometimes be achieved by hand, as the part is not necessarily be fused to the build plate; however, more broadly within PBF techniques, electric discharge machining (EDM) is used to separate the part and build plate. Typically, removal of the support material from the part is achieved via manual cutting pliers (Figure 88) followed by further subtractive machining depending on the quality of the surface finish required.



Figure 88: removal of metal supports using cutting pliers, image credit: TNO.

3.8.3.1 Laser powder bed fusion

Figure 89 highlights how support material (red) has been added to a mirror design for printing. The circular holes, shown in the design, allow unfused powder to be removed from the internal cavity.

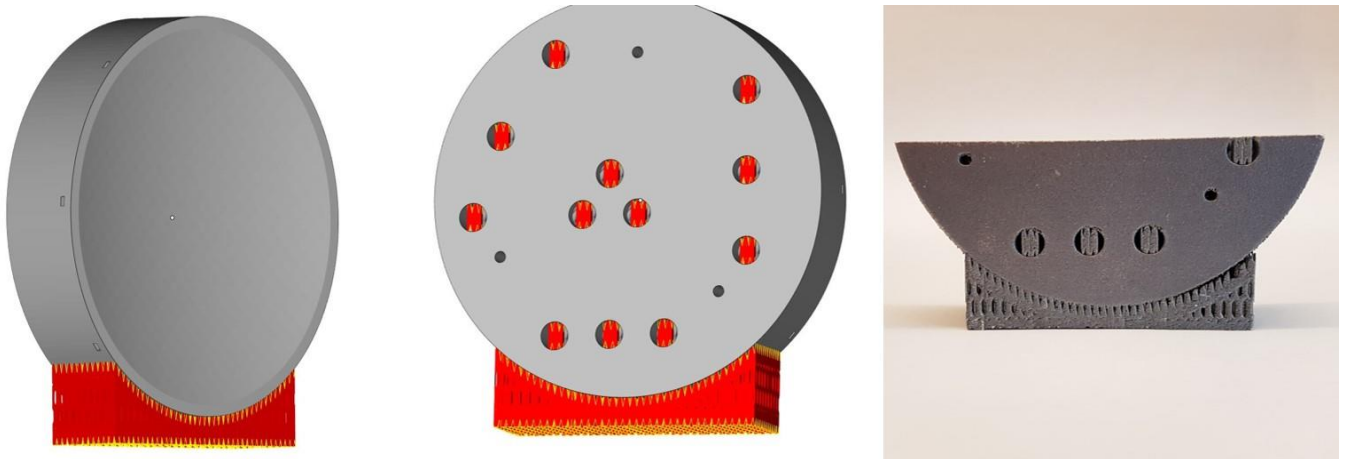


Figure 89: *left & middle* - support material generated for an aluminium L-PBF circular mirror substrate and *right* – printed example, image credit: CA Models & NSTP3-PF2-008 team.

The support material does create increased roughness in the region of interface and this roughness should be considered at the design stage depending on the post-processing route that is desired. Figure 90 highlights a second example of an L-PBF circular mirror and demonstrates how the support material has been orientated with respect to the part. The image on the *right* identifies the increased roughness caused at the interface of the mirror substrate and the supports.



Figure 90: *left & middle* - support material generated for an aluminium L-PBF circular mirror substrate; *right* – roughness observed at the support – substrate interface, image credit CA Models & NSTP3-PF-007.

3.8.3.2 Electron Beam Powder Bed fusion

EB-PBF semi sinters the build volume of the part prior to the fusion/melting of the required geometry. The advantage of this method is that the semi-sintered powder provides a better foundation to build upon than loose powder; however, heat dissipation via support structures is still required albeit not providing a direct link to the build plate – as demonstrated by the shortened supports in Figure 91.

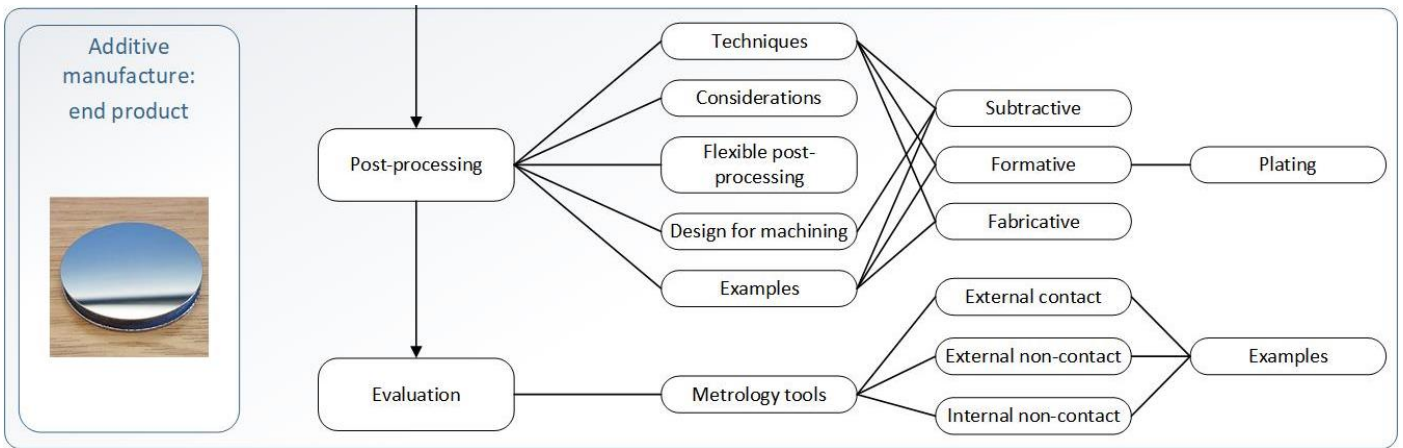


Figure 91: examples of three different types of support structure geometry used within EB-PBF, image credit: NSTP3-PF2-008 team.

Figure 92 highlights an example where a design has not been made appropriately for EB-PBF and as a result, support material has not been able to be removed from the design. The image on the left of the figure is the part as removed from the EB-PBF machine, support material has been used to ensure circular geometry of the powder removal holes. In this example, the access to remove the support material and the type of support geometry meant that the support material could not be removed and the semi sintered powder remained within the cavity. This is an example where an improvement in communication between investigator, engineer and AM machine operator could have prevented this part failure by either accepting non circular holes (the chosen solution as demonstrated in Figure 91 *middle & right*), or by using a diamond/ tear drop geometry.



Figure 92: support removal problems; the example highlights the support material used to support the vertical circular holes and the failure at the support removal. Image credit: STFC & UoS.



3.9 Post-processing

3.9.1 The importance of post-processing

Substrates created via AM do not have the required surface quality to achieve reflection at the shorter wavelengths (near-IR and shorter). In addition, the geometric tolerances on substrates are unlikely to be adequate to integrate directly within a component/instrument, therefore post-processing will usually be required. For example, Figure 93 presents profilometry data measured from three different materials, where each material was printed via a different AM methodology: Bluestone (high performance polymer) printed via SLA, glass filled nylon printed using SLS, and AlSi10Mg printed via L-PBF [42]. The profilometry data demonstrates the influence that AM method has upon the shape of the profile, in terms of both form error and surface roughness.

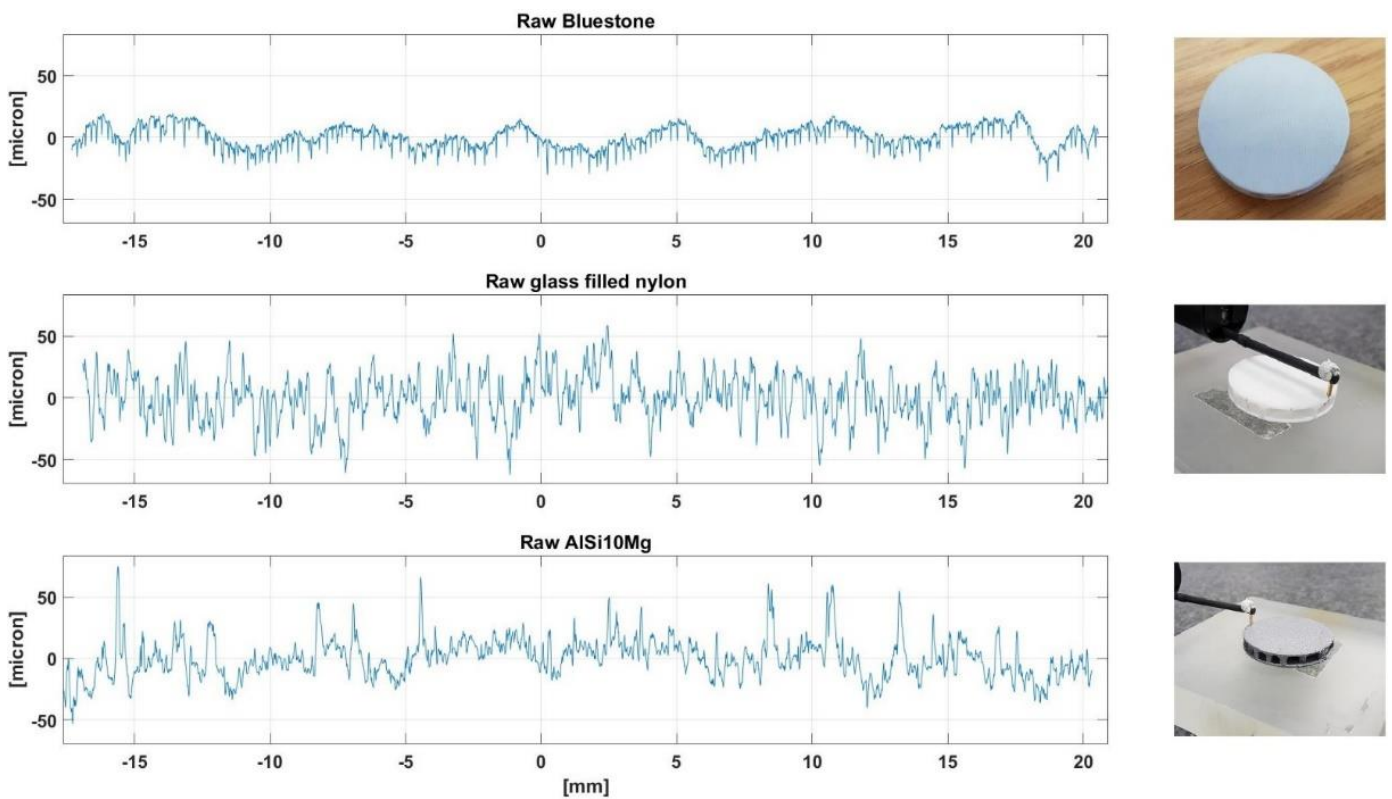


Figure 93: profilometry data for different AM materials and methods prior to post-processing. Image credit: NSTP3-PF-007 team [42].

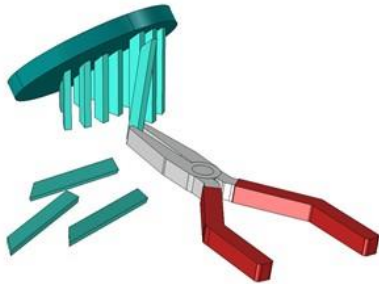
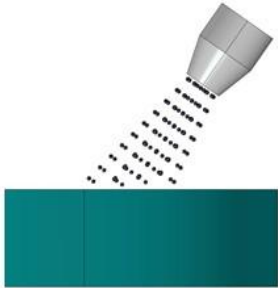
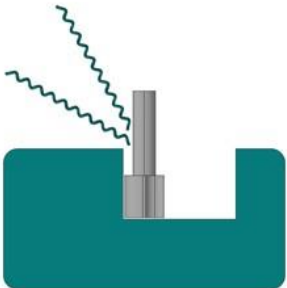
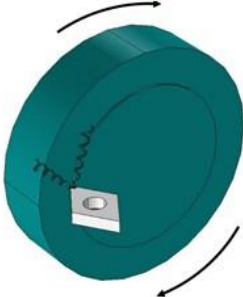
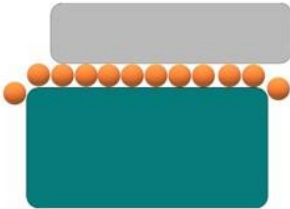


Within this section a broad range of topics are discussed which highlight not only the different post-processing techniques that can be applied (Section 3.9.2), but also introducing considerations for post-processing (Section 3.9.3), design for machining (Section 3.9.7) and future hybrid manufacture techniques (Section 3.9.8). In addition to the reference material, three examples (Sections 3.9.9 to 3.9.11) describe how different AM processes have been post-processed via different techniques to generate reflective surfaces. Two of these examples describe the process of metal plating where the polymer AM substrates have been metalised; the process of metal plating is described in further detail in Section 3.9.12.

3.9.2 Post-processing techniques

Drawing on the terminology discussed in Section 3.1, the post-processing techniques applied to an AM substrate are grouped into subtractive, formative and fabricative methods. Due to the broad scope of post-processing techniques available to astronomical components and mirror fabrication, only a short summary of each technique is discussed. Tables Table 12, Table 13 and Table 14 present the different techniques, characterised by method and listed in descending order by the spatial domain on which they act – i.e. the scale of the method nm -> cm. Within the tables, the teal objects, represent the AM substrate.

Table 12: subtractive post-processing methods, image credits: STFC.

Subtractive post-processing		
Method [scale]	Diagram	Description
Tools and solvents [mm -> cm]		Removal of support material via manual tools or solvents. Increased roughness (μm -> mm) in the vicinity of the support material is expected.
Rough finishing [μm -> mm]		The removal/smoothing of (μm -> mm) roughness often in a non deterministic manner, such as bead blasting and vibration finishing.
Mill, drill & lathe [μm -> cm]		The removal of macro scale artefacts typically via a cutting tool. Applications include: screw holes, removal of support material interfaces, and smoothing surfaces.
Diamond turning [μm]		Removal of small scale material (sub-mm) to create a precision surface or structure, for example creating an mirror surface using diamond turning.
Grinding [μm]		Removal of micron scale material using a grinding tool and slurry (water and particulates). An abrasive action is created on the surface via motion of tool in-plane with the surface.

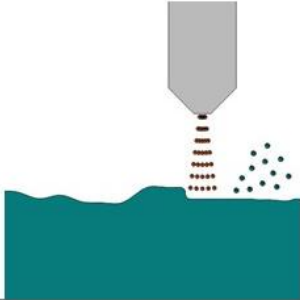
Method [scale]	Diagram	Description
<p>Polishing [nm]</p>		<p>Removal of nanometre scale material using a polishing tool and slurry. An abrasive action is created on the surface via motion of tool in-plane with the surface.</p>
<p>Finishing [nm]</p>		<p>Localised removal of material on the nanometre scale: for example, ion-beam figuring of precision optical surfaces.</p>

Table 13: formative post-processing methods, image credits: STFC.

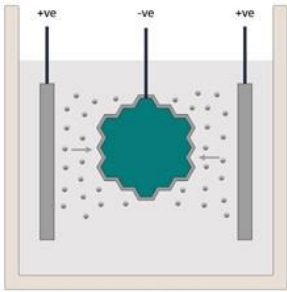
Formative post-processing		
Method [scale]	Diagram	Description
Casting [mm -> cm]		The creation of macro sized components from a mould of the inverse geometry.
Plating [μm -> mm]		The deposition of a thin layer of material on a surface that replicates the structure below it. For example, metallisation of polymers via electroplating, and electroless Ni plating.
Coating [nm -> μm]		The deposition of a nanometre scale thin layer of material for aesthetic or functional applications, for example: optical coatings via metallic sputtering.

Table 14: fabricative post-processing methods, image credits: STFC.

Fabricative post-processing		
Method	Diagram	Description
Joining		The combining of two parts via bonding/adhesion, welding, brazing or soldering.
Component assembly		Integration of individual parts, via bonding, fixing etc., to create a functional component. For example, the bonding of actuators to a structure to create a deformable mirror.
Instrument assembly		The integration of all components to create a final functional system. For example the integration of optical and mechanical components to assemble a telescope.

3.9.3 Post processing considerations

AM post-processing cost should not be underestimated. According Wohlers Report 2019 [43], an annual report on the AM industry, 26% of a part’s cost is from post-processing steps (Figure 94). Post-processing may include steps such as; powder removal, thermal stress relief, surface treatment, subtractive processing and inspection. A good and well thought Design for Additive Manufacturing (DfAM) strategy is a major factor in the economy and the success of an AM part.

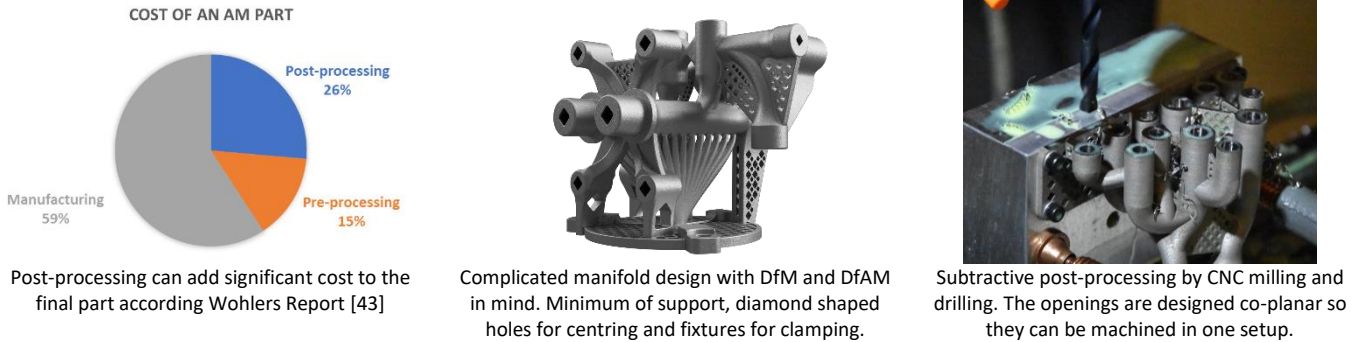


Figure 94: Post-processing is an essential part of the AM workflow, image credits: Wohlers Report [43] & Gen3D.

The workflow of designing, printing and post-machining of an AM part can be extensive, complex and involves multiple parties and expertise. Clear communication and clearly defined procedures are essential for good results (Figure 95).

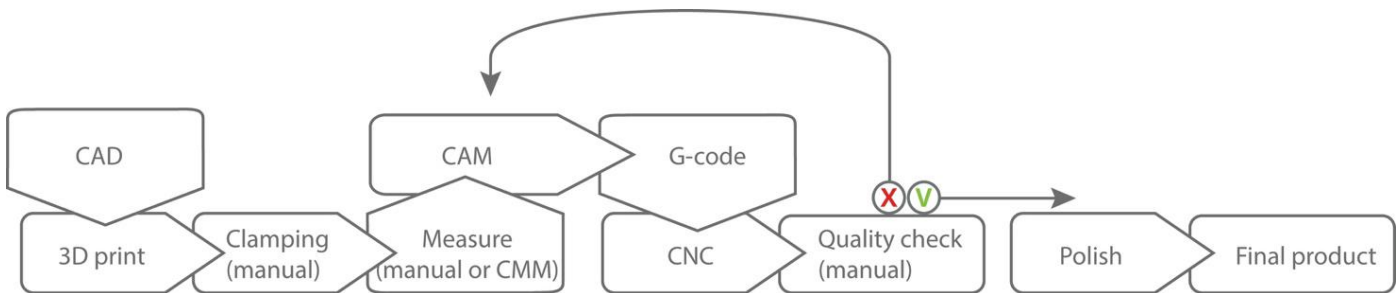


Figure 95: Conventional workflow of post processing, image credits: 3D&FPP Project - Integrating Metal 3D Printing & Flexible Post Processing.

One of the challenges with 3D printed parts after manufacture is reference loss to the exact location and orientation. It is essential for post-machining to find the correct origin and offsets. This can be a complex and time consuming process. Generally, most 3D printed parts are freeform and flat surfaces to clamp to are not available. Furthermore, clamping could deform the shape, or endanger the integrity of printed part. For subtractive processing, the designers must consider fixturing (i.e. how the part is held) within the CNC machine for ease of clamping and referencing.

3.9.4 Fixtures and clamping.

One challenge is the positioning and fixation of the printed geometry in the CNC or conventional metalworking machine. Often, special tooling and jigs are required (Figure 96). One solution is to include reference and additional fixation points or handles within the AM design.



Dedicated jig to position the part used to place treaded inserts.



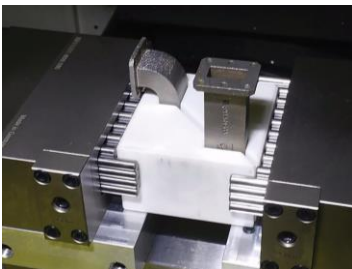
(Photocurable) adhesives, wax or hot melts can be used to keep the AM part in place during post processing



Flexible pin clamp by Matrix innovation

Figure 96: Multiple type of machine clamping solutions, image credits: BMW group - Rolls Royce, Blue Photon Grip, Matrix innovation.

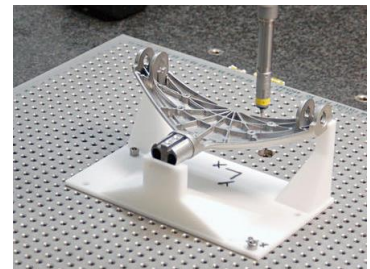
Jigs for detailed processing of connection points and surfaces can be very complex for free-form additive manufactured parts. One option is to use 3D printing technology to produce the work-holding tool. Polyamide parts created by powder bed fusion are well suited for this type of application Figure 97.



3D printed microwave guide clamped in a Matrix-innovation clamp combined with AM fixture



A SLS fixture design to match the AM part



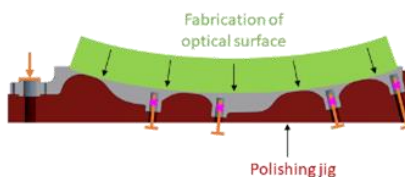
3D printed measuring jig for CMM

Figure 97: Bespoke 3D printed jigs and fixtures, image credits: Renishaw, 3DSystems.

For the post-processing of the OPTICON FAME mirror concept, a bespoke 3D printed clamping tool was designed (Figure 98). The fixation points for the piezoelectric actuators on the underside of the mirror substrate side locate the 3D printed mirror onto the polishing jig [44].



Rear side of the 3D printed FAME Active mirror concept.



Possible post-machining method with the use of a bespoke polishing jig



Exploded view of the mirror and polishing jig.

Figure 98: FAME mirror concept with bespoke 3D printed polishing jig, image credits: Konkoly Observatory

3.9.5 Current development - Flexible post processing

The ongoing automation of traditional and industrial practices using smart technology is termed the Fourth Industrial Revolution or Industry 4.0. Technologies, such as Computer Aided Design (CAM), Additive and Subtractive manufacturing methods (CNC), Assembly and digital available information, are all linked seamlessly together by large-scale machine-to-machine communication and the Internet of Things (Figure 99). The “smart factory” concept is currently under development and implemented by numerous companies such as Siemens, AutoDesk, Bosch, EOS and GE.

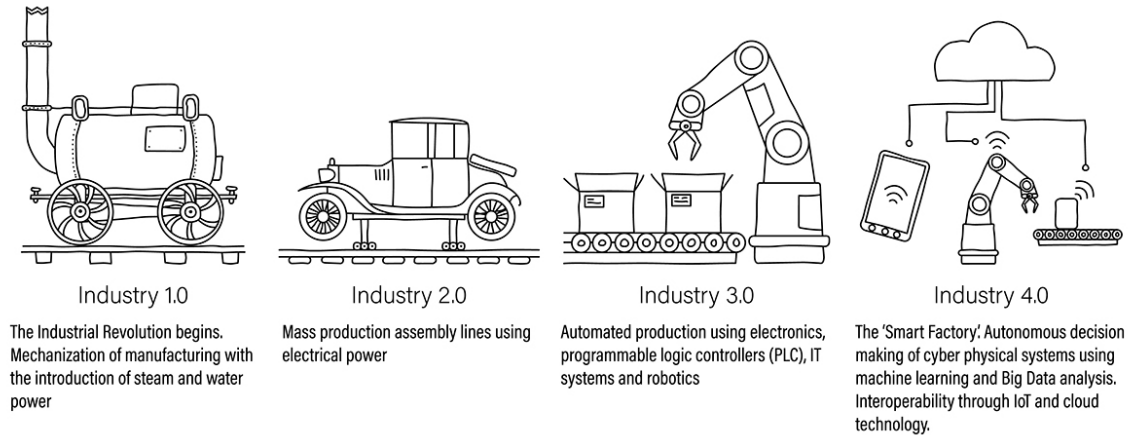


Figure 99: The four generations of Industrial Revolution, image credit: www.behance.net.

Steps have also taken place in the implementation of Industry 4.0 in workflow of post-machining of 3D metal printed parts. The objective of an Interreg project *Integrating Metal 3D printing & Flexible Post Processing*, or 3D&FPP, was to develop an efficient, fast and affordable post-processing solution based upon existing technologies that can be part of an integrated system for post processing of AM components (Figure 100).

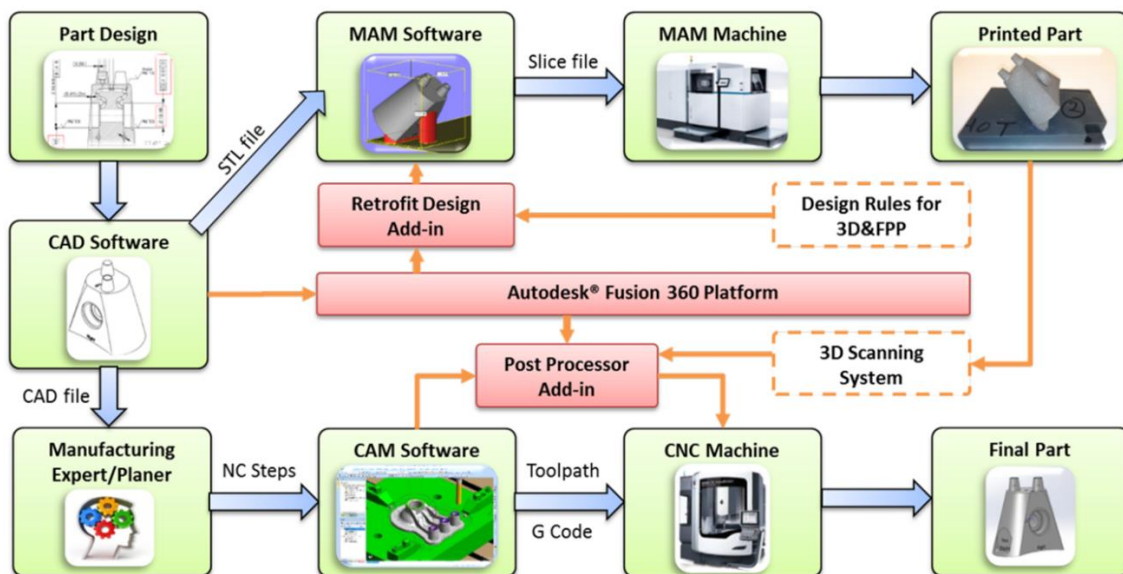


Figure 100: Integrated CAD/CAM solution for 3D&FPP, image credit: 3D&FPP Project - Integrating Metal 3D Printing & Flexible Post Processing.

Within the 3D&FPP research project, post-processing mainly consists of clamping, scanning, polishing, and CAD/CAM system. These elements are integrated within a workflow and then validated by user cases (Figure 101). Included within the user cases is an example of a mirror object from the semiconductor industry (Figure 102).

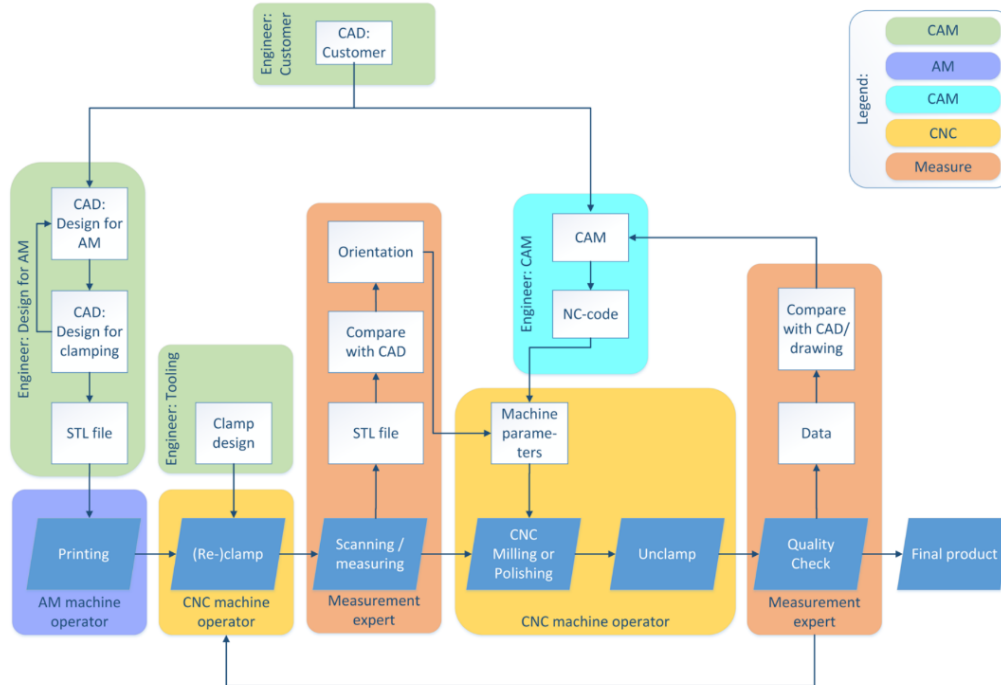


Figure 101: Integrated workflow of post-machining of 3D metal printed parts, image credit: 3D&FPP Project - Integrating Metal 3D Printing & Flexible Post Processing.

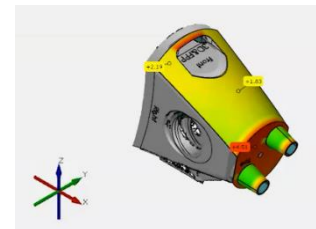
3.9.6 Flexible Post Processing User case - Freeform mirror



Parts can be equipped with an additional handle in the CAD file on a non-critical place.



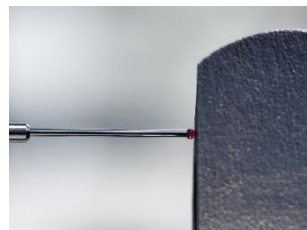
The handle is used to ease clamping. A 3d scan is made of the part positioned in the clamp.



3D scanning information is compared with the STL file and used to determine the reference and offsets



Subtractive processing of the printed part. In a second milling step, the fixture will be removed.



Quality check after CNC milling



Final product

Figure 102: A fixed reference point during process steps can be implemented adding and additional handle or fixation point onto a 3D printed part, image credit: 3D&FPP Project.

3.9.7 Subtractive Machining Guidelines – Design for Manufacturing (DfM)

To facilitate the post-processing of AM substrates, there are some simple design guidelines for subtractive machining processes (mill, drill and lathe) that can be implemented within the AM design (Figure 103 to Figure 105). An important issue encountered by AM substrates for example, is tool access to the faces that require machining, which results from the increased AM design freedom. CAD-integrated design for manufacturing software is available to help the engineer to identify and correct issues early in the design stage. This will lead to a reduction of cycle time and lower product development costs. DFMPPro and DFMPXpress are examples of such software-based programs.

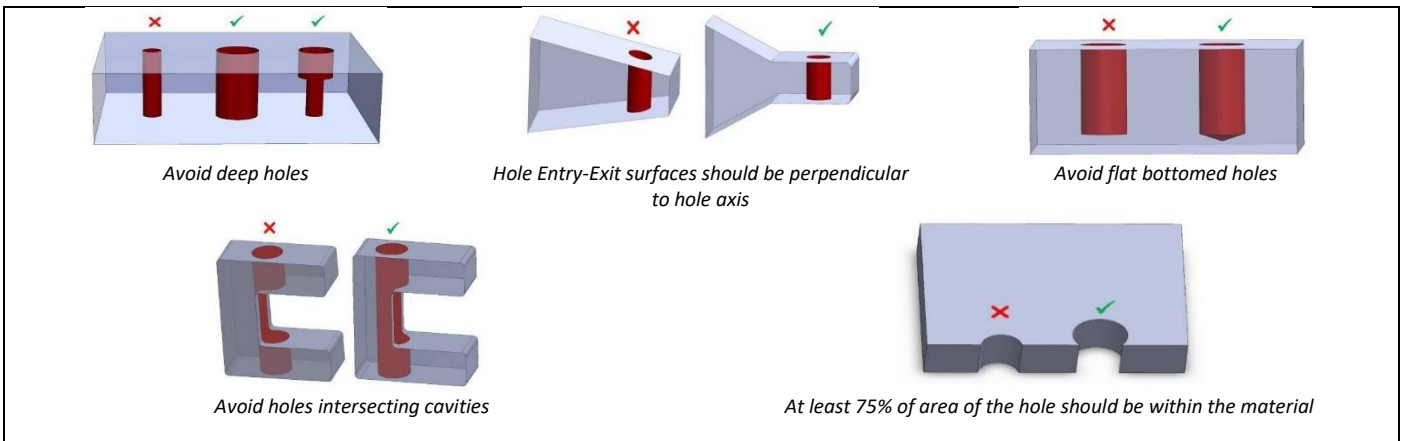


Figure 103: Drilling of holes - guidelines for drilled part design, image credit: DFMPPro.

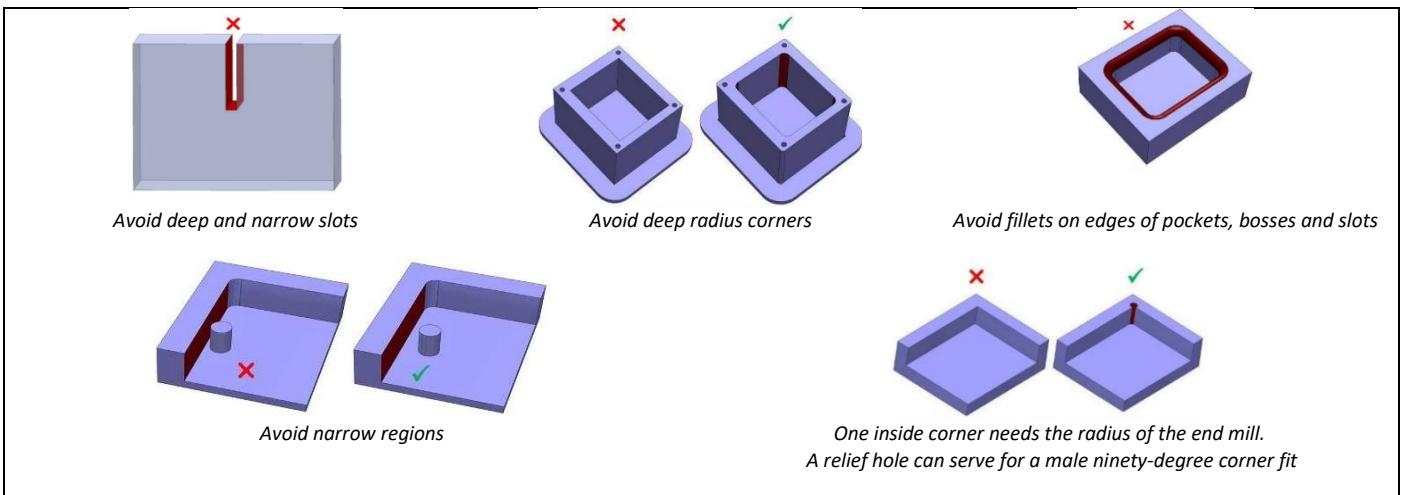


Figure 104: Milling - recommended design practices for milled parts, image credit: DFMPPro.

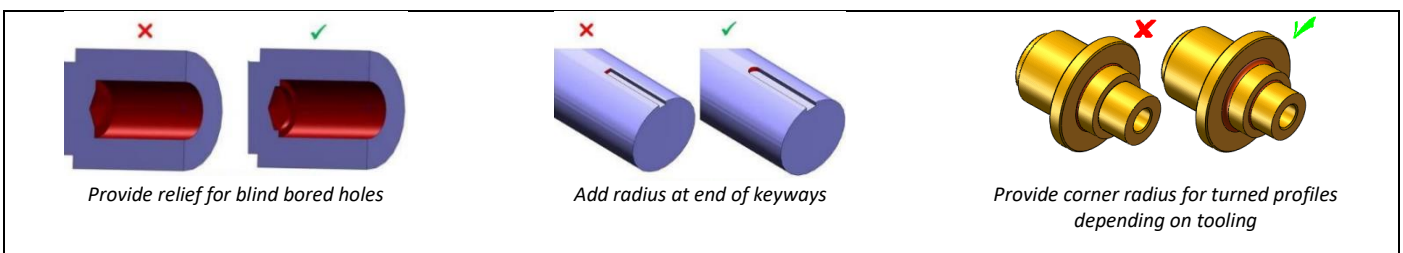


Figure 105: Turning - general guidelines for design of turned parts, image credit: DFMPPro.

3.9.8 Future developments – Hybrid Machining

Some manufacturers have developed post-processing machines that combine Additive and Subtractive processes. Direct Energy Deposition (DED) or PDF can be used to add material at dedicated places. Following, CNC milling takes place to apply detailed features to meet tolerances and improved surface finish. Hybrid machining tools are currently a niche field and development is ongoing (Figure 106). To date, this methodology has mainly been implemented for the injection moulding and tooling industry.

- DED based processes combined with CNC Milling
 - DMD Mori – LaserTEC65
 - Hybrid Manufacturing Technologies / ROMI
- PBF based process combined with CNC Milling
 - Matsuura Lumex Advance 25 & 60



Direct Energy Deposition (DED) Laser cladding process combined with CNC 5 axis milling.



Matsuura combines the PBF process with CNC milling in their LUMEX Advance-25 machine to produce tooling with internal cooling channels



Romi CNC milling machine equipped with an Ambit DED head developed by Hybrid Manufacturing technologies.

Figure 106: Hybrid machining combines additive and subtractive processes in a single production machine, image credits: DMG Mori, Matsuura & Romi.

3.9.9 Example 1: a lightweight Ti64 mirror

Additive manufacture

Ti alloy via EB-PBF

Excess powder is removed from around the fused Ti alloy parts. The excess powder is sieved and then reused within the machine.

Subtractive manufacture

The raw Ti alloy parts are oversized and include build support structures. **Subtractive** machining (mill, drill & lathe) is used to convert the raw parts to the functional dimensions.

Subtractive manufacture

Further material is removed abrasively to generate the reflective surface via grinding and polishing.

Optical metrology is used to iterate with grinding and polishing to achieve the optical prescription.

Fabricative manufacture

Ti mirror integrated for use.

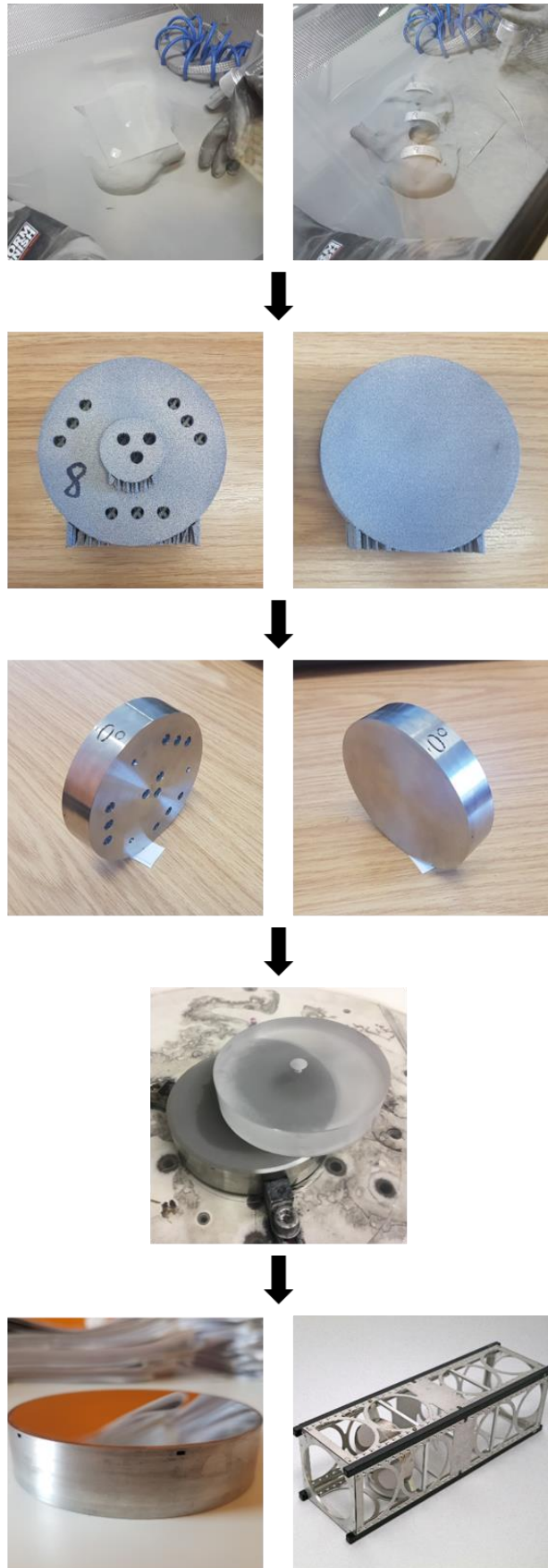


Figure 107: post-processing steps to create a Ti64 lightweight mirror. Image credit: NSTP3-PF2-008 team [45].

3.9.10 Example 2: a metallised polymer mirror

Additive manufacture

Bluestone (high performance polymer) via SLA.

Clean and support removal

Subtractive manufacture

Abrasive smoothing to remove build defects.

Formative manufacture

The part is metallised via a conductive paint and then electroplated in copper and then nickel ($\sim 100\mu\text{m}$).

Subtractive manufacture

Iterations of abrasive grinding and polishing are required to converge on the optical prescription.

Metrology to inform the iterations of grinding and polishing, contact (non specular surface; grinding phase) and non-contact (specular surface; polishing phrase) metrology methods are used, including: profilometers, interferometers and surface texture interferometers.

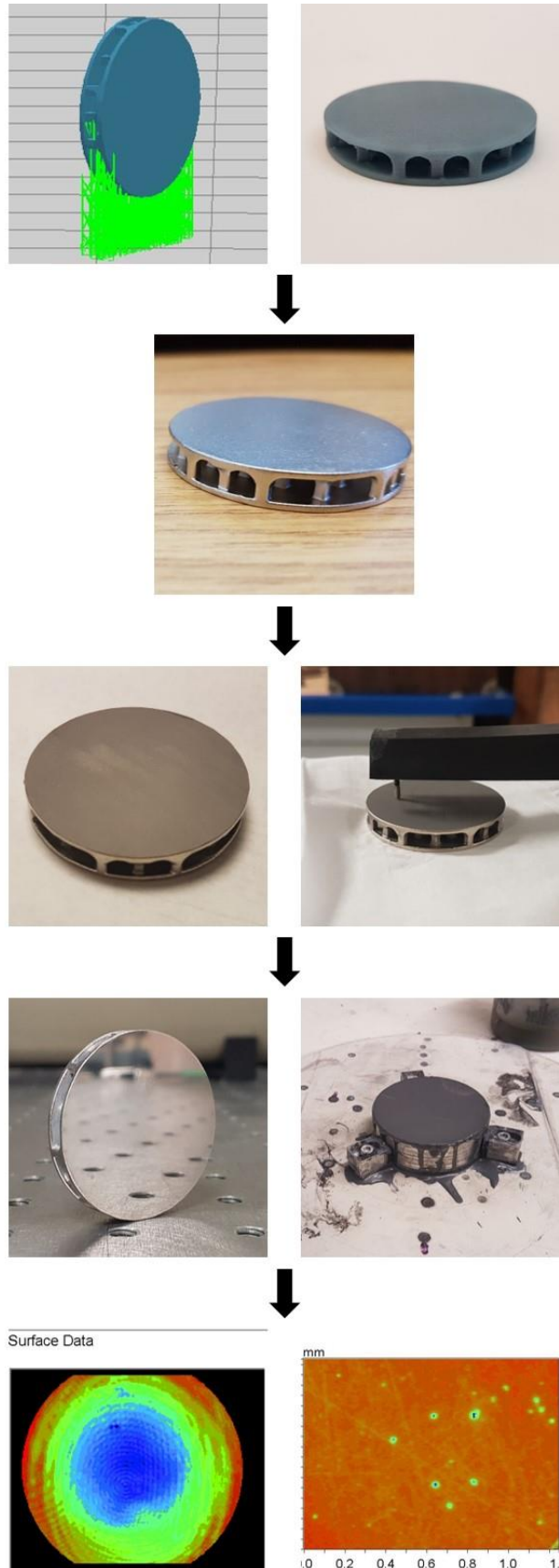
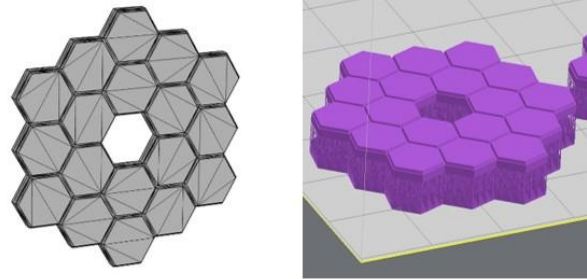


Figure 108: the post-processing steps to create a reflective surface on a polymer mirror. Image credit: NSTP3-PF-007 team & CA Models [42].

3.9.11 Example 3: metallisation of polymer components

Additive manufacture

Visijet Flex (polymer) via SLA.



Subtractive manufacture

The raw Visijet Flex parts are cleaned and the support material removed. **Subtractive** smoothing with abrasive paper is used to remove support material artefacts/interfaces.



Formative manufacture

To create a reflective surface, the polymer part is metallised. A conductive paint is applied followed by electroplating in copper, nickel and finally a thin layer of gold.



Visual inspection is used to ensure that a uniform metallic layer is plated, which is devoid of air bubbles.



Fabricative manufacture

To integrate the gold replica within the main component

Second example of an at scale polymer replica of a metallic mirror created via polymer SLA and electroplating



Figure 109: the post-processing steps in the metallisation of polymer components. Image credits STFC, CA Models & 3DDC Ltd.

3.9.12 Plating of AM substrates

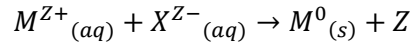
The examples shown in Figures Figure 108 and Figure 109, Figure 108, Figure 109 demonstrate how AM components can be metallised via plating to improve function. Plating is a formative process in which a metal is deposited onto a surface; it is a process that is regularly used within mirror/optical fabrication. By applying a thin metal coating on 3D printed part, multiple properties can be improved, including:

- Increase stiffness
- Durability
- Wear resistance
- Corrosion resistance
- Dust & dirt repellent
- Create fully dense material
- Cold and heat resistance
- Chemical resistance
- Conductivity
- EMC shielding
- Aesthetic

There are two main plating technologies available to apply a functional metal coating onto an AM part: electroless plating and galvanic-/electro-plating.

3.9.12.1 Electroless plating

Electroless plating involves the deposition of a coating from solutions of metal ions without the use of an external source of electrical energy. With Electroless plating, an even layer is applied regardless of the geometry of the surface and can be applied on non-conductive surfaces and parts (Figure 110). The general chemical reaction is:



Where M represents the metal, X^z the reducing agent, and Z the oxidized by-products, which may be liquids, solids, or gases.

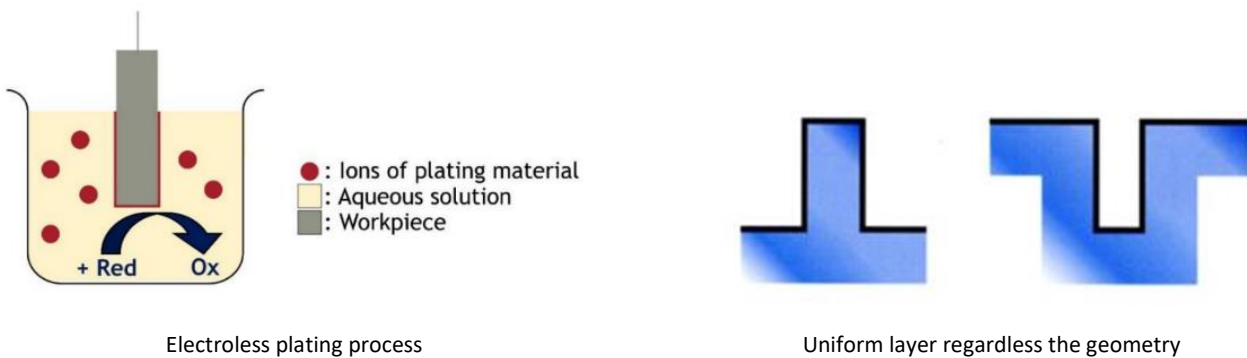


Figure 110: Schematic representation of the electroless plating process. A conformal and uniform layer is applied regardless the geometry, image credits: Interplex.

3.9.12.2 Electroless plating benefits

The plating process is more suited for parts requiring a high degree of uniformity and for plating non-metallic parts such as polymers and ceramics; however, the low deposition rate of 5 to 8 $\mu\text{m/hr}$ is a potential disadvantage.

3.9.12.3 Electro Plating

Electro plating is a process by which metal ions migrate via a solution from a positive electrode (anode) to a negative electrode (cathode). An electrical current passing through the solution causes the work-piece at the cathode to be coated by the metal in the solution - Figure 111.

Special preparation is necessary prior to plating on plastic. The material is initially etched in a chromic acid-based solution to enhance its adhesive capabilities. Any excess chromic acid that is produced must be neutralized. A solution consisting of palladium and tin salts is applied to the material. Next, the surface of the material is coated with either nickel or copper from an electroless plating solution. The palladium and tin salt solution serves as catalyst when combined with the nickel or copper. The material is now ready for electroplating using standard plating technology (

Figure 112).

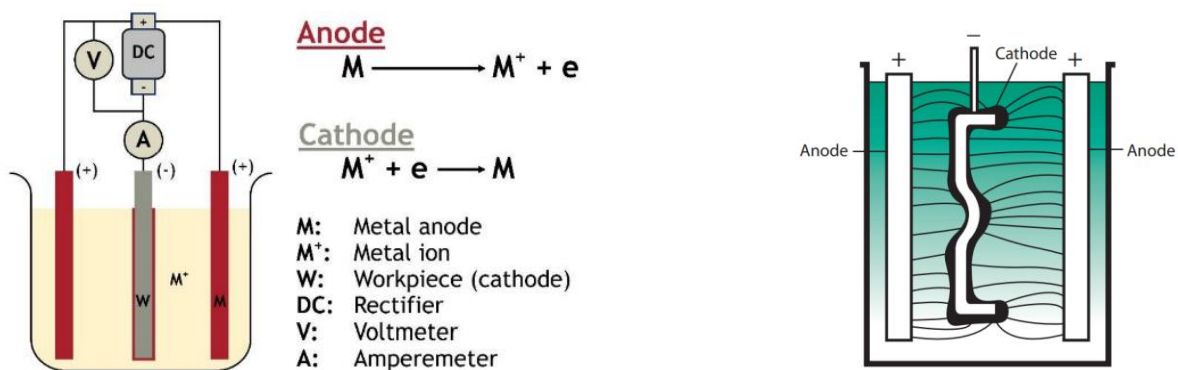


Figure 111: Schematic representation of the electro plating process; a thickness variation will occur resulting from a non-uniform current distribution, image credits: Interplex.



Seed layer
Polymer PBF part in Palladium Chloride bath
(PdCl₂ / HCl)



First plating
Electroless nickel plating
(nickel salts)



Second plating step.
Electro plating bath - Nickel

Figure 112: Process flow of plating a polymer 3D printed structure. After a palladium seed layer, an electroless nickel plating process takes place, which is then followed by an electro plating step to thicken the nickel layer, image credits: TNO.

3.9.12.4 Electro plating benefits

The primary advantage of electro plating is the overall faster dispositioning. Depending on current density (A dm⁻²), depositing speeds of 10 – 100 μm/hr can be achieved, 10x greater than electroless plating. The process is more applicable for metallic parts that need to be produced at low cost and high volumes. The disadvantage of this process is the non-uniform deposited layer and the potential for overplating.

3.9.13 Plating of Additive Manufacturing parts

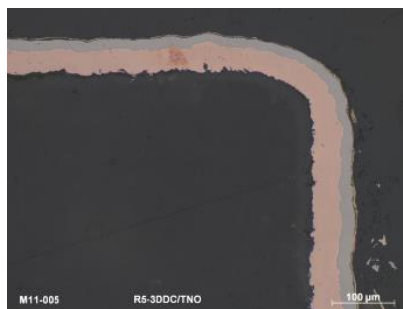
The plating process usually consists of multiple depositing steps in which several materials are applied (described previously). Copper typically serves as a base for further electroplated coatings, such as tin or nickel (Figure 113). The procedure starts with the deposition of microcrystalline and ductile copper coating in an electrolytic process. A copper-nickel coating system has several advantages:

- Good covering properties of copper
- High ductility
- Excellent electrical and thermal conductivity

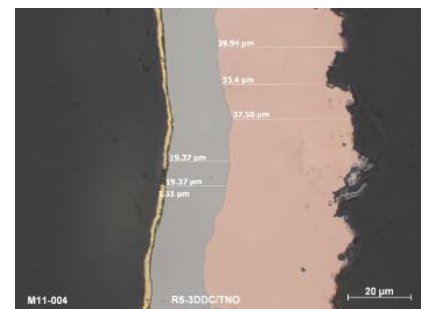
When copper is applied as a base coating, it also counteracts strains between the component and the coating system, thereby reducing the stress in the plating layer.



Copper Nickel Gold plated 3D Printed acrylic sample manufactured by Vat Photo Polymerisation.



Microscopic image of polished cross section. Magnification factor: 100x



Microscopic image of polished cross section. The Cu, Ni, Au plated layers can be clearly distinguished. Magnification factor: 500x

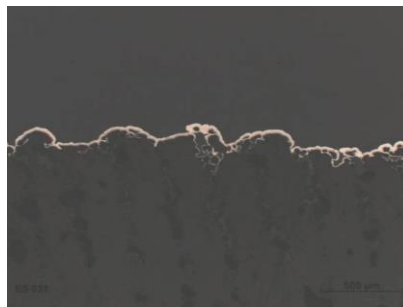
Figure 113: Cross-sectional view of the multiple metal coating layers on a stereo lithography polymer part, image credits: TNO.

3.9.13.1 Conformal technology

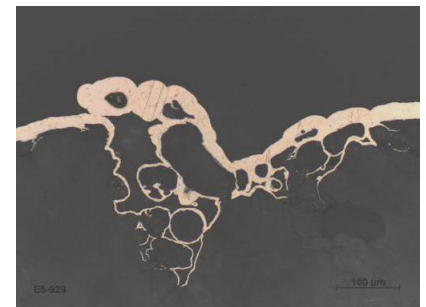
Metal plating is a formative process and it will conform to the part geometry, including the surface roughness. However, reduction of the high frequency component of roughness does take place depending on the thickness of deposit (Figure 114).



Nickel plating on a Polymer Powder Bed Fusion part



Surface roughness is still present after plating. Magnification factor: 50x

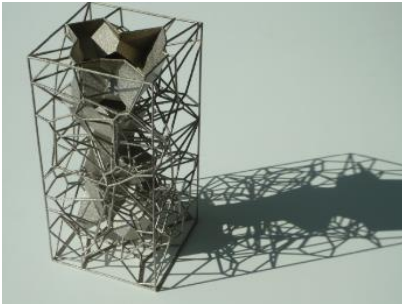


Non-uniform plating thickness on porous surface. Magnification factor: 100x

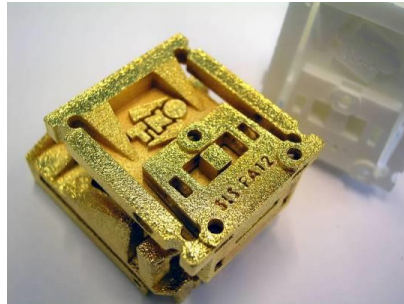
Figure 114: A cross-section view of a Ni layer on a nylon PBF printed part, image credits: TNO.

3.9.13.2 Applications

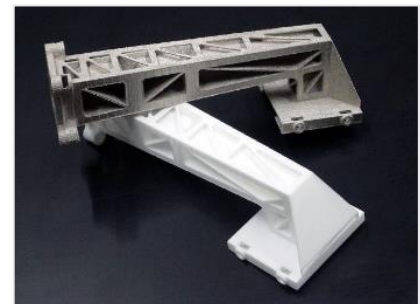
Figure 115 presents a variety of applications of metal plating of polymer 3D printed substrates.



Nickel plated 3D printed Vase
112 x 112 x 250 mm (LxWxH)



Ni + Au Plating of adjustment mechanism –
Polymer PBF in PA12



Nickel plated mechanical arm
Polymer PBF
Weight increase: 60%
Increase stiffness: 300%

Figure 115: Additive manufactured parts with an additional functional plating to improve mechanical strength, image credits: TNO

3.9.14 Mechanical properties

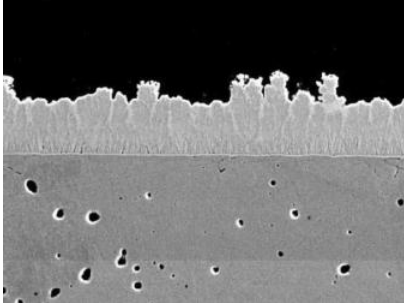
The mechanical properties of a 3D printed polymer parts will increase when a metal coating is applied. Research demonstrates increased Ultimate Tensile Strength (UTS), higher Young's modulus and impact energy [46]. The increase is dependent upon the thickness of applied coating.

	Density	width	thickness	E_{modul} E_{mod}	Tensile strength $\sigma-s$	Elongation ϵ	Tensile strength _{max} $\sigma-max$
	[g/cm ³]	[mm]	[mm]	[MPa]	[MPa]	[%]	[MPa]
SLS PA 2200	0.9	10.38	4.12	1667	49.1	10.71	49.1
SLS metalised 100µm	1.32	10.58	4.33	5230	65.1	2.96	65.1
SLS metalised 150µm	1.49	10.62	4.46	8585	78.1	2.09	77.3
% SLS - 100µm	147%			314%	133%	28%	133%
% SLS - 150µm	166%			515%	159%	20%	157%
SLA (ceramic filled)	1.6	12.02	1.45	9,967	60.20		63.1
SLA metalised 100µm	1.95	12.03	1.45	23,986	109.80		152.9
SLA metalised 150µm	2.1	12.04	1.45	31,234	133.80		197.6
SLA metalised 200µm	2.26	12.05	1.45	49,587	202.90		276.8
% SLA - 100µm	122%			241%	182%		242%
% SLA - 150µm	131%			313%	222%		313%
% SLA - 200µm	141%			498%	337%		439%

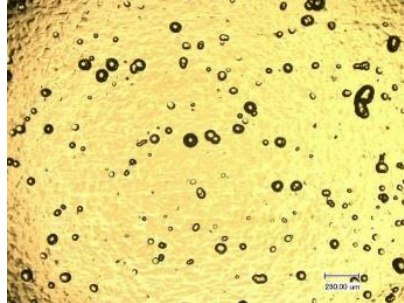
Table 15: Improvement of material properties by application of a plating layer, table credit: 3DDC [47].

3.9.15 Metal coating for optical post-processing: nickel phosphor (NiP)

Inconsistent material structures and (closed) porosity are common for parts produced by AM technologies. For optical surfaces these issues unfavourable. The application of a uniform and conformal electroless NiP coating creates a non-porous metal layer with a fine even microstructure that can be diamond turned or optically polished.



SEM image of cross section of NiP coating on substrate (image credit: Karabük University)



100 µm thick NiP coating on Optical surface before diamond turning
Magnification factor: 100x



PBF TiAl6V4 mirror with NiP coating applied by AHC (Aalberts Surface Technologies)

Figure 116: a nickel phosphor coating allows AM substrates to be coated in a suitable material for precision optical processing via diamond turning or polishing, image credits: TNO.

3.9.15.1 Phosphorus content

The material structure of the nickel plating depends on the phosphorus content and can range from micro crystalline for low content (3-4%) to amorphous for high content (11-12%). The variance of the phosphorus content in the electroless nickel plating has significant impact on the mechanical properties and the suitable application. The increase of phosphorus content results in an increased hardness and corrosion resistance.

	Low Phosphorus	Mid Phosphorus	High Phosphorus
Content	3 – 4 %	6 – 9 %	10 – 12 %
Structure	Micro Crystalline	Mixed	Amorphous
Thermal Conductivity	0.6 W/cm.K	0.05 W/cm.K	0.08 W/cm.K
Tensile Strength	300 MPa	900 MPa	800 MPa
Hardness (as deposited)	700 HV100	600 HV100	530 HV100
Hardness (Heat treated)	960 HV100	1000 HV100	1050 HV100
	0.7%	0.7%	1.5%
Corrosion protection	10 – 24 hr	10 – 192 hr	10 – 1000 hr

Table 16: Material properties of electroless nickel depending on content phosphorus [48]

3.9.16 Companies involved

Several service bureaux offer a NiP plating service on AM parts – listed below.

- 3DDC
- SAT Plating
- SPC – Sharretts plating
- CLZ Tilburg
- Repliccoat
- Protolabs
- Aalberts Surface Technologies



3.10 Evaluation via dimensional metrology

3.10.1 Overview

Post-processing a substrate to obtain a functional part, regardless of accuracy, requires measurement – *you cannot make what you cannot measure*. When considering AM, the maximum scale of measurement is the build volume of the part (max. decimetres) and the minimum scale is the required accuracy/tolerance on a given surface (min. nanometres). There are a multitude of options to evaluate a surface via dimensional metrology that depend upon the accuracy required, the access of the part to be measured with the measuring head, contact or non-contact, and cost. This section provides a brief summary of the different tools that can be employed to dimensionally evaluate an AM object.

3.10.2 Tools and examples

Table 17 provides a simplistic summary of the different tools that are available to evaluate an object or surface dimensionally. The emphasis in the table is on metrology tools to evaluate optical/mirror surfaces and the information provided is general and does not cover the specifics of a given manufacturer for instance.

Examples shown in Figures Figure 117, Figure 118 and Figure 119 that highlight how the different dimensional tools have been used to evaluate AM parts and surfaces.

Table 17: different tools available to evaluate dimensionally a part or surface.

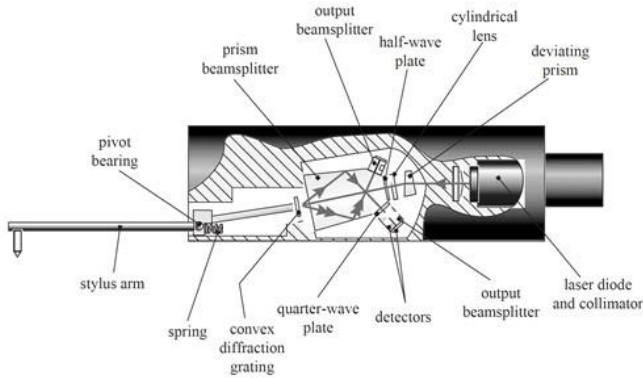
Measuring tool / system	Use	Measurement scale / accuracy			Contact / non-contact	Cost
	[insp. / eval.]	[m → mm]	[mm → μm]	[μm → nm]		€ → €€€
Squares	Inspection	Y / N	N / N	N / N	Contact	€
Callipers	Inspection	Y / N	Y / Y	N / N	Contact	€
Micrometer	Inspection	Y / N	Y / Y	N / N	Contact	€
Coordinate measuring machine (CMM)	Evaluation	Y / N	Y / Y	N / N	Contact	€€€
Profilometry	Evaluation	Y / N	Y / Y	N / Y	Contact	€€ -> €€€
Optical microscopes	Insp. & Eval.	N / N	Y / Y	N / N	Non-contact	€
3D optical imaging/scanning	Evaluation	Y / N	Y / Y	N / N	Non-contact	€€
Chromatic confocal microscopy	Evaluation	N / N	Y / Y	Y / N	Non-contact	€€
Confocal laser scanning microscopy	Evaluation	N / N	Y / Y	Y / N	Non-contact	€€
Scanning electron microscopy	Evaluation	N / N	Y / Y	Y / Y	Non-contact	€€€
Interferometry (surface form error)	Evaluation	Y / N	Y / N	N / Y	Non-contact	€€€
Interferometry (surface roughness)	Evaluation	N / N	Y / N	Y / Y	Non-contact	€€€
X-ray computed tomography (XCT)	Insp. & Eval.	Y / Y	Y / Y	N / Y	Non-contact	€€€

Evaluation: external contact		
Method [scale]	Example	Description
Manual measuring tools [inspection]		Manual measuring tools, such as callipers, micrometres, flat edges etc., are highly beneficial for a first approximation of how the built dimensions match the digital design file. These tools are in physical contact with the measurement surface and therefore are not recommended for precision surfaces
Coordinate measuring machine (CMM) [μm -> cm]		A CMM typically uses a spherical ball on the end of a stylus to measure a location of a point on a surface relative to a known coordinate system. The output data is digital 'cloud' of x, y & z coordinates. Unlike manual tools, the risk of damage to the surface caused by the probe is relatively low.
Profile measurements [nm -> mm]		A profilometer measures height data at a given scanning position. Both surface form error and roughness can be measured depending on the stylus tip – a smaller tip allows for shorter spatial frequencies to be sampled. Damage to a precision surface is possible when measuring roughness of soft metals.

Figure 117: contact evaluation methods. Image credits - STFC, TNO, Renishaw [49] & Kacmarcik et al. [50]

Example: external contact

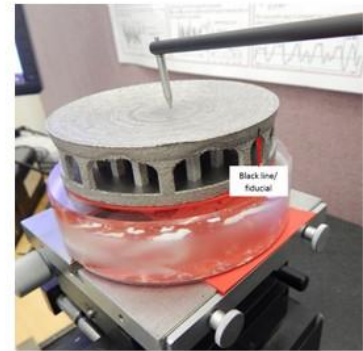
Contact profilometry



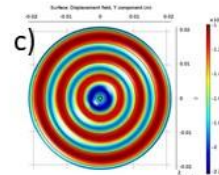
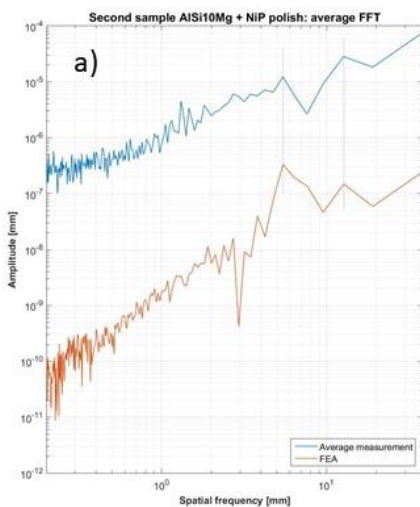
An example of the internal operations of a contact profilometer arm - Jiang, X. et al. (2007).

Contact profilometry uses a stylus to contact the object, the stylus is then drawn across the surface to generate a profile highlighting the position data (x) and height data (y). The scale of the features that are measurable depend upon the diameter of the tip. A ruby ball tip (radius: $150\ \mu\text{m} \rightarrow 500\ \mu\text{m}$) is ideal for measuring the form error of a profile, whereas, a diamond conisphere (radius: $2\ \mu\text{m} \rightarrow 5\ \mu\text{m}$) can probe the roughness of the object.

Examples of profilometers in use are shown below.



Study: Lightweight mirror development - optimization (Case study 2)



- The fast Fourier transform of the average of four contact profilometry measurements. The objective of this analysis was to investigate the *print-through effect* of the lightweight structure upon the optical surface.
- The lightweight polished mirror under measure. It has an AM aluminium substrate which is coated in NiP.
- The finite element analysis of the structure to provide a prediction of the *print-through effect*.

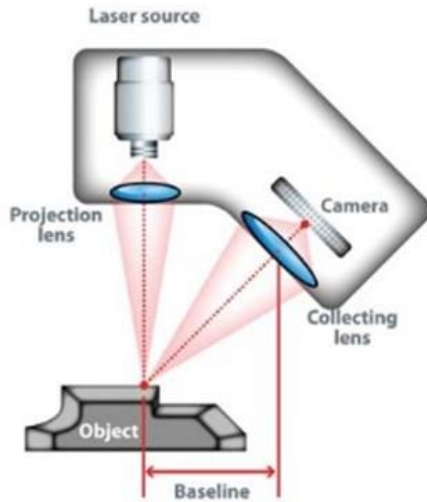
Image credits: STFC, Atkins, C. 2010 & Jiang, X. et al., Proc. R. Soc. A (2007) 463, 2049–2070

Evaluation: external non contact		
Method [scale]	Example	Description
Optical imaging [Inspection]		Optical microscopy is a powerful tool for visual inspection of AM components. It is a non destructive technique providing a magnification of the surface. Dimensional data can be retrieved if the microscope is calibrated.
Optical imaging [$\mu\text{m} \rightarrow \text{cm}$]		Optical imaging, such as confocal and scanning electron microscopy and 3D optical imaging, allows for the 3D evaluation of a surface. In these techniques a laser/electron source is scanned over an area to create the 3D image. Dimensional data can be retrieved from these measurements.
Optical surface imaging [nm]		Evaluating an optical surface, i.e. mirror or lens, requires high accuracy (nm) and often over a large area. Form error is typically evaluated via optical interferometers and microscope interferometry used to evaluate surface roughness. Accurate calibration and environment conditions are required for optimum measurements.

Figure 118: external non-contact evaluation methods. Image credits - STFC & TNO

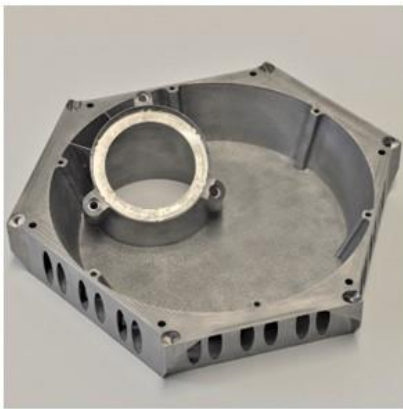
Example: external non contact

3D scanning: laser triangulation

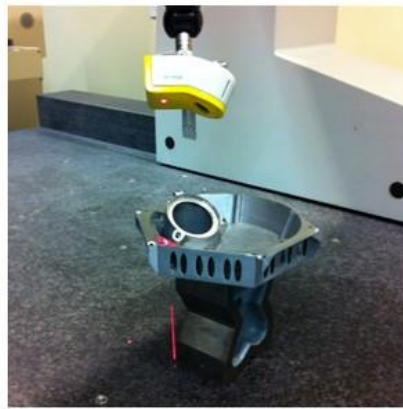


Laser triangulation scanners use a laser point to scan across an object. A sensor picks up the laser light that is reflected off the object, and using trigonometric triangulation, the system calculates the distance from the object to the scanner. The distance between the laser source and the sensor is known, as well as the angle between the laser and the sensor. As the laser light reflects off the scanned object, the system can detect the angle it is returning to the sensor, and therefore the distance from the laser source to the object surface.

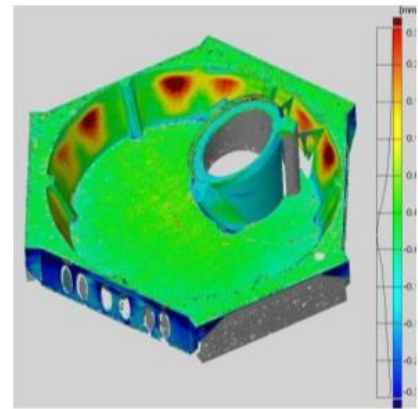
Study: AM aluminium VISCAL baseplate (Case study 12)



a.



b.



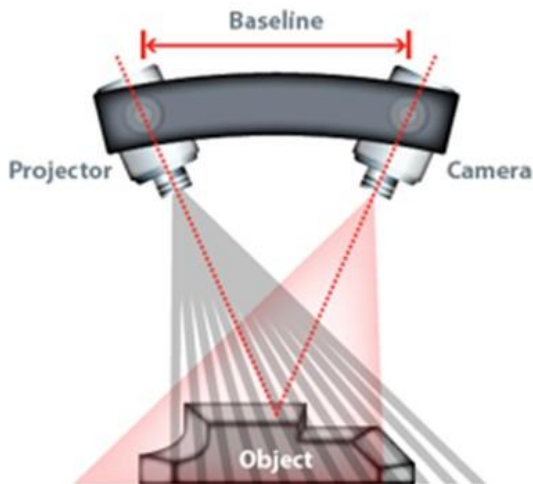
c.

- a. Additive manufactured aluminium VISCAL baseplate for the Sentinel 3 satellite
- b. Laser triangulation scanner mounted within a CMM.
- c. The 3D scanned part compared against the CAD-file.

Image credits: TNO & NeoMetrix

Example: external non contact

3D scanning: structured light



Structured light scanners also use trigonometric triangulation, but instead of looking at laser light, these systems use a projector to display a series of linear patterns onto an object. Then, by examining the edges of each line in the pattern, they calculate the distance from the scanner to the object surface. Essentially, instead of the camera seeing a laser line, it sees the edge of the projected pattern, and calculates the distance similarly.

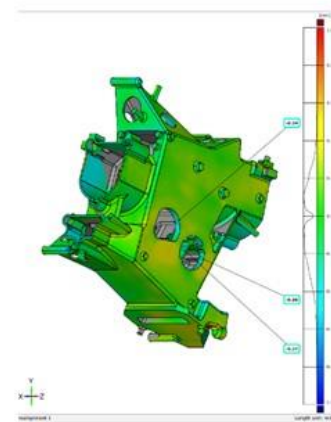
Study: Aluminium housing for SPECTROLITE (Case study 13)



a.



b.



c.

- Aluminium cast Tropo-Lite housing created via a 3D printed wax model.
- Nub3D SIDIO XR Structured light 3D scanner
- Visual inspection of 3D scan file compared with 3D CAD file.

Image credits: TNO & NeoMetrix

Evaluation: internal non contact

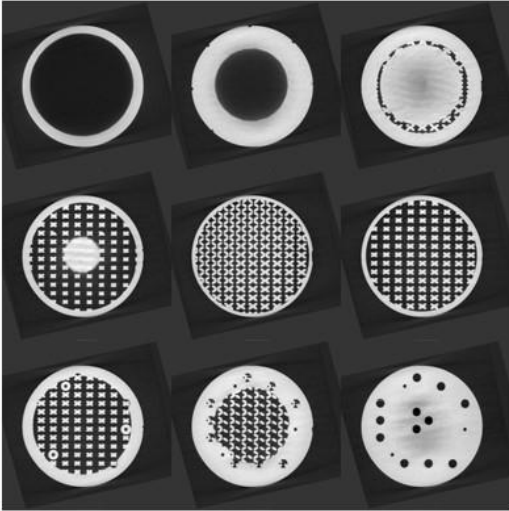
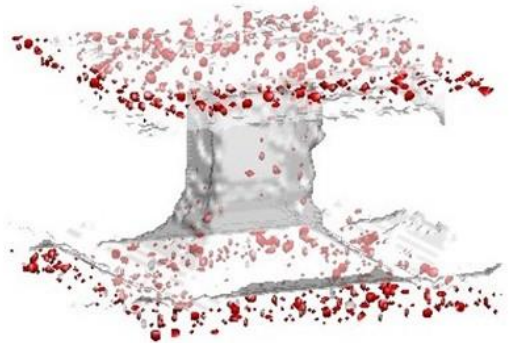
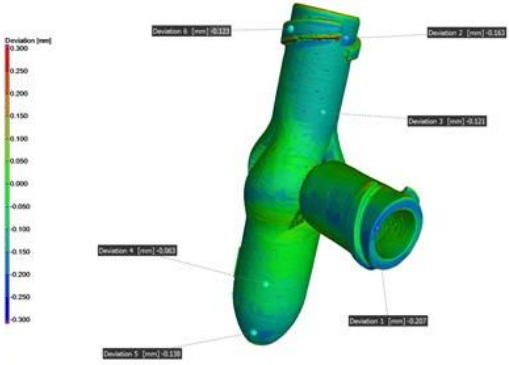
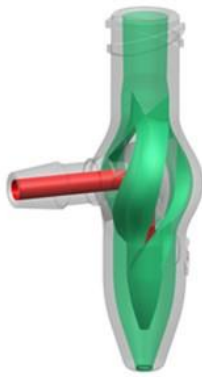
Method [scale]	Example	Description
<p>X-ray computed tomography (XCT)/micro CT (μCT)</p>		<p>XCT/μCT is a valuable tool to evaluate the internal structure of an AM build – particularly where inaccessible internal structures have been implemented. A 3D object of the AM part is constructed via successive layers of x-ray imagery and can be used to explore build quality and identify defects.</p>
		<p>The analysis of XCT/μCT data can be used to quantify the density and location of pores (small voids) with an AM substrate, which is particularly beneficial to ensure that the optical surface is not going to be generated at a depth that has high porosity.</p>
		<p>XCT/μCT data provides 3D structural information of the part which can be then be compared to the input CAD. In the example shown, green represents good fidelity with the CAD, whereas regions in red and blue highlight deviations up to ~ 0.3 mm w.r.t. the CAD.</p>

Figure 119: internal non-contact evaluation methods. Image credits – NPL, Cooper et al. [51] & TNO.

Example: internal non contact

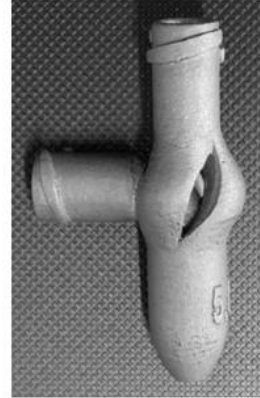
Additive manufactured concentric dispense nozzle with spiralling internal channels



a.



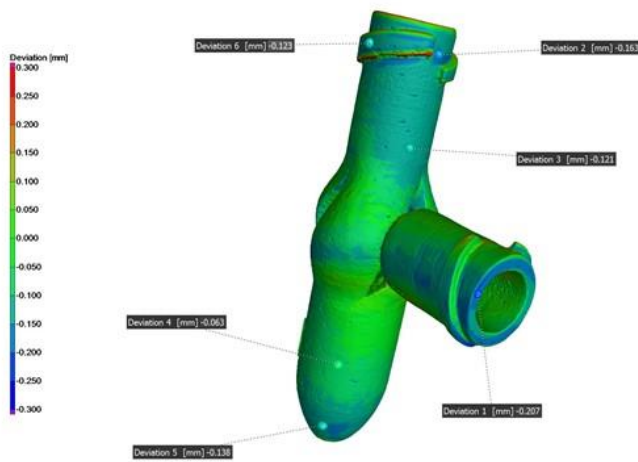
b.



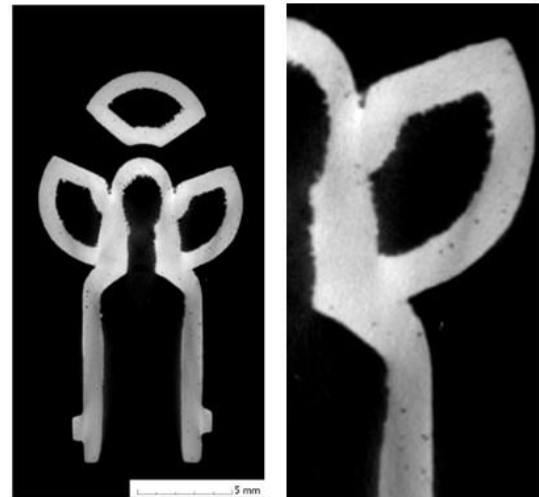
c.

- A concentric dispense nozzle designed to mix two materials; height: 35 mm.
- CAD cross section of the CAD model to visualize the internal channels.
- AM stainless steel 316L nozzle; layer thickness 20 μm and print resolution 30 – 50 μm .

μCT scan data can be converted to a 3D model, which can then be compared with the original 3D CAD print file. The deviation between the two files can be measured and visualised. Depending on scan resolution and size, micro porosity can also be detected and measured.



a.



b.

- The measured deviation by comparing the μCT data with the CAD.
- μCT image slices depicting the internal structure and the presence of porosity (pore size ~ 0.1 mm).

Image credits: TNO



REFERENCES

- [1] S. A. M. Tofail, E. P. Koumoulos, A. Bandyopadhyay, S. Bose, L. O'Donoghue and C. Charitidis, "Additive manufacturing: scientific and technological challenges, market uptake and opportunities," *Materials Today*, vol. 21, no. 1, 2018.
- [2] G. N. Levy, R. Schindel and J. P. Kruth, "RAPID MANUFACTURING AND RAPID TOOLING WITH LAYER MANUFACTURING (LM) TECHNOLOGIES, STATE OF THE ART AND FUTURE PERSPECTIVES," *CIRP Annals*, vol. 52, no. 2, pp. 589-609, 2003.
- [3] D. Vukobratovich, "Chapter 5: Lightweight Mirror Design," in *Optomechanical Engineering Handbook*, CRC Press LLC, 1999.
- [4] K. Schwertz and J. H. Burge, *Field Guide to Optomechanical Design and Analysis*, SPIE Press, 2012.
- [5] H. Martin, "Making mirrors for giant telescopes," in *Proc. SPIE 11116*, San Diego, CA, 2019.
- [6] SCHOTT AG, "ZERODUR - zero expansion glass ceramic," SCHOTT AG, Mainz, 2011.
- [7] D. Ebbets, C. K. Stewart, P. Spuhler, P. Atcheson, J. van Cleve, S. T. Bryson, A. R. Clarkson and J. Barentine, "Telescope with 100 square degree field-of-view for NASA's Kelper mission," *Optical Engineering*, vol. 52, no. 2, 2013.
- [8] M. Sweeney, M. Acreman, T. Vettese, R. Myatt and M. Thompson, "Application and testing of additive manufacturing for mirrors and precision structures," in *Proc. SPIE Vol. 9574*, 2015.
- [9] H. Herzog, J. Segal, J. Smith, R. Bates, J. Calis, A. De La Torre, D. W. Kim, J. Mici, J. Mireles, D. M. Stubbs and R. Wicker, "Optical fabrication of lightweighted 3D printed mirrors," in *Proc. SPIE Vol. 9573*, 2015.
- [10] E. Hilpert, J. Hartung, H. von Lukowicz, T. Herffurth and N. Heidler, "Design, additive manufacturing, processing, and characterization of metal mirror made of aluminum silicon alloy for space applications," *Opt. Eng.*, vol. 58(9), 2019.
- [11] C. Wang, X. P. Tan, S. B. Tor and C. S. Lim, "Machine learning in additive manufacturing: State-of-the-art and perspectives," *Additive Manufacturing*, vol. Volume 36, 2020.
- [12] J. Raplee, A. Plotkowski, M. M. Kirka, R. Dinwiddie, A. Okello, R. R. Dehoff and S. S. Babu, "Thermographic Microstructure Monitoring in Electron Beam Additive Manufacturing.," *Sci Rep*, vol. 7, p. 43554, 2017.
- [13] O. Rehme, "Cellular Design for Laser Freeform Fabrication," CUVILLIER Verlag - Technische Universität Hamburg-Harburg Institut für Laser- und Anlagensystemtechnik, Hamburg, 2010.
- [14] M. C. Sow, T. De Terris, O. Castelnau, Z. Hamouche, F. Coste, R. Fabbro and P. Peyre, "Influence of beam diameter on Laser Powder Bed Fusion (L-PBF) process," *Additive Manufacturing*, vol. 36, p. 101532, 2020.



- [15] G. Manuela and M. Paolo, "Analysis of Density, Roughness, and Accuracy of the Atomic Diffusion Additive Manufacturing (ADAM) Process for Metal Parts," *Materials*, vol. 12, no. 24, p. 4122, 2019.
- [16] R. M. Snell, C. Atkins, L. Brouwers, S. Farkas, F. Feenstra, G. Kroes, R. Haynes, W. Holland, E. Hugot, D. Jager, G. Mezo, C. Miller, K. Morris, M. Roulet, H. Schnetler, F. Tenegi and I. Todd, "Report on Additive Manufacturing Materials," Zenodo, 2020.
- [17] E. Hilpert, J. Hartung, S. Risse, R. Eberhardt and A. Tunnermann, "Precision manufacturing of a lightweight mirror body made by selective laser melting," *Precision Engineering*, vol. 53, pp. 310-317, 2018.
- [18] S. Tan, Y. Ding, Y. Xu and L. Shi, "Design and fabrication of additively manufactured aluminum mirrors," *Opt. Eng.*, vol. 59(1), 2020.
- [19] C. Miller, D. Montgomery, M. Black and H. Schnetler, "Thermal expansion as a precision actuator," in *Proc. SPIE 9912*, Edinburgh, UK, 2016.
- [20] I. A. Steele, H. Jermak, S. Bates and I. Baker, "3D-printed optical instrumentation: practical starter designs and initial experiences," in *Proc. SPIE 10706*, Austin, TX, 2018.
- [21] M. Roulet, "PhD Thesis: 3D printing for astronomical mirrors," Laboratoire d'Astrophysique de Marseille, Marseille, 2020.
- [22] W. A. Goodman, M. N. Ghasemi Nejjad, B. M. Minei, J. N. Stuecker and T. M. Anderson, "Ultra-lightweight ultra-stable RoboSiC additively manufactured lasercom telescope," in *Proc. SPIE 11101*, San Diego, CA, 2019.
- [23] X. Liu, K. Sekizawa, A. Suzuki, N. Takata, M. Kobashi and T. Yamada, "Compressive Properties of Al-Si Alloy Lattice Structures with Three Different Unit Cells Fabricated by Laser Powder Bed Fusion," *Materials*, vol. 13, no. 2902, 2020.
- [24] J. Mueller, K. H. Matlack, K. Shea and C. Daraio, "Energy Absorption Properties of Periodic and Stochastic 3D Lattice Materials," *Advanced Theory and Simulations*, vol. 2019, no. Metamaterials, pp. 1900081 (1-11), 2019.
- [25] Westminster University School of Architecture, "We Want to Learn," Diploma Studio 10, [Online]. Available: <https://wewanttorearn.wordpress.com/2019/02/03/triply-periodic-minimal-surfaces/>. [Accessed 11 June 2021].
- [26] E. Hilpert, "Design, additive manufacturing, processing, and characterization of metal mirror made of aluminum silicon alloy for space applications," *Optical Engineering*, vol. 58(9), p. 092613, 2019.
- [27] C. Mattheck, "Prof. Dr. Claus Mattheck," Seminarbüro Erika Koch, 2021. [Online]. Available: <http://www.mattheck.de/> - <http://www.mattheck.de/english/english2.htm>. [Accessed 14 June 2021].
- [28] Biomimicry Institute, "Asknature," 2021. [Online]. Available: <https://asknature.org/>. [Accessed June 2021].
- [29] D. Leidenfrost and B. Moarefi, "Generative-Engineering-Ansatz für einen B-Säulen-Karosserieknoten," *ATZ - Automobiltechnische Zeitschrift*, no. 112, pp. 68-71, 2020.



- [30] BMW Group, "Industrial-scale-3d-printing-continues-to-advance-at-bmw-group," 10 December 2020. [Online]. Available: <https://www.press.bmwgroup.com/global/article/detail/T0322259EN/industrial-scale-3d-printing-continues-to-advance-at-bmw-group>. [Accessed 13 June 2021].
- [31] B. Garret, B. Redwood and F. Schoffer, *The 3D Printing Handbook: Technologies, design and applications*, 3D Hubs B.V., 2017.
- [32] 3D Hubs, *Design Rules for 3D Printing*, 3D Hubs.
- [33] J. Kranz, D. Herzog and C. Emmelmann, "Design guidelines for laser additive manufacturing of lightweight structures in TiAl6V4," *J. Laser Appl.*, vol. 27, no. S14001, 2015.
- [34] O. Diegel, A. Nordin and D. Motte, *A Practical Guide to Design for Additive Manufacturing*, Singapore: Springer, 2020.
- [35] A. Y. Al-Maharma, S. P. Patil and B. Markert, "Effects of porosity on the mechanical properties of additively manufactured components: a critical review," *Mater. Res. Express*, vol. 7, p. 122001, 2020.
- [36] D. Frydryk, "Get the Facts on... Porosity in Metal Additive Manufacturing," GE Additive, 10 March 2020. [Online]. Available: www.ge.com/additive/blog/get-facts-porosity-metal-additive-manufacturing. [Accessed 17 May 2021].
- [37] D. B. N. P. W. M. K. W. R. P. Christian Weingarten, "Formation and reduction of hydrogen porosity during selective laser melting of AlSi10Mg," *Journal of Materials Processing Technology*, vol. Volume 221, pp. 112-120, 2015.
- [38] S. Ritt, "Will Metal Additive Manufacturing Technology be able to fulfil the customers' requirements?," in *RobTec Workshop*, Brasil, 2012.
- [39] E. Yasa and J. Kruth, "Application of Laser Re-Melting on Selective Laser Melting Parts," *Advances in Production Engineering & Management*, vol. 6, no. 4, pp. 259-270, 2011.
- [40] R. Frykholm, Y. Takeda, B.-G. Andersson and R. Carlstrom, "Solid State Sintered 3-D Printing Component by using Inkjet (Binder) Method," *J. Jpn. Soc. Powder Powder Metallurgy*, vol. Vol.63, no. No. 7, 2016.
- [41] Z. Xiang, L. Wang, C. Yang, M. Yin and G. Yin, "Analysis of the quality of slope surface in selective laser melting process by simulation and experiments," *Optik - International Journal for Light and Electron Optics*, vol. 176, no. 1, pp. 68-77, 2019.
- [42] C. Atkins, C. Feldman, D. Brooks, S. Watson, W. Cochrane, M. Roulet, P. Doel, R. Willingale and E. Hugot, "Additive manufactured x-ray optics for astronomy," in *Proc. SPIE 10399-52*, 2017.
- [43] Wohlers Associates, "Wohlers Report 2019," Wohlers Associates, Fort Collins, Colorado, 2019.
- [44] S. Farkas, T. Agocs, C. Atkins, L. Brouwers, J. Dufils, A. Joo, G. Mezo, K. Morris, M. Rodenhuis, R. Melanie, H. Schnetler, R. Snell, F. Tenegi-Sanginés, A. Vega-Moreno and B. van de Vorst, "Freeform active mirror designed for additive manufacturing," in *Proc. SPIE 11451*, 2020.



- [45] C. Atkins, W. Brzozowski, N. Dobson, M. Milanova, S. Todd, D. Pearson, C. Bourgenot, D. Brooks, R. Snell, W. Sun, P. Cooper, S. G. Alcock and I.-T. Nistea, "Additively manufactured mirrors for CubeSats," in *Proc. SPIE 11116*, 2019.
- [46] N. Sahel, N. Hopkinson, R. J. M. Hague and S. Wise, "Effects of electroplating on the mechanical properties of stereolithography and laser sintered parts," *Rapid Prototyping Journal*, vol. 10 (5), no. DOI:10.1108/13552540410562340, pp. 305-315, 2004.
- [47] 3DDC, "Mechanical Properties Test SLA - SLS," [Online]. Available: https://3ddc.eu/pdfs/metal/MechanicalPropertiesTest_SLASLS_V1.0.pdf. [Accessed 7 May 2021].
- [48] Mac Dermid Enthone, "Electroless Nickel Properties," [Online]. Available: industrial.macdermidenthone.com/products-and-applications/electroless-nickel/properties. [Accessed 7 May 2021].
- [49] Renishaw, "CMM inspection of AM part using REVO 5-axis," [Online]. Available: [https://resources.renishaw.com/details/CMM+inspection+of+AM+part+using+REVO+5-axis\(254123\)\(93694\)](https://resources.renishaw.com/details/CMM+inspection+of+AM+part+using+REVO+5-axis(254123)(93694)). [Accessed 16 02 2021].
- [50] J. Kacmarcik, D. Spahic, K. Varda, E. Porca and N. Zaimovic-Uzunovic, "An investigation of geometrical accuracy of desktop 3D printers using CMM," *IOP Conf. Series: Materials Science and Engineering*, no. 393, 2018.
- [51] P. Cooper, W. Sun, S. B. Brown and C. Atkins, "Micro CT measurements of defects in light-weighted mirrors for applications in space imaging," in *58th Annual Conference of the British Institute of Non-Destructive Testing (NDT 2019)*, Telford, UK, 2019.
- [52] N. Horvath and M. A. Davies, "Advancing lightweight mirror design: A paradigm shift in mirror preforms by utilizing design for additive manufacturing," *Applied Optics*, 2020.
- [53] N. Heidler, E. Hilpert, J. Hartung, H. von Lukowicz, C. Damm, T. Peschel and S. Risse, "Additive manufacturing of metal mirrors for TMA telescope," in *Proc. SPIE 10692*, 2018.
- [54] M. Roulet, C. Atkins, E. Hugot, S. Lemared, S. Lombardo and M. Ferrari, "3D printing for astronomical mirrors," in *Proc. SPIE Vol. 10675*, 2018.
- [55] C. Atkins, C. Feldman, D. Brooks, S. Watson, C. William, M. Roulet, E. Hugot, M. Beardsley, M. Harris, C. Spindloe, S. G. Alcock, I.-T. Nistea, C. Morawe and P. Francois, "Topological design of lightweight additively manufactured mirrors for space," in *Proc. SPIE Vol. 10706*, 2018.
- [56] K. Woodard and M. Bruce, "Progress on high-performance rapid prototype aluminum mirrors," in *Proc. SPIE 10181*, 2017.
- [57] M. Brunelle, I. Ferralli, W. Rebecca and K. Medicus, "Current use and potential of additive manufacturing for optical applications," in *Proc. SPIE 10448*, Rochester, 2017.
- [58] B. Goodman, "The results of Goodman Technologies NASA Phase II SBIRs for additive manufacturing of mirrors and telescopes," in *Proc. SPIE 11487*, Digital, 2020.



- [59] N. Horvath, A. Honeycutt and M. A. Davies, "Grinding of additively manufactured silicon carbide surfaces for optical applications," *CIRP Annals*, vol. 69, no. 1, pp. 509-512, 2020.
- [60] Senvol, "Senvol | Data to help companies implement additive manufacturing," [Online]. Available: <http://senvol.com/database/>. [Accessed 19 05 2021].
- [61] NeoMetrix, "NeoMetrix," [Online]. Available: <http://3dscanningservices.net/blog/need-know-3d-scanning/>. [Accessed 7 May 2021].



4 PARADIGM SHIFT: METAL AM MIRROR DEVELOPMENT

Section 3 presented the key reference material required for the use of AM within astronomical components and, in particular, telescope mirrors. Within this section, the implementation of the reference material specifically for mirror development is discussed. The *paradigm shift* is a description of the change in mind-set that is required to transition from conventional mirror fabrication to AM mirror fabrication.

4.1 Fabrication chain

Figure 120 presents the generic process chain for the fabrication of mirrors via AM. The process chain assumes production in metal via powder bed fusion; however, many of the described steps are invariant of AM machine type and material.

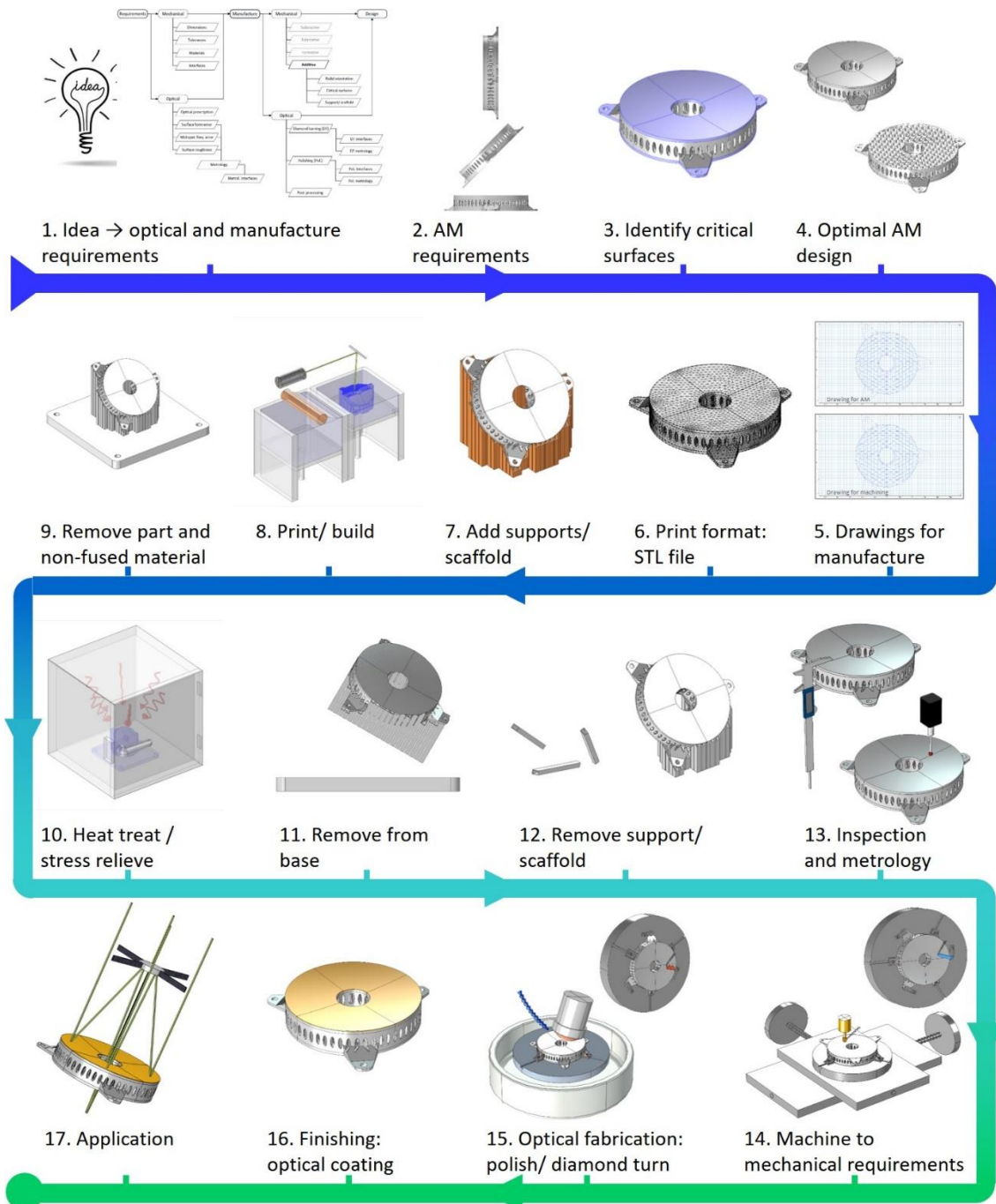


Figure 120: generic AM mirror fabrication chain, image credit: STFC.

4.2 Optical and manufacture requirements

Figure 121 presents how a mirror component design requires significant upstream considerations to converge upon an optimal solution. The use of AM introduces new variables in the mirror design which propagate through into the design process – such as build orientation and identifying critical surfaces. The broad *design-space* of AM facilitates the use of generative design software to produce lightweight organic structures; however, care should be taken to ensure that it is still possible to post-process the critical surfaces on this style of structure.

To move from *requirements* to *design* via AM relies on a holistic approach. The scientists, engineers, AM machine operators and conventional machinists need to work together to converge on the optimal design. An engineer may design an intricate, optimised design for function, but if it cannot be printed or machined then the time spent in the design is lost.

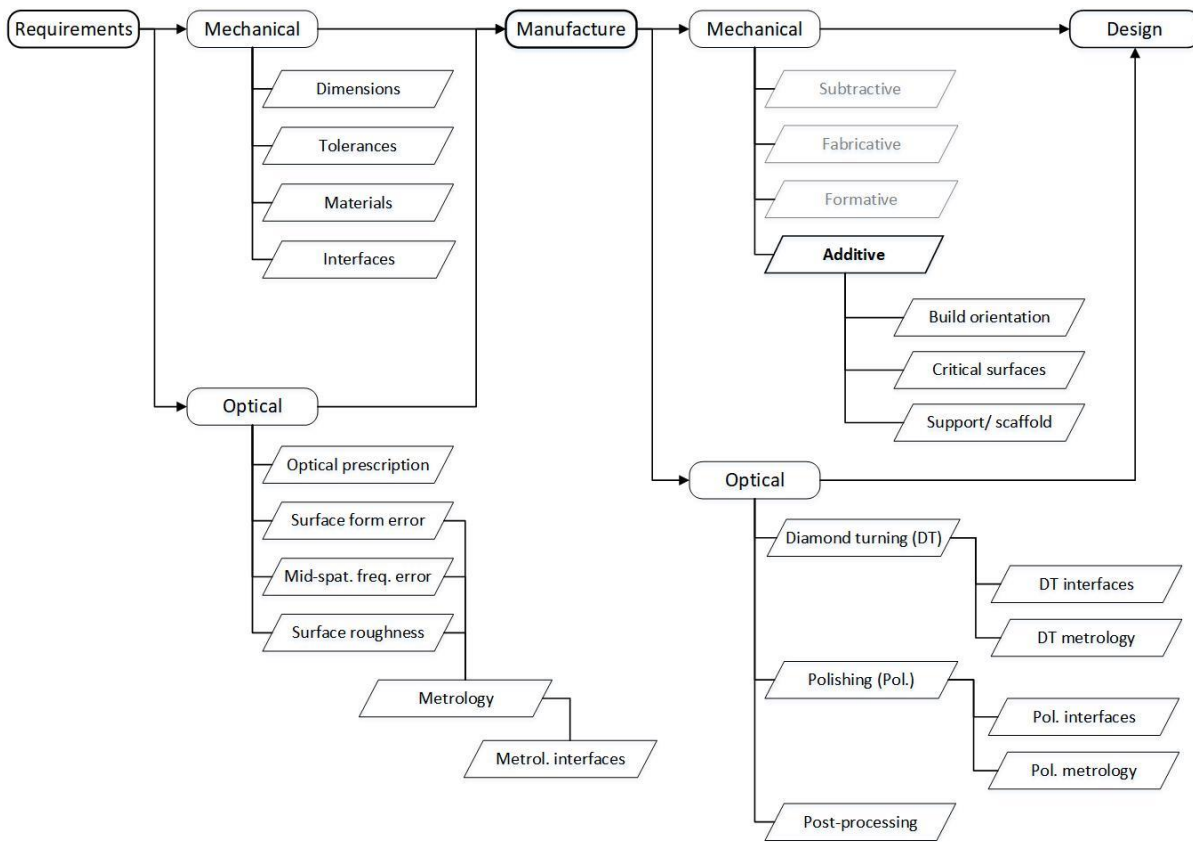


Figure 121: generic considerations from mirror requirements, to manufacture selection and optimal AM design, image credit: STFC.

4.3 Design for additive manufacture

Figure 122 highlights some of the design for additive manufacture (DfAM) benefits available for a lightweight metal mirror production. Immediate benefits of AM include integrated mounting and a sandwiched lightweight structure; however, the removal of loose powder from within the lightweight structure must be considered. The ease of powder removal is dependent upon material, process settings and AM method. It is expected that some of the surfaces will require machining to enable integration within the instrument, these surfaces should be identified and defined with the appropriate tolerances. Figure 123 highlights four examples of DfAM in lightweight mirror applications.

Section 3.6 discussed the design rules for AM and provides an example of the paradigm shift in design. A further discussion on the benefits of the AM design space on advancing lightweight mirror production, is presented in the paper by N. Horvath et al. 2020 [52].

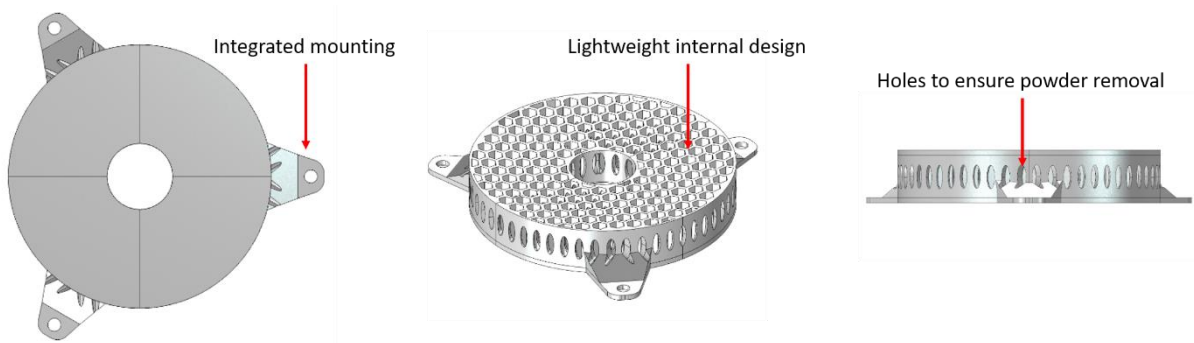
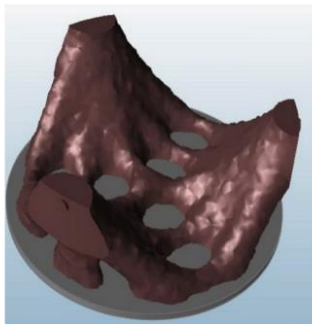
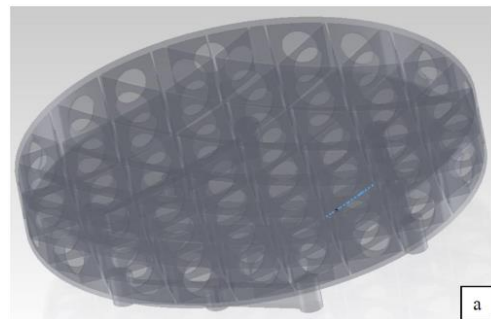


Figure 122: a demonstration of design for additive manufacture, image credit: STFC.



A topology optimised mirror (grey) plus mount (burgundy). 101.6 mm diameter. *H. Herzog et al. (2015)*



A semi transparent CAD rendering of an AM mirror. 150 mm diameter aperture. *M. Sweeney et al. (2015)*

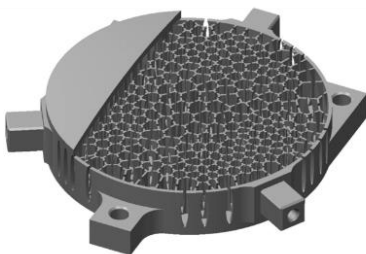


Fig. 6 Cut view of CAD model with interior lightweight structure. A: Mounting plane for first subsequent cutting process; B, C: mounting structures for fabrication and integration processes.

Use of Voronoi cells for a lightweight 'honeycomb' design. 72 mm diameter. *E. Hilpert et al. (2019)*



Fig. 1 CAD model of an additively manufactured aluminum mirror.

A fast steering mirror design for additive manufacture. 67 mm × 50 mm. *S. Tan et al. (2020)*

Figure 123: examples of DfAM in lightweight mirror development. Image credits: H. Herzog et al (2015) [9], M. Sweeney et al. (2015) [8], E. Hilpert et al. (2019) [10] and S. Tan et al. (2020) [18].

4.4 Critical surfaces and drawing generation

The surface texture of an AM object is rough immediately post build and therefore machining is required to bring the AM object into a functional component. Therefore, the critical surfaces that either interface with other components or provide a function, such as a mirror surface, need to be identified for machining and, unlike subtractive manufacture, not all surfaces will require machining. It is considered good practice to produce a minimum of two technical drawings for the component in manufacture: one for the AM machine operator and one for the post-processing machinist (Figure 124).

Technical drawing for AM – at a minimum this is the ‘as built’ geometry where certain dimensions have been oversized to allow for post-processing machining and could include sacrificial features to aid fabrication. Additional information, such as: build orientation, powder recycling, layer thickness, etc. can all be defined in this drawing (Figure 125 *top right*).

Technical drawing for machining – this drawing describes the dimensions, tolerances and finishing of the functional component and is comparable to a conventional drawing for a machined part (Figure 125 *bottom right*).

The design of an AM structure requires both input and visibility from all parties (engineers, AM machine operators, machinists etc.) to ensure that the part takes advantage of the AM design space, is optimally designed for build and can be machined to be made functional.

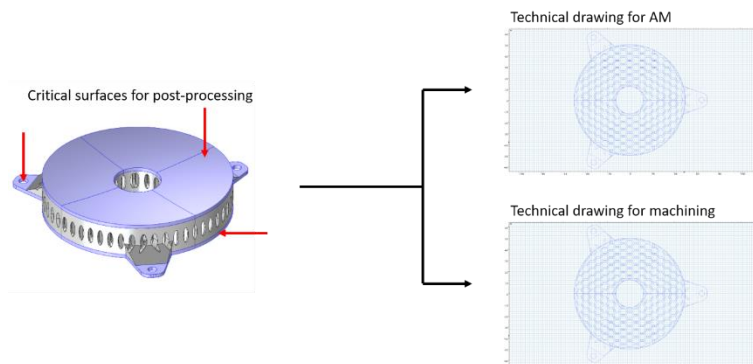


Figure 124: Identify critical surface and produce two drawings for manufacture (additive and subtractive), image credit: STFC.

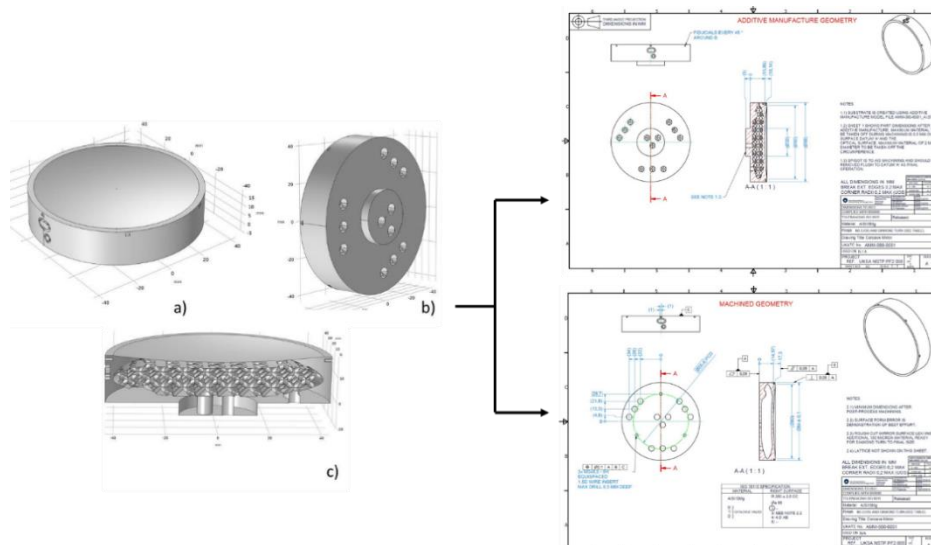


Figure 125: an example highlighting two drawings generated for AM mirror fabrication – source material C. Atkins et al. (2019) [45].

4.5 Preparation for build

Once a final design has been approved by all parties, the CAD representation of the ‘as built’ design is converted to an STL file (AMF and 3MF file types are also possible). The STL format has been used since the 1980s and converts the parametric CAD model into a series of tessellating triangles. Within the STL file, each triangle is represented by 3 vertices and a vector normal to the triangular plane – thereby indicating the external surface of the part – because triangles are used to describe the surface, faceting occurs on curved surfaces as demonstrated in Figure 126. To obtain the optimum build from the CAD design, especially for curved surfaces, care must be taken to balance mesh density and file size.

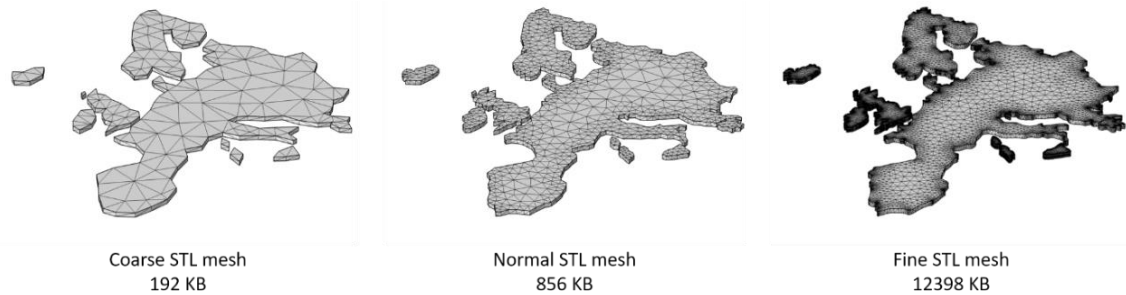


Figure 126: Europe represented in three STL files of different mesh sizes - a loss of detail is demonstrated in the coarse mesh in comparison to the fine mesh, image credit: STFC.

Figure 127 highlights how the example mirror is processed as an STL file and then how it is used within AM specific software to generate the support material and to define the orientation for printing relative to the build plate. Four worked examples, demonstrating different build orientations relative to the mirror surface, are shown in Figure 128.

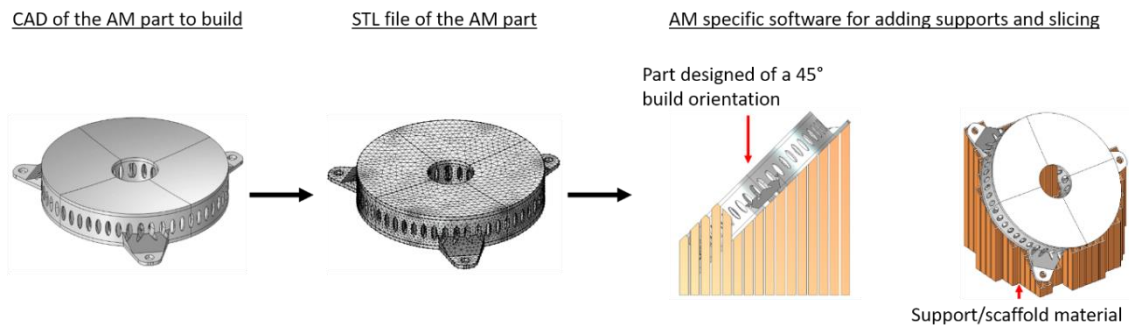


Figure 127: a CAD file is first converted to an STL file and then edited in AM specific slicing software to add orientation, scaffold and AM build parameters (scaling), image credit: STFC.

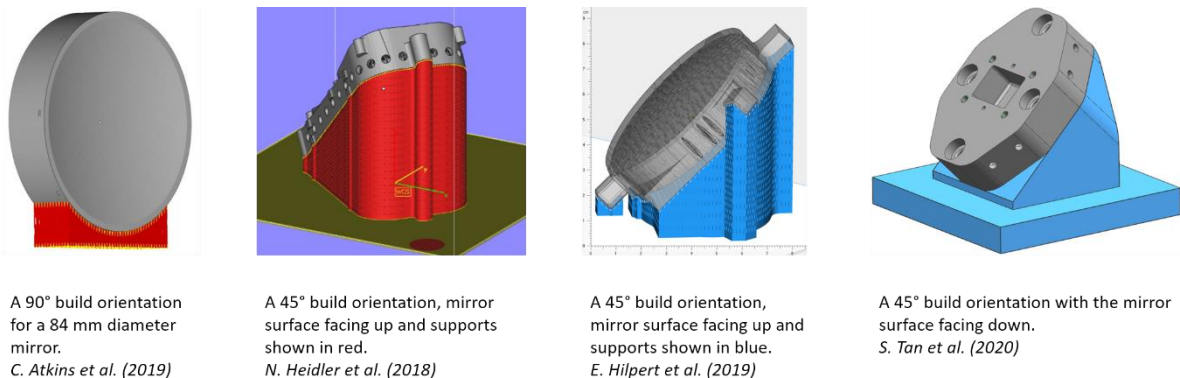


Figure 128: four examples of AM mirrors highlighting build orientation and supports. Source material (left to right) Atkins et al. (2019) [45], N. Heidler et al. (2018) [53], E. Hilpert et al. (2019) [10] and S. Tan et al. (2020) [18].

4.6 Build

The build phase of the mirror is dependent on the material selected and type of printer. In the example below, Figure 129, a simplified laser powder bed fusion (L-PBF) setup is shown during mid-build. The build starts with the build platform positioned at the top of its travel and a thin layer of powder (10 - 100 μm) is raked across the surface using the recoating blade/roller. The laser is scanned on the thin powder layer to fuse the required cross-section and then the build platform is moved downwards by the powder thickness to allow another layer of powder to be raked across. The process of laser scanning, downward platform movement and new powder layer, continues until the object is complete.

Upon completion of the print process the printed part is encapsulated within a volume of powder. The unfused powder is removed from the part and recycled for future builds. To maintain the powder quality, the powder is sieved to remove any small fused beads of metal that might be present within the loose powder.

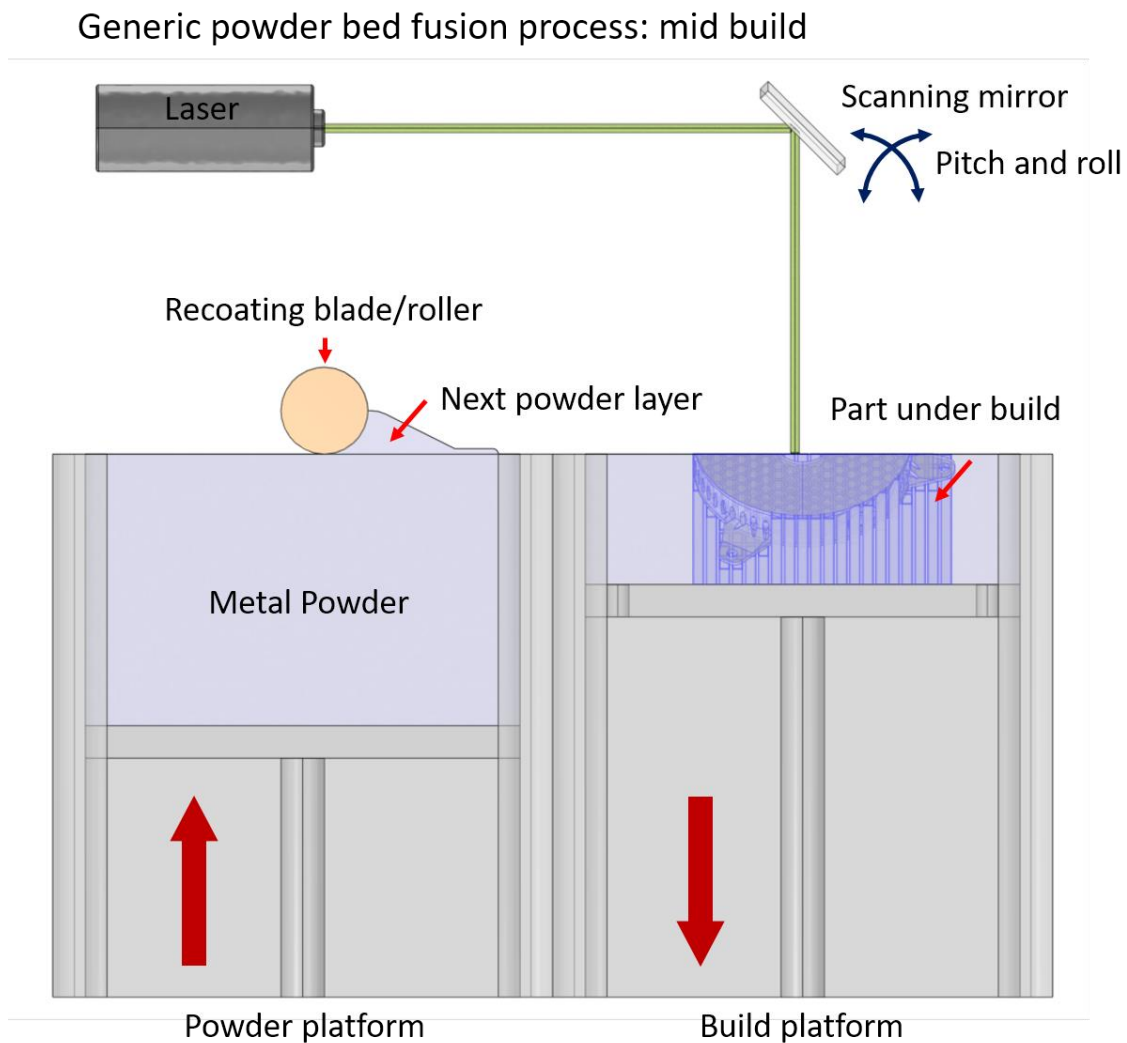


Figure 129: the generic case for metal laser powder bed fusion (L-PBF) in mid build, image credit: STFC.

4.7 Post build

Figure 130 highlights the generic process steps for metal PBF after build. First, the parts are removed from a volume of powder within an enclosed powder management housing (Figure 131). Heat treatment for some processes is recommended before the parts are removed from the build plate; however, some processes can be undertaken after removal, such as hot isostatic pressing (HIP). Temperature cycling is typically employed to reduce stress within a metallic build, whereas HIP is used to close pores and increase material density. The method used in the removal of the part from the build plate is dependent upon whether support material has been used and the print process. In Figure 131, the parts were removed by hand, whereas, in Figure 132 E. Hilpert *et al.* [17] removed the substrate from the build plate using a saw. An alternative removal method is electrical discharge machining (EDM), which is often used for this task. Finally, the support material is designed to be removed manually, by hand, using pliers, files etc.; however, some machining maybe required.

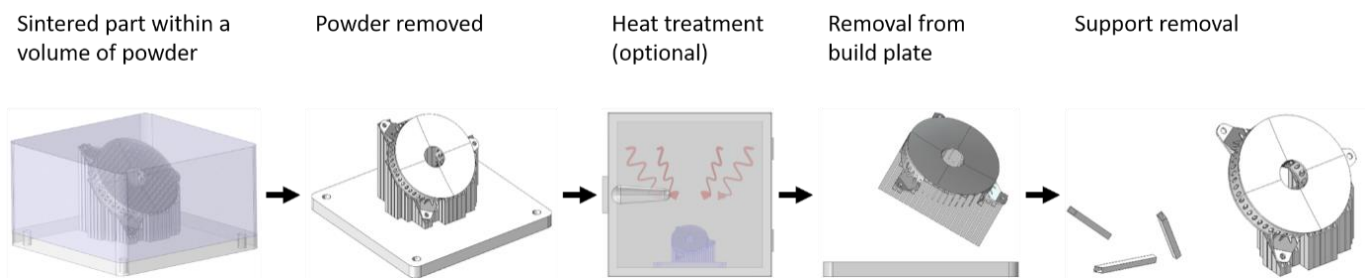


Figure 130: generic steps required in a metallic post build part.

EB – PBF example: Ti64 powder removal within an enclosed environment

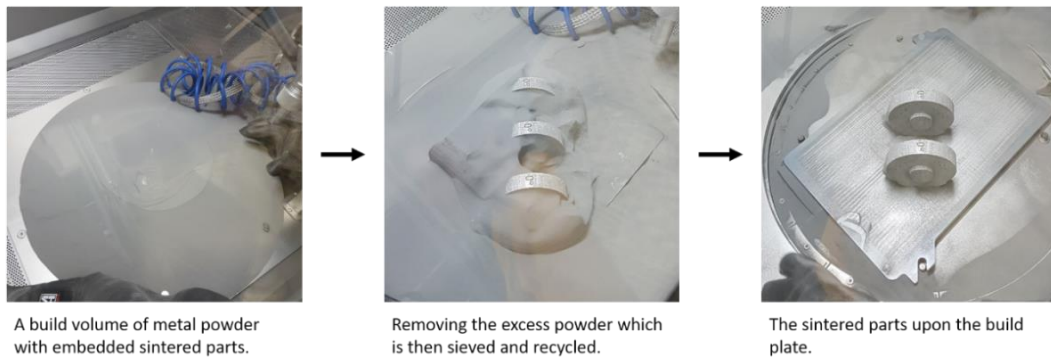


Figure 131: powder removal process for electron beam - powder bed fusion (EB-PBF), image credit: C. Atkins *et al.* (2019).

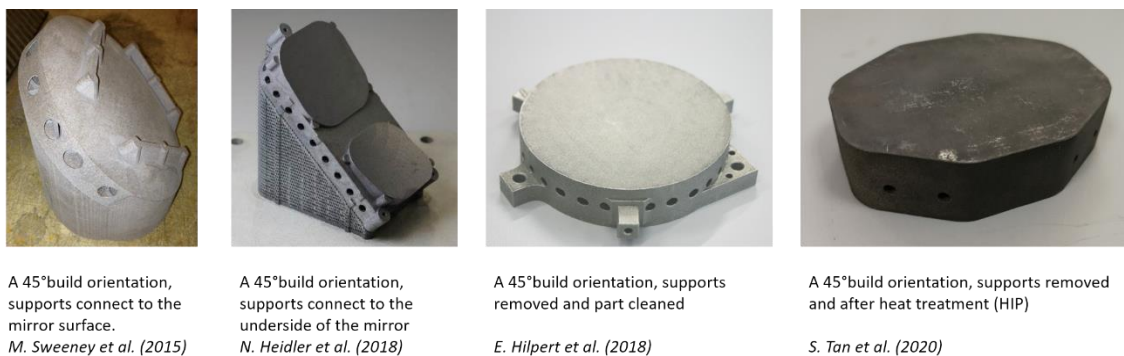


Figure 132: examples of mirror substrates after build with supports attached (left) and with supports removed (right). Image credits: M. Sweeney *et al.* (2015) [8], N. Heidler *et al.* (2018) [53], E. Hilpert *et al.* (2018) [17] and S. Tan *et al.* (2020) [18].

4.8 Inspection and metrology

AM creates a near net shape; however, deviations from the CAD in terms of shape and the creation of roughness leads to the requirement for post-processing. Section 3.10 outlined different methodologies for the inspection of the AM substrates post-build and the application of the method is dependent upon the post-processing required. For example, Figure 133 highlights the surface profile of an aluminium substrate before post-processing, the profile data informs the machining requirements to ensure the surface tolerances are achieved.

Where the shape of the AM part is of greater importance, CMM and 3D scanning techniques can be utilised and compared against the CAD. Distortion of the printed geometry is common, but there are mitigation techniques, such as adding material or extra structural supports. Figure 134 presents the application of 3D scanning to an aluminium base plate and the comparison to the CAD.

The use of XCT/ μ CT is invaluable to determine the quality of internal cavities. Figure 135 a) and b) highlight the internal cavities of two lightweight mirror designs. Figure 135 c) demonstrates how μ CT can be utilised to compare the geometry to the CAD and to assess the printed material for porosity.

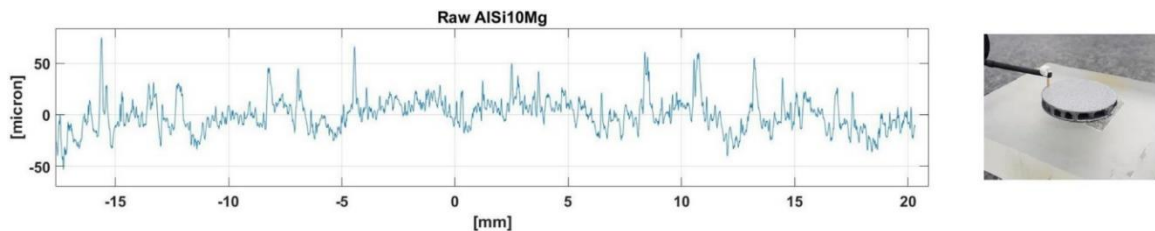


Figure 133: contact profilometry of a raw aluminium build substrate prior to post-processing.



Figure 134: 3D scanning and comparison to the original CAD file of a Viscal base plate, image credits TNO.

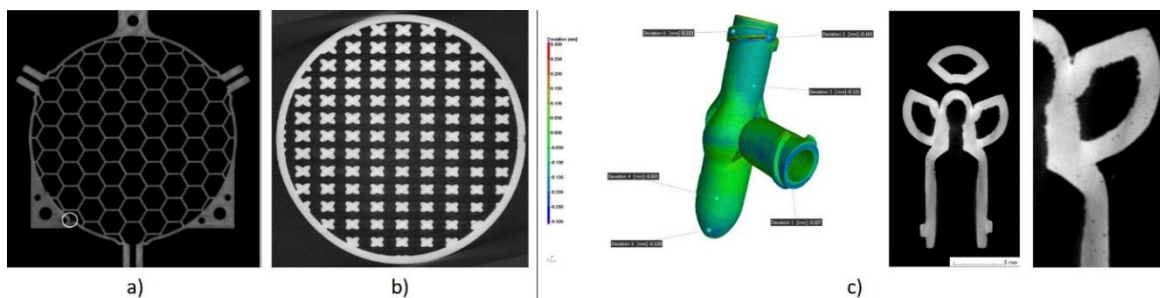


Figure 135: a) & b) the use of XCT to assess the internal cavity of a lightweight mirror substrate (image credits: Fraunhofer IOF) and c) an example of how microCT has been utilised to assess the fidelity of a part relative to the CAD and to quantify porosity within the substrate. Image credits: TNO.

4.9 Post-processing – subtractive machining

A raw metallic AM substrate has a rough texture post build. Profilometry measurements from an L-PBF aluminium substrate have shown ~10 µm RMS roughness and ~90 µm PV when using a 0.8 mm Fourier filter to remove low- and mid-spatial frequency contributions from the profile data (Figure 136; [54]). These values demonstrate the importance of post-processing, not only to obtain the optical surface, but also to ensure accuracy where parts interface.

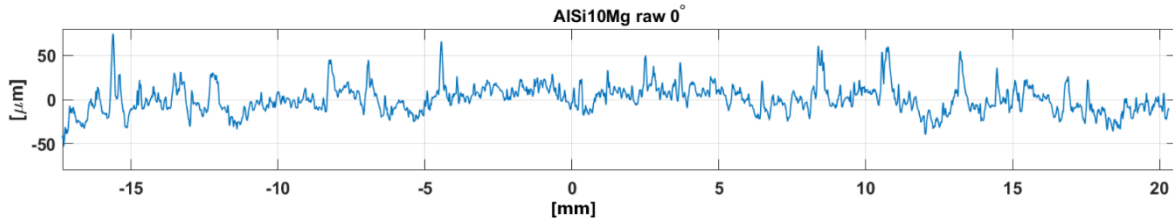


Figure 136: a contact profilometer measurement of a raw aluminium substrate, image credit: M. Roulet et al. (2018) [54].

However, it may not be necessary to post-process every surface, it is only the *critical surfaces*, as identified in Figure 124 for example, which require post-processing. The typical methodology at this stage in production is subtractive machining: mill, drill or lathe (Figure 137). Examples of AM mirrors substrates that have undergone subtractive machining are shown in Figure 138.

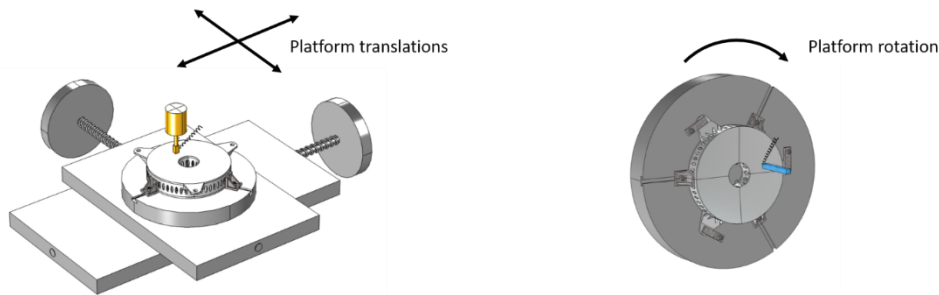
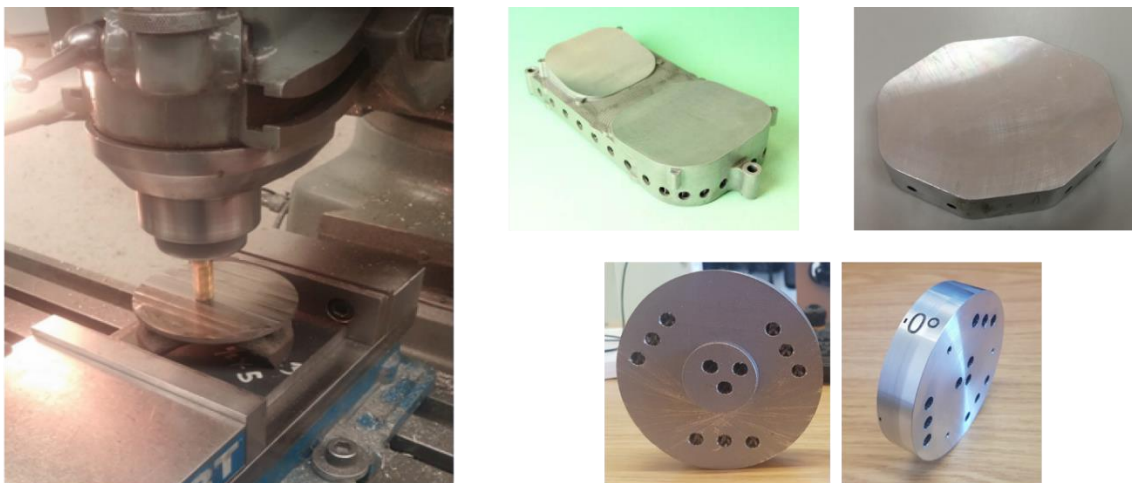


Figure 137: sketches of typical subtractive machining methods. Left - mill/drill using a simple translation stage. Right - a rotating lathe platform with a cutting tool shown in blue. Image credits: STFC.



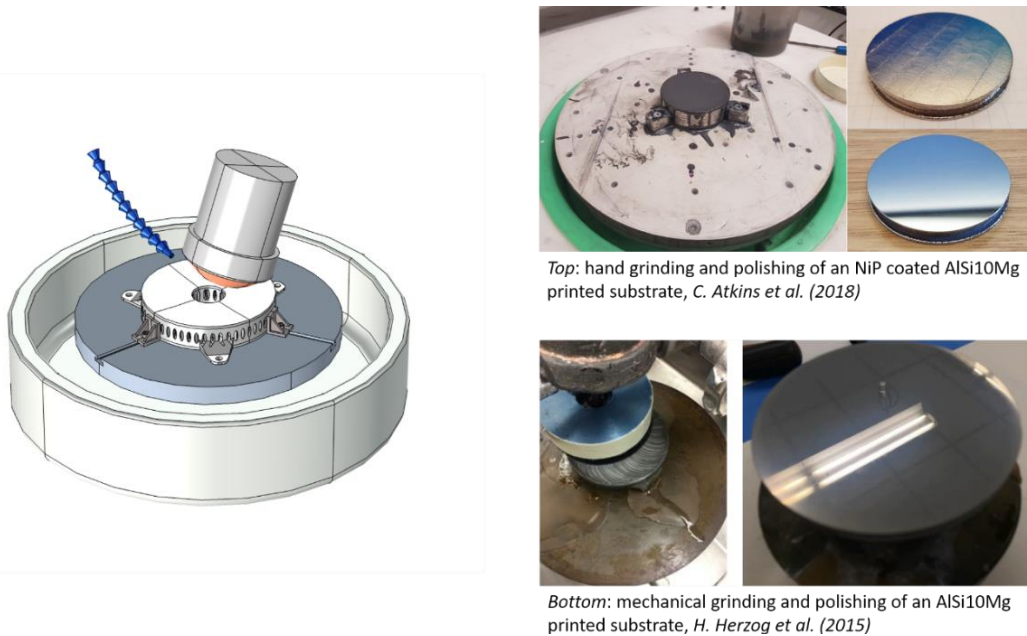
Subtractive machining of AM mirrors: left milling of an Ti alloy AM mirror substrate H. Herzog et al. (2015); top-left a machined AlSi40 mirror substrate N. Heidler et al. (2018); top-right a machined AlSi10Mg substrate S. Tan et al. (2020); bottom an AlSi10Mg substrate before (left) and after (right) machining C. Atkins et al. (2019).

Figure 138: example of subtractive machining used in AM mirror fabrication. Image credits: H. Herzog et al. (2015) [9], N. Heidler et al. (2018) [53], S. Tan et al. (2020) [18] and C. Atkins et al. (2019) [45].

4.10 Optical fabrication: polishing and SPDT

The generation of an optical surface is a subtractive method where material is either removed via abrasion (polishing), or cutting (single point diamond turning; SPDT). Depending on the quality of the surface required, which is typically dependent upon the wavelength of operation, additional optical post-processing maybe required, such as Ion Beam Figuring (IBF) or MagnetoRheological Finishing (MRF). In general, polishing and SPDT follow the same operation procedures as they would for a conventional substrate; however, extra considerations may have to be given to incorporating integrated mounting features or an open lattice structure within the set-up.

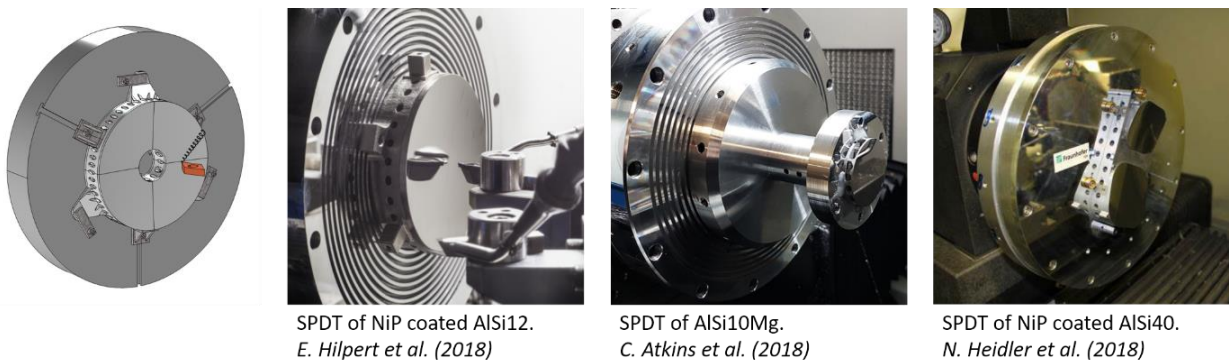
Figure 139 provides examples of AM substrates via optical polishing. In the *top* example, the AlSi10Mg alloy was first coated in ~100 μm of nickel phosphorous (NiP) prior to grinding and polishing to ensure a high quality polished surface could be achieved (i.e. to minimise the risk of porosity). In the *bottom* example, the AlSi10Mg alloy was polished directly. Figure 140 provides three examples of SPDT of AM substrates. In two cases the AM aluminium alloy substrate was coated in NiP prior to SPDT, in the third case the AM substrate (AlSi10Mg) was cut directly.



Top: hand grinding and polishing of an NiP coated AlSi10Mg printed substrate, C. Atkins et al. (2018)

Bottom: mechanical grinding and polishing of an AlSi10Mg printed substrate, H. Herzog et al. (2015)

Figure 139: optical polishing used on AM mirror substrates. Left – a simplified sketch of a CNC polishing head, part and slurry delivery (blue tubing), image credit: STFC; right – examples of hand and mechanical polishing of AM substrates. Image credits: C. Atkins et al. (2018) [55] and H. Herzog et al. (2015) [9].



SPDT of NiP coated AlSi12. E. Hilpert et al. (2018)

SPDT of AlSi10Mg. C. Atkins et al. (2018)

SPDT of NiP coated AlSi40. N. Heidler et al. (2018)

Figure 140: SPDT of AM mirror substrates. Left – a simplified sketch of an AM substrate attached to the SPDT spindle and the diamond cutting tool (orange), image credit: STFC; right – three examples of AM substrates attached to a spindle for SPDT. Image credits: E. Hilpert et al. (2018) [17], C. Atkins et al. (2018) [55] and N. Heidler et al. (2018) [53].

4.11 Applications

Table 18 presents published works in AM mirror fabrication from 2015 to date. The key motivations listed for this research are aerospace, defence, space-based imagery and precision optical components. Note, the measurements of the optical surfaces are not comparable between references, as different procedures and equipment have been used.

Table 18: reported AM mirror fabrication in published literature since 2015.

Ref./ Yr	Concept/ Sector/ application	Mirror material	DIM [mm]	Post-processing	Form error PV [nm] ^a	Form error RMS [nm] ^a	Rough. RMS [nm] ^a
[8] / 2015	Aerospace, defence & precision optics	AlSi10Mg	150 Ø	MRF polish	290	43	< 8
		AlSi10Mg	Rect.	SPDT fly-cutting	-	-	< 5
[9] / 2015	Feasibility → spaceflight	AlSi10Mg	102 Ø	Polishing	-	-	> 20
		Ti64	102 Ø	Polishing	-	-	-
[42] / 2017	Feasibility → space telescopes	AlSi10Mg	40 Ø	Polishing	520	-	10
[56] / 2017	Aerospace & defence	AlSi7Mg0.3 ^b	~ 51 Ø	Corning ^c	-	-	< 2
		AlSi7Mg0.3 ^b	Rect.	SPDT	-	-	< 3
		AlSi7Mg0.3 ^b	Rect.	SPDT + polish	-	-	1
		AlSi7Mg0.3	Coupon	SPDT	-	-	5
[57] / 2017	Feasibility → Optics manufacture	FeNi36	Spherical	-	-	-	-
		Steel	Rect. Plano	-	-	-	-
[55] / 2018	Feasibility → space telescopes	AlSi10Mg	40 Ø	SPDT	590	concave	< 4
		AlSi10Mg + NiP	40 Ø	Polishing	320	83	> 3
		AlSi10Mg + NiP	40 Ø	Polishing	200	31	6
[53] / 2018	Feasibility → TMA space telescope	AlSi40 + NiP	Rect [58]. dual mirror system	SPDT	-	-	20
[17] / 2018	Feasibility → space-based optical systems	AlSi12 + NiP	86 Ø	SPDT/ MRF/ CMP	110	13	0.6
[10] / 2019	Feasibility → space-based optical systems	AlSi40 + NiP	72 Ø	SPDT/ MRF/ CMP	80	7.3	1
[45] / 2019	Feasibility → space telescopes / nanosat applications	AlSi10Mg	84 Ø	Polishing	590	83	-
		AlSi10Mg	84 Ø	SPDT	230	28	< 5
		AlSi10Mg + NiP	84 Ø	Polishing	270	35	-
		AlSi10Mg + NiP	84 Ø	SPDT	180	30	< 6
		Ti64	84 Ø	Polishing	230	28	-
[22] / 2019	Feasibility → space flight demonstrators	RoboSiC™	25 Ø	Polishing	-	-	~2
[18] / 2020	Feasibility → infrared optical system	AlSi10Mg	67 x 50	SPDT	240	59	< 8 ^d
[58] / 2020	Feasibility → balloon, gondola, optical telescope assembly	RoboSiC™	A ¼ segment of a 250 Ø	Polishing	-	-	-
[59] / 2020	Feasibility -> bulk SiC & AM SiC comparison.	SiC + CVI ^e	50 mm inscribed circle hexagon	Grinding only	-	-	800
MRF	Magnetorheological finishing				Ø = diameter; Rect. = rectangular		
CMP	Chemical Mechanical Polishing				PV = peak to valley		
DT	Diamond turning				RMS = root mean square		
^a – Form error and roughness values have been rounded to 2 significant figures (s. f.) and 1 s. f. respectively. Less than (<) and greater than (>) symbols have been used to provide additional distinction.							
^b – AlSi7Mg0.3 alloy implied. The paper suggests an additional coating on the AM substrate in at least one case.							
^c – Quoted as ‘ <i>Corning Enhanced Performance Surfacing Process</i> ’							
^d – This reference represents the roughness as an average (Ra), rather than an RMS (Rq).							
^e – Chemical vapour infiltration							



REFERENCES

- [1] S. A. M. Tofail, E. P. Koumoulos, A. Bandyopadhyay, S. Bose, L. O'Donoghue and C. Charitidis, "Additive manufacturing: scientific and technological challenges, market uptake and opportunities," *Materials Today*, vol. 21, no. 1, 2018.
- [2] G. N. Levy, R. Schindel and J. P. Kruth, "RAPID MANUFACTURING AND RAPID TOOLING WITH LAYER MANUFACTURING (LM) TECHNOLOGIES, STATE OF THE ART AND FUTURE PERSPECTIVES," *CIRP Annals*, vol. 52, no. 2, pp. 589-609, 2003.
- [3] D. Vukobratovich, "Chapter 5: Lightweight Mirror Design," in *Optomechanical Engineering Handbook*, CRC Press LLC, 1999.
- [4] K. Schwertz and J. H. Burge, *Field Guide to Optomechanical Design and Analysis*, SPIE Press, 2012.
- [5] H. Martin, "Making mirrors for giant telescopes," in *Proc. SPIE 11116*, San Diego, CA, 2019.
- [6] SCHOTT AG, "ZERODUR - zero expansion glass ceramic," SCHOTT AG, Mainz, 2011.
- [7] D. Ebbets, C. K. Stewart, P. Spuhler, P. Atcheson, J. van Cleve, S. T. Bryson, A. R. Clarkson and J. Barentine, "Telescope with 100 square degree field-of-view for NASA's Kelper mission," *Optical Engineering*, vol. 52, no. 2, 2013.
- [8] M. Sweeney, M. Acreman, T. Vettese, R. Myatt and M. Thompson, "Application and testing of additive manufacturing for mirrors and precision structures," in *Proc. SPIE Vol. 9574*, 2015.
- [9] H. Herzog, J. Segal, J. Smith, R. Bates, J. Calis, A. De La Torre, D. W. Kim, J. Mici, J. Mireles, D. M. Stubbs and R. Wicker, "Optical fabrication of lightweighted 3D printed mirrors," in *Proc. SPIE Vol. 9573*, 2015.
- [10] E. Hilpert, J. Hartung, H. von Lukowicz, T. Herffurth and N. Heidler, "Design, additive manufacturing, processing, and characterization of metal mirror made of aluminum silicon alloy for space applications," *Opt. Eng.*, vol. 58(9), 2019.
- [11] C. Wang, X. P. Tan, S. B. Tor and C. S. Lim, "Machine learning in additive manufacturing: State-of-the-art and perspectives," *Additive Manufacturing*, vol. Volume 36, 2020.
- [12] J. Raplee, A. Plotkowski, M. M. Kirka, R. Dinwiddie, A. Okello, R. R. Dehoff and S. S. Babu, "Thermographic Microstructure Monitoring in Electron Beam Additive Manufacturing.," *Sci Rep*, vol. 7, p. 43554, 2017.
- [13] O. Rehme, "Cellular Design for Laser Freeform Fabrication," CUVILLIER Verlag - Technische Universität Hamburg-Harburg Institut für Laser- und Anlagensystemtechnik, Hamburg, 2010.
- [14] M. C. Sow, T. De Terris, O. Castelnau, Z. Hamouche, F. Coste, R. Fabbro and P. Peyre, "Influence of beam diameter on Laser Powder Bed Fusion (L-PBF) process," *Additive Manufacturing*, vol. 36, p. 101532, 2020.



- [15] G. Manuela and M. Paolo, "Analysis of Density, Roughness, and Accuracy of the Atomic Diffusion Additive Manufacturing (ADAM) Process for Metal Parts," *Materials*, vol. 12, no. 24, p. 4122, 2019.
- [16] R. M. Snell, C. Atkins, L. Brouwers, S. Farkas, F. Feenstra, G. Kroes, R. Haynes, W. Holland, E. Hugot, D. Jager, G. Mezo, C. Miller, K. Morris, M. Roulet, H. Schnetler, F. Tenegi and I. Todd, "Report on Additive Manufacturing Materials," Zenodo, 2020.
- [17] E. Hilpert, J. Hartung, S. Risse, R. Eberhardt and A. Tunnermann, "Precision manufacturing of a lightweight mirror body made by selective laser melting," *Precision Engineering*, vol. 53, pp. 310-317, 2018.
- [18] S. Tan, Y. Ding, Y. Xu and L. Shi, "Design and fabrication of additively manufactured aluminum mirrors," *Opt. Eng.*, vol. 59(1), 2020.
- [19] C. Miller, D. Montgomery, M. Black and H. Schnetler, "Thermal expansion as a precision actuator," in *Proc. SPIE 9912*, Edinburgh, UK, 2016.
- [20] I. A. Steele, H. Jermak, S. Bates and I. Baker, "3D-printed optical instrumentation: practical starter designs and initial experiences," in *Proc. SPIE 10706*, Austin, TX, 2018.
- [21] M. Roulet, "PhD Thesis: 3D printing for astronomical mirrors," Laboratoire d'Astrophysique de Marseille, Marseille, 2020.
- [22] W. A. Goodman, M. N. Ghasemi Nejjad, B. M. Minei, J. N. Stuecker and T. M. Anderson, "Ultra-lightweight ultra-stable RoboSiC additively manufactured lasercom telescope," in *Proc. SPIE 11101*, San Diego, CA, 2019.
- [23] X. Liu, K. Sekizawa, A. Suzuki, N. Takata, M. Kobashi and T. Yamada, "Compressive Properties of Al-Si Alloy Lattice Structures with Three Different Unit Cells Fabricated by Laser Powder Bed Fusion," *Materials*, vol. 13, no. 2902, 2020.
- [24] J. Mueller, K. H. Matlack, K. Shea and C. Daraio, "Energy Absorption Properties of Periodic and Stochastic 3D Lattice Materials," *Advanced Theory and Simulations*, vol. 2019, no. Metamaterials, pp. 1900081 (1-11), 2019.
- [25] Westminster University School of Architecture, "We Want to Learn," Diploma Studio 10, [Online]. Available: <https://wewanttorearn.wordpress.com/2019/02/03/triply-periodic-minimal-surfaces/>. [Accessed 11 June 2021].
- [26] E. Hilpert, "Design, additive manufacturing, processing, and characterization of metal mirror made of aluminum silicon alloy for space applications," *Optical Engineering*, vol. 58(9), p. 092613, 2019.
- [27] C. Mattheck, "Prof. Dr. Claus Mattheck," Seminarbüro Erika Koch, 2021. [Online]. Available: <http://www.mattheck.de/> - <http://www.mattheck.de/english/english2.htm>. [Accessed 14 June 2021].
- [28] Biomimicry Institute, "Asknature," 2021. [Online]. Available: <https://asknature.org/>. [Accessed June 2021].
- [29] D. Leidenfrost and B. Moarefi, "Generative-Engineering-Ansatz für einen B-Säulen-Karosserieknoten," *ATZ - Automobiltechnische Zeitschrift*, no. 112, pp. 68-71, 2020.



- [30] BMW Group, "Industrial-scale-3d-printing-continues-to-advance-at-bmw-group," 10 December 2020. [Online]. Available: <https://www.press.bmwgroup.com/global/article/detail/T0322259EN/industrial-scale-3d-printing-continues-to-advance-at-bmw-group>. [Accessed 13 June 2021].
- [31] B. Garret, B. Redwood and F. Schoffer, *The 3D Printing Handbook: Technologies, design and applications*, 3D Hubs B.V., 2017.
- [32] 3D Hubs, *Design Rules for 3D Printing*, 3D Hubs.
- [33] J. Kranz, D. Herzog and C. Emmelmann, "Design guidelines for laser additive manufacturing of lightweight structures in TiAl6V4," *J. Laser Appl.*, vol. 27, no. S14001, 2015.
- [34] O. Diegel, A. Nordin and D. Motte, *A Practical Guide to Design for Additive Manufacturing*, Singapore: Springer, 2020.
- [35] A. Y. Al-Maharma, S. P. Patil and B. Markert, "Effects of porosity on the mechanical properties of additively manufactured components: a critical review," *Mater. Res. Express*, vol. 7, p. 122001, 2020.
- [36] D. Frydryk, "Get the Facts on... Porosity in Metal Additive Manufacturing," GE Additive, 10 March 2020. [Online]. Available: www.ge.com/additive/blog/get-facts-porosity-metal-additive-manufacturing. [Accessed 17 May 2021].
- [37] D. B. N. P. W. M. K. W. R. P. Christian Weingarten, "Formation and reduction of hydrogen porosity during selective laser melting of AlSi10Mg," *Journal of Materials Processing Technology*, vol. Volume 221, pp. 112-120, 2015.
- [38] S. Ritt, "Will Metal Additive Manufacturing Technology be able to fulfil the customers' requirements?," in *RobTec Workshop*, Brasil, 2012.
- [39] E. Yasa and J. Kruth, "Application of Laser Re-Melting on Selective Laser Melting Parts," *Advances in Production Engineering & Management*, vol. 6, no. 4, pp. 259-270, 2011.
- [40] R. Frykholm, Y. Takeda, B.-G. Andersson and R. Carlstrom, "Solid State Sintered 3-D Printing Component by using Inkjet (Binder) Method," *J. Jpn. Soc. Powder Powder Metallurgy*, vol. Vol.63, no. No. 7, 2016.
- [41] Z. Xiang, L. Wang, C. Yang, M. Yin and G. Yin, "Analysis of the quality of slope surface in selective laser melting process by simulation and experiments," *Optik - International Journal for Light and Electron Optics*, vol. 176, no. 1, pp. 68-77, 2019.
- [42] C. Atkins, C. Feldman, D. Brooks, S. Watson, W. Cochrane, M. Roulet, P. Doel, R. Willingale and E. Hugot, "Additive manufactured x-ray optics for astronomy," in *Proc. SPIE 10399-52*, 2017.
- [43] Wohlers Associates, "Wohlers Report 2019," Wohlers Associates, Fort Collins, Colorado, 2019.
- [44] S. Farkas, T. Agocs, C. Atkins, L. Brouwers, J. Dufils, A. Joo, G. Mezo, K. Morris, M. Rodenhuis, R. Melanie, H. Schnetler, R. Snell, F. Tenegi-Sanginés, A. Vega-Moreno and B. van de Vorst, "Freeform active mirror designed for additive manufacturing," in *Proc. SPIE 11451*, 2020.



- [45] C. Atkins, W. Brzozowski, N. Dobson, M. Milanova, S. Todd, D. Pearson, C. Bourgenot, D. Brooks, R. Snell, W. Sun, P. Cooper, S. G. Alcock and I.-T. Nistea, “Additively manufactured mirrors for CubeSats,” in *Proc. SPIE 11116*, 2019.
- [46] N. Sahel, N. Hopkinson, R. J. M. Hague and S. Wise, “Effects of electroplating on the mechanical properties of stereolithography and laser sintered parts,” *Rapid Prototyping journal*, vol. 10 (5), no. DOI:10.1108/13552540410562340, pp. 305-315, 2004.
- [47] 3DDC, “Mechanical Properties Test SLA - SLS,” [Online]. Available: https://3ddc.eu/pdfs/metal/MechanicalPropertiesTest_SLASLS_V1.0.pdf. [Accessed 7 May 2021].
- [48] Mac Dermid Enthone, “Electroless Nickel Properties,” [Online]. Available: industrial.macdermidenthone.com/products-and-applications/electroless-nickel/properties. [Accessed 7 May 2021].
- [49] Renishaw, “CMM inspection of AM part using REVO 5-axis,” [Online]. Available: [https://resources.renishaw.com/details/CMM+inspection+of+AM+part+using+REVO+5-axis\(254123\)\(93694\)](https://resources.renishaw.com/details/CMM+inspection+of+AM+part+using+REVO+5-axis(254123)(93694)). [Accessed 16 02 2021].
- [50] J. Kacmarcik, D. Spahic, K. Varda, E. Porca and N. Zaimovic-Uzunovic, “An investigation of geometrical accuracy of desktop 3D printers using CMM,” *IOP Conf. Series: Materials Science and Engineering*, no. 393, 2018.
- [51] P. Cooper, W. Sun, S. B. Brown and C. Atkins, “Micro CT measurements of defects in light-weighted mirrors for applications in space imaging,” in *58th Annual Conference of the British Institute of Non-Destructive Testing (NDT 2019)*, Telford, UK, 2019.
- [52] N. Horvath and M. A. Davies, “Advancing lightweight mirror design: A paradigm shift in mirror preforms by utilizing design for additive manufacturing,” *Applied Optics*, 2020.
- [53] N. Heidler, E. Hilpert, J. Hartung, H. von Lukowicz, C. Damm, T. Peschel and S. Risse, “Additive manufacturing of metal mirrors for TMA telescope,” in *Proc. SPIE 10692*, 2018.
- [54] M. Roulet, C. Atkins, E. Hugot, S. Lemared, S. Lombardo and M. Ferrari, “3D printing for astronomical mirrors,” in *Proc. SPIE Vol. 10675*, 2018.
- [55] C. Atkins, C. Feldman, D. Brooks, S. Watson, C. William, M. Roulet, E. Hugot, M. Beardsley, M. Harris, C. Spindloe, S. G. Alcock, I.-T. Nistea, C. Morawe and P. Francois, “Topological design of lightweight additively manufactured mirrors for space,” in *Proc. SPIE Vol. 10706*, 2018.
- [56] K. Woodard and M. Bruce, “Progress on high-performance rapid prototype aluminum mirrors,” in *Proc. SPIE 10181*, 2017.
- [57] M. Brunelle, I. Ferralli, W. Rebecca and K. Medicus, “Current use and potential of additive manufacturing for optical applications,” in *Proc. SPIE 10448*, Rochester, 2017.
- [58] B. Goodman, “The results of Goodman Technologies NASA Phase II SBIRs for additive manufacturing of mirrors and telescopes,” in *Proc. SPIE 11487*, Digital, 2020.



- [59] N. Horvath, A. Honeycutt and M. A. Davies, "Grinding of additively manufactured silicon carbide surfaces for optical applications," *CIRP Annals*, vol. 69, no. 1, pp. 509-512, 2020.
- [60] Senvol, "Senvol | Data to help companies implement additive manufacturing," [Online]. Available: <http://senvol.com/database/>. [Accessed 19 05 2021].
- [61] NeoMetrix, "NeoMetrix," [Online]. Available: <http://3dscanningservices.net/blog/need-know-3d-scanning/>. [Accessed 7 May 2021].



5 CASE STUDIES

This section provides a series of one-page case study examples that describe different AM design, manufacture and post-processing methodologies used primarily within astronomy or Earth Observation. The information within the case studies highlights some of the key AM considerations: size, material, method, time and cost. References are provided at the end of the case studies to provide a broader picture of the project and application – a summary of the different studies is provided in Table 19.

Table 19: case studies highlighting different aspects of AM design, manufacture and post-processing.

#	Case Study title	Sector
1	Lightweight mirror development: nanosat application	Astronomy / Earth Observation
2	Lightweight mirror development: optimization study	Astronomy
3	Frame – Flying Copter	Aeronautical
4	Hydraulic Manifold Crossing	Industrial / Hydraulic systems
5	Optical Mirror - SiSiC	Astronomy
6	Lightweight Optical Mirror Designs	Astronomy
7	Lightweight mirror development: novel conformal lattice	Earth Observation
8	Ceramic Deformable Mirror	Astronomy
9	Freeform Mirror	Astronomy
10	Sentinel 5 Tropomi Mirror	Earth Observation
11	Actuator flexure	Astronomy
12	Sentinel 3 Viscal base-plate	Earth Observation
13	SPECTROLITE: hyperspectral imaging spectrometer	Earth Observation

1. Lightweight mirror development: nanosat application

An investigation into AM materials and post-processing for lightweight mirror development towards nano-satellites



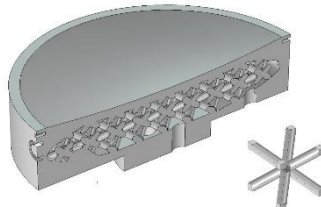
Specifications:

Dimensions (lxbxh):	84 mm \varnothing x 17.3 mm
Volume:	65130.0 mm ³
Application:	Astronomical
Design:	UKRI STFC UKATC
Software:	Autodesk Inventor
AM Process:	Laser Powder Bed Fusion
System:	SLM 500HL
Material:	Aluminium AlSi10Mg
Supplier:	CA Models, UK
Lead time	2 weeks
Cost:	£ 325,- excl. post-processing, VAT and shipping cost
Surface finish:	All external surfaces machined (lathe)
Post processing:	Diamond turning (Durham University, UK)
Year of Production:	2019

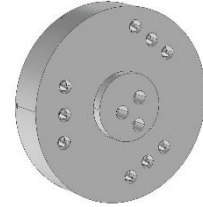
Additive Manufacturing Re-Design considerations:



The nominal design is a concave mirror which connects from the base to the mount



The lightweight internal structure of the mirror is created using a BCC (body-centered cubic) lattice.



The base of the mirror has holes to allow the removal of un-sintered metal powder and a sacrificial spigot to facilitate machining.



The aluminum substrate prior to machining



The aluminum substrate after machining



The aluminium substrate after diamond turning.

Reference:

1. 'Additively manufactured mirrors for CubeSats', C. Atkins et al., Proc. SPIE 11116, 2019 [45]
2. 'Lightweighting design optimisation for additively manufactured mirrors', C. Atkins et al., Proc. SPIE 11116, 2019
3. Research funded by the UK Space Agency under grant number NSTP3-PF2-008

2. Lightweight mirror development: optimization study

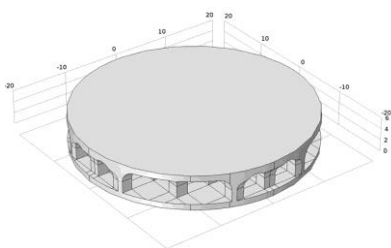
Investigation into the use of topology optimization for mirror lightweight structures



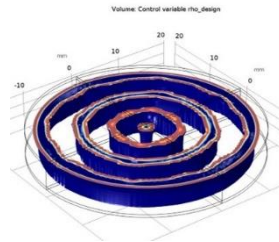
Specifications:

Dimensions (lxbxh):	40 mm \varnothing x 6 mm
Volume:	3449 mm ³ (initial design) -> 2347 mm ³ (after optimisation)
Application:	Astronomical
Design:	UKRI STFC UKATC
Software:	COMSOL Multiphysics & Autodesk Inventor
AM Process:	Laser Powder Bed Fusion
System:	SLM 500HL
Material:	Aluminium AlSi10Mg
Supplier:	CA Models, UK
Lead time	2 weeks
Cost:	£ 250,- ex post-processing, VAT and shipping cost
Surface finish:	CNC milled flat & NiP electroless plating
Post processing:	Optical polishing (University College London, UK)
Year of Production:	2017

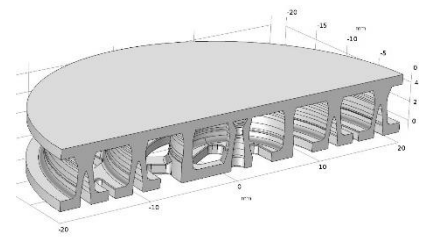
Additive Manufacturing Re-Design considerations:



Initial design with a 40 mm diameter and 4 mm lightweight height between the two face plates.



The topology optimized lightweight structure designed to ensure rigidity under a polishing pressure.



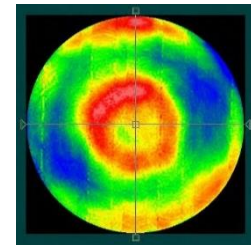
A cross section of the final optimized design.



The polished non-optimized design with a weight of 14.3 g.



The polished topology optimized design with a weight of 11.7 g.



An interferometer image ($\lambda = 633$ nm) of the optimized sample demonstrating a peak to valley of ~ 200 nm and a root mean square of ~ 30 nm.

Reference:

4. 'Additive manufactured x-ray optics for astronomy', C Atkins et al., Proc. SPIE 10399, 2017
5. 'Topological design of lightweight additively manufactured mirrors for space', C Atkins et al., Proc. SPIE 10706, 2018
6. Research funded by the UK Space Agency under grant number NSTP3-PF-007

3. Frame – Flying Copter

Topology optimized Lightweight structure of a UAV Helicopter frame

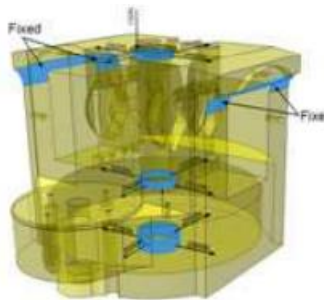


Specifications:	
Dimensions (lxbxh):	147 x 160 x 128 mm
Volume:	158.330 mm ³
Application:	Aeronautical
Design:	Flying Cam – Sirris – Mbproto
Software:	Unigraphics NX, Materialise Magics,
AM Process:	PBF
System:	SLM Solutions
Material:	AlSi12
Supplier:	MB Proto / 3DS Group France / Volum-e (www.volum-e.com)
Production time:	68 hours
Cost:	€ ---
Surface finish:	Shot peening
Post processing:	Subtractive machining, Milling
Year of Production:	2010

Additive Manufacturing Re-Design considerations:



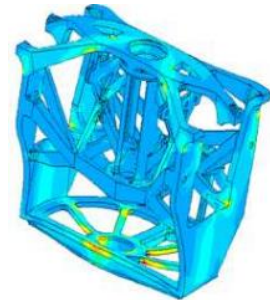
Material efficiency and lightweight structures in a 3D-printed helicopter frame for Flying Cam’s unmanned aerial vehicle (UAV), lowering the weight from 530 g to 392 g and thereby prolonging the drone’s battery life.



Setting boundaries



Topology optimization



Stress verification

Reference:

COMPOLIGHT Grant agreement ID: 213477 - FP7-NMP project 2008 – 2011

4. Hydraulic Manifold Crossing

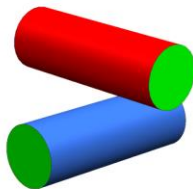
The part shows complex internal channels improving the fluid flow and making possible the reduction of the volume and mass.



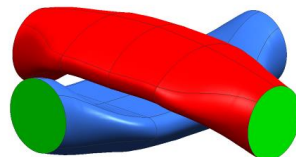
Specifications:

Dimensions (lxbxh):	85 x 85 x 38 mm (LxWxH)
Volume:	135.331 mm ³
Application:	Industrial / Hydraulic systems
Design:	Hydrovision in cooperation with TNO and Fraunhofer IFAM
Software:	Unigraphics NX, Materialise Magics,
AM Process:	Powder Bed Fusion
System:	EOS M270
Material:	316L / GP1 EOS
Supplier:	Fraunhofer IFAM
Production time:	40 hr 1pc / 137 h
Cost:	...
Surface finish:	Shot peening
Post processing:	Non
Year of Production:	2010

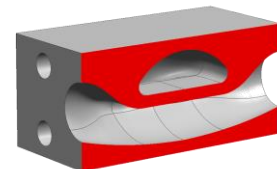
Additive Manufacturing Re-Design considerations:



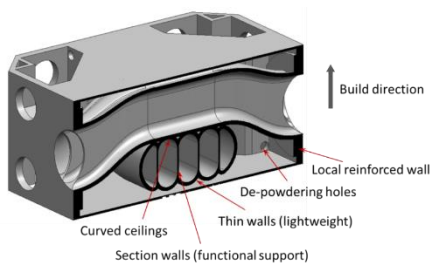
How to design a pipe crossing in a limited space?



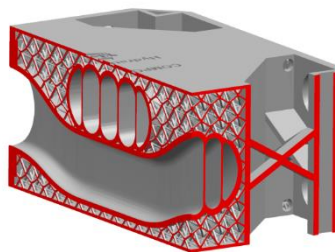
Flat Pipes to limit height while maintain flow



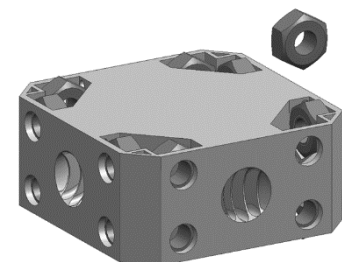
Cross sectional view



Wall act as support during build and strengthen "flat pipe" in final product.



Improved design with thin wall and internal lattice structure.



Slots for standard hexagonal nuts instead of threaded holes.

Reference:

COMPOLIGHT Grant agreement ID: 213477 - FP7-NMP project 2008 – 2011

5. Optical Mirror - SiSiC

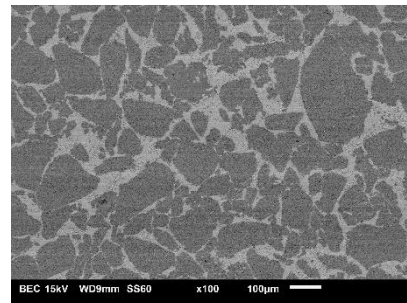
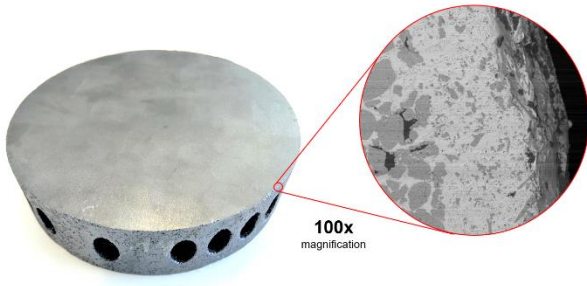
Feasibility study on 3D printing of Silicon Carbide.



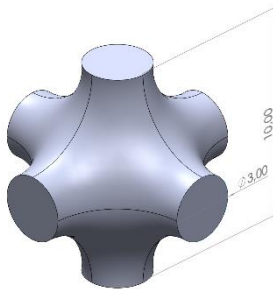
Specifications:

Dimensions (lxbxh):	100 x 100 x 26 mm
Volume:	95.737 mm ³
Application:	Astronomical
Design:	IAC Tenerife, TNO
Software:	SolidWorks, Materialise Magics
AM Process:	Binder Jetting
System:	ExOne
Material:	SiSiC - SicaPrint® Si
Supplier:	SGL Carbon - Germany
Lead time	6 weeks
Cost:	€ 820,-
Surface finish:	Shot peening
Post processing:	Grinded top surface
Year of Production:	2020

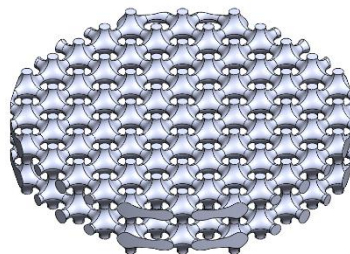
Additive Manufacturing Re-Design considerations:



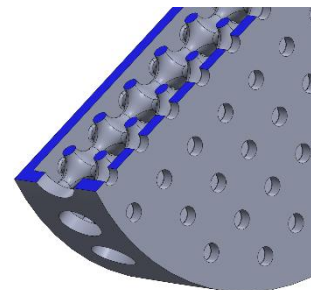
The grinded top surface of the printed mirror. Binder Jet 3D printing is used to reaction bond Silicon Carbide powder with phenolic resin. Fully dense functional parts are realized after capillary liquid silicon infiltration. With Scanning Electron Microscopy in back-scatter mode, the SiC particles embedded in the Si matrix can be clearly distinguished.



TPMS - Schwarz P based lattice structure.
Unit size 10x10x10 mm (XYX)
3 mm strut size.



Internal Primitive Cubic based lattice structure. Non-conformal to outer surface.



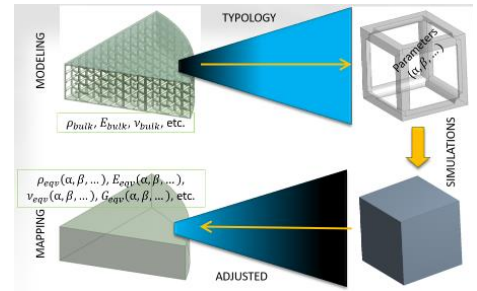
Powder escape holes of 4 mm at rear side.
0.5 mm Radius fillets to prevent sharp corners and improve power removal

Reference:

OPTICON H2020 program – grant agreement No. 730890 - JRA5 - Additive Astronomy Integrated-Component Manufacturing (A2IM)

6. Lightweight Optical Mirror Designs

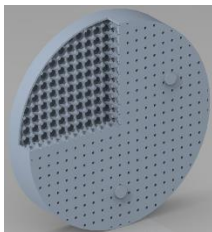
Develop of a methodology to reduce the time-consuming in the analysis of very complex geometry



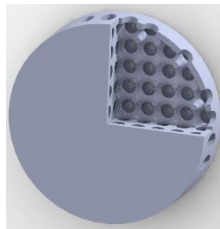
Specifications:

Dimensions (dxh):	100 x 16.667 mm
Volume:	Variable (less than 130cm ³)
Application:	Astronomical
Design:	IAC Tenerife - TNO
Software:	Creo Parametrics, Ansys Workbench, Spaceclaim
AM Process:	Varioust (Ceramic Binder Jetting & Liquid Silicon Infiltration, EBM, Powder Bed Fusion)
System:	Various
Material:	Several Materials Used (SiSiC, AlSiMg, PA12)
Supplier:	SGL Carbon, Sheffield University, RP2 Prototyping
Lead time	1 to 5 weeks
Cost:	From € 30,- pc (PA12) to € 820,- (SiSiC)
Surface finish:	Not finish
Post processing:	-
Year of Production:	2020

Additive Manufacturing Re-Design considerations:



Initial model, designed by IAC



Modified Model, proposed by TNO



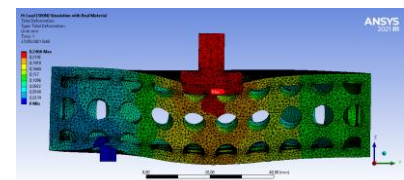
Manufactured by TNO in PA 12



Manufactured by SGL CARBON, supplied by TNO in Sicaprint® Si (Si-SiC)



Test Bench for the TNO Sample in PA12



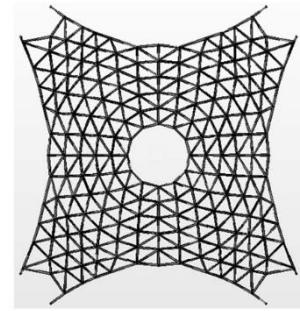
Simulation of TNO Sample (PA12) in Test Bench

Reference:

'Design for additive manufacture (DfAM): the "equivalent continuum material" for cellular structures analysis', A Vega et al., Proc. SPIE 11450, 2020 OPTICON H2020 program – grant agreement No. 730890 - JRA5 - Additive Astronomy Integrated-Component Manufacturing (A2IM)

7. Lightweight mirror development: novel conformal lattice

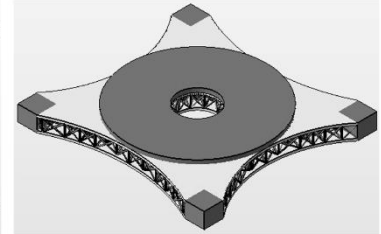
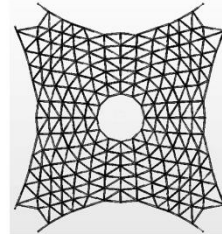
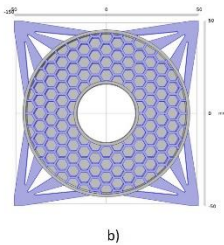
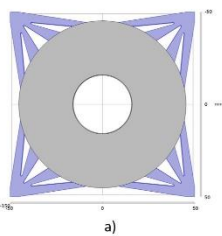
Part consolidation of a mirror with a mounting structure intended for nanosat applications. The consolidated structure incorporates a lightweight conformal lattice. This case study details a first design iteration.



Specifications:

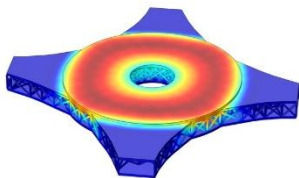
Dimensions (lxbxh):	90 mm x 90 mm x 9mm
Volume:	~ 37% of an equivalent solid
Application:	Earth observation & space science
Design:	University of Sheffield
Software:	Rhino
AM Process:	Electron Beam Powder Bed Fusion (prototype only)
System:	ARCAM Q20
Material:	Titanium (Ti64 – prototype only)
Supplier:	University of Sheffield
Lead time	In-house
Cost:	In-house
Surface finish:	Top and base machined (Future work)
Post processing:	Diamond turning (Future work by RAL Space, UK)
Year of Production:	2021

Additive Manufacturing Re-Design considerations:

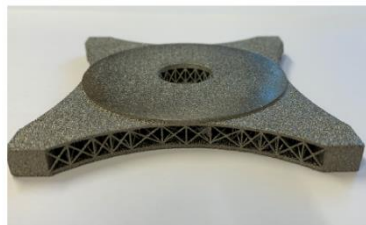


Initial concept: there are four arms to connect the mirror to the nanosat chassis and an open-back lightweight structure.

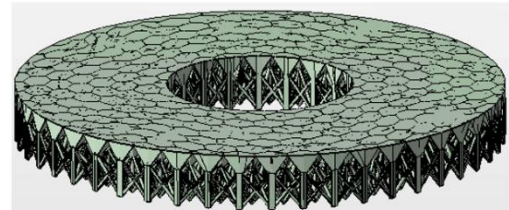
First design iteration: the conformal internal lattice (*left*) links the mirror to the supports; the lightweight structure is held between to face plates to create a sandwich mirror (*right*).



A finite element simulation of the first iteration investigating the expected distortions.



A titanium (Ti64) prototype printed using electron-beam powder bed fusion.



A second iteration of the lattice structure to allow the part to be printed horizontal to the build plate.

Reference:

1. 'An additive manufactured CubeSat mirror incorporating a novel circular lattice', R. Snell, et al., Proc. SPIE 11451, 2020
2. 'Lightweighting design optimisation for additively manufactured mirrors', C. Atkins et al., Proc. SPIE 11116, 2019

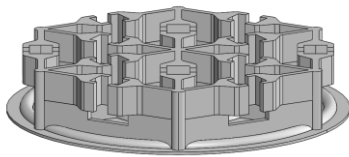
8. Ceramic Deformable Mirror

Feasibility study on 3D printing of Al₂O₃ ceramics.

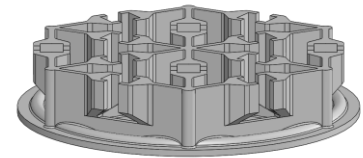
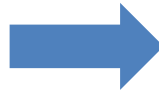


Specifications:	
Dimensions (lxbxh):	Ø 52 x 10,1 mm
Volume:	6.222 mm ³
Application:	Astronomical
Design:	LAM - Laboratoire d'Astrophysique de Marseille, TNO
Software:	SolidWorks, Materialise Magics
AM Process:	Vat Photopolymerisation, debinding and sintering
System:	Admaflex 130
Material:	AluminaOxide - Al ₂ O ₃
Supplier:	Formatec, The Netherlands
Lead time	5 weeks
Cost:	€ 225,-
Surface finish:	non
Post processing:	Grinded top surface
Year of Production:	2020

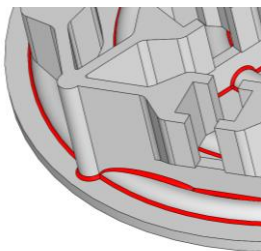
Additive Manufacturing Re-Design considerations:



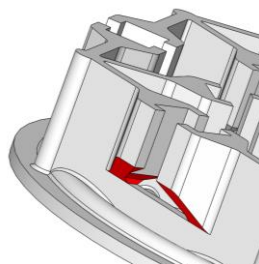
AM design concept



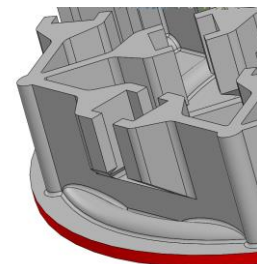
Design modifications for Ceramic Vat Photo polymerization.



Addition of fillets. Internal radius: 0,5mm



Addition of chamfers. Angle: 45°



Addition of material. Thickness: 1 mm

Reference:

OPTICON H2020 program – grant agreement No. 730890 - JRA5 - Additive Astronomy Integrated-Component Manufacturing (A2IM)

9. Freeform Mirror

Deformable freeform mirror mock-up. The integrated optical structure (IOS) has a variable thickness (and stiffness), mounting features for separate actuators and an integrated kinematic mount. The components are made for presentational purposes, not functional models.



Specifications:	Concept 1	Concept 2
Dimensions (lxbxh):	102 x 101 x 13 mm	116 x 114 x 22,5 mm
Volume:	... mm ³	21.880 mm ³
Application:	Astronomical	
Design:	Konkoly Observatory,	
Software:	Ansys, Autodesk Inventor	
AM Process:	Material Extrusion	Multi Jet
System:	Ultimaker	HP Jet Fusion 3D 4200
Material:	1612 PLA Silver metallic	PA12
Supplier:	Konkoly Observatory	Rp2
Lead time	5 weeks	1 week
Cost:	€ ..., -	€ 23,-
Surface finish:	non	non
Post processing:	non	non
Year of Production:	2020	2020

Additive Manufacturing Re-Design considerations

The performance and residuals of the generated shape. 1.5mm Thickness between active array nodes.

Ansys Topology optimisation to create the design of the Freeform Mirror

Inventor CAD model to generate and surface model.

Concept 01	Concept 02
<p>Material extrusion model printed with a layer thickness of 0.1 mm and a nozzle diameter of 0.4 mm.</p>	<p>Multi Jet Fusion model printed with a layer thickness of 0,08 mm and a printing resolution of 1200 dpi (X,Y)</p>

Reference:

- OPTICON H2020 program – grant agreement No. 730890 - JRA5 - Additive Astronomy Integrated-Component Manufacturing (A2IM)
- Freeform active mirror designed for additive manufacturing, Proc. SPIE 11451, Advances in Optical and Mechanical Technologies for Telescopes and Instrumentation IV, 114512M (13 December 2020); Szigfrid Farkas et.al. Konkoly Observatory for Astronomy and Earth Sciences,

10. Sentinel 5 Tropomi Mirror

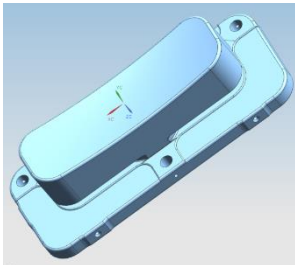
Feasibility study on 3D printing of a lightweight mirror



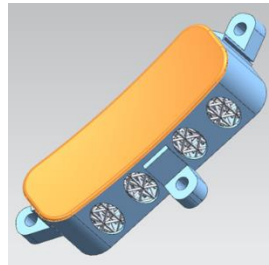
Specifications:

Dimensions (lxbxh):	121,5 x 50 x 32.6 mm
Volume:	30.295 mm ³
Application:	Earth Observation
Design:	TNO, LayerWise, ESA
Software:	UniGraphics NX, Materialise Magics
AM Process:	PBF
System:	DMP Layerwise
Material:	Ti6Al4V
Supplier:	Layerwise / 3DSystems Belgium
Lead time	5 weeks
Cost:	€ ~12.000,- Including Milling (2013)
Surface finish:	Shot peening
Post processing:	Milling, NiP Coating (AHC Benelux), Diamond turning, Polishing
Year of Production:	2014

Additive Manufacturing Re-Design considerations:



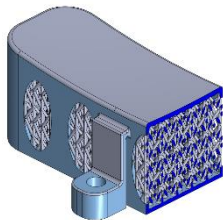
Conventional design based upon milling
Material: Al6061
Mass: 284.6 gr
1st eigen freq ~2100 Hz



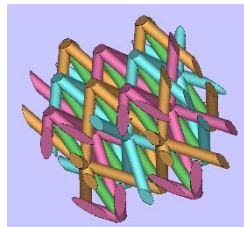
Additive Manufacturing optimized design
Mass: 129.7 gr
Weight reduction of 54%



Additive Manufacturing optimized design
Material: Ti6Al4V / NiP Coating
Mass: 127.7 gr
1st eigen freq ~2100 Hz



Cross section of mirror with the lattice structure visible



Combined Triangular lattice structure with vertical struts
Strut diameter: 0.8 mm Pitch: 3.35 mm
Unit-cell height: 10mm



Oval holes to ease powder removal and to reduce weight

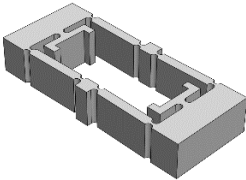
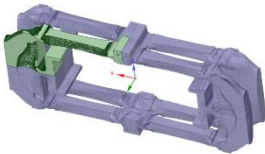
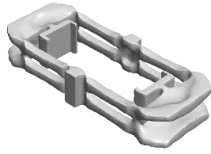
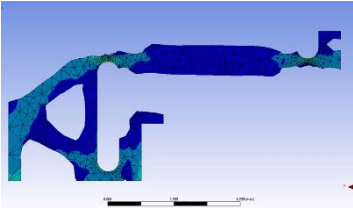
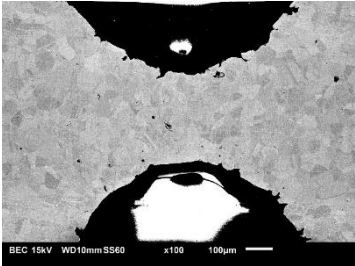
Reference:

Rapid Manufacturing for Space application – A. Hoogstrate TNO, Precisiebeurs 2014
Project: Advanced Manufacturing Methods for Systems-of-Microsystems Nano spacecraft – ESA T723-184QM

11. Actuator flexure

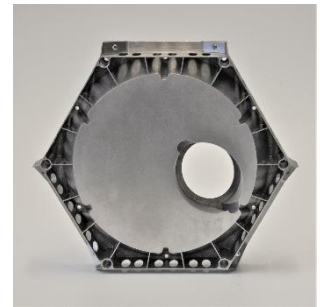
Feasibility study on 3D printing detailed small metallic components



Specifications:		
Dimensions (lxbxh):	30 x 13 x 5 mm	
Volume:	850 mm ³	
Application:	Astronomical	
Design:	UKRI STFC - TNO	
Software:	Ansys Workbench, Spaceclaim, Magics	
AM Process:	Metal Binder Jetting debinding and sintering	
System:	Höganäs DM P2500	
Material:	Stainless Steel 316L	
Supplier:	i-Materialise , Belgium	
Lead time	3 weeks	
Cost:	€ 30,- ex VAT and shipping cost	
Surface finish:	Shot Peening / Satin	
Post processing:	-	
Year of Production:	2021	
Additive Manufacturing Re-Design considerations:		
 <p>Initial design optimized for wire EDM</p>	 <p>Topology optimization was performed on 1/8 of functional geometry.</p>	 <p>Topology optimized design</p>
 <p>With Ansys WorkBench CAE software a weight reduction of 47% was realized.</p>	 <p>Polished and etched Cross sectional view of the Flexural hinge. Low intra granular porosity. Grain size of approx. 50 µm</p>	 <p>3D printed Stainless steel actuator.</p>
Reference:		
OPTICON H2020 program – grant agreement No. 730890 - JRA5 - Additive Astronomy Integrated-Component Manufacturing (A2IM)		

12. Sentinel 3 VISCAL base-plate

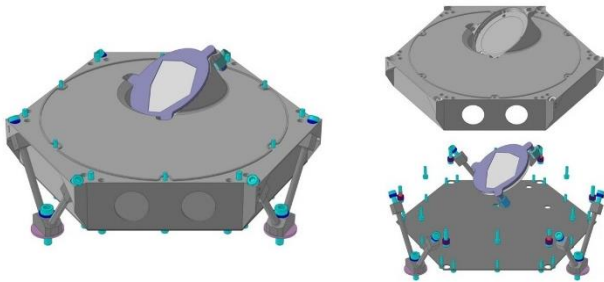
Feasibility study on 3D printing of an Aluminum instrumentation base plate



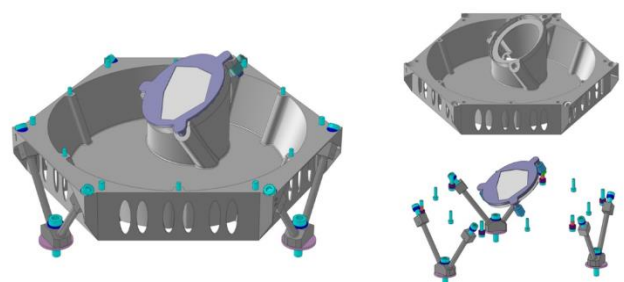
Specifications:

Dimensions (lxbxh):	241 x 209 x 67,50mm
Volume:	141.212 mm ³ after printing (113.557 mm ³ after milling)
Application:	Earth Observation
Design:	TNO, LayerWise, ESA
Software:	UniGraphics NX, Materialise Magics
AM Process:	PBF
System:	DMP Layerwise
Material:	AlSi10Mg
Supplier:	Layerwise / 3DSystems Belgium
Lead time	5 weeks
Cost:	€ ~12.000,- Including Milling (2013)
Surface finish:	Shot peening
Post processing:	HIP, milling, Alodine finish
Year of Production:	2013

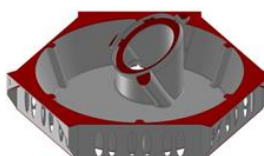
Additive Manufacturing Re-Design considerations:



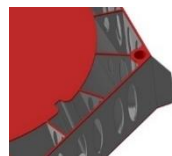
Conventional design based upon milling
2 parts, 18 bots
mass: 367 gr
Eigen-frequency: 230 Hz



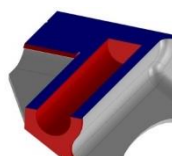
Additive Manufacturing optimized design
One part
mass: 316 gr
Eigen-frequency: 596 Hz



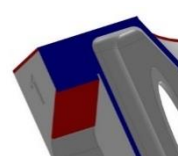
Additional material for post processing milling



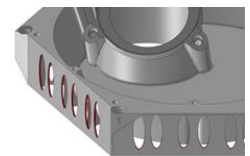
Ribs for additional stiffness



Pocket hole for post processing



Intentional undercuts for ease of postprocessing milling



Oval holes for weight reduction

Reference:

Rapid Manufacturing for Space application – A. Hoogstrate TNO, Precisiebeurs 2014
Project: Advanced Manufacturing Methods for Systems-of-Microsystems Nano spacecraft – ESA T723-184QM

13. SPECTROLITE: hyperspectral imaging spectrometer

3D Wax printing and precision casting of an Aluminum instrument housing.

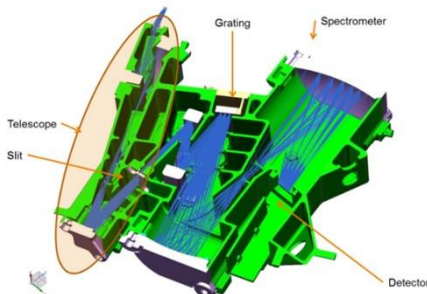
Spectrolite: an instrument for measuring air pollution (for example, NO₂, SO₂) and greenhouse gases (for example, CH₄ and CO₂), based on technology used in the ground-breaking TROPOMI satellite instrument.



Specifications:

Dimensions (lxbxh):	241 x 209 x 95 mm
Volume:	141.212 mm ³ after printing (113.557 mm ³ after milling)
Application:	Earth Observation
Design:	TNO
Software:	UniGraphics NX
AM Process:	SLS of PS infiltrated with wax, Aluminum Investment Casting
System:	Sophia [®] process by Zollern
Material:	A.357 Aluminum Silicon Magnesium
Supplier:	Zollern Germany
Lead time	~ 8 weeks
Cost:	Total price: 9k EURO/pc – 15k EURO/pc depending on order quantity.
Surface finish:	Shot peening,
Post processing:	Heat treatment, finish milling, Anodizing
Year of Production:	2014

Additive Manufacturing Re-Design considerations:



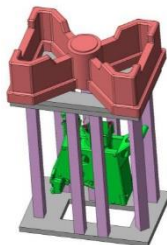
Optical path



Spectrolite fits into the standardized mechanical structure of a large CubeSat.



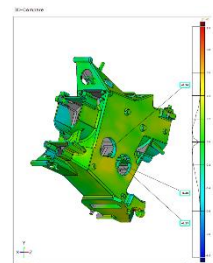
Wax model of the housing made by additive manufacturing.



Wax model with supply chains and reservoir for Investment casting



Spectrolite housing finished milled and black anodized



'Best fit' of the optical scan, indicating the difference between casting and CAD model

Reference:

- L.F. van der Wal, et.al "High-grade, compact spectrometers for Earth Observation from SmallSats" – TNO. SPIE - Conference on Remote Sensing Technologies and Applications for Urban Environments. 26-27 September 2016, 10008
- Hoogstrate TNO Rapid Manufacturing for Space application –, Precisiebeurs 2014
Project: Advanced Manufacturing Methods for Systems-of-Microsystems Nano spacecraft – ESA T723-184QM



6 APPENDIX: AM MATERIAL PROPERTIES REFERENCES

The following tables provide information regarding the material properties used within Section 3.3.7.6. The online resource Senvol [60], a database of AM material properties, is a practical tool to provide a list of properties for a given AM material and is referenced often within the tables below.

It should be noted that the material properties quoted often refer to a given machine and print parameters and therefore may not be accurate for all applications.

6.1 Metals

Metal alloy	Manufacturer	Reference
Titanium alloys		
Ti64	APWORKS	Senvol database [60]
Ti64	EOS Titanium	Senvol database [60]
Ti Gr 23	3D Systems LaserForm	Senvol database [60]
Zti-Powder	Z3DLAB	Senvol database [60]
Ti6Al4V ELI-0406	Renishaw	Senvol database [60]
Ti6Al4V 30 µm	SLM-solutions	https://www.slm-solutions.com/fileadmin/user_upload/MDS_Ti-Alloy_TiAL6V4_ELI_0719.pdf
Ti6Al4V 60 µm 400W	SLM-solutions	https://www.slm-solutions.com/fileadmin/user_upload/MDS_Ti-Alloy_TiAL6V4_ELI_0719.pdf
Ti6Al4V 60 µm 700W	SLM-solutions	https://www.slm-solutions.com/fileadmin/user_upload/MDS_Ti-Alloy_TiAL6V4_ELI_0719.pdf
Ti6Al4V 90 µm	SLM-solutions	https://www.slm-solutions.com/fileadmin/user_upload/MDS_Ti-Alloy_TiAL6V4_ELI_0719.pdf
Ti grade 2 30 µm	SLM-solutions	https://www.slm-solutions.com/fileadmin/user_upload/MDS_Ti-Alloy_Ti_Grade_2_0519.pdf
Ti6Al4V (grade 5)	3D systems LaserForm	https://www.3dsystems.com/sites/default/files/2017-12/3d-systems-laserform-stainless-ti-gr5%28a%29-datasheets-us-a4-2017-12-07-web.pdf
Ti6Al4V (grade 23)	3D systems LaserForm	https://www.3dsystems.com/sites/default/files/2018-03/3d-systems-laserform-ti-gr23%28a%29-datasheet-us-a4-2018.03.21-web.pdf
Ti48Al2Cr2Nb	Heraeus	Senvol database [60]
Ti (grade 1)	3D systems LaserForm	https://www.3dsystems.com/sites/default/files/2017-12/3d-systems-laserform-ti-gr1%28a%29-datasheet-a4-us-2017-12-07-web.pdf
Steel alloys		
316L	LWP	https://www.camodels.co.uk/media/1315/metal-am-stainless-steel-316-datasheet-ca-models.pdf
316L (B)	3D systems LaserForm	Senvol database [60]
SS 316L	APWORKS	Senvol database [60]
SS 316L	EOS	Senvol database [60]
SS 316L	GKN Additive	Senvol database [60]
316L 1.4404 / A276	SOLIDTEQ	Senvol database (values averaged) [60]
SS 316L	Sondasys	Senvol database [60]



SS 316L-0407	Renishaw	Senvol database [60]
316L 30 µm	SLM-solutions	https://www.slm-solutions.com/fileadmin/user_upload/MDS_FE-Alloy_316L_0219.pdf
316L 50 µm	SLM-solutions	https://www.slm-solutions.com/fileadmin/user_upload/MDS_FE-Alloy_316L_0219.pdf
316L SS (A)	LaserForm	https://www.3dsystems.com/sites/default/files/2017-06/3D-Systems_LaserForm_316L_%28A%29_DATASHEET_A4_US_2017.06.21_WEB.pdf
316L SS (B)	LaserForm	https://www.3dsystems.com/sites/default/files/2019-05/3d-systems-laserform-316L%28B%29-datasheet-a4-us-2019-05-03-web.pdf
Maraging steel M300 (200W)	Renishaw	https://resources.renishaw.com/en/details/data-sheet-maraging-steel-m300-for-200-w-powder-for-additive-manufacturing--96325
Maraging steel M300 (400W)	Renishaw	https://resources.renishaw.com/en/details/data-sheet-maraging-steel-m300-for-400-w-powder-for-additive-manufacturing--96326
Aluminium alloys		
AlSi10Mg	CA Models	https://www.camodels.co.uk/media/1316/metal-am-aluminium-alsi10mg-datasheet-ca-models.pdf
AlSi10Mg	EOS aluminium	Senvol database [60]
AlSi10Mg	GKN Additive	Senvol database [60]
AlSi10Mg	SOLIDTEQ	Senvol database [60]
AL1000-AM	Elementum	Senvol database [60]
AlSi7Mg0.6	3D systems Laser form	Senvol database [60]
AlSi10Mg 0403 (400W)	Renishaw	http://resources.renishaw.com/en/download/data-sheet-alsi10mg-0403-400-w-powder-for-additive-manufacturing--73122
AlSi10Mg 0403 (200W)	Renishaw	https://resources.renishaw.com/en/details/data-sheet-alsi10mg-0403-200-w-powder-for-additive-manufacturing--73121
Nickel (Inconel) alloys		
In 718	EOS Nickel alloy	Senvol database [60]
In 718 30 µm	Renishaw	https://resources.renishaw.com/en/details/data-sheet-in718-0405-powder-for-additive-manufacturing--94192
In 718 60 µm	Renishaw	https://resources.renishaw.com/en/details/data-sheet-in718-0405-powder-for-additive-manufacturing--94192
In718 30 µm	SLM-solutions	https://www.slm-solutions.com/fileadmin/user_upload/MDS_Ni-Alloy_IN718_2.4668_0719.pdf
In718 60 µm	SLM-solutions	https://www.slm-solutions.com/fileadmin/user_upload/MDS_Ni-Alloy_IN718_2.4668_0719.pdf
Ni625	LaserForm (Inconel 625)	https://uk.3dsystems.com/sites/default/files/2018-09/3D-Systems_LaserForm_Ni625%28B%29_DATASHEET_A4_US_2018.09.06_WEB.pdf
IN625	APWORKS Nickel alloy	Senvol database [60]
In 625	EOS Nickel alloy	Senvol database [60]
In 625 30 µm	Renishaw	http://resources.renishaw.com/en/download/data-sheet-in625-0402-powder-for-additive-manufacturing--97039
In 625 60 µm	Renishaw	http://resources.renishaw.com/en/download/data-sheet-in625-0402-powder-for-additive-manufacturing--97039



In625 20 microns	SLM-solutions	https://www.slm-solutions.com/fileadmin/user_upload/MDS_Ni-Alloy_IN625_0819.pdf
In625 30 microns	SLM-solutions	https://www.slm-solutions.com/fileadmin/user_upload/MDS_Ni-Alloy_IN625_0819.pdf
In625 60 microns	SLM-solutions	https://www.slm-solutions.com/fileadmin/user_upload/MDS_Ni-Alloy_IN625_0819.pdf
Cu alloys		
(AM Copper-100)	Elementum Copper	Senvol database [60]
CuCr1Zr	GKN Additive	Senvol database [60]
Copper alloy BR6-P6	Sondasys	Senvol database [60]
CuNi2SiCr	SLM-solutions Cu-alloy	https://www.slm-solutions.com/fileadmin/user_upload/MDS_Cu-Alloy_CuNi2SiCr_1909.pdf
CuNi2-A LMF	TRUMPF CuNi2-A LMF	Senvol database [60]

6.2 Polymers

Polymer	Manufacturer	Reference
Polypropylene (PP) or PP like		
Accura 25	3D Systems	https://www.ame-group.co.uk/Data/Prototype_Downloads/Accura_25_Plastic_A4_UK.pdf
Accura PP White (SL 7811)	3D Systems	https://www.3dsystems.com/sites/default/files/2017-11/3d-systems-accura-pp-white-sl7811-datasheet-us-a4-2017-11-08-web.pdf
DuraForm EX Plastic	3D Systems	https://www.3dsystems.com/sites/default/files/2018-09/3d-systems-duraFormex-datasheet-usen-2018-09-24-web.pdf
VisiJet ProFlex (M2G-DUR) (MJP)	3D Systems	https://www.3dsystems.com/sites/default/files/2020-01/3d-systems-visiJet-m2-material-selection-guide-a4-us-2020-01-08-web.pdf
Figure 4® FLEX-BLK 20 ASTM	3D Systems	https://www.3dsystems.com/sites/default/files/2020-03/3d-systems-figure-4-FLEX-BLK-20-datasheet-usa4-2020-03-13-web.pdf
Figure 4® FLEX-BLK 20 ISO	3D Systems	https://www.3dsystems.com/sites/default/files/2020-03/3d-systems-figure-4-FLEX-BLK-20-datasheet-usa4-2020-03-13-web.pdf
FabPro Flexible BLK	3D Systems	https://www.3dsystems.com/materials/fabpro-flexible-blk
DuraForm ProX EX NAT	3D Systems	https://www.3dsystems.com/sites/default/files/2019-05/3d-systems-duraform-prox-ex-nat-datasheet-us-a4-2019-05-01-a-print.pdf
Figure 4 FLEX-BLK 10	3D Systems	https://www.3dsystems.com/sites/default/files/2019-06/3d-systems-figure-4-flex-BLK-10-datasheet-us-a4-2019-06-18-a-web.pdf
9120	Somos	https://www.dsm.com/content/dam/dsm/additive-manufacturing/en_US/documents/somos-9120-ss-pds-letter.pdf



Nylon (polyamide)		
DuraForm PA Plastic	3D Systems	https://www.3dsystems.com/sites/default/files/2017-03/3D-Systems_DuraForm_PA_DATASHEET_A4_US_2017.03.22_WEB.pdf
DuraForm ProX PA Plastic	3D Systems	https://www.3dsystems.com/sites/default/files/2018-07/3d-systems-duraform-prox-sls-datasheet-us-a4-2018-07-17-a-print.pdf
DuraForm FR1200	3D Systems	https://www.3dsystems.com/sites/default/files/2018-03/3d-systems-duraform-fr1200-datasheet-a4-us-2018-03-19-web.pdf
DuraForm ProX EX BLK	3D Systems	https://www.3dsystems.com/sites/default/files/2017-10/3d-systems-duraform-prox-ex-blk-datasheet-a4-us-2017-10-10-web.pdf
DuraForm ProX PA Plastic	3D Systems	https://www.3dsystems.com/sites/default/files/2018-07/3d-systems-duraform-prox-sls-datasheet-us-a4-2018-07-17-a-print.pdf
DuraForm PA Plastic	3D Systems	https://www.3dsystems.com/sites/default/files/2017-03/3D-Systems_DuraForm_PA_DATASHEET_A4_US_2017.03.22_WEB.pdf
DuraForm EX Plastic	3D Systems	https://www.3dsystems.com/sites/default/files/2018-09/3d-systems-duraFormex-datasheet-usen-2018-09-24-web.pdf
ABS or ABS-like		
DuraForm ProX EX BLK	3D Systems	https://www.3dsystems.com/sites/default/files/2017-10/3d-systems-duraform-prox-ex-blk-datasheet-a4-us-2017-10-10-web.pdf
VisiJet Armor M2G-CL	3D Systems	https://www.3dsystems.com/sites/default/files/2020-01/3d-systems-visiJet-m2-material-selection-guide-a4-us-2020-01-08-web.pdf
Figure 4® TOUGH-BLK 20	3D Systems	https://www.3dsystems.com/sites/default/files/2020-03/3d-systems-figure-4-TOUGH-BLK-20-datasheet-usa4-2020-03-16-web.pdf
VisiJet M3-X	3D Systems	https://www.3dsystems.com/sites/default/files/2018-11/3d-systems-proJet-mjp-3600-plastic-tech-specs-a4-us-2018-11-08-web.pdf
Accura ABS Black (SL 7820)	3D Systems	https://www.3dsystems.com/sites/default/files/2018-11/3D-Systems_Accura_ABS_Black_SL7820_Datasheet_USEN_11-01-18-web.pdf
Accura ABS White (SL 7810)	3D Systems	https://www.3dsystems.com/sites/default/files/2017-02/3D-Systems_Accura_ABS_White_SL7810_DATASHEET_A4_01.22.17_UKEN_WEB.pdf
Accura 55	3D Systems	https://www.3dsystems.com/sites/default/files/2017-03/3D-Systems_Accura_55_DATASHEET_A4_US_2017.03.21_a_WEB.pdf
GP Plus 14122	Somos	https://www.dsm.com/content/dam/dsm/additive-manufacturing/en_US/documents/Brand-Status-Sell-Sheets/English-Letter/Somos%20GP%20Plus%2014122%20SS-PDS%20Letter.pdf
WATERSHED XC 11122	SOMOS	https://www.dsm.com/content/dam/dsm/additive-manufacturing/en_US/documents/somos-watershed-xc-11122-leaflet-v2.pdf
Elastomers		
VisiJet M2 ENT	3D Systems	https://www.3dsystems.com/sites/default/files/2020-01/3d-systems-visiJet-m2-material-selection-guide-a4-us-2020-01-08-web.pdf
Figure 4® RUBBER-BLK 10	3D Systems	https://www.3dsystems.com/sites/default/files/2020-03/3d-systems-figure-4-RUBBER-BLK-10-datasheet-usa4-2020-03-13-web.pdf
FabPro Elastic BLK	3D Systems	https://www.3dsystems.com/materials/fabpro-elastic-blk



DuraForm TPU Elastomer	3D Systems	https://www.3dsystems.com/sites/default/files/2017-02/3D-Systems_DuraForm_TPU_Elastomer_SLS_Datasheet_10.17.16_USA4_WEB.pdf
DuraForm Flex	3D Systems	https://www.3dsystems.com/sites/default/files/2017-02/DuraForm_Flex_SLS_DATASHEET_01.08.17_USEN_WEB.pdf
Polymer composites		
Accura Bluestone	3D Systems	https://uk.3dsystems.com/sites/default/files/2017-01/DS_Accura_Bluestone_US.pdf
DuraForm ProX AF+ (Al + nylon)	3D Systems	https://www.3dsystems.com/sites/default/files/2017-12/3d-systems-duraform-prox-af%2B-datasheet-a4-us-2017-10-10-web.pdf
DuraForm ProX HST	3D Systems	https://www.3dsystems.com/sites/default/files/2017-02/3D-Systems_DuraForm_ProX_HST_Composite_SLS_Datasheet_10.17.16_USA4_WEB.pdf
DuraForm ProX GF plastic	3D Systems	https://www.3dsystems.com/sites/default/files/2017-08/3D-Systems_DuraForm_ProX_GF_Plastic_SLS_Datasheet_USA4_2017.08.18_WEB.pdf
DuraFormHST Composite	3D Systems	https://www.3dsystems.com/sites/default/files/2017-03/3D-Systems_DuraForm_HST_DATASHEET_A4_US_03.27.17_WEB_0.pdf
DuraFormGF plastic	3D Systems	https://www.3dsystems.com/sites/default/files/2017-06/3D-Systems_DuraForm_GF_DATASHEET_A4_US_2017.06.8_WEB.pdf
Accura® HPC	3D Systems	https://www.3dsystems.com/sites/default/files/2018-08/3d-systems-accura-hpc-sla-datasheet-us-a4-2018-08-21-web.pdf
Accura CeraMAX	3D Systems	https://www.3dsystems.com/sites/default/files/2017-02/3D-Systems_Accura_CeraMAX_DATASHEET_A4_01.22.17_UKEN_WEB.pdf
Carboprint C (resin)	SGL Carbon	https://www.sglicarbon.com/pdf/SGL-Brochure-The-3Designers-EN.pdf
Carboprint P-1 (polymer)	SGL Carbon	https://www.sglicarbon.com/pdf/SGL-Brochure-The-3Designers-EN.pdf
Carboprint P-2 (polymer)	SGL Carbon	https://www.sglicarbon.com/pdf/SGL-Brochure-The-3Designers-EN.pdf
SICAPRINT P-100 (polymer)	SGL Carbon	https://www.sglicarbon.com/pdf/SGL-Brochure-The-3Designers-EN.pdf
SICAPRINT P-200 (polymer)	SGL Carbon	https://www.sglicarbon.com/pdf/SGL-Brochure-The-3Designers-EN.pdf
SICAPRINT P-210 (polymer)	SGL Carbon	https://www.sglicarbon.com/pdf/SGL-Brochure-The-3Designers-EN.pdf

6.3 Ceramics

Ceramic	Manufacturer	Reference
Alumina		
Al ₂ O ₃	Admatek	https://admateceurope.com/ceramics
Al ₂ O ₃	3D Ceram	http://3dceram.com/wp-content/uploads/2019/11/Technical-ceramics-by-3DCeram.pdf
HP 500 - Alumina	LithaLox	https://www.lithoz.com/application/files/2315/5197/6789/2019_1_Materialfolder_EN_Print-1.pdf



Zirconia		
ZrO ₂	Admatek	https://admateceurope.com/ceramics
Al ₂ O ₃ toughened ZrO ₂ 20 / 80	3D Ceram	http://3dceram.com/wp-content/uploads/2019/11/Technical-ceramics-by-3DCeram.pdf
Zirconia 8Y	3D Ceram	http://3dceram.com/wp-content/uploads/2019/11/Technical-ceramics-by-3DCeram.pdf
Zirconia 3Y	3D Ceram	http://3dceram.com/wp-content/uploads/2019/11/Technical-ceramics-by-3DCeram.pdf
LithaCon 3Y 210 & 3Y 230	Lithoz	https://www.lithoz.com/application/files/2315/5197/6789/2019_1_Materialfolder_EN_Print-1.pdf
Si+SiC (SiC infused with Si)		
SICAPRINT Si-10	SGL Carbon	https://www.sglcarbon.com/pdf/SGL-Brochure-The-3Designers-EN.pdf
SICAPRINT Si-100	SGL Carbon	https://www.sglcarbon.com/pdf/SGL-Brochure-The-3Designers-EN.pdf
SICAPRINT Si-200	SGL Carbon	https://www.sglcarbon.com/pdf/SGL-Brochure-The-3Designers-EN.pdf
Si + C (C infused with Si)		
Carboprint Si-1	SGL Carbon	https://www.sglcarbon.com/pdf/SGL-Brochure-The-3Designers-EN.pdf
Carboprint Si-2	SGL Carbon	https://www.sglcarbon.com/pdf/SGL-Brochure-The-3Designers-EN.pdf
Carboprint Si-3	SGL Carbon	https://www.sglcarbon.com/pdf/SGL-Brochure-The-3Designers-EN.pdf
Silicon nitride		
Silicon Nitride	3D Ceram	http://3dceram.com/wp-content/uploads/2019/11/Technical-ceramics-by-3DCeram.pdf
LithaNit 720	Lithoz	https://www.lithoz.com/application/files/2315/5197/6789/2019_1_Materialfolder_EN_Print-1.pdf
Other		
Aluminium nitride	3D Ceram	http://3dceram.com/wp-content/uploads/2019/11/Technical-ceramics-by-3DCeram.pdf
Cordierite	3D Ceram	http://3dceram.com/wp-content/uploads/2019/11/Technical-ceramics-by-3DCeram.pdf

◆◆◆ End of document ◆◆◆